BEAM PROFILE CHARACTERIZATION OF LIGHT-EMITTING-DIODE CURING UNITS AND ITS EFFECT ON POLYMERIZATION OF A RESIN-MATRIX COMPOSITE

Afnan Omar AlZain

Submitted to the faculty of the University Graduate School
in partial fulfillment of the requirements
for the degree
Doctor of Philosophy
in the School of Dentistry,
Indiana University

May 2017

Accepted by the Graduate Faculty, Indiana University, in partial fulfillment of the requirements for the degree of Doctor of Philosophy.

Jeffrey A. Platt, D.D.S., M.S., Chair

Doctoral Committee

Tien-Min G. Chu, D.D.S., Ph.D.

Marco C. Bottino, D.D.S, M.Sc, Ph.D.

Anderson T. Hara, D.D.S, M.Sc, Ph.D.

John V. Goodpaster, B.A, M.S, Ph.D.

November 28, 2016

Jean-Francois Roulet, D.D.S, Ph.D.

DEDICATION

I would like to dedicate this dissertation to my parents and siblings, a great source of encouragement, inspiration, support, unconditional love and prayers.

ACKNOWLEDGMENTS

I am thankful to Allah for guiding me and giving me strength during my education journey. I would not be where I am today without Him being by my side.

I would like to convey my deepest gratitude to King Abdulaziz University for their scholarship and support to earn my graduate degree.

I would like to express my deepest appreciation to my mentor Dr. Jeffrey A. Platt, for his continuous guidance and support during my Ph.D. journey. Dr. Platt is not only a mentor for my Ph.D. dissertation project, but is a role model. His teaching skills, research experience and patience significantly impacted my professional and personal growth. Dr. Platt helped expand my critical thinking, research independence and leadership skills. I am privileged, honored and grateful to have Dr. Platt as my mentor.

I would like to give a special gratitude to Dr. Richard Gregory and Dr. Michael Kowolik for their engorgement and support throughout my time in the Ph.D. program. Without Dr. Gregory, Dr. Kowolik and Dr. Platt's help, my Ph.D. dissertation would not have been completed. They stood by my side when I needed them the most.

I would like to thank my advisory and research committee professors, Dr. Tien-Min Chu, Dr. Marco Bottino, Dr. Anderson Hara, Dr. John Goodpaster and Dr. Jean-Francois Roulet for their help and advice during my Ph.D. dissertation project.

I would like to also express my gratitude to Mr. Gorge Eckert for his statistical expertise and help during my Ph.D. experience. I would like to acknowledge David Reagan from the Advanced Visualization Laboratory for all of his assistance with ParaView imaging program. Also, I would like to thank laboratory managers and technicians for their assistance in the laboratories I have worked in, Clif Duhn, Nyi-Nyi Tin and Joseph Joseph at the Oral Health and Research Institute laboratories, Gina Londino and Donna Roskowski at the Department of Forensic and Investigative Sciences Laboratory.

I would like to give special thanks to the Department of Dental Illustrations, Tim Centers, Nicole Alderson, Mark Dirlam and Terry Wilson for their kindness and their continuous help in everyway they can. Exceptional gratitude and appreciation goes to Tim for his genuine assistance throughout my Ph.D. journey and his help photographing the experimental laboratory procedures. Special credit goes to Tim and Nicole for their remarkable help with Photoshop and Illustrator programs.

I would like to express my sincere appreciation to the American Dental Association Laboratory for their collaboration and allowing me to conduct part of my Ph.D. dissertation project in their laboratory. Thanks to Dr. Spiro Megremis, Henry Lukic and Vicrotia Ong for their assistance in using the Beam Profiler System equipment, without their help and collaboration, I would not be able to perform that experiment.

I would like to thank all of my friends and colleagues who stood by my side and helped me in my time of need, namely, Maria Tereza Pedrosa Albuquerque, Eliseu Münshow, Hawazen Radhwan, Divya Pankajakshan, Maryam Al-Ghilan, Sarah Al-Angari, Hadeel Ayoub, Amnah Al-Garni, and Ghaeth Yassen.

Finally, a heartfelt thanks to my parents and siblings for all they have done, care, help, support, love and prayers.

Afnan Omar AlZain

BEAM PROFILE CHARACTERIZATION OF LIGHT-EMITTING-DIODE CURING UNITS AND ITS EFFECT ON POLYMERIZATION OF A RESIN-MATRIX COMPOSITE

The general aim of this study was to investigate the influence of the localized irradiance beam profiles from multiple light-emitting-diode (LED) light-curing units (LCUs) on the polymerization pattern within a resin-matrix composite (RMC). Irradiance beam profiles were generated from one quartz-tungsten-halogen and various single and multiple emission peak LED LCUs using a camera-based beam profiler system combined with LCU power measurements obtained using an integrating sphere/spectrometer assembly. The influence of distance on irradiance, radiant exposure (RE) and degree of conversion (DC) on the top and bottom surfaces of a RMC increment, using various LCUs, at two clinically relevant distances was investigated. Molar absorptivity of the photoinitiators present in the nano-hybrid RMC (Tetric EvoCeram-bleaching shade-XL) assessed was using UV-spectrophotometry. The correlation among irradiance, RE and DC was explored. A mapping approach was used to investigate DC, microhardness and cross-link density (CLD) within 5×5×2 mm specimens at various depths; top, 0.5, 0.7, 0.9, 1.1, 1.3,1.5 mm and bottom. The localized irradiance correlation with its corresponding DC, microhardness and CLD was explored, and localized DC correlation with microhardness was assessed. The DC was measured using micro-Raman spectroscopy, and CLD was assessed by an ethanol-softening method (%KHN reduction) using an automated microhardness tester.

Molar absorptivity of diphenyl (2,4,6-trimethylbenzoyl) phosphine oxide was 20-fold higher than camphorquinone. Non-uniform LCU beam profiles caused localized polymerization discrepancies that were significant at specific depths and points within the specimens with respect

to DC, microhardness and CLD, which did not follow a specific pattern regardless of the LCU or curing distance assessed.

A moderate correlation was displayed among irradiance, RE and DC. The localized irradiance from the LCUs was weakly correlated with the corresponding DC, microhardness and CLD on the top surface of a RMC at both curing distances. The localized microhardness was moderately correlated with DC. In conclusion, polymerization within the RMC investigated was non-uniform and did not reflect the LCU irradiance pattern at the area assessed. Also, a mapping approach within the specimens provided a detailed polymerization pattern assessment occurring within a RMC increment. Therefore, the LCUs explored may potentially increase the risk of RMC fracture.

Jeffrey A. Platt, D.D.S., M.S., Chair

TABLE OF CONTENTS

LIST OF TABLES ix

LIST OF FIGURES xii

LIST OF APPENDICES xix

LIST OF ABBREVIATIONS xxiv

INTRODUCTION 1

MATERIALS AND METHODS 24

RESULTS 44

DISCUSSION 70

SUMMARY 95

CONCLUSION 99

CLINICAL IMPLICATIONS 105

TABLES 106

FIGURES 134

APPENDICES 224

REFERENCES 710

CURRICULUM VITAE

LIST OF TABLES

Table 1. The LCUs explored and materials used in this study....106

Table 2. Mean (SD) irradiance (mW/cm^2) and RE (J/cm^2) detected by the top and bottom MARC-RC sensors and received on the top and bottom RMC surfaces cured at 2 mm distance by an LED (BS) LCU and a QTH (O) LCU....107

Table 3. Mean (SE) DC (%), KH-BE, KH-AE (kg/mm^2) and %KH reduction for the RMC light cured using an LED (BS) LCU and a QTH (O) LCU at 2 mm curing distance....108

Table 4. Curing times (seconds) needed to achieve 10-11 J/cm^2 RE from the LCUs explored at multiple distances (mm) as detected by the top MARC-RC sensor....109

Table 5. Regression trendline, R^2 and percent increase in curing time and percent decrease in irradiance to achieve 10-11 J/cm^2 RE from the LCUs explored as detected by the top MARC-RC sensor....110

Table 6. Mean (SE) irradiance (mW/cm^2), RE (J/cm^2), DC (%) and percent decrease in irradiance, RE and DC between the top and bottom surfaces of the RMC specimens....111

Table 7. ANOVA table of the effect of the LCUs and curing distances on irradiance (mW/cm^2), RE (J/cm^2) and DC (%) on the top and bottom surfaces of the RMC specimens....112

Table 8. Correlation among the irradiance (Irr) (mW/cm^2) , RE (J/cm^2) and DC (%) on the top and bottom surfaces of the RMC specimens light cured using the LCUs explored at 2 and 8 mm distances....113

Table 9. Mean (SD) radiant power (mW) and irradiance (mW/cm^2) from the QTH and multiple emission peak LED LCUs explored at various spectral ranges and distances using the integrating sphere/spectrometer assembly....114

Table 10. Mean (SD) radiant power (mW) and irradiance (mW/cm^2) measurements from the pulsating single emission peak LED LCUs over the full spectral range (380-700 nm) at multiple curing distances....115

Table 11. Characterization of the LCUs explored....116

Table 12. Number of localized significant comparisons (*) among the %KH reduction measurement points (x-y coordinates) of the RMC specimens at each depth and curing distance using the LCUs explored 117

Table 13. ANOVA table for the %KH reduction significant of x, y and x-y coordinates using the individual LCU across each depth at 2 and 8 mm curing distances....118

Table 14. Mean (SD) KH-BE, KH-AE (kg/mm^2) and %KH reduction of the RMC specimens across each depth at 2 and 8 mm curing distances using the LCUs explored....119

Table 15. ANOVA table for LCU and curing distance effect on the %KH reduction across each depth of the RMC specimens....120

Table 16. Correlation between the localized irradiance beam profiles (mW/cm^2) and localized %KH reduction on the top surfaces of the RMC specimens using the various filters for the multiple LCUs explored at 2 and 8 mm curing distances from the RMC specimens....121

Table 17. Number of localized significant comparisons (*) among the KH (kg/mm^2) measurements (x-y coordinates) of the RMC specimens across each depth and curing distance using the LCUs explored 122

Table 18. Number of localized significant comparisons (*) among the DC (%) measurement points (x-y coordinates) across each depth and curing distance of the RMC specimens using the LCUs explored 123

Table 19. ANOVA table for KH (kg/mm^2) significant effect of x, y, x-y coordinates for the individual LCU across each depth at 2 and 8 mm curing distances 124

Table 20. ANOVA table for DC (%) significant effect of x, y, x-y coordinates for the individual LCU across each depth at 2 and 8 mm curing distances 125

Table 21. Mean (SE) KH (kg/mm^2) and DC (%) of the RMC specimens across each depth using the LCUs explored at 2 and 8 mm curing distances....126

Table 22. ANOVA table of the LCU and curing distance effect on KH (kg/mm^2) across each depth of the RMC specimens....128

Table 23. ANOVA table of the LCU and curing distance effect on the DC (%) across each depth of the RMC specimens....129

Table 24. Correlation of the localized irradiance beam profiles with KH and DC values of the RMC specimens using the various LCUs explored and beam profile filtersat 2 and 8 mm distances....130

Table 25. Correlation between the localized (x-y coordinates) DC with KH-BE, KH-AE and %KH reduction using the LCUs explored at 2 and 8 mm curing distances....131

Table 26. Correlation between the average DC values with KH-BE, KH-AE and %KH reduction values across each depth using the LCUs explored at 2 and 8 mm curing distances ...132

Table 27. Collective significant comparisons (*) summary for the DC, KH, %KH reduction and bottom/top KH ratios of all the data points collected within the entire RMC specimens cured using the LCUs explored at 2 and 8 mm distances 133

LIST OF FIGURES

Figure 1. Specific aim 1 phases 134

Figure 2. Research questions based on specific aim 1 findings 135

Figure 3. Specific aim 2 phases 136

Figure 4. Specific aim 3 phases 137

Figure 5. Specific aim 4 phases 138

Figure 6. Optilux 401 QTH LCU 139

Figure 7. Bluephase Style multiple emission peak LED LCU 140

Figure 8. Beam profiler system 141

Figure 9. LCU setup on a beam profiler system with the light guide tip at 2 mm distance from a ground glass diffuser 142

Figure 10. Integrating sphere/spectrometer assembly components and setup 143

Figure 11. Representative adapter assembly and a LCU setup on an integrating sphere for collecting LCU power measurements 144

Figure 12. Specific aim 1, phase 2 experimental design 145

Figure 13. MARC-RC system 146

Figure 14. Representative of a LCU setup on the top MARC-RC sensor 147

Figure 15. Custom-designed mold for the RMC specimen fabrication 148

Figure 16. Representative of a LCU setup on the bottom MARC-RC sensor and setup RMC specimen fabrication 149

Figure 17. Setup of the RMC specimen sectioning 150

Figure 18. Representative sectioned RMC specimen for depth characterization 151

Figure 19. RMC specimens finishing and polishing procedure 152

Figure 20. Knoop microhardness test setup 153

Figure 21. Illustration of the DC and KH mapping on the RMC specimens 154

Figure 22. Micro-Raman spectroscopy experiment 155

Figure 23. Representative spectra measurement of the peaks of interest collected using a micro-Raman spectroscopy instrument 156

Figure 24. Soaking the RMC specimens in absolute ethanol 157

Figure 25. Specific aim 2, phase 1 experimental design 158

Figure 26. SmartLite Max multiple emission peak LED LCU 159

Figure 27. VALO Cordless multiple emission peak LED LCU 160

Figure 28. DEMI single emission peak LED LCU 161

Figure 29. Demi Ultra single emission peak LED LCU 162

Figure 30. Setup of VALO Cordless on a top MARC-RC sensor 163

Figure 31. Setup of VALO Cordless on a bottom MARC-RC sensor 164

Figure 32. Serial dilutions of the photoinitiator molar absorptivity experiment 165

Figure 33. Ultraviolet (UV) spectrophotometry instrument 166

Figure 34. LCU setup against a ground glass diffuser 167

Figure 35. VALO Cordless setup against a ground glass diffuser 168

Figure 36. Custom-made 3D printed adapters for placement on an integrating sphere opening 169

Figure 37. Specific aim 3, phase 2 experimental design 170

Figure 38. Specific aim 4, phase 2 experimental design 171

Figure 39. Representative 2D and 3D irradiance beam profiles from the multiple emission peak LED (BS) LCU and QTH (O) LCU measured through a 425 nm longpass or shortpass filter with the light emitting tip at 2 mm distance from a glass diffuser 172

Figure 40. Representative spectral emission curves for the LED (BS) and QTH (O) LCUs 173

Figure 41. Representative images for the Knoop microhardness indentations BE and AE 174

Figure 42. Representative DC (%) 2D contour maps and 3D renderings of RMC specimens light cured with the LED (BS) LCU and the QTH (O) LCU 175

Figure 43. Representative KH (kg/mm^2) 2D contour maps and 3D renderings of the RMC specimens BE and AE that were light cured with the LED (BS) LCU and QTH (O) LCU.....176

Figure 44. Mean (SE) DC (%), KH-BE and KH-AE (kg/mm^2), and %KH reduction measurements of the RMC specimens cured by the multiple emission peak LED (BS) LCU and the QTH (O) LCU 177

Figure 45. Representative irradiance (mW/cm^2) and spectral distribution curves of the LCUs explored at 0 mm distance from the top MARC-RC sensor needed to achieve 10-11 J/cm^2 to the top surfaces of the RMC specimens 178

Figure 46. Irradiance mean (SD) and curing times needed to achieve 10-11 J/cm^2 at multiple distances collected using the top MARC-RC sensor for the LCUs explored.....179

Figure 47. Polynomial (order 2) trendline of the irradiance and curing needed to reach 10-11 J/cm^2 at multiple distances collected using the top MARC-RC sensor.....180

Figure 48. Representative irradiance (mW/cm^2) measurements of the LCUs explored collected using the top and bottom MARC-RC sensors at multiple distances 181

Figure 49. Representative spectral emission curves of the LCUs explored collected using the top and bottom MARC-RC sensors at multiple distances 182

Figure 50. Mean (SE) DC (%) measurements collected from the top and bottom surfaces of the RMC specimen at 2 and 8 mm curing distances.....183

Figure 51. Mean (SE) DC (%) significant differences between top and bottom surfaces for each LCU at 2 and 8 mm curing distances.....184

Figure 52. CQ photoinitiator spectral distribution at multiple concentrations measured using a UV-spectrophotometry 185

Figure 53. TPO photoinitiator spectral distribution at multiple concentrations measured using a UV-spectrophotometry 186

Figure 54. Molar absorptivity of CQ and TPO photoinitiators.....187

Figure 55. Representative LCU spectral distribution curves collected using the top and bottom MARC-RC sensors combined with the CQ and TPO absorbance spectrum at 0.005M concentration 188

Figure 56. Representative 2D irradiance distribution images measured through a 425 nm longpass filter at multiple distances between each LCU guide tip and glass diffuser 189

Figure 57. Representative 3D irradiance distribution images explored measured through a 425 nm longpass filter at multiple distances between each LCU guide tip and glass diffuser 190

Figure 58. Representative 2D irradiance distribution images measured through a 425 nm shortpass filter at multiple distances between each LCU tip and glass diffuser 191

Figure 59. Representative 3D irradiance distribution images measured through a 425 nm shortpass filter at multiple distances between each LCU guide tip and glass diffuser 192

Figure 60. Representative 2D and 3D irradiance distribution images from the LCUs explored measured through a 425 nm longpass filter with the light tip at 2 and 8 mm distance from a glass diffuser 193

Figure 61. Representative 2D and 3D irradiance distribution images from the LCUs explored measured through a 425 nm shortpass filter with the light tip at 2 and 8 mm distance from a glass diffuser 194

Figure 62. Representative 2D localized irradiance distribution images from the LCUs that were received on the top RMC surfaces measured through a 425 nm longpass filter 195

Figure 63. Representative 2D localized irradiance distribution images from the LCUs that were received on the top RMC surfaces measured through a 425 nm shortpass filter 196

Figure 64. Percent contribution (%) from the blue (425-700 nm) and violet (380-425 nm) spectral region of the LCUs explored at 2 mm curing distance from the integrating sphere opening 197

Figure 65. Representative 3D renderings of the localized Knoop microhardness BE and AE (kg/mm^2) of the RMC specimens light cured using the LCUs explored at 2 and 8 mm curing distances....198

Figure 66. Representative 2D renderings of the localized KH-BE (kg/mm^2) contour maps of the RMC specimens light cured using the LCUs explored 199

Figure 67. Representative 2D renderings of the localized KH-AE (kg/mm^2) contour maps of the RMC specimens light cured using the LCUs explored 200

Figure 68. Representative 3D renderings of the localized %KH reduction for the RMC specimens light cured using the LCUs explored at 2 and 8 mm curing distances....201

Figure 69. Representative 2D renderings of the localized %KH reduction contour maps of the RMC specimens light cured using the LCUs explored 202

Figure 70. Representative 3D renderings of the localized %KH reduction measurement points at each depth of the RMC specimens light activated using the LCUs explored at 2 and 8 mm distances 203

Figure 71. Representative 3D renderings of the localized %KH reduction significant points at each depth of the RMC light cured using the LCUs explored at 2 and 8 mm distances 204

Figure 72. Representatives 2D localized irradiance beam profiles from the LCU explored measured through a 425 nm longpass filter coupled with the corresponding 2D localized %KH reduction contour maps on the top surfaces of the RMC specimens at 2 and 8 mm distances....205

Figure 73. Representative 3D renderings for localized KH (kg/mm^2) and DC (%) values from the RMC specimens light cured using the LCUs assessed at 2 mm and 8 mm curing distances....206

Figure 74. Representative 2D contour maps for the localized DC (%) values light cured using the LCUs assessed at 2 mm and 8 mm curing distances....207

Figure 75. Representative 3D renderings of the localized KH (kg/mm^2) measurement points at each depth of the RMC specimens light cured using the LCUs explored at 2 and 8 mm curing distances 208

Figure 76. Representative 3D renderings of the localized KH (kg/mm^2) significant measurement points at each depth of the RMC specimens light cured using the LCUs explored at 2 and 8 mm distances 209

Figure 77. Representative 3D renderings of the localized DC (%) measurement points at each depth of the RMC specimens cured using the LCUs explored at 2 and 8 mm curing distances 210

Figure 78. Representative 3D renderings of the localized DC (%) significant measurement points at each depth of the RMC specimens light cured using the LCUs explored at 2 and 8 mm curing distances 211

Figure 79. 2D contour plots to visualize the localized bottom/top KH ratios (%) at each measurement point on the RMC specimens cured using the LCUs explored at 2 and 8 mm curing distances.....212

Figure 80. 2D contour plots to visualize the localized %bottom/top KH ratios that are less than 80% at each point on the RMC specimens cured using the LCUs explored at 2 and 8 mm distances.....213

Figure 81. 2D contour plots to visualize the localized significant %bottom/top KH ratios among the point on the RMC light cured using the LCUs explored at 2 and 8 mm distances.....214

Figure 82. Representative 3D renderings of the localized minimum DC (%) measurement points at each depth of the RMC specimens light cured using the LCUs explored at 2 and 8 mm curing distances 215

Figure 83. Representative 3D renderings of the localized minimum DC values that are less than 50% on the RMC specimens light cured using the LCUs explored at 2 and 8 mm distances.....216

Figure 84. Representative 2D images of the localized irradiance beam profiles from the LCU explored measured through a 425 nm longpass filter coupled with the corresponding 2D localized KH and DC contour maps at 2 mm distance from the target surface 217

Figure 85. Representative 2D images of the localized irradiance beam profiles from the LCU explored measured through a 425 nm longpass filter coupled with the corresponding 2D localized KH and DC contour maps at 8 mm distance from the target surface 218

Figure 86. Diameter of the fiber optic light guide tip entry and exit for the removable light guide tips of the LCUs explored 219

Figure 87. Differences between the original and updated BS fiber optic light guide tip.....220

Figure 88. Illustration of the Spectral Reflection Law.....221

Figure 89. Representatives 2D images of the localized irradiance beam profiles from the LCUs explored measured through a 425 nm longpass filter coupled with the corresponding 2D localized DC, KH and %KH reduction values on the top surfaces of the specimens at 2 mm distance from the target surface 222

Figure 90. Representatives 2D images of the localized irradiance beam profiles from the LCUs explored measured through a 425 nm shortpass filter coupled with the corresponding 2D localized DC, KH and %KH reduction values on the top surfaces of the specimens at 8 mm distance from the target surface 223

LIST OF APPENDICES

Appendix 1. Descriptive details for the irradiance (mW/cm^2) and RE (J/cm^2) received on the top and bottom surfaces of the RMC specimens cured at 2 mm distance using an LED (BS) LCU and a QTH (O) LCU as detected by the MARC-RC sensors 224

Appendix 2. Mean (SE) DC (%) and significant differences for the between curing the RMC with an LED (BS) LCU and a QTH (O) LCU across various depths within the specimens cured at 2 mm distance 225

Appendix 3. Descriptive details for the DC (%) across various depths within the RMC specimens cured using an LED (BS) LCU and a QTH (O) LCU at 2 mm distance from the top surfaces of the specimens 226

Appendix 4. Mean (SE) and significant difference of the KH-BE, KH-AE (kg/mm^2) and %KH reduction across various depths of the RMC specimens cured at 2 mm curing distance from the top surfaces of the RMC specimens using an LED (BS) LCU and a QTH (O) LCU 227

Appendix 5. Descriptive details for the KH-BE, KH-AE (kg/mm^2) and %KH reduction across various depths of the RMC specimens cured by an LED (BS) LCU and a QTH (O) LCU cured at 2 mm distance 228

Appendix 6. DC, KH-BE, KH-AE and %KH reduction significant differences (*) among the various depths of the RMC specimens cured using an LED (BS) LCU and a QTH (O) LCU 229

Appendix 7. ANOVA table and significant differences (*) of the LCU, x, y and x-y coordinates effect on DC, KH, %KH reduction across each depth of the RMC specimens cured using an LED (BS) LCU and a QTH (O) LCU 231

Appendix 8. Descriptive details of the irradiance (mW/cm^2), RE (J/cm^2) and DC (%) on the top and bottom RMC specimen surfaces cured by the LCUs explored at 2 and 8 mm distances 233

Appendix 9. Descriptive details of the irradiance (mW/cm^2), RE (J/cm^2) and DC (%) significant comparisons between 2 and 8 mm curing distances on the top and bottom surfaces of the RMC specimens cured using the LCUs explored 235

Appendix 10. Descriptive details of the irradiance (mW/cm^2), RE (J/cm^2) and DC (%) significant comparisons among LCUs on the top and bottom surfaces of the RMC specimens cured using the LCUs explored at 2 and 8 mm curing distances 237

Appendix 11. Localized average radiant power values from the LCUs explored within the 3×3 mm area investigated using the longpass and shortpass filters at 2 and 8 mm distances 243

Appendix 12. Localized average irradiance distribution (mW/cm^2) from the LCUs explored within the 3×3 mm area investigated using the longpass and shortpass filters at 2 and 8 mm distances 255

Appendix 13. Localized mean (SE) KH-BE and KH-AE (kg/mm^2) values (x-y coordinates) on the top and bottom surfaces of the RMC specimen at 2 and 8 mm curing distances 267

Appendix 14. Localized mean (SE) KH-BE and KH-AE (kg/mm^2) measurement points at each depth of slices-a, -b and –c of the RMC specimens cured using the LCUs explored at 2 and 8 mm distances 291

Appendix 15. Descriptive details for the KH-BE, KH-AE (kg/mm^2) and %KH reduction measurement values (x-y coordinates, mm) on the top (T), bottom (B) surfaces and various depths (mm) of the RMC specimens cured using the LCU explored at 2 mm distance 303

Appendix 16. Descriptive details of the KH-BE, KH-AE (kg/mm^2) and %KH reduction measurement values (x-y coordinates, mm) on the top (T), bottom (B) surfaces and depths (mm) of the RMC specimens cured using the LCU explored at 8 mm distance 346

Appendix 17. Localized mean (SE) %KH reduction values and significant points among the top (T) and bottom (B) RMC surface cured using the LCUs explored at 2 or 8 mm distances 389

Appendix 18. Localized mean (SE) %KH reduction values and significant points (x-y coordinates, mm) among each depth (mm) and distance of the RMC specimens cured using the LCUs explored 401

Appendix 19. Localized %KH reduction significant comparisons among points (x-y coordinates) on the top (T), bottom (B) surfaces and at the various depths of the RMC specimens and curing distances using the LCUs explored at 2 and 8 mm curing distances 407

Appendix 20. Descriptive details of the average KH-BE, KH-AE (kg/mm^2) and %KH reduction values across each depth of the RMC specimens at 2 and 8 mm curing distances using the LCUs explored 451

Appendix 21. Significant differences of the average %KH reduction between 2 and 8 mm curing distances across each depth using the LCUs explored 457

Appendix 22. Significant differences of the average %KH reduction amongst specimens cured using the LCUs explored across the top (T) and bottom (B) surfaces and across each depth at 2 and 8 mm curing distance 459

Appendix 23. Localized irradiance (Irr) distribution (mW/cm^2) from the LCUs explored using a longpass filter coupled with the corresponding %KH reduction value on the top RMC surfaces at 2 mm distance 468

Appendix 24. Descriptive details of the localized DC (%) values at each point on the top (T), bottom (B) surfaces and various depths of the RMC specimens cured at 2 and 8 mm distances 480

Appendix 25. Localized mean (SE) KH-BE (kg/mm^2) values and significant points (x-y coordinates) among the top (T) and bottom (B) RMC surface cured using the LCUs explored at 2 or 8 mm distances 507

Appendix 26. Localized mean (SE) KH-BE (kg/mm^2) values and significant points (x-y coordinates) among each depth and distance of the RMC specimens cured using the LCUs explored....519

Appendix 27. Significant localized KH-BE (kg/mm^2) comparisons among points (x-y coordinates) at the various depths of the RMC specimens cured using the LCUs explored at 2 and 8 mm distances....525

Appendix 28. Localized mean (SE) DC (%) values and significant points (x-y coordinates) among the top (T) and bottom (B) RMC surface cured using the LCUs explored at 2 or 8 mm distances....569

Appendix 29. Localized mean (SE) DC (%) values and significant points (x-y coordinates) among each depth and distance of the RMC specimens cured using the LCUs explored....581

Appendix 30. Localized significant DC (%) points (x-y coordinates) and p-values at the various depths of the RMC specimens cured using the LCU explored at 2 and 8 mm distances....587

Appendix 31. Localized mean (SE) and significant bottom/top (B/T) KH ratio (%) when curing the RMC specimens using the LCUs explored at 2 and 8 mm distances....633

Appendix 32. Localized significant B/T KH ratio (%) comparisons of the RMC specimens light cured using the LCUs explored at 2 and 8 mm distances....645

Appendix 33. Descriptive details of the localized DC (%) values (x-y coordinates) that are less than 50% from all specimens at the various depths when curing specimens using the LCUs explored at 2 and 8 mm distances....657

Appendix 34. Location and values of the DC (%) measurement points (x-y coordinates) that are less than 50% from all specimens when cured using the LCUs explored at 2 and 8 mm curing distances....659

Appendix 35. Descriptive details for the average DC (%) values across each depth of the RMC specimens cured using the LCUs explored at 2 and 8 mm distances....675

Appendix 36. Significant differences of the average KH (kg/mm^2) comparisons between 2 and 8 mm curing distances across each depth using the LCUs explored 677

Appendix 37. Significant differences of the average KH (kg/mm^2) comparisons amongst light curing specimens using the LCUs explored across each depth at 2 and 8 mm curing distances 679

Appendix 38. Significant differences of the average DC (%) comparisons between 2 and 8 mm curing distances across each depth using the LCUs explored 687

Appendix 39. Significant differences of the average DC (%) comparisons amongst light curing specimens using the LCUs explored on the top (T) and bottom (B) surfaces, across each depth and curing distance 689

Appendix 40. Localized irradiance (Irr) distribution (mW/cm^2) from the LCUs explored coupled with the corresponding KH-BE (kg/mm^2) and DC (%) values on the top specimen surfaces at 2 and 8 mm distances 698

LIST OF ABBREVIATIONS

%KH reduction	Percent Knoop microhardness reduction
AE	After soaking the RMC specimens in absolute ethanol
BE	Before soaking the RMC specimens in absolute ethanol
BS	Bluephase Style
CLD	Cross-link density
CQ	Camphorquinone
D	DEMI
DC	Degree of conversion
DU	Demi Ultra
KH	Knoop microhardness
KH-AE	Knoop microhardness after soaking specimens in ethanol
KH-BE	Knoop hardness before soaking specimens in ethanol
LCU	Light-curing unit
LED	Light-emitting-diode
MARC-RC	Managing Accurate Resin Curing-Resin Calibrator
O	Optilux 401
QTH	Quartz-tungsten-halogen
RE	Radiant exposure
RMC	Resin-matrix composite
SM	SmartLite Max
TPO	Diphenyl (2,4,6-trimethylbenzoyl) phosphine oxide
V	VALO Cordless

INTRODUCTION

Light activated resin-matrix composite (RMC) has become the material of choice for direct restorative materials (Rasines Alcaraz et al. 2014). The median longevity of posterior RMC restoration was reported to be six years compared to 16 years of amalgam restorations (Sunnegardh-Gronberg et al. 2009). A recent Cochrane review, several literature reviews and a retrospective study reported that secondary caries and fracture of the restoration are the two most common causes of RMC restoration failure (Rasines Alcaraz et al. 2014, Opdam et al. 2007, Demarco et al. 2015, Astvaldsdottir et al. 2015, Moraschini et al. 2015, Alvanforoush et al. 2016, Rho et al. 2013). The Cochrane review reported that the failure rate of a RMC restoration due to secondary caries was significantly higher compared to amalgam restorations, but there were no significant differences in fracture failure rate between RMC and amalgam restorations (Rasines Alcaraz et al. 2014). A recent literature review reported the failure rate of RMC restorations in the past two decades was 10.59% from 1995 to 2005, and 13.13% from 2006 to 2016 (Alvanforoush et al. 2016). The literature review reported that RMC failure due to its fracture increased in the past decade, where the percentage of RMC failure between 1995-2005 was 29.47% due to secondary caries and 28.84% due to RMC fracture, compared 2006-2016 where failure due to secondary caries was 25.68% and 39.07% due to RMC fracture (Alvanforoush et al. 2016).

Premature failure of a RMC restoration is multifactorial in nature including the individual's caries risk, experience of the operator, adhesive technique, material type, and location of the restoration in the oral cavity (Nedeljkovic et al. 2015, Astvaldsdottir et al. 2015, Sunnegardh-Gronberg et al. 2009). A literature review suggested that secondary caries could be associated with the restorative material type and patient-related factors (Nedeljkovic et al. 2015). Failure of the restoration due to fracture may be a result of stresses generated from subjecting a restoration to masticatory loads specifically at high stress bearing areas (Demarco et al. 2015). Also, non-uniform polymerization could adversely impact the physical, chemical and mechanical

properties of RMC restorations (Leprince et al. 2013, Santini et al. 2012, Price, Ferracane, and Shortall 2015, Price et al. 2014, Megremis et al. 2014, Arikawa et al. 2011, Price, Fahey, and Felix 2010, Harlow et al. 2016, Price et al. 2011, Rueggeberg 2011). Therefore, it is critical to investigate polymerization uniformity within the bulk of the restoration as one of the factors that could contribute to fracture of RMC restorations.

The effectiveness of RMC polymerization is dependent on several intrinsic and extrinsic factors. The intrinsic factors are related to the physio-chemical properties of the RMC, such as the type and concentration of photoinitiator system, monomer composition and viscosity, filler particle size and geometry, and optical properties (Leprince et al. 2013). The extrinsic factors are related to the operator's technique, and characteristics of a light-curing unit (LCU), such as the light source, spectral emission, beam profile, light guide tip effective light-emitting area, orientation and positioning of the LCU over the tooth cavity, distance from the restoration, number and type of the LED chips, radiant exposure (RE), irradiance, irradiation time, irradiation mode, and temperature (Price, Ferracane, and Shortall 2015, Leprince et al. 2013, Shortall et al. 2016a). Due to various factors that can impact RMC polymerization effectiveness, it is critical to educate practitioners about these factors and to take them into consideration when using a LCU to polymerize RMC restorations. One of the most common overlooked factors by clinicians is the non-uniform irradiance beam profile distribution across a LCU guide tip, specifically the LED LCUs (Price, Ferracane, and Shortall 2015). Only in the past decade, researchers started to investigate the impact of the non-uniform irradiance beam profile from a LCU on polymerization effectiveness. However, further investigation in this area is still warranted.

The following areas were explored in this study:

1. Irradiance beam profile from a LCU

The LCUs have become an integral part of the dental practice and are used to polymerize resin-based materials such as a RMC. When using a LCU, clinicians assume that the irradiance

beam profile across the light guide tip is uniform, and that the LCU emits the same level of power and wavelength of light across its light guide tip (Price, Ferracane, and Shortall 2015); therefore, usually practitioners place a LCU guide tip centered over the tooth cavity to polymerize the RMC. A LCU irradiance is the radiant power on a surface of known dimensions; therefore, it reflects the average power value received over a RMC surface area (irradiance = power × surface area), and is represented in mW/cm^2 (Platt and Price 2014, Price, Ferracane, and Shortall 2015, Leprince et al. 2013, Shortall et al. 2016a). Manufacturers and researchers usually report the irradiance from a LCU as one average value using conventional methods such as thermopile and a radiometer (ISO 2004, 2007, Price, Ferracane, and Shortall 2015), or using a spectrophotometer, such as an integrating sphere/spectrometer assembly or a cosine corrector (Price, Ferracane, and Shortall 2015). However, these methods do not evaluate the degree of light beam uniformity nor they consider the presence of "hot" and "cold" irradiance regions across the light guide tip (Price, Ferracane, and Shortall 2015).

Now, it is well demonstrated in studies that the irradiance beam profiles and power distribution across the light guide tips of various LCUs could be inhomogeneous and non-uniform (Price, Rueggeberg, et al. 2010, Price et al. 2011, Price, Labrie, et al. 2010, Price et al. 2014, Michaud et al. 2014, Price, Ferracane, and Shortall 2015, Megremis et al. 2014). This was established using a laser beam analyzer that is commonly used now in research to measure the power distribution across the light beam (Price et al. 2014, Michaud et al. 2014, Megremis et al. 2014, Price et al. 2011, Price, Ferracane, and Shortall 2015). Thereby, the assumption that the beam profile is uniform across the light guide tip is no longer valid and reporting the irradiance as one average value is inaccurate. Furthermore, it is more accurate to measure the irradiance using the effective dimension of the light-emitting portion of the LCU guide tip instead of its physical diameter (Price et al. 2014, Michaud et al. 2014, Megremis et al. 2014, Price et al. 2011, Haenel et al. 2015). Because using the physical diameter of the light guide tip will produce substantially lower mean irradiance values (Price et al. 2014).

Beam profile inhomogeneity was not a critical issue with a quartz-tungsten-halogen (QTH) LCU, which has a broad spectral emission (375-510 nm), that is relatively uniform across the light guide tip, and includes wavelengths needed by most RMC photoinitiators (Price, Labrie, et al. 2010, Megremis et al. 2014, Rueggeberg 2011, Jandt and Mills 2013). However, with the development of the light-emitting-diode (LED) LCUs, the irradiance beam profile from a LCU is more of a concern since they include LED chips that are typically side-by-side making complete uniformity across the light tip a challenge. A single emission peak LED LCU contains a blue LED chip that has a narrow spectral emission at the longer wavelength (blue) region (400-520 nm) that peaks near 460 nm (Rueggeberg 2011, Jandt and Mills 2013, Harlow et al. 2016, Miletic and Santini 2012). This blue region includes wavelengths that fall within the absorbance range of camphorquinone (CQ), which is the most commonly used photoinitiator in the RMCs (Rueggeberg 2011, Jandt and Mills 2013, Harlow et al. 2016, Miletic and Santini 2012).

CQ has a yellowish color that can be problematic in esthetic regions (Rueggeberg 2011, Jandt and Mills 2013, Ogunyinka et al. 2007, Harlow et al. 2016, Miletic and Santini 2012). Due to the high esthetic demand, specifically in the anterior region of the oral cavity, various alternative photoinitiators were introduced, such as diphenyl (2,4,6-trimethylbenzoyl) phosphine oxide (TPO), which are commonly used in bleaching shades, and have a spectral range at the shorter wavelength region compared to CQ (Rueggeberg 2011, Jandt and Mills 2013). Therefore, multiple emission peak LED LCU were developed that contain an additional violet LED chip that has a narrow range at the shorter wavelength (violet) region (380-420 nm) and peaks near 409 nm, which includes wavelengths within the absorption range of the alternative photoinitiators (Rueggeberg 2011, Jandt and Mills 2013, Ogunyinka et al. 2007, Harlow et al. 2016, Miletic and Santini 2012). Due to the differences between the single and multiple emission peak LED LCUs, clinicians should select the appropriate LED LCU type depending on the photoinitiator system within a RMC. Unfortunately, manufacturers do not report all the components within a RMC, including the type and concentration of the photoinitiator system, which makes proper LCU

selection for a given RMC a challenge. Therefore, QTH LCUs and multiple emission peak LED LCUs were suggested to polymerize most RMCs (Rueggeberg 2011, Jandt and Mills 2013).

Achieving satisfactory polymerization across the entire surface of the restoration may be highly dependent on the position and orientation of the LCU, and location of the blue and violet LED chips over the uncured RMC (Price et al. 2014, Michaud et al. 2014, Price, Ferracane, and Shortall 2015). As mentioned previously, clinicians usually position the LCU centered over the uncured RMC without taking into account the LCU beam profile across its tip. Thus, the non-uniform beam distribution across its tip can result in a restoration receiving high or low irradiance across its surface, which could affect the amount of photoinitiator activated and, thereby, impact the quantity of free radical generated (Leprince et al. 2013). This in turn can result in localized discrepancies in the polymerization reaction rates when using an LED LCU (Michaud et al. 2014, Price et al. 2014, Haenel et al. 2015, Price, Fahey, and Felix 2010). This suggests that localized regions within a restoration may exhibit high or low degree of polymerization that may positively or negatively influence its physical, mechanical and chemical properties (Price, Ferracane, and Shortall 2015, Price et al. 2014, Megremis et al. 2014, Arikawa et al. 2011, Price, Fahey, and Felix 2010, Harlow et al. 2016, Price et al. 2011, Rueggeberg 2011, Price and Felix 2009, Leprince et al. 2013, Haenel et al. 2015), such as microhardness (Haenel et al. 2015, Price et al. 2014, Arikawa et al. 2011, Price, Fahey, and Felix 2010), the degree of conversion (DC) (Haenel et al. 2015, Megremis et al. 2014), or the depth of cure (Megremis et al. 2014). The localized polymerization differences can lead to stresses generation within a restoration, specifically during occlusal loading, which may result in premature fracture of the restoration. Insufficient polymerization of a RMC restoration may lead to leaching of the unreacted monomers to the oral environment, which may ultimately compromise the durability and quality of the final restoration (Durner et al. 2012, Knezevic et al. 2008). A study reported that adding an optical element within the LCU enhanced light homogeneity and improved hardness of the RMC specimens (Arikawa et al. 2011). Manufacturers now are aware of the beam inhomogeneity across the LCU tip. Some

manufacturers developed light guide tips that diffuse the light output so a relatively uniform radiant power is emitted, such as the updated light guide tip of Bluephase Style LCU manufactured by Ivoclar Vivadent. This way, the various regions of a RMC may receive a relatively homogeneous irradiance, at the correct wavelength required to sufficiently activate photoinitiators, and generate free radicals to effectively polymerize a RMC (Price, Ferracane, and Shortall 2015, Leprince et al. 2013). Nevertheless, not every inhomogeneous LCU results in unsatisfactory properties at all regions of the restorations if sufficient light irradiance is received by the RMC (Haenel et al. 2015, Price, Ferracane, and Shortall 2015, Price, Felix, and Andreou 2005, Price et al. 2014).

Several studies explored the influence of beam profile uniformity on RMC polymerization through a mapping approach of the top and bottom surfaces of the specimens. One study explored the efficacy of various LCU types by microhardness mapping of the top and bottom surfaces of RMCs at one curing distance (Price, Fahey, and Felix 2010). Another study explored the correlation between the localized irradiance beam profile from a LCU with microhardness mapping on the top and bottom surfaces of various RMCs using at multiple curing times at one curing distance (Price et al. 2014). Furthermore, a study evaluated the effect of irradiance distribution from multiple LCUs on mapping the localized microhardness on the top surfaces of the specimens, and assessed the average, not localized, DC on the bottom surfaces of the RMC specimens at one curing distance (Haenel et al. 2015). These studies found a relationship between the non-uniform LCU beam profile and KH on the top and bottom RMC surfaces. In an effort to decrease the prevalence of premature fracture of the restoration, investigating the influence of LCU non-uniform beam profile on polymerization pattern uniformity may contribute to a greater understanding of fracture etiology.

2. LCU irradiance, curing time and radiant exposure

A light-cured RMC will perform as the manufacturer's instructions intends when it receives the required amount of energy at the appropriate wavelengths, to produce enough free radicals and achieve satisfactory polymerization (Price et al. 2011, Rueggeberg 2011, Price and Felix 2009, Price, Ferracane, and Shortall 2015, Leprince et al. 2013, Price et al. 2014, Shortall et al. 2016a). This means that the correct irradiance, exposure duration, and spectral emission should be delivered from the curing unit to the RMC. Also, as mentioned earlier, LCU positioning over the RMC, distance between the light guide and restoration, RMC composition, shade and translucency can play a significant role in photoinitiator activation and thereby, free radical production, the extent of DC, hardness, and depth of cure of the final restoration (Leprince et al. 2013).

The RE is the total amount of irradiance received by a surface over an irradiation procedure or (irradiance × time) and is expressed in units of J/cm^2 (Platt and Price 2014, Leprince et al. 2013, Price, Ferracane, and Shortall 2015, Shortall et al. 2016a). It has been suggested that a given material will exhibit similar properties and degree of polymerization as long as it receives the same amount of RE, regardless of how it was achieved, by various irradiance and curing time combinations (Leprince et al. 2011, Selig et al. 2015, Leprince et al. 2013). This phenomenon is described as the "Exposure Reciprocity Law" (Leprince et al. 2011, Selig et al. 2015, Leprince et al. 2013). However, the literature demonstrated that exposure reciprocity is not a general rule, as some RMCs may follow this rule (Leprince et al. 2011, Hadis et al. 2011, Feng and Suh 2007, Leprince et al. 2013), but others may not (Musanje and Darvell 2003, Selig et al. 2015, Wydra et al. 2014). This law makes high-power LCUs attractive to dentists, because they can use high-power LCUs to light cure RMC in shorter periods of time. This in turn encourages manufacturers to develop high-power LCUs (Hadis et al. 2011). Studies reported that RMC exposure reciprocity mainly depended on the number of carbon double bonds, viscosity, filler content (Feng and Suh 2007, Hadis et al. 2011), and photoinitiator type (Leprince et al. 2013, Leprince et al. 2011),

where monomers with similar viscosities and number of carbon double bonds were more likely to follow the exposure reciprocity rule (Feng and Suh 2007, Hadis et al. 2011), and low viscosity flowable RMC were less likely to follow this rule compared to their counterpart higher viscosity paste material (Feng and Suh 2007, Hadis et al. 2011, Selig et al. 2015).

A study reported that calculations based on the RE delivered to a restoration to guide the clinician's curing protocol is invalid and should no longer be used, because the calculation does not recognize product behavior (Musanje and Darvell 2003). This means that delivering the same irradiance value and curing time combination to a RMC restoration does not necessarily indicate that restorations will exhibit similar material properties (Feng and Suh 2007). For example, A study showed that model TPO-based RMCs exhibited higher DC when the irradiance increased regardless of the curing time, and the opposite was true for model CQ-based RMCs, where higher DC was detected when the curing duration increased regardless of the irradiance values (Leprince et al. 2011). Also, the literature reported that the DC extent is highly dependent on the amount of free radical production and irradiance (Feng and Suh 2007), because a high LCU irradiance received by a RMC will activate more photoinitiators, resulting in the generation of a greater amount of free radicals (Leprince et al. 2011, Leprince et al. 2013). However, this may lead to the early vitrification of the polymer network and the radical entrapment or radical loss by the early recombination termination (Leprince et al. 2011, Leprince et al. 2013). Therefore, depending on the rate of cure, some RMC restorations can exhibit different physical properties although the same DC was achieved due to the complexity of polymerization kinetics (Feng and Suh 2007, Wydra et al. 2014). Unfortunately, manufacturers do not disclose all of their product components, photoinitiator system, and concentrations. Manufacturers also do not supply graphs indicating the required energy for each RMC product and shade using various LCUs, as suggested in the literature (Musanje and Darvell 2003). Furthermore, manufacturers do not provide curing protocols according to the material resin composition, viscosity and filler content, regardless of the evidence in the literature encouraging manufacturers to provide such valuable information

(Leprince et al. 2011, Hadis et al. 2011). Therefore, clinicians usually follow the manufacturer instructions when curing light activated resin-based materials.

Increasing the distance between the LCU tip and the floor of the cavity may result in a decreased irradiance and RE received by the RMC when using the same curing times instructed by the manufacturer. So, the irradiance at the surface of a restoration decreases because of the movement of the curing unit tip away from the surface as reported in the literature (Shortall et al. 2016b, Price et al. 2011, Beolchi et al. 2015). Therefore, increasing the distance between the light guide tip and restoration may lead to a restoration surface being exposed to decreased irradiance distribution, which could negatively impact the reaction rates and polymerization effectiveness, based on the RE equation (Price et al. 2011, Megremis et al. 2014, Rueggeberg 2011, Nomoto 1997, Price and Felix 2009, Leprince et al. 2013, Musanje and Darvell 2003). This will lead to formation of a polymer network with less than ideal polymerization that can leach the unreacted monomers into the oral environment compromising the overall properties and ultimately the longevity of the final restoration (Price et al. 2011, Price et al. 2000, Felix and Price 2003, Ferracane et al. 1997, Sobrinho et al. 2000, Knezevic et al. 2008, Durner et al. 2012, Michaud et al. 2014, Silikas, Eliades, and Watts 2000, Ferracane 2006).

The RE value required to achieve satisfactory RMC polymerization varies from one product to another because RMCs differ in composition, photoinitiator, shade and translucency (Michaud et al. 2014, Beolchi et al. 2015, Yap and Seneviratne 2001, Gritsch et al. 2008). However, it is important for a clinician to have an understanding of the factors that can impact polymerization to properly estimate an appropriate curing time, specifically when the curing distance is increased. Due to the variation in resin matrix composition, viscosity, filler content and photoinitiator systems, variation in LCU irradiance, curing time and RE required for optimum RMC polymerization makes determining irradiation protocols a challenge for clinicians. This becomes important specifically when curing at a distance since manufacturers supply information for curing at 0 mm distance, and manufacturers do not provide detailed information

of the energy required for each RMC using various LCUs, as previously mentioned. Therefore, clinicians usually follow the manufacturer instructions in terms of the curing time needed for a given RMC.

Although the literature reported that calculating RE is no longer valid, a clinician needs a guide for the required RE and curing times at various clinically relevant distances using various LCUs. Therefore, RE calculations based on the information provided by the manufacturer may be a helpful guide for clinicians until manufacturers supply sufficient information with the irradiance and curing time combinations needed for each RMC and shade at multiple clinically relevant distances.

As mentioned in the previous section, most studies and manufacturers report the average irradiance from an LCU using an integrating sphere/spectrometer assembly, cosine corrector, or a radiometer (ISO 2004, 2007, Price, Ferracane, and Shortall 2015). All of which typically represent the irradiance amount that will be received on a top surface of a RMC restoration. A Managing Accurate Resin Calibrator (MARC-RC) system can measure the irradiance and RE received on the top and bottom surfaces of a RMC because the MARC-RC system includes two cosine corrector optical fiber irradiance probes or sensors (a top and a bottom sensor). The top MARC-RC sensor measures the spectral emission, irradiance, and RE that is expected to be received on the top surface of a RMC specimen, and the bottom MARC-RC sensor detects the irradiance and RE passing through a specimen during its polymerization, reflecting the spectral emission, irradiance and RE values received on the bottom surfaces of a specimen (Arikawa et al. 1998, Beolchi et al. 2015).

A study reported a decrease in the LCUs irradiance values with increasing the distance between the light guide tip and a top MARC-RC sensor (Beolchi et al. 2015). Also, LCU beam profile studies demonstrated the irradiance beam profile distribution decreased with increasing the distance between a LCU guide tip and a ground glass diffuser, when quantifying the localized irradiance beam profile from a LCU (Price et al. 2011, Megremis et al. 2014). The literature

reported that a LCU can deliver less than 200 mW/cm^2 at a curing distance of 7 mm from the light guide tip (Felix and Price 2003); therefore, it was suggested that restorations of approximately 7 mm depth may receive less than 2 J/cm^2 at the bottom of the restoration if cured for 10 seconds (Price, Fahey, and Felix 2010). The decrease in RE, which is most likely due to the absorption, refraction or scattering of the light as it passes through a restoration, can result in a RE that may be insufficient for satisfactory polymerization on the bottom surfaces of the restorations (Price, Fahey, and Felix 2010, Leprince et al. 2013). However, additional research with respect to the irradiance and RE received at the bottom of a RMC restoration with increasing the curing distance is warranted. Also, exploring influence of distance on polymerization effectiveness, with respect to DC on the top and bottom RMC surfaces, when a restoration receives similar RE using multiple LCUs may provide guidance to clinicians on the appropriate curing protocols.

3. Cross-link density (CLD)

Light-activated RMC consists of monomers that undergo polymerization upon light exposure that results in the development of a highly cross-linked polymer structure (Cramer, Stansbury, and Bowman 2011, Ferracane et al. 1997). However, the monomer conversion is never complete, and the polymer network contains a considerable amount of pendent and unreacted double bonds that affect the CLD of the final polymer network (Ferracane et al. 1997, Soh and Yap 2004). The CLD distribution provides an estimate of the network heterogeneity that cannot be achieved by measuring the DC, because DC is an average measure of the percentage of double bonds that are converted into single bonds (Asmussen and Peutzfeldt 2001a, b). Therefore, the DC does not consider the heterogeneity of the polymer network, and it alone is insufficient as a measure of the RMC polymerization effectiveness because it does not provide a complete characterization of the polymerized network (Leprince et al. 2012, Asmussen and Peutzfeldt 2001b). Consequently, polymers may have similar DC, yet differ in CLD due to differences in the

linearity of the polymer chains (Schneider, Moraes, et al. 2008). The CLD can be correlated to the mechanical properties of the RMC. For instance, the monomer structure has a great influence on the ultimate physical properties of the polymer network (Soh and Yap 2004). In addition, it was previously demonstrated that a polymer network with high CLD is more resistant to degradation and is associated with increased fracture resistance compared to low CLD networks (Ferracane 2006).

Currently, there is no method that directly evaluates CLD of a polymer network; however, it can be estimated indirectly by measuring the glass transition temperature (Tg) or by an ethanol softening method (Leprince et al. 2013). Measuring the Tg can be accomplished using a dynamic mechanical analysis, differential scanning calorimetry or thermogravimetric analysis, because the Tg represents the temperature where the polymer vitrifies during the polymerization reaction (Dewaele et al. 2009). However, measuring the Tg requires the use of highly sophisticated instruments that may not be readily available. On the other hand, the ethanol softening method estimates CLD of a RMC by repeated hardness measurements on the RMC specimens before and after immersion in an organic solvent, which is a method that can be readily performed in most laboratories (Asmussen and Peutzfeldt 2001b, Schneider, Moraes, et al. 2008, Yap et al. 2004, Soh and Yap 2004, Ferracane 2006). As a RMC gets exposed to ethanol, the three-dimensional cross-linked dimethacrylate network swells per the degree of polymer cross-linking (Soh and Yap 2004, Ferracane 2006, Brandt et al. 2008). The polymer network swelling occurs because the solvent molecules penetrate and replace the secondary inter-chain bonds and the unreacted chains get dissolved to a certain extent, which results in softening of the polymer network according to the degree of cross-linking (Soh and Yap 2004, Ferracane 2006, Brandt et al. 2008). A cross-linked network is insoluble because the solvent-polymer secondary bonds cannot surpass the primary cross-linked bonds (Soh and Yap 2004, Ferracane 2006, Brandt et al. 2008). Therefore, a highly cross-linked network is more resistant to degradation and solvent uptake, swells less and exhibits a less softening effect compared to a linear polymer network that

is comprised of more pathways for the organic solvent molecule diffusion (Soh and Yap 2004, Ferracane 2006, Brandt et al. 2008).

Most studies that evaluated CLD using the ethanol softening method achieved it by obtaining a few microhardness measurements on the top and bottom surfaces of RMC specimens (Schneider, Moraes, et al. 2008, Alshali et al. 2015, Yap et al. 2004, Feitosa et al. 2012). Nevertheless, obtaining only few measurements on the top and bottom specimens surfaces may not be sufficient to completely characterize RMC polymerization, due to the non-uniform and inhomogeneous LCU irradiance beam profiles across the light guide tips. Therefore, an approach that can provide details with respect to CLD of RMC restorations is worth investigating.

4. Degree of conversion (DC) and Knoop microhardness (KH)

Sufficient conversion of monomer into polymer during RMC polymerization is essential to produce a RMC with satisfactory properties (Leprince et al. 2013, Leprince et al. 2012). When characterizing polymerization, the DC or microhardness measurement may estimate the properties of the final restoration, because a correlation was suggested between DC or microhardness with several mechanical and physical properties of a RMC (Dewaele et al. 2006, Li et al. 2009, Ferracane et al. 1997, Ferracane 1994, Vandewalle et al. 2004, Durner et al. 2012, Santini et al. 2012, Leprince et al. 2012). Additionally, a strong positive correlation was suggested between DC of a RMC, and their microhardness (Li et al. 2009, Asmussen 1982, Ferracane 1985, Vandewalle et al. 2004, Leprince et al. 2012).

Most of the polymerization reaction takes place during irradiation but continues for 24 hours, as measured by the DC (Truffier-Boutry et al. 2006). Other studies showed that the majority of polymerization occurs within minutes after light irradiation, continues to increase significantly in the first 24 hours, and the DC may show a minor increase up to one week but does not increase much after that, as estimated by microhardness (Pilo and Cardash 1992, Hansen 1983, Watts, Amer, and Combe 1987). Therefore, most studies evaluate the DC immediately after

the light irradiation procedure and after 24 hour post-cure (Par et al. 2014, Alshali, Silikas, and Satterthwaite 2013). The DC is highly dependent on the amount of free radical production and irradiance values (Feng and Suh 2007). However, some RMCs with high DC could exhibit dissimilar physical properties depending on the rate of polymerization, irrespective of their similar DC values, as mentioned in the second section (Feng and Suh 2007).

The DC can be assessed by attenuated total reflection accessory Fourier transform infrared (ATR-FTIR) spectroscopy or Raman and micro-Raman spectroscopy (Park et al. 2009). The main advantage of Raman or micro-Raman spectroscopy over FTIR is that it is not destructive to the specimen, because the specimen it is not in contact with an ATR crystal accessory (Park et al. 2009, Soh et al. 2004). Micro-Raman spectroscopy also permits mapping of the specimens surface through a focused beam that enables assessment of DC at a specific location on the specimen (Leprince et al. 2013). Moreover, the micro-Raman spectroscopy is more accurate because its infrared intensity (IR) is high, which gives a more distinctive C=C band compared to the medium-strong IR intensity in the case of FTIR (Park et al. 2009, Soh et al. 2004). However, both methods depend on the sensitivity to molecular vibration, which is a direct approach to quantify the conversion ratio of monomer into polymer (Ferracane 1985, Schneider, Pfeifer, et al. 2008). In addition, both methods have nearly the same molecular vibrational frequencies but the vibrational band intensity differs, because the intensity of the Raman measurements depends on the relevant quantity change in the polarizing tensor, whereas FTIR intensity is determined by the change in the dipole moments of the vibration (Park et al. 2009).

Most studies evaluated microhardness or DC by measurements on the top and bottom surfaces of a RMC, or by sectioning the specimen in half longitudinally and obtaining microhardness measurements along the specimen (Price, Felix, and Andreou 2005, Price, Fahey, and Felix 2010, Price et al. 2014, Selig et al. 2015, Santini et al. 2012, Rencz, Hickel, and Ilie 2012, Leprince et al. 2012, Ilie and Stark 2014, MM et al. 2016). As previously discussed in the first section, studies have demonstrated an association between the irradiance beam profile from

various LCUs and microhardness through microhardness mapping of the top and bottom surfaces of a RMC (Price et al. 2014, Price, Fahey, and Felix 2010, Haenel et al. 2015). Nevertheless, additional research is needed to investigate polymerization within a RMC restoration.

Based on the four areas mentioned, the following are the rational behind each aim, and the specific aim investigated in this study:

- **Novelty of the studies conducted**
    1. Investigating the localized irradiance beam profile from multiple LCUs on DC, microhardness and CLD within a RMC increment through mapping the top and bottom surfaces, as well as multiple internal locations, at two clinically relevant distances.
    2. Investigating the irradiance and RE received on the bottom surfaces of a RMC increment using various LCUs at multiple clinically relevant distances.

- **General aim**

The general aim of this study was to investigate the influence of a non-uniform irradiance beam profile area from multiple LED LCUs on polymerization pattern within a RMC.

The following four specific aims were conducted:

1. SPECIFIC AIM 1

1.1. Rational of specific aim 1

As previously mentioned, most studies evaluated the effectiveness of a LCU and polymerization efficiency of a RMC by obtaining a few DC, microhardness and CLD measurements on the top, bottom surfaces of RMC specimens (Alshali et al. 2015, Selig et al. 2015, MM et al. 2016, Santini et al. 2012, Feitosa et al. 2012, Yap et al. 2004). Also as stated in

an earlier section, few studies evaluated the influence of the localized irradiance beam profile from multiple LCUs on RMC microhardness through a mapping approach of the top and bottom surfaces of the specimens at one curing distance (Price et al. 2014, Price, Fahey, and Felix 2010, Haenel et al. 2015). Furthermore, the irradiance and RE received on the bottom of RMC restorations at a clinically relevant distance is not well documented in the literature and needs further investigation.

In an attempt to further understand the influence of the non-uniform irradiance beam profile across an LED LCU guide tip on polymerization pattern, an assessment of polymerization effectiveness within a RMC specimen at a clinically relevant distance is necessary. In addition, investigating the influence of the non-uniform beam on the assessed RMC parameters may be accentuated using a bleaching shade TPO-containing dual photoinitiator RMC. To our knowledge, investigating the influence of irradiance beam profile from a QTH LCU and a LED LCU on polymerization pattern within a RMC by mapping the DC and CLD on the top, bottom surfaces of a RMC increment, within different internal locations, and at various depths of a RMC increment, and at a clinically relevant distance was not yet performed.

1.2. Specific aim 1

The first aim was to explore the influence of a localized irradiance beam profile area of an LED LCU and a QTH LCU on the corresponding DC and CLD mapping within a RMC increment as well as to explore the average irradiance at the center of each LCU beam and its corresponding average RE received by the top and bottom surfaces of a RMC increment.

1.3. Specific aim 1 was comprised of two phases (Figure 1):

1.3.1. Phase 1

- *The working hypothesis*

  The localized irradiance beam profile from one LED LCU at a clinically relevant distance is not uniform compared to one QTH LCU.

- *The null hypothesis*

  The localized irradiance beam profile from one LED LCU at a clinically relevant distance is uniform compared to a QTH LCU.

1.3.2. Phase 2

- *The working hypotheses*

  1. A localized non-uniform irradiance beam profile area from an LED LCU will have an influence on the corresponding DC and CLD mapping on the top, bottom, within different internal locations and at different depths of a 2 mm RMC increment at a clinically relevant distance compared to the relatively uniform QTH LCU.
  2. The average irradiance at the center of one LED LCU beam and the corresponding average RE received on the top surfaces of a RMC increment cured by one LED LCU and one QTH LCU at a clinically relevant distance is significantly higher compared to that on the bottom surfaces of a RMC increment.

- *The null hypothesis*

  1. A localized non-uniform irradiance beam profile area from one LED LCU will not have an influence on the corresponding DC and CLD mapping on the top, bottom, within different internal locations and at different depths of a 2 mm RMC increment at a clinically relevant distance compared to the relatively uniform QTH LCU.
  2. The average irradiance at the center of an LED LCU beam and the corresponding average RE received on the top surfaces of a RMC increment cured by one LED LCU

and a QTH LCU at a clinically relevant distance is not significantly different compared to that on the bottom surfaces of a RMC increment.

Based on the findings from specific aim 1, the following three specific aims were investigated (Figure 2):

2. SPECFIC AIM 2

2.1. Rational for specific aim 2

As mentioned in the second section of the introduction, most studies report a LCU's irradiance received on the top surfaces of the RMC specimens (Price et al. 2011, Rueggeberg 2011, Price and Felix 2009, Price, Ferracane, and Shortall 2015, Leprince et al. 2013, Price et al. 2014). However, little research was conducted that assessed the irradiance received on the bottom RMC surfaces (Bucuta and Ilie 2014). Since clinicians need a guide for light curing RMC restorations at clinically relevant distances; RE calculations based on the irradiance and curing time information provided by the manufacturer followed by assessment of the polymerization efficiency with respect to the DC may provide guidance for clinicians when light curing a restoration at a distance. So, investigating the irradiance and RE values received on the bottom surfaces of the RMC specimens cured by multiple LCUs, at clinically relevant distances is warranted. Also, exploring the influence of distance on irradiance and curing time using various LCUs at multiple curing distances to achieve a specific RE needs further investigation. Furthermore, the irradiance, RE and DC on the top and bottom surfaces of a RMC increment and the correlation among them using multiple LCUs at clinically relevant distances needs to be explored.

2.2. Specific aim 2

The aim was to explore the influence of distance on LCU irradiance on its corresponding curing time and DC when similar RE is received by a RMC using multiple LCUs as well as explore the correlation among irradiance, RE and DC on the top and bottom surfaces of a RMC increment cured by various LCUs at multiple clinically relevant distances**.**

2.3. Specific aim 2 was comprised of two phases (Figure 3):

2.3.1. Phase 1

- *The working hypotheses*
    1. The average irradiance of multiple LED LCUs, and the corresponding RE and DC on the top surfaces of a RMC increment at two clinically relevant distances is significantly higher compared to the bottom surfaces of a RMC increment.
    2. A correlation among irradiance and the corresponding RE and DC exists, on the top and bottom surfaces of a RMC increment cured by various LED LCUs at multiple clinically relevant distances**.**
- *The null hypotheses*
    1. The average irradiance of multiple LED LCUs, and the corresponding RE and DC on the top surfaces of a RMC increment at two clinically relevant distances is not significantly different compared to a RMC increment bottom surfaces.
    2. A correlation among irradiance and the corresponding RE and DC does not exist, on the top and bottom surfaces of a RMC increment cured by various LED LCUs at multiple clinically relevant distances**.**

2.3.2. Phase 2

- *The working hypothesis*

    The molar absorptivity of TPO is significantly higher than that of CQ.

- *The null hypothesis*

  The molar absorptivity of TPO is not significantly different than that of CQ.

3. SPECIFIC AIM 3

3.1. Rational for specific aim 3

Based on specific aim 1 rationale and findings, an assessment of the influence of a localized irradiance beam profile area on its corresponding CLD mapping within a RMC cured by multiple LED LCUs at two clinically relevant distances was not explored. Furthermore, the correlation between a localized irradiance beam profile area from multiple LED LCUs at two clinically relevant distances, with its corresponding CLD mapping was not yet assessed. Therefore, this area was worth investigating to give an insight on the influence of irradiance beam profile on polymerization pattern uniformity that occurs within a restoration.

3.2. Specific aim 3

The aim was to explore the influence of a localized irradiance beam profile area from multiple LED LCUs on the corresponding CLD mapping within a RMC increment as well as to explore the correlation between a localized irradiance beam profile area with its corresponding CLD mapping on the top surfaces of a RMC increment cured by multiple LED LCUs at two clinically relevant distances.

3.3. Specific aim 3 was comprised of two phases (Figure 4):

3.3.1. Phase 1

- *The working hypothesis*

  The localized irradiance beam profiles from multiple LED LCUs at various distances are different.

- *The null hypothesis*

  The localized irradiance beam profiles from multiple LED LCUs at various distances are not different.

3.3.2. Phase 2

- *The working hypotheses*
  1. A localized non-uniform irradiance beam profile area from multiple LED LCUs has a significant effect on the corresponding CLD mapping within a RMC increment at two clinically relevant distances.
  2. A correlation exists between a localized non-uniform irradiance beam profile area from multiple LED LCUs at two clinically relevant distances and its corresponding CLD mapping on the top surfaces of a RMC.
- *The null hypotheses*
  1. A localized non-uniform irradiance beam profile area from multiple LED LCUs does not have significant effect on the corresponding CLD mapping within a RMC increment at two clinically relevant distances.
  2. A correlation does not exist between a localized non-uniform irradiance beam profile area from multiple LED LCUs at two clinically relevant distances and its corresponding CLD mapping on the top surfaces of a RMC.

4. SPECIFIC AIM 4

4.1. Rational for specific aim 4

Based on specific aim 1 rationale and findings, investigating the localized correlation of an irradiance beam profile from a multiple LED LCU with its corresponding DC and microhardness of a RMC cured by the lights, through a mapping approach at two clinically relevant distances from a RMC is not yet explored. Furthermore, the localized correlation

between microhardness and DC through RMC mapping, at several depths cured by various LED LCUs, at two clinically relevant distances from a RMC is not investigated. Exploring this area can provide a better understanding of the influence of LCU irradiance beam profiles and distance on polymerization pattern within a restoration. Also, it will provide information regarding the localized versus the average correlation between DC and microhardness and if the strength of the correlation is LCU dependent.

4.2. Specific aim 4

The aim was to investigate the correlation of a localized irradiance beam profile area from multiple LED LCUs with its corresponding DC and KH mapping on the top surfaces of a RMC at two clinically relevant distances. Additionally, the aim was to explore the localized and average correlation between DC and KH across various depths within a RMC increment cured by various LED LCUs at two clinically relevant distances and to assess if the correlation is LCU and distance dependent.

4.3. Specific aim 4 was comprised of two phases (Figure 5):

4.3.1. Phase 1

- *The working hypothesis*

  The localized irradiance beam profiles from multiple LED LCUs at various distances are different.

- *The null hypothesis*

  The localized irradiance beam profiles from multiple LED LCUs at various distances are not different.

4.3.2. Phase 2

- *The working hypotheses*

    1. A correlation exists between the localized irradiance beam profile area from multiple LED LCUs with its corresponding DC and KH mapping on the top surfaces of a RMC at two clinically relevant distances.
    2. A correlation exists between the localized DC and KH across various depths of a RMC increment at two clinically relevant distances cured by multiple LED LCUs.
    3. A correlation exists between the average DC and KH across various depths of a RMC increment at two clinically relevant distances using multiple LED LCUs.
    4. The localized DC and KH correlations are more accurate than the average DC and KH correlations, and the correlations are LCU and distance dependent.

- *The null hypotheses*

    1. A correlation does not exist between the localized irradiance beam profile area from multiple LED LCUs with its corresponding DC and KH mapping on the top surfaces of a RMC at two clinically relevant distances.
    2. A correlation does not exist between the localized DC and KH across various depths of a RMC increment at two clinically relevant distances using multiple LED LCUs.
    3. A correlation does not exist between the average DC and KH across various depths of a RMC increment at two clinically relevant distances using multiple LED LCUs.
    4. The localized DC and KH correlations are not different than the average DC and KH correlations, and the correlations are not LCU and distance dependent.

MATERIALS AND METHODS

1. SPECIFIC AIM 1

The influence of an irradiance beam profile area from one LED LCU and one QTH LCU on the corresponding CLD and DC mapping within a RMC increment

1.1. Specific aim 1, phase 1

1.1.1. LCU irradiance beam profile characterization

One QTH LCU (Optilux 401, Kerr, Orange, CA) (O) (Figure 6), and one multiple emission peak LED LCU (Bluephase Style, Ivoclar Vivadent, Amherst, NY) (BS) that had the updated fiber optic light guide tip, which was claimed by the manufacturer to emit a relatively uniform beam profile compared to the original light guide tip (Figure 7), were investigated. The LED LCU had an effective light-emitting diameter of 9 mm and the QTH LCU had an effective light-emitting diameter of 10.8 mm.

Beam profile quantification for each LCUs was accomplished using radiant power values from an optical spectrometer (FLAME-S-VIS-NIR, Ocean Optics, Dunedin, FL) combined with measurements made with a commercially available CCD camera-based beam profiler system (BGP-USB-SP620 with a FL-50 CCTV lens, Ophir-Spiricon, North Logan, UT). A ground glass diffuser (DG100mm×100mm, 1500 grit, Thorlabs, Newton, NJ) was held in place between the guide tip of the LCU being characterized and the beam profiler camera so that the light projected onto the diffuser could be captured with the camera. The beam profiler camera was positioned at a fixed distance to the ground glass diffuser. The diffuse side of the glass diffuser was positioned facing away from the camera and toward the LCU guide tip being characterized.

The beam profile images were collected in dark conditions, where only minimum light was available to operate the equipment during the entire experiment, in order to eliminate the surrounding light from interfering when capturing the image. Before collecting the beam profile

images, the CCD camera was calibrated for background noise and the optical scaling value of the pixel dimensions on the screen were determined to allow precise linear measurements of each image. The system was corrected for pixel response and ambient light using the "UltraCal" baseline correction algorithm of the software (BeamGage Professional 5.11, Ophir-Spiricon, North Logan, UT). To compensate for differences in the spectral response of the photo diode within the CCD camera, a shortpass optical filter (#84-703, 425 nm, 25mm diameter, OD 4, Edmund Optics, Barrington, NJ) and a longpass optical filter (#84-742, 425nm, 25mm diameter, high performance, Edmund Optics, Barrington, NJ), both having a cut-off wavelength of 425 nm, were used to separate violet light from blue light with peaks at 409 nm and 456 nm, respectively. Each filter was attached to the CCD camera lens with an M30.5×0.5 filter mount (#65-801, 25 mm diameter, Edmund Optics, Barrington, NJ). The shortpass filter was used to allow wavelengths below than 425 nm to "pass" through to the CCD camera (violet spectrum), while the longpass filter was used only to allow wavelengths greater than 425 nm to reach the CCD camera (blue spectrum) (Figure 8). For measurements made with each LCU, the tip of the individual LCU was positioned parallel to the diffuse side of the glass diffuser at a 2 mm distance using a 2 mm gauge block (Figure 9). Then, each LCU was activated and images were collected using the longpass and shortpass filters. Captured images were then processed using the data acquisition and analysis software of the beam profiler system.

Radiant power values were measured using a 6-inch integrating sphere (Labsphere, North Sutton, NH) connected to the Ocean Optics optical spectrometer, which was calibrated using a NIST-traceable light source (HL-3plus-INT-CAL, Ocean Optics, Dunedin, FL) with a specific file provided by the manufacturer for the integrating sphere (Figure 10). For each LCU, a custom-made adapter was fabricated to match the dimensions of the effective light-emitting portion of its guide tip (Selig et al. 2015). The surface of the adapter facing the inside of the integrating sphere was coated with a highly reflective barium sulfate material to match the inside of the integrating sphere. When collecting the radiant power measurements for each LCU, the corresponding LCU

custom adapter assembly was placed on the integrating sphere opening so that the light radiated from the individual LCU was collected at a 2 mm distance from the opening of the integrating sphere (Figure 11). The radiant power measurements from the individual LCU were collected from the integrating sphere/spectrometer assembly from the entire spectral range (380-700 nm), the shorter wavelength spectral range between 380-425 nm, and the longer wavelength spectral range between 425-700 nm (n=3/spectral range/LCU). Then the average power values were calculated for each LCU at each spectral range.

Finally, using the beam profiler software, each average radiant power value for the individual LCU was applied to its corresponding beam profile image, and calibrated two-dimensional (2D) and three-dimensional (3D) images of the average irradiance distribution values were generated for each LCU. Note that for each LCU, the area of its LCU adapter assembly, which equaled its guide tip area, was matched to the corresponding area of the beam profile collected by the CCD camera to generate the calibrated irradiance maps.

1.2. Specific aim 1, phase 2

The experimental design of specific aim 1, phase 2 is illustrated in Figure 12.

1.2.1. Irradiance, radiant exposure, spectral emission received by the RMC specimens, and specimen preparation

For each LCU explored, the spectral emission, irradiance and radiant exposure received by the top and bottom surfaces of the RMC specimens were measured using a MARC-RC system (BlueLight Analytics, Halifax, Canada). The MARC-RC contains a NIST-referenced miniature spectrometer (USB4000, Ocean Optics, Dunedin, FL, USA) with a 3,648-element linear CCD array detector (TCD1304AP, Toshiba, Tokyo, Japan) that is custom designed to collect LCU wavelengths between 360-540 nm, and two 4 mm custom designed cosine corrector sensors (top and bottom sensors) fixed within the MARC-RC, which are connected to the spectrophotometer with a bifurcated fiber optic cable (BlueLight Analytics, Halifax, Canada) (Figure 13). The

sensors are designed to collect the light output at 180° to eliminate any optical interference issues associated with the light collection sampling geometry (Bucuta and Ilie 2014). The measurements collected from the 4 mm top sensor represented the irradiance and RE delivered to the top surface of a RMC increment. The bottom sensor detects the spectral distribution, irradiance and RE passing through a RMC increment representing what would be received on the bottom surfaces of the specimens. The MARC-RC is connected to a laptop computer provided by the manufacturer pre-loaded with custom MARC-RC software for data acquisition and analysis. A limitation of the MARC-RC device is that the two 4 mm CC3 sensors collect the irradiance, radiant exposure and spectral emission measurements with respect to a limited area of the LCU guide tip that falls over the sensor, and do not reflect the measurements of the entire light guide tip. Therefore, small square specimens with dimensions that fell over the MARC-RC sensor collection area were fabricated in this study.

The LCU measurements and specimen preparation were performed in a constant temperature room (21°C) with filtered light that absorbed wavelength between 380-520 nm. Each LCU position was standardized using a mechanical arm with a metric gauge. Each LCU guide tip was centered over the top sensor using custom-made Mylar targets that matched the dimension of each LCU guide tip, and was removed before collecting the measurements. Each LCU guide tip and LCU body (wand) was aligned with the MARC-RC crosshead on the surface to standardized the x- and y-directions, and the light guide tip was positioned flat and perpendicular against the sensor to standardize the z-direction (Figure 14). The LED LCU was fully charged before obtaining measurements, and the QTH LCU fan was allowed to completely turn off between measurements. Prior to specimens preparation, the irradiance, RE and curing time measurements were collected for each LCU with a 2 mm distance between the light guide tip and the 4 mm top sensor (n=6/LCU). The curing time for each LCU was adjusted so that each RMC specimen received 10-11 J/cm^2 on the top surface. The RE was calculated based on the irradiance and curing time specified by the manufacturer for the dual photoinitiator system RMC investigated

(Tetric EvoCeram bleaching shade-XL, Ivoclar Vivadent, Amherst, NY, Lot# T25427). The manufacturer instructed that a 10 and 20 second curing time is required when a LCU irradiance ≥1000 and ≥500 mW/cm^2, respectively. As a result, the LED LCU needed 10 seconds and the QTH LCU needed 14 seconds to deliver a RE of 10-11 J/cm^2, as measured by the top MARC-RC sensor. This particular RMC was selected because it contains both CQ and TPO photoinitiator systems, with less concentration of CQ compared to other Tetric EvoCeram shades (Palin et al. 2008). Therefore, the influence of the non-uniform beam from a multiple emission peak LED LCU on its corresponding polymerization pattern of a RMC may be better assessed using a high TPO-containing dual photoinitiator RMC.

After that, each LCU position was standardized over the center of the bottom sensor in a setup similar to the top sensor using the custom-made Mylar targets. Square RMC specimens (5×5×2 mm) were prepared using custom Delrin molds (n=6/LCU). Each custom mold was designed with a square opening centered over the 4 mm bottom sensor and with outer borders that followed the shape of the sensor well to prevent mold rotation and standardize the position of the specimens (Figure 15). The selected RMC was placed in the square mold opening and sandwiched between two 0.002 mm thick Mylar strips (Matrix Strips, DuPont MYLAR, Chester, VA) and 1 mm thick glass slides to remove excess material. The glass slides were removed, the mold with Mylar strips on each side was placed over the bottom sensor, and the light guide was positioned at a 2 mm distance from the top of the RMC specimens, which was polymerized from the top surface only to simulate a clinically relevant setting (Figure 16). During specimens curing, irradiance, RE and spectral distribution readings were collected to determine the amount of irradiance and RE and spectral distribution detected on the bottom surface of the RMC specimens. The Mylar strip placed on the top surface of the specimens in this study absorbed 3.5%-5% of the LCU irradiation, which was similar to what is reported in the literature (Haenel et al. 2015). The Mylar strips were peeled off, the lower right corner of the top surface of each specimen was marked outside the measurement collection area for the experiments being

performed, and the specimens were removed from the molds. Then, specimens were placed in a container and wrapped with aluminum foil to prevent specimen exposure to the light. The containers were then stored dry in the dark in a 37°C incubator for 24 hours (Price et al. 2014, Schneider, Moraes, et al. 2008, Brandt et al. 2008).

From the six specimens fabricated for each LCU, three squares were used to characterize the top and bottom RMC surfaces and three squares were used to characterize polymerization at different depths of a RMC specimen. After 24 hours, each specimen designated for depth characterization was mounted on an acrylic rod using a cyanoacrylate glue to secure the position of each specimen during sectioning. Each rod with mounted specimen was placed in the brass mandrill and sectioned into five slices perpendicular to the top surface using a microtome (Hard tissue microtome, Series 1000 Deluxe, Scientific Fabrications, Littleton, CO). The microtome uses a 0.2-mm thick rotating wafer blade (Buehler, Lake Bluff, IL, USA) to harvest thin slices. The outer 0.6 mm slices were discarded and only the three 1-mm middle slices (a, b and c) were used for the depth characterization (Figure 17). For each of the three slices, only the surface furthest from the first cut was characterized. Thus, the characterized slice surfaces were at the following distances from the edge of each specimen: slice-a=1.8 mm, slice-b=3 mm and slice-c=4.2 mm (Figure 18).

The RMC specimens designated for top and bottom characterization were finished on both sides, and the slices designated for depth characterization were finished on the characterized surface only using a Struers Rotopol 4 polishing unit with 1200-, 2400- and 4000-grit SiC abrasive paper (Struers, Ballerup, Denmark). Specimens were rinsed under running water for three minutes, ultrasonically cleansed for three minutes in deionized water followed by another cycle of three minutes of rinsing in running deionized water to remove any debris from the surfaces before the polishing procedure. All specimens were polished using a 1-μm alcohol-based diamond polishing suspension (Struers, Ballerup, Denmark) for three minutes and rinsed under running deionized water for three minutes. Polished specimens were ultrasonically cleaned for 20

minutes in deionized water to remove any remnants on the surface and finally rinsed for a final cycle under running deionized water for three minutes to produce smooth clean surfaces before chemical (DC) and physical (KH) analysis, in order to obtain smooth and clear DC peaks, and accurate KH indents (Figure 19).

1.2.2. Characterization of polymerization pattern through CLD and DC mapping

The RMC specimens were characterized by measuring the CLD and DC through a mapping approach. The CLD mapping was determined using the ethanol softening method by repeated KH measurement, and DC mapping was accomplished by micro-Raman spectroscopy. After 24h of specimen storage, Knoop hardness (KH) mapping of the specified surfaces (top, bottom, slice-a, -b and –c) was performed using an automated hardness stage (Clemex ST-2000 automatic stage, Norwood, MA) with specimens mounted on an acrylic block using a removable mounting putty (Scotch, removable mounting putty, 3M, St. Paul, MN) and placed on the hardness tester (Instron, Wilson-Tukon model 2100B, Norwood, MA). Indentations were obtained using a 50-gram load and 10-second dwell time (Price, Fahey, and Felix 2010) (Figure 20). On the top and bottom surfaces of each specimen, a 3×3 mm checkerboard grid pattern was created and 50 indentations were made. The grid was 1 mm away from all edges of the specimen, with a 600-μm distance in the x-direction and 300-μm distance in the y-direction created between indentations.

On each of the three slices, a 3×1 checkerboard pattern with 30 indentations was made with a 1 mm distance from the right and left edges of the specimen and 0.5 mm from the top and bottom surfaces of the specimen. The distance between every two indentations was 600-μm in an x-direction and 200-μm in a y-direction (Figure 21). Thus, each slice was evaluated at the following depths: 0.5, 0.7, 0.9, 1.1, 1.3 and 1.5 mm.

The following day, DC micro-Raman spectra mapping was generated for each specimen immediately next to each indentation using micro-Raman spectroscopy (FORAM, CRAIC

technologies, San Dimas, CA) with a 785 nm laser excitation wavelength (Figure 22). Five scans for each spectrum measurement were collected. Spectra of the uncured composites (n=3) were recorded in the same manner. The spectra were processed with FORAM PC-software. The DC calculations were performed by comparing the relative change of the band peak height at 1640 cm^{-1}, representing the C=C stretch before and after the polymerization, to an aromatic C=C reference band peak height at 1610 cm^{-1}, which remains unchanged during the polymerization reaction initiated by light curing (Figure 23). DC calculation was performed by the following equation (Albino et al. 2011, Goncalves et al. 2007, Cassoni et al. 2008, Lucey, Santini, and Roebuck 2015):

$$\text{DC } \% = \left(1 - \frac{\text{cured (peak height under 1640/peak height under 1610)}}{\text{uncured (peak height under 1640/peak height under 1610)}}\right) \times 100$$

Subsequent to the micro-Raman spectra measurements, a physical scratch was placed at the edge of each specimen that was away from the KH indents to identify the specimen surface and orientation after soaking the specimens in absolute ethanol. Then, each specimen was placed in a 2 ml specimen cup with a conical bottom (#2544131, Fisherbrand, Pittsburg, PA) that contained 1 ml of absolute ethanol (Sigma-Aldrich, St. Louis, MO, Lot# SHBF5121V), to expose all specimen surfaces of the specimen to ethanol (Figure 24). Absolute ethanol was selected in this study because it potentially increases the rate of dissolution of pendent and unreacted C=C double bonds, and leaching of non-polymerized and unreacted components of the RMC (Asmussen and Peutzfeldt 2001a, Aguiar et al. 2005, Schneider, Moraes, et al. 2008). Also, absolute ethanol possibly simulates extreme conditions of the oral cavity (Moin Jan et al. 2001). After 24 hours of soaking in ethanol, specimens were removed and blot dried with Kimwipes (Kimberly-Clark professional, Roswell, GA). Then, KH mapping was performed in the same checkerboard pattern described earlier between every two indents that were created before soaking in absolute ethanol as illustrated in Figure 21. To estimate the localized CLD, the %KH reduction was calculated from each localized KH-BE and its corresponding KH-AE.

1.2.3. 2D contour plots and 3D renderings

The average values for each localized DC and KH measurement points obtained from the three specimens for top and bottom surface characterization, and the three specimens for the depth characterization were used to generate colored 2D contour plots and 3D renderings, which combined all surfaces characterized to visualize the KH and DC mapping within a RMC specimen using ParaView 5.0 (Ayachit, Utkarsh, The ParaView Guide: A Parallel Visualization Application, Kitware, 2015, ISBN 978-1930934306). Data was imported into ParaView and sphere glyphs were attached to each measurement point. A 3D mesh was created from the input points using a Delaunay triangulation filter and volume renderings were used to show the DC and KH values. A slice filter was used to isolate surfaces from the 3D mesh, which corresponded to the measurement planes. Diverging color scale was selected to illustrate the DC and KH uniformity because the diverging color maps allows a quick identification of the middle point on the scale and highlights the two extremes (Moreland 2009). Default blue-red scale was used for DC renderings, and a green-pink color scale from the boundary colors was used for the %KH renderings (Brewer 2017). ParaView's default linear interpolation and data processing algorithm were used for the 2D and 3D renderings. The data processing algorithm allowed slicing of a 3D floating point values to produce an image by converting the numerical values into colors (Ayachit 2015). The effect of the combination of low spatial resolution for the measurements and linear interpolation lead to the generation of non-smooth-looking plots, which can be specifically evident for neighboring points with wildly different values.

1.3. Statistical analysis

Two-specimen t-tests with unequal variances were used to compare the differences in irradiance and RE detected by the top and bottom MARC-RC sensors for both LCUs. To compare between the LED LCU and QTH LCU, a specimen-level comparisons for KH and DC of both LCUs at each depth, averaging across multiple locations on each specimen were made using two-

specimen t-tests with unequal variances. Surface-level analyses for comparisons among depths by LCU were made using paired t-tests and two-specimen t-tests as appropriate for the specific depths because the top and bottom measurements were obtained from the same specimen and depth measurements were obtained from multiple slices of different sets of specimens. Ideally, the comparisons between LCUs and between depths would have been performed within the framework of a mixed-model ANOVA, but with the small specimen size in this study and data obtained from different specimens with respect to specimens designated for top and bottom characterization, and different specimens designated for depth characterization, an appropriate ANOVA was unable to fit the data.

The effects at each depth of location on the specimen and LCU were tested using mixed-model ANOVA. The ANOVA included fixed effects for the LCU, x-direction location and y-direction location and all two-way and three-way interactions effect for LCU, x-direction location and y-direction location. Normality assumptions were assessed and met for all analyses. The homogeneous variance assumption was met for the ANOVAs. A 5% significance level was used for all tests, with no adjustment for multiple testing. All statistical analyses were performed using SAS version 9.4 (SAS Institute Inc., Cary, NC).

2. SPECIFIC AIM 2

The influence of distance on irradiance, RE and DC on the top and bottom surfaces of a RMC increment

2.1. Specific aim 2, phase 1

The experimental design of specific aim 2, phase 1 is illustrated in Figure 25.

2.1.1. Irradiance, RE, curing time and spectral emission measurement on the top RMC surfaces

Six LCUs were explored in this study: one QTH LCU, three multiple emission peak LED LCUs and two single emission peak LED LCUs. The QTH LCU selected was O, the same LCU used in specific aim 1 study, and it served as the control. The three multiple emission peak LED LCUs were: BS that was used in the specific aim 1 study, SmartLite Max (SM) (Densply, York, PA) (Figure 26) and VALO Cordless (V) (Ultradent, South Gordon, UT) (Figure 27). The two single emission peak LED LCUs were: DEMI (D) that has a "Turbo" light guide tip (Kerr, Orange, CA) (Figure 28) and Demi Ultra (DU) (Kerr, Orange, CA) (Figure 29).

The irradiance, RE and spectral distribution at the center of the LCUs were explored using the MARC-RC system as described in specific aim 1, phase 2 (section 1.2.1) with a few modifications. In this study, the irradiance, RE, spectral emission and curing time measurements were collected for each LCU at 0, 2, 4, 6 and 8 mm distance between the light guide tip and the top sensor, to assess the effect of distance on irradiance and RE (n=6). Each LCU was centered over the top sensor using custom-made Mylar targets as described in specific aim 1, phase 2 (section 1.2.1). Since the V LCU has a concave light guide head, a custom-made adapter was machined with dimensions that matched the V light guide head and allowed its seating accurately to aid its alignment in the x-, y- and z-directions (Figure 30). The crossheads and circles around the sensors in addition to the custom-made Mylar targets, as seen in Figures 13 and 14, also assisted the exact centering and placement of the V light guide head over the sensor. After the

LCU alignment, the adapter was removed and the LCU distance was adjusted so the most concave point of the light guide head was placed against the top sensor, and this location was considered the 0 mm distance (Figure 30). Then, the desired distance was adjusted using the metric gauge on the MARC-RC system (Figure 13). The light curing time for each LCU at each curing distance was adjusted so the top sensor received 10-11 J/cm^2 per the manufacturer's instructions for the selected RMC as described in specific aim 1, phase 2 (section 1.2.1).

2.1.2. Specimen preparation, irradiance, RE and spectral emission measurement received on the bottom RMC surfaces

Each LCU was centered over the bottom MARC-RC sensor and square specimens (5×5×2 mm) were fabricated for each LCU (n=3) as described in specific aim 1, phase 2 (section 1.2.1), using the same dual photoinitiator RMC (Tetric EvoCeram bleaching shade XL). In this study, the average irradiance, RE and spectral distribution at the center of the LCUs were detected by the sensors and the corresponding average DC were characterized on the top and bottom surfaces of the RMC specimens. Each LCU guide tip was positioned at 2 or 8 mm distance from the top surface of each specimen to represent the best and worst clinical case scenario setting, respectively (Price et al. 2011). The specimens were prepared and polymerized over the bottom sensor at 2 or 8 mm distances between the light guide tip and top surface of the specimens (n=3/LCU/distance). The V LCU was adjusted over the bottom sensor in a similar setup to the top sensor using the custom-made adapter (Figure 31). Like specific aim 1, phase 2 study, each LCU was activated to polymerize the specimens from the top surfaces only, and the bottom sensor collected measurements through the 2 mm thick RMC specimens. Polymerized specimens were placed in a container covered with aluminum foil and stored dry in a 37°C incubator for 24 hours. After that, prepared specimens were finished and polished per the protocol described in specific aim 1, phase 2 (section 1.2.1). As mentioned previously, the Mylar strip

placed on the top surface of the specimens in this study absorbed approximately 5% of the LCU irradiation (Haenel et al. 2015).

2.1.3. DC measurements

On the fourth day after specimen preparation, the DC mapping was performed on the top and bottom surfaces of the RMC specimens only. The DC was measured using micro-Raman spectroscopy as previously described in the specific aim 1, phase 2 (section 1.2.1). In this study, the 50 measurements on the top surface and on the bottom surfaces were averaged to obtain one mean value for the top and for the bottom surfaces. Note that the specimens prepared in specific aim 2 were the same specimens used in specific aim 3 and 4.

2.2. Specific aim 2, phase 2

2.2.1. Molar absorbability of the photoinitiator systems

This test was performed to assess molar absorbability of CQ (Sigma-Aldrich, St. Louis, MO, Lot#09003AQ) and TPO (Tokyo Chemical Industry Co., Tokyo, Japan, Lot# N74HG-CB), which are the photoinitiators present in Tetric EvoCeram bleaching shade XL used in all experiments. For each photoinitiator, eight calibrant solutions were prepared in serial dilutions by mixing CQ or TPO with 20 ml methanol (Fisher Scientific, Pittsburg, PA, Lot#112195) starting from a concentration of 0.01M (Figure 32). Ultraviolet (UV) spectrophotometry (Evolution 201, UV-spectrophotometer, Thermo Fisher scientific, Waltham, MA) was used to analyze the solutions in the wavelength range between 200-700 nm (Figure 33). All materials used in the studies conducted are listed in Table 1.

2.3. Statistical analyses

The percent change in curing time or irradiance between 2 and 8 mm needed to reach 10-11 J/cm^2 was calculated. The effects of the LCUs and distance from the specimen (2 or 8mm) on

irradiance, RE and DC on the top and bottom surfaces were analyzed using ANOVA, with each LCU-distance combination allowed having a different variance. Pearson correlation coefficients were calculated to evaluate the linear associations among irradiance, RE and DC. The percent change in irradiance, RE and DC between the top and bottom surfaces of the RMC specimens light cured with each LCU were calculated using a student t-test. The regression trendline and R^2 were assessed and calculated. The molar absorptivity was calculated from the slope of a plot that displayed the absorbance as function of concentration for CQ and TPO at 470 and 380 nm, respectively. Normality assumptions were assessed and met for all analyses. The homogeneous variance assumption was met for the ANOVAs. A 5% significance level was used for all tests, with no adjustment for multiple testing. All statistical analyses were performed using SAS version 9.4 (SAS Institute Inc., Cary, NC).

3. SPECIFIC AIM 3

The influence of a localized irradiance beam profile area from multiple LED LCUs on the corresponding CLD mapping within a RMC increment

3.1. Specific aim 3, phase 1

3.1.1. LCU irradiance beam profile characterization

The irradiance beam profiles were collected from all six LCUs: O, BS, SM, V, D and DU that were used in the second study. The irradiance beam profiles were quantified using a Beam Profiler system as explained in specific aim 1, phase 1 (section 1.1.1) with a few alterations. The irradiance beam profiles from the LCUs explored were quantified at 0, 2, 4, 6 and 8 mm distances using gauge blocks (Figure 34). The beam profile images were collected in three setups; without placement of a filter over the camera lens to quantify the light output from the entire LCU spectral range, using the longpass filter to quantify the LCU output from the blue spectral range, and using the shortpass filter to quantify the LCU output from the violet spectral range. The V

LCU was placed against the ground glass diffuser using the custom-made adapter described in specific aim 2, phase 1 (section 2.1.1). After the LCU alignment, the adapter was removed and the LCU distance was adjusted so the most concave point of the light guide head was placed against the glass diffuser, and this location was considered the 0 mm distance, then, the LCU was activated and the image was captured (Figure 35). After that, the remaining desired distances were adjusted using the gauge blocks and images were captured. For the single emission peak LED LCUs, the camera recorded 50 frames to capture their pulsating high and low light outputs.

The irradiance measurements were collected using an integrating sphere/spectrometer assembly at 0, 2, 4, 6 and 8 mm distances from the integrating sphere opening utilizing custom-made adapters that matched the dimensions of the individual light guide tip as described in specific aim 1, phase 1 (section 1.1.1) (Figure 36). Each beam profile image was combined with its corresponding average power value collected from the integrating sphere/spectrometer assembly. For the single emission peak LED LCUs, the average power values were calculated, since the power pulsed between two levels, and then applied to the corresponding images.

In this study, the numerical power values of the 3×3 mm center of each image at 2 and 8 mm distances were exported. This area corresponded to the location that the KH measurements were collected (Figure 21) and corresponded to the area where the %KH reduction values were collected on the top surfaces of the RMC specimens. The exported power values from the 3×3 mm area of each beam profile image were used to calculate a 10×10 grid of average irradiance values within that 3×3 mm area providing 100 localized irradiance values. Only 50 values in a checkerboard pattern, which corresponded to the 50 %KH reduction measurements on the RMC specimens, were used to explore the correlation between the irradiance and %KH reduction on the top surfaces of the specimens for the individual LCU.

3.2. Specific aim 3, phase 2

The experimental design of specific aim 3, phase 2 is illustrated in Figure 37.

3.2.1. Specimen preparation

As mentioned in specific aim 2, phase 1 (section 2.1.3), one set of specimens was used for specific aims 2, 3, and 4. So, the irradiance, RE and spectral emission measurements collected were used in specific aim 2, phase 1. However, separate specimens were prepared for depth characterization, as described in specific aim 1, phase 2 (section 1.2.1).

Briefly, square RMC specimens (5×5×2 mm) were prepared using the same RMC used in the specific aim 1 and 2 experiments. In this study, specimens were prepared and polymerized over the bottom MARC-RC sensor at 2 or 8 mm distances between the light guide tip and top surfaces of the specimens (n=6/LCU/distance), as described in specific aim 1, phase 2, and specific aim 2, phase 1. Three squares were prepared for top and bottom surface characterization and three squares were prepared for the depth characterization. All specimens were stored dry in a 37°C incubator for 24 hours. After that, the squares designated for depth characterization were sectioned and all prepared specimens were finished and polished as described in specific aim 1, phase 2 (section 1.2.1).

3.2.2. Polymerization pattern characterization through CLD mapping

The polymerization pattern was characterized using the ethanol softening method by repeated KH measurements mapping (KH-BE and KH-AE) as described in specific aim 1, phase 2 (section 1.2.2). Briefly, the day after finishing and polishing of the specimens, KH-BE mapping was performed. The next day, specimens were soaked in absolute ethanol for 24 hours, and then the KH-AE mapping was performed. After that, the %KH reduction was calculated from the KH measurements BE and AE.

3.2.3. 2D contour plots and 3D renderings

Colored contour plots and 3D renderings were used to visualize the KH-BE, KH-AE and %KH reduction maps using ParaView 5.0, as described in specific aim 1, phase 2 (section 1.2.3).

3.3. Statistical analyses

The effects of the multiple LCUs assessed and curing distance from a RMC specimen (2 or 8 mm) on the %KH reduction by depth were analyzed using ANOVA, with each LCU-distance combination allowed to have a different variance. The ANOVA was extended to analyze repeated measures for the measurements (x-y coordinates) for each specimen rather than the average across the specimen. The correlations among the measurements at the x and y locations were based on the distance between the measurements. Linear mixed models were used to calculate the correlations across multiple locations on each specimen while accounting for within-specimen correlations. Pearson correlation coefficients were also used for the associations of the irradiance beam profile with %KH reduction on the top surfaces of the RMC specimens. Normality assumptions were assessed and met for all analyses. The homogeneous variance assumption was met for the ANOVAs. A 5% significance level was used for all tests, with no adjustment for multiple testing. All statistical analyses were performed using SAS version 9.4 (SAS Institute Inc., Cary, NC).

4. SPECIFIC AIM 4

The correlation of a localized irradiance beam profile area from multiple LED LCUs with the corresponding KH and DC mapping of a RMC increment

4.1. Specific aim 4, phase 1

4.1.1. Beam profile characterization of the LCUs

Like the second study, six LCUs were explored: O, BS, SM, V, D and DU. The irradiance beam profiles collected from specific aim 3, phase 1 (section 3.1.1) were used in this study. Briefly, the irradiance beam profiles from all six LCUs explored were quantified using a beam profiler system combined with irradiance measurements collected using an integrating sphere/spectrometer assembly at 2 or 8 mm distance from the integrating sphere opening. Then, the numerical power values of a 3×3 mm center of each image at 2 and 8 mm distances were exported as described in specific aim 3, phase 1 (section 3.1.1). The 3×3 mm area corresponded to the KH and DC measurement area on the top surfaces of the RMC specimens (Figure 21). The localized average irradiance values on the grid were correlated with the corresponding localized average KH and DC measurement points in a checkerboard pattern for each LCU.

4.2. Specific aim 4, phase 2

The experimental design of specific aim 4, phase 2 is illustrated in Figure 38.

4.2.1. Specimen preparation

Square RMC specimens (5×5×2 mm) were prepared (n=6/LCU/distance), as described in the specific aim 3, phase 2 (section 3.2.1). Briefly, the specimens were fabricated and polymerized on the bottom MARC-RC sensor at 2 or 8 mm distance between the top surfaces and light guide tip. Three squares were prepared for the top and bottom surface characterization and three squares were prepared for depth characterization. Specimens were stored dry in a 37°C

incubator for 24 hours. Then, the squares assigned for depth characterization were sectioned and slices-a, -b and -c were harvested then finished and polished.

4.2.2. Polymerization pattern characterization through DC and KH mapping

The polymerization pattern was characterized using KH and DC mapping, as described in specific aim 1, phase 2 (section 1.2.2). The KH mapping was performed utilizing an automated stage, and on the following day, DC mapping was performed using micro-Raman spectroscopy, as formerly explained.

4.2.3. 2D contour plots and 3D renderings

Colored contour plots and 3D renderings were used to visualize the KH and DC maps using ParaView 5.0, as described in specific aim 1, phase 2 (section 1.2.3).

4.3. Statistical analyses

The effects of the LCUs explored and distance from a specimen at 2 or 8 mm distance on DC by depth were analyzed using ANOVA, with each LCU-distance combination allowed to have a different variance. The analysis model was unable to perform comparisons for the 0.9 mm depth data, most likely due to complexities in the data that could not be overcome with the small sample size. The ANOVA was extended to analyze repeated measures for the data points (x-y coordinates) for each specimen rather than the average across the specimen. The correlations among the measurements were based on the distance between the measurements. Correlations between KH and DC were calculated using Pearson correlation coefficients for each depth after averaging across multiple locations on each specimen. Linear mixed effects models were used to calculate the correlations across multiple locations on each specimen while accounting for within-specimen correlations. Pearson correlation coefficients were also used for the associations of the irradiance beam profile with KH and DC on the top surface of a RMC specimen. Normality

assumptions were assessed and met for all analyses. The homogeneous variance assumption was met for the ANOVAs. A 5% significance level was used for all tests, with no adjustment for multiple testing. All statistical analyses were performed using SAS version 9.4 (SAS Institute Inc., Cary, NC).

RESULTS

1. SPECIFIC AIM 1

The influence of a localized irradiance beam profile area from one LED LCU and one QTH LCU on the corresponding CLD and DC mapping within a RMC increment

1.1. Specific aim 1, phase 1

1.1.1. LCU irradiance beam profile characterization

The 2D and 3D images (Figure 39) demonstrate the irradiance beam profiles of the LED and QTH LCUs collected from the Beam Profiler system using the longpass and shortpass filters, combined with the average power measurements collected from the long and short wavelength spectrum using the integrating sphere/spectrometer assembly. It is evident that the beam profile for the LED LCU was non-uniform with high irradiance "hot-spot" regions. On the other hand, the QTH LCU had a relatively homogenous irradiance beam profile compared to the BS LED LCU.

1.2. Specific aim 1, Phase 2

1.2.1. Irradiance, RE and spectral emission received on the top and bottom surfaces of the RMC

For each LCU, Table 2 and Appendix 1 show the average RE and irradiance values detected by the top and bottom MARC-RC sensors for each LCU, which correspond to the values delivered to the top surfaces, and received on the bottom surfaces of the 2 mm RMC specimens. Significantly higher irradiance values were measured from the LED compared to those from the QTH LCU at the top ($p=0.0006$) and bottom sensors ($p=0.0009$). Neither LCU had significantly different RE values for the top or bottom sensors.

For both LCUs, the irradiance and RE values detected on the bottom sensor decreased approximately 90% from the values detected on the top sensor. Furthermore, for both LCUs,

Figure 40 shows spectral distribution curves collected by the top sensor and through a 2 mm specimen at the bottom sensor. For both LCUs, it was found that the spectral distribution curves detected by the bottom sensor showed low irradiance values in the TPO absorbance range of the curves.

1.2.2. Polymerization pattern characterization through DC and CLD (KH) mapping

Figure 41 show representative images of the RMC surface and KH indentations BE and AE. It is evident in Figure 41 (a and b) that the RMC surface was smooth after finishing and polishing of the specimens. Figure 41 (a) displays that the KH indents BE are placed in a checkerboard pattern. In addition, Figure 41 (c and d) shows that the RMC surface became rougher AE. Also, it is clear that the KH indentations AE became longer compared to BE. Figure 41 (c) displays that the KH indentations AE placed in a checkerboard pattern between the KH indents placed BE.

Figure 42 (a) reveals the 3D renderings of a representative RMC specimen and displays the distribution of the DC values within the specimen. The 2D DC contour maps in Figure 42 (b) demonstrate the differences in DC on the characterized surfaces. The localized DC means within the specimens ranged from 50%-80%. It is evident that the DC in specimens cured with either LCU was not uniform on the top or bottom surfaces. Additionally, the characterized surfaces cured by both LCUs demonstrated a non-uniform and non-gradual decrease in DC from the top to the bottom. Figure 43 (a) reveals the 3D rendering of representative specimens illustrating the distribution of KH values. Figure 43 (b) shows the 2D KH maps and localized differences in KH on the characterized surfaces BE and AE cured with both LCUs. The localized mean KH values BE ranged from 40-67 kg/mm^2, and ranged from 22-43 kg/mm^2 AE. Like DC characterization, it is apparent that KH values with both LCUs were non-uniform on the top and bottom surfaces. However, a relative gradual decrease in KH values was observed from the top to the bottom of the specimens.

Table 3 and Figure 44 show the mean DC, KH-BE, KH-AE, and %KH reduction for specimens cured with each of the LCUs. The mean DC values across the top and bottom surfaces ranged between 62%-74%. The DC of the specimen-level analysis showed that the specimens cured using the LED LCU had significantly higher DC at a depth of 1.3 mm ($p=0.0112$), and significantly lower DC on the top ($p=0.0010$) and on the bottom ($p=0.0027$) compared to the specimens cured using the QTH LCU (Appendix 2 and 3). Curing with the LED LCU presented a significantly lower DC at a depth of 1.1 mm ($p\leq0.02$) compared to the top surfaces and a depth of 0.7 mm. Curing with the QTH LCU, the top surface had significantly higher DC than all the other depths except at a depth of 0.5 mm ($p\leq0.05$). Similar to the specimen-level analyses, the surface-level analysis showed localized differences in DC distribution that did not have a specific pattern on the surfaces characterized when comparing the curing between both LCUs. Also, localized discrepancies in DC were observed on the surfaces cured by the same LCU. When comparing between specimens cured by each LCU at all the points measured, only few points were significantly different from the DC mean that were mainly located on the top and at the depth of 1.3 mm ($p\leq0.05$). Additionally, within specimens cured by the same LCU, those cured by the LED LCU revealed fewer random measurements that were significantly different from the DC mean compared to the QTH LCU ($p\leq0.05$), respectively.

The KH specimen-level analysis in Table 3 and Figure 44 specimens cured with the QTH LCU had significantly higher KH values BE than those cured using the LED LCU at the depths of 0.9 mm ($p=0.0246$), 1.1 mm ($p=0.0186$) and 1.5 mm ($p=0.0034$). However, the bottoms cured using the LED LCU had significantly higher KH values than the bottoms cured using the QTH LCU BE ($p=0.0157$) and AE ($p=0.0244$). Also, the specimens cured using the LED LCU had significantly higher bottom/top KH ratio values that were greater than 80% compared to the specimens cured by the QTH LCU BE ($p=0.0454$) (Appendix 4 and 5). For the specimens cured using the LED LCU BE, the top surfaces, at a depth of 0.5 mm, and the bottom surfaces were not significantly different from each other. However, AE, the top had significantly higher KH values

than the surfaces at all other depths ($p \leq 0.046$). For the specimens cured using the QTH LCU, both BE and AE, the top had significantly higher KH values than all other depths ($p \leq 0.043$).

Like the specimen-level analyses, the KH surface analyses comparison between the surfaces cured using the LED and QTH LCUs revealed that 68/190 and 54/190 of the total points measured BE and AE were significantly different from the KH mean values ($p \leq 0.05$), respectively, and did not have a certain pattern. For the specimens cured using the LED LCU, 22/190 and 38/190 of all the points BE and AE, respectively, were significantly different from the KH mean values ($p \leq 0.05$). Also, for the specimens cured using the QTH LCU, 19/190 and 24/190 of all the points measured BE and AE, respectively, were significantly different from the KH mean ($p \leq 0.05$).

The %KH reduction specimen-level analysis in Table 3 and Figure 44 revealed that curing using the LED LCU had significantly higher %KH reduction values at a depth of 0.5 mm compared to curing using the QTH LCU ($p=0.0390$). However, curing with either LCU displayed that the top surface exhibited a significantly lower ($p \leq 0.044$) %KH reduction than all the other depths. Furthermore, a gradual increase in reduction of KH values was observed from the top to the bottom of specimens cured using either LCU. The surface-level analysis comparison between the LCUs showed that 24 measurements for the LED LCU had a significantly higher %KH reduction values compared to the QTH LCU ($p \leq 0.05$). Additionally, the LED LCU resulted in 90/190 measurement points that are significant from the mean ($p \leq 0.05$) compared to 75/190 significant points for the QTH LCU ($p \leq 0.05$). All the significant data points (x-y coordinates) for the DC, KH-BE, KH-AE and %KH reduction did not seem to follow a particular pattern (Appendix 6 and 7).

2. SPECIFIC AIM 2

The influence of distance on irradiance, RE and DC on the top and bottom surfaces of a RMC increment

2.1. Specific aim 2, phase 1

2.1.1. The influence of distance on LCU curing time and irradiance

The curing time needed for each LCU explored to achieve 10-11 J/cm^2 at 0 mm distance and the corresponding spectral distribution is revealed in Figure 45. It was evident that each LCU required a different curing time to achieve 10-11 J/cm^2. The LCU that emitted higher irradiance needed less curing time to reach the target RE. In addition, the spectral distribution for each LCU was variable per the LCU type. The graph revealed that a QTH LCU had a broad spectral emission. Also, the graph shows that the single emission peak LED LCUs and the multiple emission peak LED LCUs had one and two irradiation peaks, respectively. Furthermore, the spectral curve location and peak height was shifted for each LCU. Figure 46 (a) shows an inverse relationship between irradiance and distance that had a distinct pattern for the individual LCU. Figure 46 (b) and Table 4 display the curing time needed to achieve the RE needed (10-11 J/cm^2) at multiple distances from 0 to 8 mm. The Figure demonstrates a positive relationship between distance and curing time and a negative relationship between distance and LCU irradiance that had a unique pattern for each LCU. Table 5 shows that the percent increase in curing time and percent decrease in irradiance between 2 and 8 mm was not the same for the LCUs explored. The Table revealed that the curing time and irradiance from each LCU at 0 and 2 mm distances were relatively similar except when using O and SM. However, when curing with BS, a relatively equivalent irradiance and curing time (10-11 seconds) for up to 6 mm distance from the top sensor was measured. On the other hand, using the remaining LCUs revealed a rather gradual increase in curing time and decrease in irradiance when the distance between the light guide tip and the sensor was increased from 0 to 8 mm distance. In addition, curing with SM, V and DU

displayed the most percent change in curing time and irradiance. Table 5 displays the regression equation for each LCU that fit a polynomial (order 2) trendline, as demonstrated in Figure 47 (a and b), and that R^2 ranged between 90.8%-99.8% for the LCUs.

2.1.2. The influence of LCU curing distance on RMC polymerization

Figures 48 and 49 display that irradiance and spectral emission curves for each LCU that decreased with increasing the distance from the top sensor. The graphs show that the irradiance and spectral emission passing through the 2 mm specimens dramatically decreased on the bottom sensor. Figure 49 also reveals that the short wavelength curve within the violet region is no longer evident as recorded by the bottom sensor. Also, the spectral emission curves for all LCUs encompassed the absorption ranges of CQ and TPO photoinitiators.

Table 6 shows the average irradiance and RE values measured from the top and bottom sensors, which correspond to the values received on the top and the bottom of the 2 mm RMC specimens at 2 and 8 mm curing distances (Appendix 8). In addition, Table 6 shows the DC values calculated from the micro-Raman spectroscopy on the top and bottom surfaces of the RMC specimens at 2 and 8 mm curing distances (Appendix 8). It was evident that the distance from the specimens had a significant impact on irradiance (Appendix 9). However, distance only had a significant influence on DC when light curing with SM. The irradiance was significantly higher at 2 mm compared to 8 mm distance using all the LCUs regardless of surface. The RE on the bottom surface was significantly lower at 2 mm compared to 8 mm distance when using all LCUs except when curing with O. The DC was significantly higher for 2 mm than 8 mm distance when using SM regardless of the surface ($\alpha<0.05$).

Table 6 also shows that the LCU had a significant effect on irradiance, RE or DC at the top and bottom surfaces of the RMC specimens (Appendix 10). On the top surface, the irradiance at 2 mm revealed that using V yielded significantly higher irradiance compared to the remaining LCUs, and the opposite was true when using with O. However, the irradiance on the top surfaces

of the specimens cured at 8 mm distance revealed significant differences among using all LCUs except when light curing with V and O. In addition, at 8 mm curing distance, the irradiance from BS was significantly higher than the remaining LCUs and curing with D revealed significantly lower irradiance compared to the remaining LCUs. On the bottom surfaces, the irradiance emitted when using with SM and DU at 2 mm curing distance was significantly higher than the remaining LCUs and the opposite was true when curing with O. However, the irradiance on the bottom surfaces at 8 mm curing distance showed that curing with BS delivered significantly higher irradiance compared to the remaining LCUs, and the opposite was true when light curing with SM and D ($\alpha<0.05$).

Furthermore, Table 6 displayed that the RE on the bottom surfaces at 2 mm curing distance was significantly higher when light curing with O and DU than the remaining LCUs and the opposite was true for V. On the other hand, at 8 mm curing distance, the bottom surfaces of the specimens showed significantly higher RE when using D and DU compared to the other LCUs, and the opposite was true when curing with O ($\alpha<0.05$).

The DC values in Table 6 and Figure 50 demonstrate that significant differences were detected when light curing using the QTH, multiple emission peak LED and single emission peak LED LCUs at 2 and 8 mm curing distances. It is evident that there were no significant differences in the DC values with the QTH and multiple emission peak LED LCUs at 2 mm distance on the top and bottom surfaces. Also, no significant difference was observed in the DC values among the multiple emission peak LED LCUs at 8 mm curing distance except on the bottom surfaces when curing with SM. Furthermore, no significant difference in the DC values was found between using both single emission peak LED LCUs at 2 and 8 mm curing distances. Curing using D at 2 mm distance showed that the bottom surfaces had significantly lower DC values compared to curing with O, BS and SM. On the bottom surfaces at 8 mm distance, curing with V showed significantly higher DC compared to curing with SM or DU.

Irrespective of the LCU used, Table 6 displays that the irradiance or RE percent decrease between the top and the bottom surfaces ranged between 85%-93%, which was a similar finding to that observed in specific aim 1, phase 2 (Table 2 and Figure 40). The percent decrease in DC values between the top and bottom surfaces ranged between 0.2%-7.4%. Regardless of the LCU used, irradiance and RE displayed significant decreases between the top and bottom surfaces. However, Table 6 and Figure 51 show there was significant decrease in the DC values between the top and bottom surfaces at 2 mm curing distance except with D and DU. However, at 8 mm curing distance, only curing with O or SM showed a significant decrease in DC values between the top and bottom surfaces.

Using each LCU, distance did not have an impact on the DC values except when curing with SM. However, the LCU had an impact on DC values among the LCUs at each distance. Table 7 shows that interaction between the LCU and distance has a significant effect on the irradiance, RE and DC values on the top and bottom surfaces.

2.1.3. Correlation among irradiance, RE and DC

In general, Table 8 shows that the correlation among irradiance, RE and DC was relatively moderate to strong using the LCUs evaluated. Regardless of distance, an overall strong positive correlation between irradiance and RE was detected specifically on the bottom surfaces of the 2 mm RMC specimens. Also, regardless of distance, a fairly moderate-strong correlation was found between DC and irradiance, and between DC and RE. However, the correlations varied for each LCU, at each distance, and on each RMC surface. So, a LCU that exhibited a strong correlation between irradiance and RE did not necessarily have a strong correlation with DC. Also, a LCU that showed a strong correlation at 2 mm curing distance did not necessarily exhibit a strong correlation at 8 mm curing distance. Furthermore, a LCU that exhibited a strong correlation on the top surface of the specimens did not necessarily display a strong correlation on the bottom surfaces of the specimens.

2.2. Specific aim 2, phase 2

2.2.1. Molar absorbability of the photoinitiator systems

For CQ and TPO photoinitiators, Figures 52 and 53 demonstrate the CQ and TPO spectral emission curves at the eight concentrations tested, respectively. It is evident that the CQ photoinitiator spectral distribution falls within the longer blue wavelength spectrum compared to the TPO photoinitiator spectral distribution that falls within the shorter violet wavelength spectrum. It is also clear that increasing the concentration of CQ or TPO photoinitiators resulted in a greater spectral peak height. Figure 54 displays that the molar absorptivity of TPO photoinitiator (548.89x) was approximately 20-fold more than CQ photoinitiator (28.37x) at the different concentrations tested. The UV-spectrophotometry was unable to detect TPO at the high concentration of 0.01M and data could not be plotted.

For the LCUs explored, Figure 55 reveals the spectral distribution of the LCUs assessed on the top and bottom surfaces of a 2 mm RMC specimen combined with the absorbance spectrum of equal concentrations of CQ and TPO photoinitiators. The Figure yields the broad spectrum of a QTH LCU that falls within the absorption range of CQ and TPO photoinitiators and has higher absorption at the CQ photoinitiator range compared to the TPO photoinitiator range. In addition, the Figure displays that the multiple emission peak LED LCUs emit two spectral curves, one in the blue range and one in the violet range that fall within the absorption spectrum of CQ and TPO photoinitiators, respectively. In addition, the Figure yields that the multiple emission peak LED LCUs have higher absorption at the CQ range. On the other hand, the single emission peak LED LCUs have only one spectral curve in the blue range that falls within the absorption range of CQ photoinitiator. It is shown in the Figure that each LCU has its unique peak height. Furthermore, it is evident that the irradiance dramatically deceased on the bottom surfaces after the light was transmitted through the RMC compared to the top surfaces. Also, when light curing with the multiple emission peak LED LCUs, the violet curves were no longer evident on the bottom sensor.

3. SPECIFIC AIM 3

The influence of a localized irradiance beam profile area from multiple LED LCUs on the corresponding CLD mapping within a RMC increment

3.1. Specific aim 3, phase 1

3.1.1. LCU irradiance beam profile characterization

The 2D and 3D LCUs irradiance beam profile images quantified at the various distances between the light guide tip and a ground glass diffuser using the longpass filter are displayed in Figures 56 and 57, and using the shortpass filter are presented in Figures 58 and 59. It is evident that each LCU had a unique beam profile showing "hot-spot" and "cold-spot" regions depending on the type of LCU, number and type of the LED chips within the LCU, and the location and orientation of each LED chip within the LCU body or head. In addition, as the distance between the LCU guide tips and the glass diffuser increased, the irradiance values striking the camera decreased, and each LCU exhibited a relatively more uniform irradiance distribution over a wider area, which was outside the effective light-emitting area of the light guide tip. Table 9 reveals the average radiant power values from the QTH LCU and multiple emission peak LED LCUs from the effective light-emitting area of the light guide tip at various spectral emission ranges (full spectrum, long wavelength, and short wavelength spectrum). The power measurements in the Table for each LCU were collected using an integrating sphere/spectrometer assembly at multiple distances from 0 mm to 8 mm. Each average power measurement collected from the blue or violet spectrum was applied to the corresponding beam profile image collected from the longpass filter (Figure 56 and 57) or shortpass filter (Figures 58 and 59) to generate the calibrated irradiance maps. The Table also shows the average irradiance values calculated from the average power values and the light-emitting area of each LCU. Like Table 9, Table 10 displays the average radiant power values calculated for the single emission peak LED LCUs from the full spectral emission ranges (380-700 nm) using an integrating sphere/spectrometer assembly at each

curing distance using its effective light-emitting area. Since the single emission peak LED LCUs evaluated are pulsating in nature, the minimum, maximum and mean radiant powers were calculated from the measured spectral graph. The mean power values were applied to the corresponding beam profile images. The Table also displays the average irradiance values calculated from the average power values using the light-emitting dimensions of each LCU.

Figures 60 and 61 show the 2D and 3D beam profiles emitted from the LCUs quantified at 2 and 8 mm between the LCU tip and glass diffuser using the longpass and shortpass filters, respectively. The images reveal a superimposed white square at the center of each image that corresponds to the 3×3 grid area where the KH measurements were collected on the RMC specimens. Like Figures 56-59, the "hot-spot" regions correspond to the blue of violet chips when using the longpass or shortpass filters, respectively. The irradiance distribution beam profile images reflect the irradiance emitted from the LCU tip that was received on the top surfaces of the specimens. Figures 62 and 63 show the irradiance distribution within the 3×3 grid, which was divided into 10×10 grid that corresponded to the location of the DC and KH mapping grid. The numerical power values of the 2D data were exported and the irradiance values in each square on the grid were calculated for three different beam profile quantification setups; without using a filter, using the longpass filer and using the shortpass filter (Figure 8). For each LCU investigated, the exported average power values in each square and the corresponding calculated average irradiance values for the three setups (without a filter, with the longpass and the shortpass filter) are revealed in Appendix 11 and 12.

Table 11 shows the details of each LCU spectral distribution, peaks and the LED chip type, and number. It is evident that each LCU type had a distinctive spectral range with a different peak location, as previously displayed in Figures 49 and 55. The O LCU had a broad spectral emission with a higher absorption in the longer wavelength (blue) region. The broad spectral emission of O LCU is displayed as a relatively homogenous irradiance beam profile distribution, as shown in Figures 6, 39 and 56-63. The multiple emission peak LED LCUs have

two spectral peaks in the blue and violet regions, with higher output in the longer wavelength (blue) region compared to the shorter wavelength (violet) region. BS has two blue and one violet LED chips equally separated from each other, as demonstrated in Figures 7, 39 and 56-63. SM has one blue and one violet chip opposite to each other, as shown in Figures 26 and 56-63. V has three blue chips (two blue and one longer blue wavelength) and one violet chip, as displayed in Figures 27 and 56-63. However, the single emission peak LED LCUs, D and DU, had one spectral peak at the longer wavelength region with one and three blue chips at the center of the LCU guide tip, respectively, as revealed in Figures 28, 29 and 56-63. The D image at 2 mm distance displayed that higher irradiance was projected on the peripheries than the center of the LCU guide tip where the LED chip is located. Furthermore, it is clear that the irradiance beam profile at 8 mm distance between the LCU emitting tip and the glass diffuser showed lower irradiance values captured by the beam profiler camera that were more homogenous compared to the 2 mm distance.

Figure 64 shows the percent contribution from the violet and blue spectrums for the individual LCUs at 2 mm distance that was calculated from the average power values collected from the integrating sphere/spectrometer assembly (Table 9). It is evident that the irradiance percent contribution from the blue LED chips for each LCU was more than from the violet chips. Also, the irradiance percent contribution from the blue and violet LED chips among the QTH and multiple emission peak LED LCUs was relatively similar.

3.2. Specific aim 3, phase 2

3.2.1. Polymerization pattern characterization through CLD mapping

3.2.1.1. Localized CLD characterization within the RMC specimens

The 3D and 2D rendering contour maps in Figures 65-67 were generated from the average localized KH-BE and KH-AE values at each measurement point (x-y coordinate), which are presented in Appendix 13 and 14. The average %KH reduction for each point in the Figure 68

and 69 renderings was calculated from each KH-BE value and the corresponding KH-AE value (Appendix 15 and 16). It is clear from the 3D KH measurement renderings in Figure 65 that the gradual reduction in the KH-AE values from the top to the bottom surfaces occurred regardless of the distance. This is also evident in the 2D KH contour maps in Figures 66 and 67, which show the average KH distribution on the top and bottom surfaces along with the various depths investigated, as seen slices-a and -b. However, curing with the single emission peak LCUs showed a relatively uniform KH distribution within the depths of the specimens. The 2D contour maps also show that the KH distribution was not uniform across the top and bottom specimen surfaces for the LCUs explored.

Figures 68 and 69 display the 3D and 2D renderings, respectively, of representative specimens revealing the average %KH reduction distribution values using the LCUs investigated at 2 and 8 mm curing distances. The %KH reduction was not uniform, did not have a specific pattern, and gradually increased from the top to the bottom of the specimens at both curing distances, except for the single emission peak LED LCUs that revealed a relatively uniform %KH reduction distribution. Table 12 displays the number of significant %KH reduction comparison values among the measurement points (x-y coordinates) at each surface, depth, and distance. The fewer CLD significant comparisons in the Table indicate that more consistent values were observed across each depth for the individual LCU, at each curing distance. The number of significant %KH reduction comparisons revealed in Table 12 varied for each LCU, and differed between 2 and 8 mm distances when curing with the same LCU. It is evident from Table 12 that curing specimens with O showed more significant variations at 2 mm distance compared to the remaining LCUs. In addition, curing specimens with BS or D at 2 mm distance showed the most %KH reduction discrepancy among the LCUs explored. The significant comparisons at each depth and each distance among the LCUs demonstrated that the significant points did not follow a specific pattern. Additionally, at each depth, the significant %KH reduction value comparisons between 2 and 8 mm curing distances varied for each LCU. The opacity of the 3D renderings was

adjusted in Figure 70 to clearly show the average %KH reduction measurement points. Figure 71 displays the locations of the significant %KH reduction points across each depth (Appendices 17, 18 and 19). The renderings yielded that, for the same LCU, the uniformity of %KH reduction varied between depths and between 2 and 8 mm curing distances, and also differed among the LCUs at each distance ($\alpha<0.05$, Appendix 19). Considering Figure 71 and Table 12 simultaneously, it is evident that the number of significant comparisons varied across each depth. For example, using O LCU to cure the specimens at 2 mm distance showed 100 and 159 significant comparisons among the top and bottom surfaces, respectively. This indicates that the bottom surfaces showed more polymerization discrepancies across its surface compared to the top surface. Therefore, Figure 71, Table 12 and Appendices 17-19 are complementary to each other to view polymerization uniformity across each surface.

The ANOVA results in Table 13 reveal that the x-y coordinates were significant on the bottom surfaces when using BS at 2 mm distance, at the depths of 0.9 and 0.5 mm when light curing using D and V, respectively at 8 mm distance.

3.2.1.2. Average CLD characterization across the depths of the RMC specimens

Table 14 displays the average %KH reduction at each depth using the individual LCUs (Appendix 20). It is evident that the average %KH reduction at each depth using the same LCU was not significantly affected by the curing distance except when curing with D, which showed significantly higher %KH reduction at 2 mm compared to 8 mm curing distance at the depth of 0.9, 1.3, 1.5 mm and on the bottom of the specimens. Also, curing with V and O revealed significantly higher %KH reduction at 8 mm compared to 2 mm curing distance on top and bottom surfaces, respectively ($\alpha<0.05$, Appendix 21). Comparing the average %KH reduction amongst curing with the LCUs assessed revealed significant differences that did not follow the same trend at each depth nor at each distance. Also, Table 14 yields more significant differences

between curing with the QTH or multiple emission peak LED LCUs compared to using the single emission peak LED LCUs at 2 mm curing distance ($\alpha<0.05$, Appendix 22).

At 2 mm curing distance, Table 14 revealed that only minor significant differences in %KH reduction were detected between curing with the QTH and the multiple emission peak LED LCUs. Curing with O at the depth of 0.5 mm showed significantly lower %KH reduction compared to curing with BS. In addition, using O had significantly less %KH reduction than curing with SM on the top and bottom surfaces only. On the other hand, more significant differences were displayed between using QTH and the single emission peak LED LCUs. Curing with O showed significantly less %KH reduction than using D at all depths except at 1.1 mm. Using O had significantly less %KH reduction than curing with DU from the top moving down to the depth of 0.9 mm. Regarding the significant differences among the multiple emission peak LED LCUs, the only significant difference was that using BS had significantly less %KH reduction than curing with SM at the top surface. Considering the significant differences between curing the specimens with the single emission peak LED LCUs, results revealed that using D showed significantly higher %KH reduction at the depths of 0.9, 1.3 and 1.5 mm only. Comparing between curing with the multiple emission peak and the single emission peak LED LCUs, using D showed significantly higher %KH reduction than curing with BS and V at the top, 0.5, 0.7 and 0.9 mm. Using D displayed significantly higher %KH reduction than using SM at the top, 0.5, and 0.9 mm. Also, curing with DU had significantly higher %KH reduction than using BS at the top and 0.5 mm only, and significantly higher %KH reduction than SM at the top and 0.9 mm only. Interestingly, at the depth of 1.1 mm, which is the middle of the specimen, no significant differences in %KH reduction were observed when light cured using the multiple LCUs assessed ($\alpha<0.05$, Appendix 22).

At 8 mm distance, Table 14 displayed that only minor significant differences were revealed in %KH reduction between curing with the QTH and LED LCUs. Curing with O showed significantly higher %KH reduction compared to curing specimens with BS and D on the bottom

surfaces. There were no significant differences detected between using the single emission peak LED LCUs in %KH reduction. Considering the significant differences among using the LED LCUs, curing with BS revealed significantly less %KH reduction compared to using SM on the bottom surface, curing with V at the top, 0.9, 1.1 and 1.5 mm, curing with D at the top, 0.9 and 1.1 mm, and curing specimens with DU at the top and 0.9 mm. Furthermore, using SM displayed significantly less %KH reduction compared to curing with V and DU on the top surfaces, and using D on the top, 0.5 and 0.9 mm. Also, curing with SM showed significantly higher %KH reduction compared to using V, D and DU on the bottom surfaces. Additionally, curing with V revealed significantly less %KH reduction compared to curing with D on the top and at the depth of 0.5 mm. However, at the depth of 1.3 mm, no significant differences were observed in the %KH reduction when curing using all the LCUs in this study ($\alpha<0.05$, Appendix 22).

Table 15 shows that the LCU, distance, and the LCU/distance interaction have significant effect on the %KH reduction at certain depths. The ANOVA table demonstrated that the interaction between the LCU and distance was significant only on the bottom surfaces.

3.2.2. Correlation between the localized irradiance beam profiles and CLD

Figure 72 displays the area of the localized irradiance distribution assessed and the corresponding %KH reduction values on the top surfaces at 2 and 8 mm curing distances. The average numerical localized irradiance values at each square on the 10×10 grid for the top surfaces of the LCUs explored at 2 and 8 mm distances are presented in Appendix 23. The numerical localized irradiance values were correlated to the corresponding %KH reduction value. Table 16 reveals that the localized %KH reduction was weakly correlated with the localized irradiance beam profiles from each LCU regardless of the distance or filter used. However, %KH reduction showed a significantly positive association with irradiance beam from BS at 8 mm distance when using the longpass filter ($p=0.035$).

4. SPECIFIC AIM 4

The correlation of a localized irradiance beam profile area from multiple LED LCUs with the corresponding KH and DC mapping of a RMC increment

4.1. Specific aim 4, phase 1

4.1.1. LCU irradiance beam profile characterization

Previously mentioned Figures 60 and 61 display representative 2D and 3D images of the irradiance beam profiles from the LCUs explored using the longpass and shortpass filter at 2 and 8 mm curing distances, which corresponds to the emitted light delivered on the top surface of the specimens. The beam profile images showed localized irradiance measurements across the surface for all LCUs that ranged from approximately 200-1400 mW/cm^2. The details for the irradiance beam profiles are described in specific aim 3, phase1 experiment results (section 3.1.1). Briefly, the QTH has a relatively homogenous beam profile compared to the LED LCUs. Also, the LED LCUs reveal "hot-spot" and "cold-spot" regions representing high and low irradiance zones that correspond to the location of the blue and violet LED chips.

4.2. Specific aim 4, phase 2

4.2.1. Polymerization pattern characterization through DC and KH mapping

4.2.1.1 Localized DC and KH characterization within the RMC specimens

Figure 73 reveals 3D representative renderings of the KH and DC measurements of the RMC specimens cured at 2 and 8 mm distances. Figures 66 and 74 display 2D representative contour maps of the KH and DC measurements of 2 and 8 mm distances cured using the LCUs explored. The localized KH values approximately ranged from 39-67 and 40-74 kg/mm^2 at 2 and 8 mm curing distances, respectively. The localized DC values varied between 50%-80% regardless of the curing distance. A non-uniform KH and DC distribution was detected across the top surface, which was more evident for the DC measurements. Furthermore, the single emission

peak LED LCUs showed a lower KH and DC values compared to the multiple emission peak LED LCUs. The 3D KH and DC renderings revealed the presence of localized differences within. The KH values gradually decreased from the top to the bottom surfaces when light curing using the QTH LCU and multiple emission peak LED LCUs. On the other hand, using the single emission peak LED LCUs showed relatively uniform KH values. However, DC value distribution did not follow a specific pattern. Furthermore, the renderings displayed higher KH values at 8 mm compared to the 2 mm curing distance. Also, curing with a QTH LCU and multiple emission peak LED LCUs displayed higher DC values compared to using the single emission peak LED LCUs regardless of the distance.

Tables 17 and 18 show the number of significant comparisons among the data points (x-y coordinates) for KH and DC values using the individual LCU at each depth and distance. The results demonstrate that the number of significant KH and DC comparisons at each depth varied between 2 and 8 mm distances for the individual LCU. Table 17 and 18 also shows that fewer KH and DC significant comparisons indicated that more consistent values were observed across each depth for the individual LCU, at each curing distance. The significant comparisons between KH and DC at each depth for each LCU showed that curing with BS and SM had fewer significant comparisons in KH at 2 mm distance compared to the remaining LCUs. The location of the significant points for KH and DC values varied across each surface and depth for each LCU. Irrespective of the curing distance, curing the specimens with BS yielded more significant differences in KH at the depth of 0.7 mm and DC at the depth of 0.9 mm. Also, from all the significant comparisons, using BS demonstrated more significant differences in KH and DC values at 8 mm curing distance. Considering the bottom/top KH ratios, O LCU demonstrated more significant comparisons when curing specimens at 8 mm distance compared to the remaining LCUs. Similar to Figures 62 and 63, the opacity in Figures 75-78 was adjusted to clearly see all the measurement points within the specimens. Figures 75 and 77 display the average KH values (Appendices 15, 16) and average DC values (Appendix 24), respectively.

Figures 76 and 78 reveal the locations of the significant KH points (Appendices 25-27) and DC points (Appendix 28-30), respectively. The renderings demonstrated that the homogeneity at each depth for each LCU was different between 2 and 8 mm distances, and varied among the LCUs at each distance. Like the %KH reduction in specific aim 3, phase 2 experiment (section 3.2.1.1), the number of significant points across each depth in Figures 76 and 78 using the individual LCU at each curing distance, does not indicate the degree of significance among the points, unless combined with the number of significant comparisons across each depth shown in Tables 17 and 18, respectively ($\alpha<0.05$, Appendix 27 and 30). It is evident form Table 17 that light curing with V or D at 2 mm, and curing with BS at 8 mm had the least KH value uniformity. In addition, Table 18 displays that curing with O at 2 mm and curing with BS at 8 mm shows the least DC value uniformity among the LCUs explored.

Figure 79 is a 2D contour map of the bottom/top KH ratio. These renderings are not of an existing surface, but were rendered to visualize the localized bottom/top KH ratio values. Figure 80 and Appendix 31 demonstrates that the localized bottom/top KH ratios for most of the points were more than 80% regardless of the curing distance. Also, the Figure and Appendix show that most of the localized bottom/top KH ratio points were less than 80% when light curing with O or V at 2 mm. Light curing specimens using BS and SM at 8 mm showed some points with bottom/top KH ratios less than 80%. Curing specimens using the remaining LCUs and distances revealed only 0-3 points with bottom/top KH ratios less than 80%. Considering the significant differences among the measurement points across each bottom/top KH ratio surface, Figure 81 reveals that light curing the specimens with O and BS at 8 mm and DU at 2 mm had the most significant variation among the points (Appendix 32). This indicates that a LCU at a specific distance can achieve a bottom/top KH ratio greater than 80% but shows less localized polymerization uniformity between the top and bottom surfaces.

Considering the localized DC values within the RMC specimens, although the localized average measurement points varied between 50-80%, the localized measurements for a few

individual random minimum DC values were less than 50%. To illustrate this, Figure 82 shows 3D renderings of the minimum DC values from all specimens characterized when cured using the LCUs explored at each distance. These values were not all from the same specimen, but are the minimum values detected from all the specimens. Figures 83, and Appendices 33 and 34 display the location of the minimum DC values that were less than 50% for each LCU explored at each distance.

From all the LCUs explored, the ANOVA results in Table 19 revealed that the localized KH x-y coordinate values were significant on the bottom surfaces of the specimens when curing with BS at 2 mm and when evaluating the bottom/top KH ratios. However, the ANOVA results in Table 20 showed that the DC x-y coordinate values were significant when light curing with BS at the depth of 0.9 mm at 2 mm distance and on the top surfaces at 8 mm curing distance. Also, when curing with D at the depth of 1.3 mm at 2 mm curing distance and at the depths of 1.1 and 1.5 mm at 8 mm curing distance, in addition to light curing using DU at the depth of 1.1 mm at 2 mm curing distance.

4.2.1.2. Average DC and KH characterization across the depths of the RMC specimens

Table 21 and Appendix 35 reveal the average KH and DC values across each depth when light curing using the individual LCU at each curing distance. Considering the significant differences in DC and KH between 2 and 8 mm distances, the findings showed that more significant differences between 2 and 8 mm curing distances were detected for KH across most depths than for DC, regardless of the LCU used. Also, it is evident that the average KH and DC values at each depth varied for the LCUs explored, and were not consistent for the same LCU at the distances assessed.

Considering the curing distance, the findings revealed that KH values were significantly higher at 8 mm distance compared to 2 mm curing distance except at specific depths; when curing

with O on the top, 1.1, 1.3 and 1.5 mm, when using BS on the top and bottom surfaces, using V and D on the top surfaces and DU at the depth of 1.3 mm ($\alpha<0.05$,Appendix 36).

Considering the significant differences of the average KH values among the LCUs across each depth showed significant differences, which were more at 2 mm compared to 8 mm curing distance. In general, only a few significant differences in KH values were detected between curing with a QTH LCU compared to the LED LCUs regardless of the distance. Also, only a few significant differences were detected amongst using the multiple emission peak LED LCUs irrespective of the distance. However, using the multiple emission peak LED LCU yielded significantly higher KH values compared to using the single emission peak LED LCUs except at specific depths regardless of the distance. Curing with the single emission peak LED LCUs revealed only a few significant differences between them. The analysis model was unable to perform comparisons for the 0.9 mm depth data, most likely due to complexities in the data that could not be overcome with the small sample size ($\alpha<0.05$, Appendix 37).

To be more specific, at 2 mm, comparisons between curing with the QTH LCU and multiple emission peak LED LCUs displayed that using O resulted in significantly higher KH compared to using BS at the depths of 1.1 and 1.5 mm, and significantly lower KH across the bottom surfaces. Also, curing with O revealed significantly higher KH than using SM across the bottom surfaces only. However, using O did not show significant differences to using V at any depth. Comparing between using the QTH LCU and single emission peak LED LCUs demonstrated that curing with O exhibited significantly higher KH than curing with D and DU at all depths except across the bottom surfaces. Comparisons among the multiple emission peak LED LCUs showed that using BS and SM resulted in significantly higher KH than using V across the bottom surfaces only. Using SM revealed significantly higher KH values than using BS at the depth of 1.3 mm only. In addition, comparisons between the multiple and single emission peak LED LCUs showed that curing with BS demonstrated significantly higher KH values than using D at all depths except 1.3 mm and using DU at all depths except 1.1 mm and bottom surfaces.

Curing with SM showed significantly higher KH values compared to using D at all depths except 1.5 mm, and using DU at all depths. Curing with V demonstrated significantly higher KH values compared to using D and DU across the top, 0.5, 0.7 and 1.1 mm, but significantly lower KH values compared to using DU across the bottom surfaces. Comparisons between the single emission peak LED LCUs showed that using D had significantly lower KH values compared to using DU at the bottom surfaces, and significantly higher KH values on the top surfaces and at the depth of 0.5mm ($\alpha<0.05$).

At 8 mm distance, relatively more KH similarities were observed between the LCUs at each depth. Comparing between using the QTH and multiple emission peak LED LCUs displayed that using O showed significantly lower KH values compared to using BS across 1.3 and 1.5 mm only, using SM at all depths except across the top surfaces, and using V across the depths of 0.5, 0.7 and 1.5 mm. Comparing between the QTH and single emission peak LED LCUs showed that curing with O revealed significantly higher KH values compared to using D and DU across the top surfaces, and significantly lower KH values compared to using D at the depths of 1.3 and 1.5 mm. The multiple emission peak LED LCUs displayed several significant differences among them where using SM demonstrated significantly higher KH values compared to using BS across the top, 0.5, 1.1, 1.5 mm and bottom surfaces, and using V across the top and bottom surfaces. However, no significant differences in KH values were displayed between using BS and V at any depth. Comparisons between the multiple and single emission peak LED LCUs showed that curing with BS revealed significantly higher KH values compared to D and DU across the top surfaces, significantly lower KH values compared to using D at the depths of 1.1, 1.3 mm and the bottom surfaces, and using DU at the bottom surfaces. Also, curing with SM displayed significantly higher KH values compared to using D across the top, 0.5 and 1.1 mm, and using DU across the top and bottom surfaces only. Furthermore, curing with V displayed significantly higher KH compared to using D and DU across the top surfaces, and significantly less KH values compared to using D across the bottom surfaces. However, no significant differences were

detected between the single emission peak LED LCUs at any depth. The analysis model was unable to perform comparisons for the 0.9 mm depth data, most likely due to complexities in the data that could not be overcome with the small sample size ($\alpha<0.05$). The bottom/top KH ratio for the average KH on the top and bottom surfaces for all LCUs was greater than 80% except when using O and V at 2 mm distance from the top surfaces of the RMC specimens.

Table 21 reveals the DC value comparison between 2 and 8 mm for using the individual LCU at each depth. The DC values were significantly higher at 2 compared to 8 mm when curing with SM at the top and bottom surfaces, and using V at the depth of 0.5 mm. No other significant differences were found between the distances for each LCU at each depth ($\alpha<0.05$, Appendix 38).

At 2 mm distance, the DC comparisons among the LCUs across each depth and curing distance revealed that there were no significant differences detected between the depths from 0.9 to 1.5 mm ($\alpha<0.05$,Appendix 39). The DC displayed few significant differences amongst the QTH and the LED LCUs at certain depths regardless of the distance. Comparing between the QTH and the multiple emission peak LED LCUs, revealed that there were no significant differences in DC among them across each depth except when using SM that had significantly higher DC compared to O across the top surfaces. No significant differences were detected between using the QTH LCU and the single emission peak LED LCUs except that using O showed significantly higher DC compared to D across the top surfaces and DU at the top and bottom surfaces across each depth. No significant differences in DC were displayed amongst using the multiple emission peak LED LCUs at each depth. Comparisons between using the single and multiple emission peak LED LCUs showed that using BS had significantly higher DC than D across the top, 0.5, 0.7 mm and bottom surfaces, and DU at the depth of 0.5 mm. Curing with SM showed significantly higher DC than D across the top and bottom surfaces, and using V revealed significantly higher DC than D across the top, 0.5 and 0.7 mm. Curing with SM and V showed significantly higher DC than DU across the top surfaces and at the depth of 0.5 mm ($\alpha<0.05$).

At 8 mm distance, comparisons between curing with the QTH and the multiple emission peak LED LCUs revealed significant differences when using O and BS at the depths of 1.1 and 1.3 mm. No other significant differences were found ($\alpha<0.05$). Comparisons among using the multiple emission peak LED LCUs showed that using V showed significantly higher DC compared to SM across the bottom surfaces, and significantly lower DC compared to using BS across the depths of 0.7, 0.9 and 1.1 mm. Comparisons among using the single emission peak LED LCUs and the remaining LCUs revealed that D had significantly lower DC compared to using O at the top and 0.5 mm, BS at the top and 0.5 mm, V at 0.5 mm and bottom surfaces, SM at the depth of 0.5 mm, and significantly higher than SM at the bottom surfaces. DU showed significantly lower DC compared to using O, SM and V across the top surfaces, and BS at the top and 0.9 mm ($\alpha<0.05$).

Considering the KH values, the LCU, distance, and the LCU/distance interaction in the ANOVA results in Table 22 revealed that LCU, distance and their interaction had a significant effect on the KH at all depths of the RMC specimens. Considering the DC values, The ANOVA results in Table 23 demonstrated that the interaction between the LCU and distance was significant only on the bottom surfaces of the RMC specimens.

4.2.3. Correlation of the LCU irradiance beam with KH and DC

4.2.3.1. Correlation of a localized LCU irradiance beam area with KH and DC on the top surfaces of the RMC specimens

Figures 84 and 85, and Appendix 40 display 2D representative images of the localized irradiance beam profiles from the LCUs coupled with corresponding KH and DC images of the top surface at 2 and 8 mm distances, respectively. Table 24 shows that the localized correlation of the KH and DC measurement with the corresponding irradiance beam profile value for the individual LCU was weak when using the longpass or shortpass filter. Curing with BS at 8 mm distance revealed that KH was significantly associated with irradiance beam profile, where a

negative association was observed for the longpass filter (p=0.008) and a positive correlation for the shortpass filter (p=0.010). Also, using V at 2 mm distance showed a negative association with the longpass filter (p=0.014). DC was significantly correlated with irradiance beam profile from a LCU when curing with V at 2 mm distance, where a positive association was shown with the longpass filter (p=0.023) and a negative correlation with the shortpass filter (p=0.024).

4.2.3.2. Correlation between the localized DC and KH within the RMC specimens

The localized correlation between each KH and DC measurements revealed in Table 25 was not similar among the LCUs or when using each LCU at the distances assessed. Also, none of the correlations were statistically significant. In general, a moderate correlation was detected at 2 mm compared to the moderate to weak correlation at 8 mm distance when using all the LCUs assessed. Curing with O demonstrated a moderate correlation at the depths of 0.7, 0.9, 1.5 mm and bottom surfaces at 2 mm distance, and a weak correlation at the remaining depths. At 8 mm distance, using O showed a moderate to high correlation on the top, 0.7, 0.9 and 1.5 mm, and a low correlation at the other depths. Curing with BS revealed a moderate to strong association between 0.9-1.3 mm at 2 mm distance and top and bottom surfaces at 8 mm curing distance, and a weak correlation at the remaining depths. At 2 mm distance, using SM displayed a moderate association on the top, 1.1 and 1.5 mm distance, and at 8 mm using SM demonstrated a strong to moderate association on the top, 0.5 and 0.7 mm, all the remaining depths demonstrated a weak correlation. At 2 mm distance, curing with V revealed a moderate correlation at all depths except the top and bottom where the association was weak. At 8 mm distance, using V showed a weak correlation at all depths. Curing with D yielded a moderate correlation at the depths of 0.5, 0.7, 1.5 mm and bottom surfaces at 2 mm distance, and top, 0.9, 1.1 and 1.3 mm for 8 mm distance, all the remaining depths showed a weak correlation. Using DU displayed a moderate correlation at the depths of 1.3 and 1.5 mm at 2 mm distance, at the depths of 1.1, 1.5 mm and bottom surfaces at 8 mm distance, and weak for all other depths.

Although CLD was not performed in this study, the localized DC, KH-AE, and %KH reduction results from specific aim 3, phase 2 were used to explore the correlation. The results showed variations in the correlation between CLD and DC at each depth, curing distance and for each LCU.

4.2.3.3. Correlation between the average DC and KH among the depths of the RMC specimens

The correlations between the average KH and DC values across each depth in Table 26 showed a moderate to strong correlation and only few of the correlations were statistically significant. The significant correlations at 2 mm distance were with BS at the depth of 0.5 mm ($p=0.045$), D at the depth of 0.9 mm ($p=0.012$), and D at the depth of 1.1 mm ($p=0.033$). The significant correlations at 8 mm were using D at the depth of 0.5 mm ($p=0.042$), O at the depth of 0.7 mm ($p=0.034$), O at the depth of 1.1 mm, and O the B surface.

The correlation of the DC with KH-AE and CLD from specific aim 3, phase 2 was explored. The average DC correlations with the average KH-AE values across each depth was only significant at a few points; at 2 mm curing distance when using D at the depth of 0.9 ($p=0.012$), and at the depth of 1.1 ($p=0.033$). At 8 mm curing distance, the correlation was significant for KH-AE when using O on the bottom surface ($p=0.033$).

Significant correlations between the average DC and CLD were observed at 2mm curing distance when using SM at the depth of 0.5 mm ($p=0.021$), at 8 mm curing distance when using BS at the depths of 0.5 mm ($p=0.019$), using D and O on the top surface ($p=0.003$) and ($p=0.031$), respectively.

DISCUSSION

Based on the outcomes of the studies conducted, the following sections explain the findings. First, characterization of the beam profile and spectral emission from the LCUs are discussed followed by characterization of polymerization patterns with respect to DC, KH, and CLD and finally the correlations conducted.

A non-uniform irradiance beam profile across the LCU guide tip may result in localized polymerization discrepancies across the RMC surfaces. Polymerization discrepancies may affect RMC chemical, mechanical, physical properties, and may ultimately impact the longevity of the restoration (Rueggeberg 2011, Price, Rueggeberg, et al. 2010, Arikawa et al. 2011, Haenel et al. 2015, Price, Ferracane, and Shortall 2015, Price et al. 2014). Polymerization pattern characterization through DC, KH, and CLD mapping at different depths of a RMC cured by a QTH LCU, single and multiple emission peak LED LCUs may provide an insight on the influence of the localized irradiance beam profile uniformity on polymerization efficiency within the RMC.

1. Characterization of the LCUs

1.1. LCU irradiance beam profile characterization

The QTH and LED LCUs showed variations in the irradiance beam profile uniformity (Figures 6, 39 and 56-63). These differences are attributed to the light source differences between the QTH and LED LCUs. The O QTH LCU showed a relatively uniform beam profile across its tip. This can be explained by the wide spectral range of the light generated (375-510 nm) from a light bulb located in the body of the LCU. The generated light is transmitted from the LCU body to the guide tip through a straight fiber optic light guide tip. Our findings were similar to the literature (Jandt and Mills 2013, Rueggeberg 2011, Megremis et al. 2014, Price, Ferracane, and Shortall 2015).

The LED LCUs showed “hot-spot” regions in the beam profile images. The variation in location and number of the “hot-spots” in the multiple and single emission peak LED LCUs is due to the variations in the number, location and type of the LED chips within a LCU (Megremis et al. 2014, Michaud et al. 2014, Price et al. 2014, Price, Ferracane, and Shortall 2015, Corciolani et al. 2008).

For BS multiple emission peak LED LCUs, the “hot-spots” in the beam profile images can be explained by the presence of three different LED chips placed within the body of the LCU (Figure 7). BS has its LED chips within its body; therefore, like O, a straight fiber optic light guide is used to transmit the generated light to the light guide tip. When using a longpass filter with the BS LCU, two “hot-spot” regions are evident on the irradiance distribution images (Figures 39, 56, 57 and 60), which correspond to the two blue LED chips with spectral emission peaks around 456 nm (Table 11). When using a shortpass filter, a low irradiance region is visible on the irradiance distribution images, which corresponds to the violet LED chip with a spectral emission peak around 409 nm (Figures 39, 58, 59 and 61). Our findings were supported by the literature (Megremis et al. 2014, Price et al. 2014, Price, Ferracane, and Shortall 2015).

Concerning SM multiple emission peak LED LCU, the variations in mean irradiance values and presence of “hot-spots” in the LED LCU can be attributed to the presence of the two LED chips placed within the light guide head, unlike O and BS (Figure 26). The LED chips in SM are placed in different angles in the head of the light guide aiming to collimate the emitted light at the center of the restoration, which is indicated by the arrows on either side of the light guide tip. When using the longpass filter with the SM LED LCU, one “hot-spot” region is revealed on the irradiance distribution images (Figures 56, 57 and 60), which correspond to one blue LED chip with spectral emission peak around 456 nm (Table 11). The outcomes are supported by the literature (Megremis et al. 2014, Michaud et al. 2014). When using a shortpass filter, a low irradiance region is visible on the irradiance distribution images that corresponds to one violet LED chip with a spectral emission peak around 409 nm (Figures 58, 59 and 61).

Considering V multiple emission peak LED LCU, the differences in mean irradiance values and the existence of "hot-spot" regions in the irradiance distribution images can be explained by the presence of four LED chips (Figure 27). Like SM, the V has all its LED chips within the LCU head. When using a longpass filter with the V LCU, high irradiance regions corresponded to the three blue LED chips, two of which have spectral emission peaks around 439 nm located opposite to each other, and one blue chip with a longer spectral emission peak around 460 nm (Figures 56, 57 and 60, and Table 11). The findings are in agreement with the literature (Megremis et al. 2014, Price, Labrie, et al. 2010, Jandt and Mills 2013). When using a shortpass filter, a low irradiance region is visible on the irradiance distribution images, which corresponds to the violet LED chip with a spectral emission peak around 409 nm (Figures 58, 59 and 61).

Regarding D and DU single emission peak LED LCUs, the variations in mean irradiance values and the presence of "hot-spot" regions in the irradiance distribution images can be justified by the presence of one LED chip and three LED chips within the LCU, respectively. D has its LED chip within the LCU body, like O and BS (Figure 28). DU LCU has the LED chips placed in the light guide head, like SM and V (Figure 29). When using a longpass filter with the single emission peak LED LCUs, the high irradiance regions in D and DU corresponded to one and three blue LED chips, respectively, with a spectral emission peak around 456 nm (Figures 56, 57 and 60, and Table 11). Considering D LED LCU, the higher mean irradiance values observed on the peripheries of the irradiance distribution images (Figures 56, 57 and 60) may be explained by the "Turbo" fiber optic guide tip for D LCU, which has a wider light entry diameter and a smaller light exit diameter, unlike O and BS (Figure 86). The literature reported that the "Turbo" light guide tip tends to emit higher radiant power on the peripheries of the light cone (Corciolani et al. 2008, Nitta 2005).

The average power measurements collected from an integrating sphere/spectrometer assembly (Tables 9 and 10) was performed utilizing the effective light-emitting area of the light guide tip (Figures 11 and 36), and indicated by the superimposed white-circles over the beam

profile images (Figures 56-59). The effective light-emitting area of the light guide tip provides a more accurate LCU power and irradiance fingerprint (Haenel et al. 2015, Price et al. 2014, Michaud et al. 2014, Harlow et al. 2016), compared to collecting the average power or irradiance measurements from a 3.9 mm cosine corrector, or the 4 mm MARC-RC cosine corrector sensors (Figures 13-16), and then applying the value collected over the entire beam profile images (Megremis et al. 2014, Price et al. 2011, Price, Fahey, and Felix 2010).

1.2. LCU spectral emission measurements

Differences in the average irradiance values were detected among the LCUs when using the MARC-RC sensors (Tables 2 and 6, Appendices 1, 8 and 9), and the integrating sphere/spectrometer assembly (Tables 9 and 10). This can be explained by the differences in the light source and spectral distribution curves between the QTH and LED LCUs. For QTH LCUs, The generated light from the light bulb has a broad spectral range, which includes wavelengths needed by most photoinitiators, such as CQ and TPO (Figures 40, 45 and 49, and Table 11). As a result, a QTH LCU is suitable to polymerize most RMCs (Jandt and Mills 2013, Rueggeberg 2011). However, most of the light is dissipated as heat and not utilized for polymerization (Rueggeberg 2011, Jandt and Mills 2013, Stahl et al. 2000). On the other hand, an LED LCU is solid-state semiconductor that directly converts electric energy into light (Rueggeberg 2011, Jandt and Mills 2013, Mills, Jandt, and Ashworth 1999). This makes an LED LCU more efficient because it emits light within a narrow spectral curve range that falls within the maximum absorption spectral range of the photoinitiator (Figure 55). Therefore, less heat is generated in the process. Our results were like other studies in the literature (Rueggeberg 2011, Jandt and Mills 2013, Mills, Jandt, and Ashworth 1999, Megremis et al. 2014, Santini et al. 2012, de Oliveira et al. 2015).

The variations in the irradiance values collected from the 4 mm MARC-RC sensors compared to the integrating sphere/spectrometer assembly, is due to the differences in the

dimensions where the measurements were collected. The optics in V was improved as claimed by the manufacturer. However, the mean irradiance values from V received by the integrating sphere was less than the remaining LED LCUs (Figures 56, 57 and 60, and Table 9).

The differences among the LED LCUs occur because each LED chip type (blue or violet) has a different spectral emission range, and each spectral curve peak varies from one LCU manufacturer to the other (Figures 45, 49 and 55, Table 11). The single emission peak and multiple emission peak LED LCUs have blue LED chips with a narrow wavelength spectral curve. The blue LED chips emit higher irradiance output at the longer blue wavelength region (450-470 nm) that peaks near 460 nm and falls within the maximum CQ absorption range. The multiple emission peak LED LCUs have a blue chip, and an additional violet chip that emits higher irradiance output at the shorter violet wavelength region (400-420 nm) that peaks near 409 nm, which falls within the maximum TPO absorption range (Figure 55). Our findings were supported by the literature (Price, Ferracane, and Shortall 2015, Rueggeberg 2011, Jandt and Mills 2013). Although a QTH LCU has a broad spectral emission, it may not activate TPO as effectively as CQ because it has a lower power output at the TPO region compared to the CQ region (Figure 55). The outcomes are supported by the literature (Rueggeberg 2011, Jandt and Mills 2013, Mills, Jandt, and Ashworth 1999, Dunn and Bush 2002). Consequently, the LED LCUs may provide equivalent RMC polymerization in a shorter curing time because it does not require a lot of energy to activate the photoinitiators within a RMC compared to a QTH LCU (Rueggeberg 2011, Jandt and Mills 2013, Mills, Jandt, and Ashworth 1999, Dunn and Bush 2002).

During the light exposure, the relative contribution from each spectral peak to the total radiant power and irradiance from a LCU differs for the individual LCU (Figure 64 and Tables 9 and 10). Interestingly, SM showed unequal relative contribution from the blue and violet chips, although it has one blue and one violet LED chip (Figure 26). The findings of this study are like

another study that demonstrated differences in radiant power from the LED chips of multiple LCUs (Harlow et al. 2016).

In this study, 5 mm square specimens that were 2 mm in depth were cured while centered over a 4 mm MARC-RC sensor (Figures 14-16, 30 and 31). The 3×3 mm square where the DC and KH measurements were obtained relatively coincided with the 4 mm sensor as approximated by the dashed square (Figure 15). Therefore, the irradiance and RE detected by the top and bottom sensors approximately reflected the irradiance and RE received on the top and bottom surfaces of the specimens, at the location where the DC and KH measurements were obtained, which was one of the specific aims conducted in this study. When the LED LCU were centered over the MARC-RC sensors the "hot-spot" regions from BS, SM and V LCUs were located outside of the collection areas of the sensors, as approximated by the white-squares superimposed over the 2D and 3D beam profiles (Figures 39, 60 and 61). However, D and DU single emission peak LED LCUs had the "hot-spot" regions within the collection areas of the sensors. This means that movement of the light guide tip over the MARC-RC sensor would result in different mean irradiance values being recorded (Megremis et al. 2014, Price, Ferracane, and Shortall 2015, Price et al. 2014, Selig et al. 2015). Localized irradiance differences can be seen within the KH and DC measurement collection areas (Figures 62 and 63, Appendices 11 and 12). Investigating the center of each beam profile area of the light guide tip is a limitation in this study. Nevertheless, the aim of this study was to explore the influence of a non-uniform localized irradiance beam profile on polymerization pattern within a RMC increment, which was demonstrated in the findings of this study regardless of the limited area characterized. In this study, one LCU from each brand was assessed, but it is important to note that different LCUs of the same could perform differently. Nevertheless, evaluating the LCUs quality is beyond the scope of this study.

1.3. Influence of LCU distance on the irradiance and irradiance beam profile

In this study, testing was performed at 2 and 8 mm distances between the light guide tip and the top surfaces of the specimens. Because often the clinical situation does not allow for a 0 mm placement of the LCU with respect to the surface of the restoration; therefore, it is more clinically relevant to evaluate the LCU performance at some distance away from the surfaces of a specimen (Price, Fahey, and Felix 2010, Price et al. 2011). The 2 and 8 mm distances between the light guide tip and top surfaces of the specimens were selected to assess the best and worst clinical case scenarios (Price et al. 2011).

An inverse relationship was demonstrated between irradiance and distance. Increasing the distance between the light guide tip and target surface resulted in decreasing the irradiance values. This was detected in the irradiance measurements collected by the MARC-RC sensor (Figures 46 (a), 47 (a), and 49, Tables 2 and 6), radiant power and irradiance measurement collected using the integrating sphere (Tables 9 and 10, Appendices 11 and 12), and exhibited in the beam profile images (Figures 56-63). In addition, increasing the distance between the light guide tip and the top RMC surfaces had a significant impact on the mean irradiance values recorded. This can be explained by the divergence of the emitted light over a larger surface area with increasing the distance. Furthermore, the reduction in irradiance values occurs because the irradiance is expressed in units of W/m^2 (or $J/s/m^2$, power per unit area). Consequently, increasing the distance between the light guide tip and target surface causes less radiant power from the LCU to strike the target surface, which negatively affects the irradiance measurement. Therefore, increasing the curing time can compensate for the decreased irradiance, and the total amount of light energy deposited on the restoration, or RE (J/m^2, energy per unit area), remains the same. The findings in this study were consistent with the literature (Price et al. 2011, Megremis et al. 2014, Gritsch et al. 2008, Price et al. 2000, Corciolani et al. 2008). Our outcomes has a clinical implication because the clinician may need to increase the curing time when there is a need to increase the distance between the light guide tip and the surface of the restoration.

For each LCU assessed, significantly higher irradiance was delivered at 2 mm compared to 8 mm distance (Table 6, Appendices 9). This may be due to the higher radiant power striking the top surfaces denoted by the increased irradiance measurements collected by the top MARC-RC sensor (Figures 46-49). Furthermore, the significantly higher irradiance of the LED LCUs at 2 mm curing distance compared to the QTH LCU on the top and bottom surfaces may be explained by the higher power output and spectral emission curve of an LED LCU (Rueggeberg 2011, Jandt and Mills 2013).

Another factor that can influence the irradiance values is the entry and exit diameter of the light guide tip. A significantly lower mean irradiance value was detected when using D (Table 6, Appendices 8-10), which has a "Turbo" light guide tip (Figure 28), compared to the remaining LCUs. This can be explained by the entry and exit diameter of the fiber optic light guide tip. Because the light emitted through a fiber optic light guide follows the Law of Specular Reflection, which states that the cone of light generated is reflected outward in a specular manner as illustrated in Figure 88, as well as the literature (Corciolani et al. 2008). Therefore, a "Turbo" light guide tip will generate a wider cone when the tip is close to the surface and a wider cone will be produced as the distance increases between the light guide tip and a target surface (Corciolani et al. 2008).

Based on the study outcomes, the following working hypotheses were accepted: (1) Specific aim 1, phase 1, which stated: The localized irradiance beam profile from one LED LCU at a clinically relevant distance is not uniform compared to one QTH LCU. (2) Specific aims 3 and 4, phase 1, which stated: The localized irradiance beam profiles from multiple LED LCUs at various distances are different.

1.4. Influence of LCU distance on irradiance and curing time pattern

Each LCU exhibited a distinctive pattern in the irradiance reduction and curing time increase with increasing the distance between the light guide tip and the top MARC-RC sensor,

which fit a polynomial trendline (Figures 46-49, Tables 4 and 5). The irradiance pattern findings were similar to another study (Beolchi et al. 2015). Furthermore, each LED LCU exhibited a different power output due to the variations among the LED LCUs (Table 11). The outcomes are supported by the literature (Felix and Price 2003, Corciolani et al. 2008, Price et al. 2000, Price et al. 2011, Megremis et al. 2014, Price, Ferracane, and Shortall 2015). In this study, SM, V and DU LCUs had a relatively similar irradiance and curing time pattern with increasing the distance from the top sensor (Figures 46-48, Table 5). Interestingly, those are the three LCUs with the LED chips placed within the light guide head (Figures 6, 7 and 26-29). This may suggest that the irradiance values can be affected according to the location of the LED chips within a LCU. On the other hand, when keeping the RE constant, BS revealed a relatively consistent curing time (10-11 seconds) up to a 6 mm distance, which is the same curing time instructed by the manufacturer. Therefore, BS irradiance values exhibited the least percent increase in curing time as the distance increases. This may be because BS has a fiber optic guide tip that diffuses the light emitted from the blue and violet LED chips (Figure 87).

The findings of this study has a clinical implication because it suggests that using BS can be convenient for clinicians, since there will be no need to adjust the curing time when there is a need to increase the curing distance up to 6 mm from the surface being light cured, unlike the remaining LCUs. Nevertheless, increasing the curing time to deliver equivalent RE for a given RMC is not a simple task, and an arbitrary approximation of the curing time may result in a restoration receiving insufficient RE. This may lead to unsatisfactory polymerization of a restoration. Therefore, educating practitioners of the association among irradiance, curing time and RE is imperative, specifically since each LCU showed a particular irradiance and curing time pattern. Therefore, manufacturers should report the recommended curing times at multiple clinically relevant distances to guide the clinician to determine the curing time needed for each LCU at each distance. However, it may not be practical for manufacturers to report the curing

times at all clinically relevant distances, reporting the recommended curing time at the best and worst clinically relevant distances can be valuable for clinicians.

2. Characterization of the RMC polymerization pattern

2.1. Influence of the LCU on RMC polymerization

Investigating several material properties using a mapping approach to assess polymerization uniformity may provide a better understanding of polymerization occurring within the RMC. Per the study findings, non-uniform polymerization was demonstrated throughout the RMC. Also, localized polymerization discrepancies among points and depths were detected within the RMC with respect to the DC, KH and CLD, regardless of the curing distance (Figures 42, 43, 65-70, 73-75 and 77, Appendices 13-18, 24-26, 28 and 29). In addition, significant differences with respect to DC, KH and CLD values were exhibited at localized points and at certain depths within the RMC (Figures 71, 76 and 78, Tables 12, 13 and 17-20, Appendices 17-19 and 25-30), and among the average DC, KH and %KH reduction values across each depth, regardless of the curing distance (Tables 3, 6, 14 and 21, Appendices 2, 3, 6, 22 and 36-39). In this study, the RMC, specimen thickness, RE, LCU position, LCU orientation and distance between the RMC and LCU were standardized throughout the entire experiment. Therefore, polymerization pattern discrepancies may be associated with the non-uniform emitted light from the LCU and its interaction within the specimens. However, the findings revealed that the location of the DC, KH, and %KH reduction significant points varied for each LCU at each depth and curing distance (Figures 71, 76, 78, Tables 12, 17 and 18, Appendix 17-19 and 25-30). Interestingly, the polymerization pattern did not reflect the LCU irradiance pattern with respect to DC, KH and %KH reduction maps on the top surfaces of the RMC (Figures 89 and 90). This suggest that factors other than the non-uniform LCU irradiance distribution can impact polymerization pattern, and may influence the rate and quality of the RMC polymerization (Leprince et al. 2013).

Light transmission through a restoration has an impact on its polymerization (Leprince et al. 2013). On the top surfaces, sufficient polymerization was achieved, with respect to the localized and average DC and KH values, regardless of the irradiance values received (Figures 89 and 90, Appendices 23 and 40). For each LCU, the overall average irradiance values collected from the top MARC-RC sensor was greater than 400 mW/cm^2 regardless of the curing distance (Tables 2 and 6, Appendices 9 and 10), which is the minimal irradiance suggested for sufficient polymerization (Rueggeberg, Caughman, and Curtis 1994, Fan et al. 2002, ISO 2004, 2007). Nonetheless, in some regions across a LCU tip, the localized irradiance values were as low as 180 mW/cm^2, but did not necessarily result in unfavorable polymerization at that specific location on the top surfaces. For example, SM had an average irradiance value across its light guide tip of 1532 mW/cm^2 at 2 mm curing distance, when using an integrating sphere/spectrometer assembly (Table 9). However, a localized square on the 3×3 mm area had an irradiance value of 235 mW/cm^2 that decreased to 180 mW/cm^2 at 8 mm curing distance (Figures 89 and 90, Appendix 23 and 40). Nevertheless, polymerization was not compromised at that specific localized point and exhibited sufficient values for DC (59.6%) and KH values (66 kg/mm^2) when similar RE was achieved. This can be explained by the fact that satisfactory polymerization occurred on the top RMC surfaces, because there is no interference between the RMC and the LCU, although some light reflection does take place (Watts and Cash 1994).

As the light passes through the bulk of the restoration, a decreased DC, KH and %KH reduction was detected at localized points (Figures 65-70, 73-75 and 77). In addition, the irradiance and RE received on the bottom was significantly decreased (Table 2 and 6, Appendices 1, 9 and 10). Also, the LCU that showed a higher irradiance value on the top did not necessarily exhibit a higher irradiance on the bottom. These findings indicate that a relatively large proportion of the total amount of light energy deposited on the RMC surface gets absorbed, scattered or reflected when passing through it due to the presence of pigments, photoinitiators and filler particles that can impact light transmission (Leprince et al. 2011, Leprince et al. 2013,

Turssi, Ferracane, and Vogel 2005, Shortall, Palin, and Burtscher 2008, Musanje and Darvell 2006, Ogunyinka et al. 2007). The mean irradiance and RE values detected by the bottom sensor for all LCUs were 85-90% lower than those detected by the top sensor, regardless of the curing distance and irradiance value recorded (Table 2 and 6, Figures 40 and 55, Appendix 1 and 8). This may indicate that the light from all LCUs may have transmitted through the RMC specimens in a similar manner. The non-significant differences in DC, KH and %KH reduction among the points and depths may be because the RE values were kept constant. This may also explain the non-significant difference in RE values on the bottom among the LCUs. Note that the beam profiler software does not export 3D radiant power data; therefore, a dramatic decrease in the localized irradiance values can be expected as the light passes through the specimen to the bottom.

Shade of the RMC also has an influence on light transmission, where lighter and transparent shades transmit light better than darker and opaque shades (Leprince et al. 2013). In this study, the RMC selected was a bleaching shade that is light and opaque relative to the other Tertic EvoCeram shades, which may affect light transmission through the RMC specimens. These observations may translate to RMCs with similar composition, shade and translucency, and the findings may differ to some extent when using different RMCs.

The variation in the size and geometry of the filler particles has an influence on the RMC polymerization pattern because they can hinder light transmission through scattering and refraction that takes place at the resin-filler interfaces (Leprince et al. 2011, Leprince et al. 2013, Turssi, Ferracane, and Vogel 2005, Shortall, Palin, and Burtscher 2008). The literature reported that a large filler particle size (0.05-2 μm) within a RMC decreases light transmission compared to a small filler particle size (Fujita, Ikemi, and Nishiyama 2011). In this study, a nano-hybrid RMC was used with an average filler particle size of 550 nm, which may have affected light transmission because the nanoparticles were less likely to scatter light at the resin-filler interface (Bucuta and Ilie 2014).

Heat generation during the irradiation procedure can impact the localized polymerization (Leprince et al. 2013, Mousavinasab and Meyers 2011). A LCU effectiveness depends on the radiant power and the photons it emits (Soh, Yap, and Siow 2004). However, excessive energy leads to an increase in polymerization shrinkage and heat generation within a restoration (Silikas, Eliades, and Watts 2000, Hofmann, Hugo, and Klaiber 2002). During light irradiation, the RMC absorbs energy and an exothermic polymerization reaction takes place, which increases the temperature of the resin matrix (Leprince et al. 2013, Mousavinasab and Meyers 2011). Regions of higher irradiance could result in a RMC experiencing increased temperature at those locations affecting the rate of polymerization (Price, Ferracane, and Shortall 2015, Leprince et al. 2013). As a result, different regions of a RMC can exhibit different temperature changes when light activated using a LCU with non-uniform irradiance beam profile (Price, Ferracane, and Shortall 2015). This occurs by the conversion of the monomers into polymers at a faster rate due to reaching the Tg at an earlier stage (Leprince et al. 2013). In turn, local viscosity changes of the resin surrounding the filler particles occurs favoring early vitrification. Therefore, the filler particles may cause a decrease in polymer chain mobility, and restrict the diffusion of the free radicals leading to their entrapment, and entrapment of some pendent and unreacted double bonds within the resin matrix (Beun et al. 2009, Leprince et al. 2009, Leprince et al. 2013). Therefore, the variation in size, type and distribution of the inorganic filler particles not only affect light transmission through a RMC restoration, but also influence the monomer mobility and free radicals entrapment within the resin matrix (Leprince et al. 2011, Leprince et al. 2013).

The LCU irradiance and spectral emission wavelengths have an influence on the amount of free radical production (Neumann et al. 2005, Leprince et al. 2013). Consequently, the rate of polymerization is impacted. When using the QTH LCU or the multiple emission peak LED LCUs, differences were detected within the RMC with respect to the DC that did not follow a specific pattern (Figures 73, 74 and 77). However, a gradual decrease in KH and CLD from the top to the bottom of the RMC surfaces was detected (Figures 65-70). This may be partially

explained by the LCU spectral emission wavelengths. When a LCU is turned on, the radiant power strikes the photoinitiator molecules generating free radicals, then, the polymerization reaction starts (Leprince et al. 2013). The degree of photoinitiator activation within a RMC restoration depends on the photoinitiator receiving the appropriate irradiance at the correct wavelength. In this study, the selected RMC contained higher concentrations of TPO compared to CQ. Therefore, the differences in light source, spectral distribution and thermal emission between the QTH LCU and the LED LCUs may have influenced the amount of photons emitted from the LCU (Rueggeberg 2011, Yap et al. 2004). Also, the shorter wavelengths associated with the violet LED chip, with its spectral emission peak around 409 nm and meant to activate the alternative photoinitiator did not affectively reach the bottom of the specimens when using the QTH and multiple emission peak LED LCUs (Figure 40, 49 and 55). This may be due to the Rayleigh scattering of light (Arikawa et al. 1998, Jandt and Mills 2013, Price and Felix 2009). Therefore, less light energy was transmitted from the top to the bottom surface, which can lead to less free radical production and negatively affect polymerization (Lohbauer et al. 2005, Ferracane et al. 1997, Sobrinho et al. 2000, Rueggeberg, Caughman, and Curtis 1994, Manga, Charlton, and Wakefield 1995, Knezevic et al. 2008, Durner et al. 2012, Cook and Standish 1983).

The photoinitiator type, concentration, chemistry and molar absorptivity have an influence on the amount of free radical production, which can affect polymerization rate (Neumann et al. 2005, Leprince et al. 2013). TPO photoinitiator is highly reactive, has a short wavelength range (350-420 nm) that peaks approximately at 380 nm (Figure53), and tends to scatter more light compared to CQ (Leprince et al. 2011, Neumann et al. 2005, Santini et al. 2012). In addition, TPO absorbs more photons, and produces two free radicals without the aid of a co-initiator upon light exposure at the shorter wavelength (violet) region (Leprince et al. 2011, Ikemura and Endo 2010, Neumann et al. 2005). Therefore, TPO produces more radical growth centers, and forms a polymer network at a faster kinetic rate by the earlier onset of autoacceleration and the low radical termination rate compared to CQ (Leprince et al. 2011,

Ikemura and Endo 2010, Neumann et al. 2005, Vaidyanathan et al. 2017). This may lead to increasing free radical entrapment within the resin matrix moving from the top to the bottom of the specimens. Furthermore, free radicals may have been prematurely spent via bimolecular termination before the polymer network is fully established on the deeper parts of the RMC. Ineffective activation of TPO may lead to its leaching to the surrounding environment and causing a greater cytotoxic effect relative to CQ (Manojlovic et al. 2017).

On the other hand, curing specimens with the single emission peak LED LCUs exhibited relatively uniform KH and CLD values compared to the remaining LCUs (Figures 56-71 and 73-78). This suggests that TPO may not have been effectively activated compared to CQ when using the single emission peak LED LCUs, causing its scattering and entrapment within the resin matrix. CQ photoinitiator has a long wavelengths (blue) spectral emission that peaks approximately at 470 nm (Figure 52), which does not scatter as much as TPO (Leprince et al. 2011, Neumann et al. 2005, Santini et al. 2012). Also, CQ needs a co-initiator to generate one free radical upon light exposure at the longer wavelength (blue) region to initiate the polymerization reaction (Ikemura and Endo 2010, Leprince et al. 2011, Neumann et al. 2005). Therefore, CQ may have effectively reached the bottom of the restoration, regardless of the LCU used. The literature reported that resins containing the combined TPO/CQ photoinitiator system tend to entrap more free radicals within the resin matrix (Selig et al. 2015).

The molar absorptivity findings in this study showed the high reactivity and absorbance of TPO compared to CQ at multiple concentrations (Figure 54). The outcomes of this study, as well as the literature, indicate that the highly reactive alternative photoinitiators require minimal radiant power to generate more radical growth centers to start an auto-accelerated polymerization reaction (Rueggeberg 2011, Jandt and Mills 2013, Price et al. 2014, Price, Fahey, and Felix 2010, Leprince et al. 2013). Therefore, the alternative photoinitiators require minimal radiant power to reach an equivalent DC compared to CQ (Rueggeberg 2011, Jandt and Mills 2013, Price et al. 2014, Price, Fahey, and Felix 2010, Leprince et al. 2013). This may explain why typically less

TPO concentration is present within a RMC, and why a multiple emission peak LED LCU typically has fewer violet LED chips compared to the blue LED chips.

Per the outcomes of the study, the working hypothesis was accepted: specific aim 2, phase 2, which stated: The molar absorptivity of TPO is significantly higher than that of CQ.

Localized polymerization discrepancies in the DC, KH and CLD measurements within the specimens may have an influence on the localized stresses generated within a restoration upon cyclic loading. The local modulus of elasticity can be negatively impacted, generating localized stressed between the high and low modulus of elasticity regions. This may compromise the restoration when subjected to loading fatigue, such as those generated from the masticatory forces (Feng and Suh 2007, Leprince et al. 2013, Demarco et al. 2015). This is an important factor since fracture of the restoration is one of the common causes of RMC failure (Rasines Alcaraz et al. 2014, Opdam et al. 2007, Demarco et al. 2015, Astvaldsdottir et al. 2015, Moraschini et al. 2015, Alvanforoush et al. 2016). Our KH outcomes on the top and bottom surfaces are in agreement with a similar study that explored the correlation between the beam profile from a curing light with KH values of different RMCs (Price et al. 2014).

When evaluating the %KH reduction as an indicator for CLD. Larger KH indents were evident after soaking the specimens in ethanol (Fig 41). This may be explained by the fact that the process of soaking a RMC specimen in an organic solvent results in softening the polymer structure (Asmussen and Peutzfeldt 2001b, a, Schneider, Moraes, et al. 2008, Yap et al. 2004). Therefore, regions with less crosslinking increased the swelling of the polymer and had a greater softening effect (Asmussen and Peutzfeldt 2001b, Schneider, Moraes, et al. 2008, Soh and Yap 2004, Yap et al. 2004, Ferracane 2006). This can also explain the rougher RMC surfaces after soaking the specimens in ethanol due to the dissolution of the unreacted components of the resin matrix that resulted in exposing more fillers on the specimen surfaces.

Assessment of the bottom/top hardness ratio is a valuable indicator of curing effectiveness of the RMC specimens. A bottom/top hardness ratio of 80% was suggested as the

minimally acceptable ratio for RMCs (Moore et al. 2008). The outcomes showed that only few or no points that exhibited a bottom/top KH ratios that were less 80%, except when using O and V at 2 mm curing distances, and curing with BS and V at 8 mm curing distances (Figure 80, Appendix 31). The amount of light transmitted through the specimens and localized differences in polymerization and entrapment of free radicals could explain the localized bottom/top KH ratios that were less than 80%. The absence of points that were less than 80% using the single emission peak LED LCUs may indicate that various regions received sufficient irradiance values to effectively activate CQ and generate enough free radicals for satisfactory polymerization from the top to the bottom. However, a bottom/top KH ratio that is greater than 80% did not necessarily indicate that the polymerization was uniform from the top to the bottom (Figures 80 and 81, Table 17, Appendices 31and 32). For instance, curing with DU at 2 mm distance did not show any localized bottom/top KH ratio point that was less than 80%; however, significant differences existed among most of the local points. This further points to the complexity of the polymerization reaction and the suggested impact of polymerization kinetics on the quality of a restoration (Feng and Suh 2007, Leprince et al. 2013). Therefore, calculating only the average bottom/top KH ratios across the top and bottom surfaces of the specimens may not provide complete characterization of the RMC polymerization. For example, the average bottom/top KH ratio was more than 80% for all LCUs except when using O and V at 2 mm curing distance, but the localized bottom/top KH ratios show that using O and V at 2 mm curing distances, in addition to BS and V at 8 mm curing distances had localized bottom/top KH ratios that were less than 80% (Figure 80, Table 21, Appendix 31).

The outcomes showed that the localized DC values within the specimen and the average DC values across each depth were greater than 50%. This indicates that the total amount of light energy deposited on the specimens (10-11 J/cm^2) produced satisfactory conversion of the monomers (Figures 42, 73, 74 and 75, Tables 3, 6 and 21, Appendices 2, 3, 8, 28 and 29). This may be due to the controlled RE throughout the study. Per the results, 0.7 J/cm^2 RE received on

the bottom surface was sufficient for to produce satisfactory DC. Our findings The were similar to a study (Bucuta and Ilie 2014). Furthermore, 0.7 J/cm^2 was sufficient to generate satisfactory bottom/top KH ratios greater than 80% for most LCUs (Table 21, Figure 80, Appendix 31). This has a clinical implication because a clinician may use the manufacturer instructions as a guide to calculate the needed curing time for a given RMC at a given distance. It is important to note that specimen treatment by sectioning, polishing and ultrasonic cleansing, prior to obtaining the DC and KH measurements, could have affected the localized DC and KH values to a certain extent resulting in higher DC and KHN values. Nevertheless, the purpose of this study was to characterize polymerization uniformity within the RMC specimens when cured by the different LCUs, which was clearly demonstrated in the 2D maps and 3D renderings, regardless of the localized high DC and KH values, or the small area assessed.

Regardless of the specimen treatment prior to testing, few random individual DC measurements yielded DC that were less than 50% (Figure 82 and 83, Appendices 24, 33 and 34). The minimum DC values were used to generate the 3D renderings. These DC values were from among all specimens and are not all located in the same specimen. However, the renderings were generated to visualize the location of the minimum DC values. These points were no longer evident when obtaining the average of each localized point, as seen in the 2D and 3D renderings (Figures 73, 74 and 77, Appendix 33). This may indicate that insufficient polymerization can occur at random points. This may be explained by the localized entrapment of the free radicals that could cause insufficient polymerization at specific locations, resulting in regions of unreacted monomers that may leach out into the oral environment (Leprince et al. 2013). As a result, the local integrity of a restoration at those points may be compromised (Leprince et al. 2013). Unsatisfactory polymerization becomes more of a concern when it occurs at the bonding interface layer around the margins of the restoration, because it may create pathways for bacterial invasion that could lead to secondary caries formation. This may ultimately result in premature failure of a RMC restoration. Nevertheless, exploring polymerization effectiveness at the adhesive interface

is beyond the scope of this study. The DC results in this study were like a study that used micro-Raman spectroscopy (Par et al. 2015, Santini et al. 2012). Typically, using micro-Raman spectroscopy to measure the DC, reveals higher DC values compared to using an ATR-FTIR (Durner et al. 2012). These differences are probably due to the infrared intensity (IR) of Raman being comparatively high and yielding a more distinctive C=C band compared to the medium-strong IR intensity in the case of the FTIR (Park et al. 2009). The findings in this study suggest that light penetration through the specimens was not attenuated enough to significantly affect the DC at the bottom of the specimens (Miletic and Santini 2012).

2.2. Influence of distance on the DC, KH and CLD within the RMC

RMC polymerization pattern varies between 2 and 8 mm with respect to DC, KH and CLD within the RMC. Nevertheless, sufficient polymerization was achieved. Also, non-significant differences detected with respect to the DC, KH and %KH reduction values between 2 and 8 mm curing distances across each depth (Tables 6, 14 and 21, Appendices 8-10, 20-22 and 35-39) and at the localized points (Figures 71, 76 and 78, Tables 12, 17 and 18, Appendices 15-19 and 23-30). This may be attributed to the similar RE values received by each specimen. Therefore, adjusting the curing time for the individual LCU at each distance may have allowed sufficient time for the photoinitiators to generate suitable amounts of free radical growth centers for satisfactory polymerization (Price, Ferracane, and Shortall 2015, Haenel et al. 2015).

Regarding %KH reduction, significantly higher average %KH reduction values across the depths were seen when curing at 8 mm compared to 2 mm distance from the specimen using O or V (Table 14). This may be because insufficient light was transmitted to the bottom surfaces denoted by the bottom/top KH ratios, although manufacturers claim that the convex tip design of V collimates the light allowing better light transmission through a RMC increment.

Considering DC, significantly higher average DC values across the depths were detected when curing specimens with SM at 2 mm compared to 8 mm curing distance on the top and

bottom surfaces, and at the depth of 0.5 mm (Table 21). This may be because the blue and violet LED chips are positioned in an angle that may have allowed the emitted light to be more focused at 2 mm curing distance compared to 8 mm curing distance. Therefore, the number of photons hitting a RMC specimen may have been impacted, which can affect the amount of photoinitiators activated and the rate of polymerization. Also, the light transmitted at 2 mm curing distance may have reflected off the bottom MARC-RC sensor more than at 8 mm that resulted in the significant increase in DC at 2 mm distance compared with 8 mm. Curing with a single emission peak LED LCU was not significantly different from the QTH and multiple emission peak LCUs across most depths. This suggests that using a single emission peak LED LCU to light activated the RMC investigated may achieve a relatively similar DC when equivalent RE is provided. Furthermore, significant differences in DC values between the top and bottom surfaces were detected (Table 6) as denoted by the percent change in DC when using the QTH and multiple emission peak LED LCUs. This may be explained by the fact that a dual photinitiator RMC was investigated.

Concerning KH, significant differences were detected between 2 and 8 mm distances for most KH values across each depth for the LCUs, unlike DC and CLD (Table 21). At the various depths assessed, most of the LCUs investigated showed that the average KH values significantly increased on the top surfaces at 8 mm curing distance compared to 2 mm (Tables 6, 14 and 21). This may be partially explained by the early termination of the free radicals at 2 mm curing distance because less curing time was needed to achieve 10-11 J/cm^2. As a result, more radical growth centers were generated with increasing curing time at 8 mm distance (Price, Ferracane, and Shortall 2015, Haenel et al. 2015). Furthermore, a mapping approach was used in this study at specific locations; therefore, the Knoop hardness indenter may have landed at some locations on the organic phase as well as the inorganic phase, which may have resulted in the higher KH values at some locations.

Interestingly, the single emission peak LED LCUs had the lowest DC and KH values, and highest %KH reduction values on the top surface among the LCUs, but the same was not true on

the bottom surface, regardless of the curing distance. This may suggest that light was not attenuated to a degree that compromised polymerization at the bottom surface compared to the remaining LCUs (Miletic and Santini 2012). Also, this could be explained by the reflection of the light off the radiopaque bottom MARC-RC sensor and the white mold used to prepare the specimens, which may have transmitted, reflected, or refracted light off the mold that increased light exposure, which could have increased polymerization on the bottom surfaces (Price, Felix, and Andreou 2006). Our findings agreed with other studies in the literature (Sim et al. 2012, Lucey, Santini, and Roebuck 2015).

The outcomes indicate that the distance and/or LCU may have a significant influence on average irradiance, RE and extent of the DC on the top and bottom surfaces of the specimens (Table 7). Furthermore, distance and/or LCU can have a significant influence on average and localized DC, KH and %KH reduction per the depth within the RMC specimen (Tables 15, 22 and 23). This further demonstrates polymerization kinetics the complexity.

2.3. Collective overview on the influence of LCU beam profile on the localized DC, KH and CLD values within a RMC increment

Based on the collective findings of this study, it is evident that polymerization is a complex process, and does not follow a specific pattern, which varied for each LCU at each distance (Table 27, which is a collective Table from Tables 12, 17 and 18). It is important to note that regardless of the LCU used or curing distance, the location of the significant points across each surface for each testing measure is not necessarily the same.

For each LCU evaluated, there was no LCU that exhibited uniform polymerization from any of the measurements obtained with respect to DC, KH, CLD and bottom/top KH ratio at both curing distances. At 2 mm curing distance, curing with SM followed by BS yielded the most uniformity among points when evaluating the DC, KH, CLD, and bottom/top KH ratios compared to the remaining LCUs. On the other hand, curing with O displayed the least polymerization

uniformity among points when assessing the DC and KH, but not the CLD or the bottom/top KH ratios. However, curing with V and D displayed the least polymerization uniformity among the points when measuring the CLD and the bottom/top KH ratios. At 8 mm curing distance, the multiple LCUs explored did not show similar significant differences among the points for all the measurements evaluated. Furthermore, using BS revealed the least polymerization uniformity among the points for all the measurements assessed.

Based on the explanations in the previous sections, the following working hypotheses were accepted: (1) Specific aim 1, phase 2, which stated: (a) A localized non-uniform irradiance beam profile area from an LED LCU will have an influence on the corresponding DC and CLD mapping on the top, bottom, within different internal locations and at different depths of a 2 mm RMC increment at a clinically relevant distance compared to the relatively uniform QTH LCU. (b) The average irradiance at the center of one LED LCU beam and the corresponding average RE received on the top surfaces of a RMC increment cured by one LED LCU and one QTH LCU at a clinically relevant distance is significantly higher compared to that on the bottom surfaces of a RMC increment. (2) First hypothesis of specific aim 2, phase 1, which stated: The average irradiance of multiple LED LCUs, and the corresponding RE and DC on the top surfaces of a RMC increment at two clinically relevant distances is significantly higher compared to the bottom surfaces of a RMC increment. (3) First hypothesis specific aim 3, phase 2, which stated: A localized non-uniform irradiance beam profile area from multiple LED LCUs has a significant effect on the corresponding CLD mapping within a RMC increment at two clinically relevant distances.

3. Correlations

The outcomes of this study demonstrated that the localized irradiance beam profile differences from a LCU can result in a RMC with non-uniform polymerization within the specimens, which may ultimately affect the overall performance of the restoration, as discussed

throughout this study (Haenel et al. 2015, Price, Ferracane, and Shortall 2015, Price, Felix, and Andreou 2005, Price et al. 2014). Nevertheless, the findings of this study, as well as the literature demonstrated that not every inhomogeneous LCU results in unsatisfactory properties at all regions of the restorations as long as sufficient light irradiance is received by the RMC (Haenel et al. 2015, Price et al. 2014). Therefore, exploring various correlations was worth investigating to provide an insight on the strength of that association, if any.

3.1. Correlation among the average irradiance, RE and DC

The strength of the correlation among the average irradiance, RE and DC across the top and bottom surfaces, is LCU and curing distance dependent (Table 8). Although a general positive strong correlation between the average irradiance and RE values exists, this did not necessarily result in a strong correlation between the average irradiance and DC values, nor between RE and DC. Also, some LCUs at a certain curing distance or on a specific surface (top or bottom) displayed a relatively low correlation compared to the remaining LCUs. The differences in the strength of correlation may be due to the various reasons discussed throughout this dissertation; the differences in the LCU, the method of light transmission through the specimens, photoinitiator system, filler size and shape, shade and translucency of the RMC all are contributing factors to the strength of correlation. It is worth mentioning that the strength of the correlations is dependent on the sample size, so the outcomes may differ to a certain extent if the sample size is increased.

Based on the findings, the following working hypothesis was accepted: second hypothesis of specific aim 2, phase 1, which stated: A correlation among irradiance and the corresponding RE and DC exists, on the top and bottom surfaces of a RMC increment cured by various LED LCUs at multiple clinically relevant distances**.**

3.2. Correlation of the localized irradiance beam profile with DC, KH and %KH reduction on the top surfaces of the RMC specimens

The localized polymerization on the top surface was not compromised, although the irradiance beam from a LCU was weekly correlated to the top surface localized DC, KH and CLD values (Tables 16 and 24). Furthermore, it was evident that the localized irradiance pattern in the area explored was not reflected in the DC, KH and CLD pattern on the top surfaces of the RMC specimens (Figures 89 and 90). This may be explained by variations in the amount of photoinitiator activation, free radical production, and heat generation at the localized points. Note that correlations of the irradiance beam profiles with DC, KH and %KH reduction at the remaining depths could not be accomplished because the beam profile software exports only the 2D radiant power data.

Based on the outcomes, the following working hypotheses were accepted: (1) Second hypothesis of specific aim 3, phase 2, which stated: A correlation exists between a localized non-uniform irradiance beam profile area from multiple LED LCUs at two clinically relevant distances and the corresponding CLD mapping on the top surfaces of a RMC. (2) First two hypotheses of specific aim 4, phase 2, which stated: (a) A correlation exists between the localized irradiance beam profile area from multiple LED LCUs with the corresponding DC and KH mapping on the top surfaces of a RMC at two clinically relevant distances. (b) A correlation exists between the localized DC and KH across various depths of a RMC increment at two clinically relevant distances cured by multiple LED LCUs. (c) A correlation exists between the average DC and KH across various depths of a RMC increment at two clinically relevant distances using multiple LED LCUs.

3.3 Correlation of the localized vs. average DC, KH and %KH reduction values

The correlation among the average among DC, KH and %KH reduction values were generally strong compared to the moderate correlation of the localized DC, KH and %KH

reduction values. In addition, the correlations at each depth varied per the LCU used, curing distance, and whether the average or localized values were used (Tables 24 and 25). This indicates that using the average DC, KH and %KH reduction values across each depth can overestimate the correlation.

Per the outcomes of the studies conducted, the average irradiance, DC, KH, or %KH reduction values across each depth did not accurately characterize polymerization of a RMC due to the various factors that can impact the polymerization reaction. Therefore, obtaining only few DC, KH, and CLD measurements from the top and bottom surfaces of the specimens, as performed by most studies, does not provide a complete characterization of the polymerization pattern compared within a RMC.

Based on the findings, the following working hypotheses were accepted: Second two hypotheses of specific aim 4, phase 2, which stated: (a) A correlation exists between the average DC and KH across various depths of a RMC increment at two clinically relevant distances using multiple LED LCUs. (b) The localized DC and KH correlations are more accurate than the average DC and KH correlations, and the correlations are LCU and distance dependent.

SUMMARY

Based on the findings of the LCU irradiance beam profile area assessed from the LCUs explored and the corresponding polymerization pattern in the RMC investigated, the following can be summarized:

1. Summary outcomes from specific aims 1, 3 and 4

- **SPECIFIC AIM 1**

  The influence of an irradiance beam profile area from one LED LCU and one QTH LCU on the corresponding CLD and DC mapping within a RMC increment

- **SPECIFIC AIM 3**

  The influence of a localized irradiance beam profile area from multiple LED LCUs on the corresponding CLD mapping within a RMC increment

- **SPECIFIC AIM 4**

  The correlation of a localized irradiance beam profile area from multiple LED LCUs with the corresponding KH and DC mapping of a RMC increment

1.1. Summary of the influence of LCU beam profile on RMC polymerization pattern

1. The non-uniform light beam irradiance profiles from the LCUs explored at the area assessed resulted in corresponding localized DC, KH and CLD discrepancies within the RMC, which were significant at specific depths and locations. However, the localized discrepancies did not follow a specific pattern.
2. The DC, KH and CLD polymerization pattern did not reflect each LCU irradiance pattern, regardless of the curing distance.

3. From the LCUs explored, there was no LCU that exhibited the most uniform polymerization with respect to DC, KH and CLD at all depths and at both curing distances evaluated.
4. For each LCU, few significant differences were detected with respect to DC and CLD values between 2 and 8 mm curing distances at specific depths. On the other hand, KH values showed more significant differences between 2 and 8 mm curing distances at each depth.
5. At each curing distance, significant differences were detected among the LCUs when the specimens received similar RE.
6. All LCUs explored demonstrated satisfactory polymerization with respect to DC and KH values at all localized points, except using O and V at 2 mm distance, and BS and V at 8 mm distance that showed localized bottom/top KH ratios that were less than 80%.
7. The single emission peak LED LCUs effectively polymerized the dual photoinitiator RMC assessed.
8. The localized irradiance beam from a LCU was weekly correlated with the corresponding localized DC, KH and CLD, but did not necessarily compromise polymerization on the top surface of the RMC investigated.
9. The localized DC was moderately correlated with the localized KH and CLD within the specimens. On the other hand, the average DC was strongly correlated with the average KH within the specimens, indicating that using the average DC, KH, and CLD values can overestimate the existing correlations within a restoration. Also, the strength of the correlation varied for each LCU, at each depth and at each curing distance.

1.2. Summary of the LCU irradiance and RE received on the bottom RMC surfaces

The LCU irradiance and RE received on the bottom surfaces of the RMC specimens significantly decreased by approximately 90% regardless of the original LCU irradiance and RE value received on the top surfaces.

2. Summary outcomes from specific aim 2

- **SPECIFIC AIM 2**

The influence of distance on irradiance, RE and DC on the top and bottom surfaces of a RMC increment

2.1. Summary of the influence of distance on the LCU irradiance and RE received on the top and bottom RMC surfaces

1. Increasing the curing distance from a top MARC-RC sensor resulted in decreasing the irradiance and increasing the curing time in a pattern that was unique for each LCU.
2. To achieve similar RE, BS LCU showed the most stable curing time as recommended by the manufacturer up to 6 mm distance.
3. Increasing the distance between the light guide tip and top surfaces of the RMC specimens significantly decreased the average irradiance and RE on the bottom surfaces of the RMC specimens compared to the top surfaces. The significant decrease in the LCU average irradiance and RE ranged from 85-93% of its original values, as detected by a bottom MARC-RC sensor for the RMC assessed using the various LCUs explored.

2.2. Summary of the influence of distance on the LCU irradiance and RE received on the top and bottom RMC surfaces

1. For each LCU, curing distance did not have a significant impact on DC for each LCU explored except SM when the RMC specimens received similar RE.

2. At each curing distance, significant differences in DC were detected among the LCUs explored.
3. Achieving similar RE to the RMC specimens at two clinically relevant distances resulted in satisfactory polymerization on the top and bottom surfaces of the RMC specimens with respect to the average DC.
4. For all LCUs explored at two clinically relevant distances, the average irradiance values at the center of each LCU measured using the MARC-RC sensors strongly correlated with RE on the top and bottom surfaces of the specimens. Also, the average DC values revealed a moderate-strong correlation with the average irradiance and RE values on the top and bottom surfaces of the specimens. However, the LCU that showed a strong correlation between irradiance and RE did not necessarily exhibit a strong correlation with DC.
5. Using single emission peak LED LCUs did not compromise polymerization with respect to DC for the RMC explored, regardless of curing distance or RMC surface.
6. The molar absorptivity of the TPO photoinitiator was 20-fold more than the CQ photoinitiator.

CONCLUSION

Based on the outcomes of the studies conducted, the following can be concluded for each specific aim followed by an overall conclusion of the entire study:

- **Specific aims conclusions**

1. SPECIFIC AIM 1

1.1. Specific aim 1 hypotheses

1.1.1. Phase 1

- *The working hypothesis*

  The localized irradiance beam profile from one LED LCU at a clinically relevant distance is not uniform compared to one QTH LCU.

1.1.2. Phase 2

- *The working hypotheses*

1. A localized non-uniform irradiance beam profile area from an LED LCU will have an influence on the corresponding DC and CLD mapping on the top, bottom, within different internal locations and at different depths of a 2 mm RMC increment at a clinically relevant distance compared to the relatively uniform QTH LCU.
2. The average irradiance at the center of one LED LCU beam and the corresponding average RE received on the top surfaces of a RMC increment cured by one LED LCU and one QTH LCU at a clinically relevant distance is significantly higher compared to that on the bottom surfaces of a RMC increment.

1.2. Specific aim 1 conclusions

1. When using either an LED or a QTH LCU, a RMC showed localized differences in DC, KH and %KH reduction that were significant at specific depths and locations.
2. The degree of beam profile uniformity across the light emitting tips at the area investigated of the different LCUs appeared to have a minor influence on DC and percent KH reduction of the RMC material cured by the lights.
3. The RMC cured by the LED LCU demonstrated satisfactory polymerization with respect to DC and KH at all points measured.
4. The 10-11 J/cm^2 and 0.7 J/cm^2 RE received on the top and bottom surfaces of the RMC assessed, respectively, were sufficient for satisfactory polymerization with respect to the localized DC values. However, it was only sufficient to produce satisfactory polymerization with respect to KH for the LED (BS) LCU but not the QTH (O) LCU explored at the curing distance investigated.

2. SPECIFIC AIM 2

2.1 Specific aim 2 hypotheses

2.1.1. Phase 1

- *The working hypotheses*

1. The average irradiance of multiple LED LCUs, and the corresponding RE and DC on the top surfaces of a RMC increment at two clinically relevant distances is significantly higher compared to the bottom surfaces of a RMC increment.
2. A correlation among irradiance and the corresponding RE and DC exists, on the top and bottom surfaces of a RMC increment cured by various LED LCUs at multiple clinically relevant distances**.**

2.1.2. Phase 2

- *The working hypothesis*

The molar absorptivity of TPO is significantly higher than that of CQ.

2.2. Specific aim 2 conclusions

1. The curing time needed to achieve the required RE instructed by the manufacturer when the curing distance was increased exhibited a distinctive pattern for each LCU. This makes it challenging for clinicians to select the needed curing time for satisfactory polymerization activation of RMC restorations when the distance from a restoration is increased.
2. Achieving a similar RE resulted in satisfactory polymerization on the top and bottom surfaces of the RMC explored with respect to DC using the LCUs investigated, although the RMC specimens did not exhibit the same average DC values.
3. The 10-11 J/cm^2 and 0.7 J/cm^2 received on the top and bottom surfaces, respectively, were sufficient for satisfactory polymerization with respect to the DC.
4. A moderate correlation existed between irradiance, RE and DC.
5. The higher molar absorptivity of TPO photoinitiator positively impacted polymerization on the top surfaces of the RMC specimens, with respect to the average DC values when a QTH or a multiple emission peak LED LCU was used.

3. SPECIFIC AIM 3

3.1. Specific aim 3 hypotheses

3.1.1. Phase 1

- *The working hypothesis*

The localized irradiance beam profiles from multiple LED LCUs at various distances are different.

3.1.2. Phase 2

- *The working hypotheses*

    1. A localized non-uniform irradiance beam profile area from multiple LED LCUs has a significant effect on the corresponding CLD mapping within a RMC increment at two clinically relevant distances.
    2. A correlation exists between a localized non-uniform irradiance beam profile area from multiple LED LCUs at two clinically relevant distances and the corresponding CLD mapping on the top surfaces of a RMC.

3.2. Specific aim 3 conclusions

1. The degree of non-uniform irradiance beam from the LCUs explored was not reflected in the localized CLD pattern within the RMC assessed and exhibited a non-specific pattern that varied at each curing distance.
2. The localized irradiance beam profile area assessed was weekly correlated with the corresponding CLD on the top surfaces of the specimens.

4. SPECIFIC AIM 4

4.1. Specific aim 4 hypotheses

4.1.1. Phase 1

- *The working hypothesis*

    The localized irradiance beam profiles from multiple LED LCUs at various distances are different.

4.1.2. Phase 2

- *The working hypotheses*

    1. A correlation exists between the localized irradiance beam profile area from multiple LED LCUs with the corresponding DC and KH mapping on the top surfaces of a RMC at two clinically relevant distances.
    2. A correlation exists between the localized DC and KH across various depths of a RMC increment at two clinically relevant distances cured by multiple LED LCUs.
    3. A correlation exists between the average DC and KH across various depths of a RMC increment at two clinically relevant distances using multiple LED LCUs.
    4. The localized DC and KH correlations are more accurate than the average DC and KH correlations, and the correlations are LCU and distance dependent.

4.2. Specific aim 4 conclusions

1. The non-uniform irradiance from the LCUs was weakly correlated with the corresponding KH and DC of the top surface of a RMC.
2. The localized KH was moderately correlated with the corresponding DC within a RMC, regardless of the curing distance.
3. The average KH was strongly correlated with the corresponding DC within a RMC, regardless of the curing distance.
4. Using the average KH and DC values overestimated the existing correlation.

- **Overall conclusions**

1. This study showed that multiple testing measurements are necessary to provide a more accurate characterization of polymerization pattern.
2. A mapping approach within the specimens provided detailed characterization and assessment of the RMC polymerization patterns compared to using the average values across the surfaces.
3. The non-uniform irradiance beam profiles from the various LCUs explored were weakly correlated with the DC, KH and CLD, and did not strongly reflect the LCU irradiance pattern. Also, it seems to have a minor influence on the significant localized polymerization discrepancies that did not follow a specific pattern.
4. There was no LCU among the LCUs explored that demonstrated uniform polymerization at all localized points assessed with respect to DC, KH and CLD of the RMC investigated and at both curing distances.

- **Future research direction**

Future direction for this research includes exploring the influence of the entire LCU beam profile area on polymerization pattern using multiple RMCs with various compositions and shades. Also, investigating the influence of a LCU beam profile on various RMC mechanical properties and longevity through testing fatigue and fracture of a RMC restoration should occur.

CLINICAL IMPLICATIONS

Within the limitation of the *in vitro* studies conducted, the following clinical implications can be extrapolated:

1. The area assessed of the LCUs explored do not result in uniform polymerization within a dual photoinitiator RMC restoration, which may potentially increase the risk of RMC fracture.
2. From the area assessed of the LCU explored, achieving similar RE values based on the manufacturer instructions of the RMC can result in satisfactory polymerization within a restoration. This information could be a helpful guide for clinicians if manufacturers reported enough details to effectively guide polymerization of different RMCs using various LCUs at multiple clinically relevant distances.
3. There is potential benefit for practitioners to request from manufacturers a curing protocol guide for a given RMC using various LCUs at multiple clinically relevant distances in an attempt to effectively activate RMC polymerization.

TABLES

Table 1. The LCUs explored and materials used in this study

Device/Material	Device/Material type	Brand	Manufacturer
LCU	QTH	Optilux 401	Kerr, Orange, CA
	Multiple emission peak LED	Bluephase Style	Ivoclar Vivadent, Amherst, NY
		SmartLite Max	Densply, York, PA
		VALO Cordless	Ultradent, South Gordon, UT
	Single emission peak LED	DEMI	Kerr, Orange, CA
		Demi Ultra	Kerr, Orange, CA
RMC	Nano-hybrid	Tetric EvoCeram bleaching shade XL	Ivoclar Vivadent, Amherst, NY Lot# T25427
Photoinitiator	Common	CQ	Sigma-Aldrich, St. Louis, MO Lot#09003AQ)
	Alternative	TPO	Tokyo Chemical Industry Co., Tokyo, Japan Lot# N74HG-CB
Ethanol	Absolute ethanol		Sigma-Aldrich, St. Louis, MO Lot# SHBF5121V
Methanol	Methanol		Fisher Scientific, Fair Lawn, NJ Lot#112195

Table 2. Mean (SD) irradiance (mW/cm^2) and RE (J/cm^2) detected by the top and bottom MARC-RC sensors and received on the top and bottom RMC surfaces cured at 2 mm distance by an LED (BS) LCU and a QTH (O) LCU

MARC-RC Sensor	LCU	Irradiance (mW/cm^2)	RE (J/cm^2)
Top	LED	1008 (27)*	10.3 (0.1)
	QTH	775 (30)	10.4 (0.1)
Bottom	LED	104.6 (1.2)*	1.1 (0.01)
	QTH	82.2 (2.4)	1.1 (0.04)

The top sensor of the MARC-RC recorded the irradiance and RE delivered to the top surface of the RMC specimens at 2 mm distance. The bottom sensor recorded the amount of irradiance and RE passing through the 2 mm RMC specimens at 2 mm distance between the top of the specimen and light guide tip.

*Represent significant differences between the LCUs in the same column for each MARC-RC sensor.

Table 3. Mean (SE) DC (%), KH-BE, KH-AE (kg/mm^2) and %KH reduction for the RMC light cured using an LED (BS) LCU and a QTH (O) LCU at 2 mm curing distance

Depth (mm)	DC (%)		KH-BE (kg/mm^2)		KH-AE (kg/mm^2)		%KH reduction	
	LED	QTH	LED	QTH	LED	QTH	LED	QTH
T (0)	69.6 (0.4)^{a}	74.0 (0.4)^{a}*	59.7 (1.4)^{ac}	60.9 (0.4)^{a}	39.2 (1.3)^{a}	40.4 (0.4)^{a}	34.4 (1.4)^{c}	33.6 (0.7)^{e}
0.5	70.2 (1.8)^{ab}	68.8 (1.3)^{abcd}	58.2 (0.8)^{ab}	58.1 (0.3)^{b}	33.4 (0.4)^{b}	35.0 (0.6)^{b}	42.6 (0.4)^{ab}*	39.7 (0.7)^{d}
0.7	68.7 (0.6)^{a}	66.9 (1.4)^{bcd}	56.2 (0.5)^{cd}	57.3 (0.3)^{b,c}	31.5 (0.5)^{bc}	32.8 (0.5)^{c}	44.0 (0.7)^{ab}	42.7 (1.2)^{cd}
0.9	67.9 (1.1)^{ab}	67.2 (1.2)^{bc}	54.0 (0.5)^{e}	57.4 (0.02)^{bc}*	29.8 (0.6)^{d}	30.7 (0.3)^{d}	44.7 (1.2)^{ab}	46.5 (0.5)^{b}
1.1	66.7 (0.3)^{b}	66.8 (0.9)^{c}	54.1 (0.3)^{ce}	57.0 (0.6)^{b}*	29.1 (0.9)^{cd}	29.9 (0.5)^{d}	46.2 (1.9)^{b}	47.4 (0.9)^{abc}
1.3	68.7 (0.9)^{ab}*	62.6 (0.4)^{d}	53.5 (0.5)^{bde}	55.4 (0.5)^{cd}	27.8 (0.7)^{e}	29.0 (0.7)^{de}	48.1 (1.8)^{a}	47.7 (1.0)^{ab}
1.5	67.7 (1.0)^{ab}	66.1 (0.8)^{c}	52.3 (0.2)^{f}	54.2 (0.2)^{d}*	26.9 (0.7)^{f}	28.0 (0.2)^{e}	48.6 (1.2)^{ab}	48.2 (0.2)^{a}
B (2)	67.3 (0.3)^{abB}	70.4 (0.1)^{b}*	56.1 (2.3)^{abcdef}*	43.8 (1.7)^{e}	28.5 (0.9)^{cdef}*	24.3 (0.6)^{f}	48.9 (3.8)^{ab}	44.4 (1.0)^{abc}

Lowercase superscript letters represent significant differences within the same column. *Asterisk represents significant differences between the LED and QTH LCUs within the same testing property at each depth. Abbreviations: T, top; B, bottom.

Table 4. Curing times (seconds) needed to achieve 10-11 J/cm^2 RE from the LCUs explored at multiple distances (mm) as detected by the top MARC-RC sensor

LCU	Distance (mm)				
	0	2	4	6	8
O	11	14	14	17	20
BS	10	10	10	11	15
SM	6	8	12	17	22
V	8	7	11	15	19
D	10	10	12	16	20
DU	8	8	12	17	22

Table 5. Regression trendline, R^2 and percent increase in curing time and percent decrease in irradiance to achieve 10-11 J/cm^2 RE from the LCUs explored as detected by the top MARC-RC sensor

LCU	Irradiance			Curing time		
	% Decrease between 2 and 8 mm distances	Polynomial trendline	R^2	% Increase between 2 and 8 mm distances	Polynomial trendline	R^2
O	37	$y = 0.7906x^2 - 57.746x + 906.66$	0.99764	43	$y = 0.0536x^2 + 0.6214x + 11.429$	0.95604
BS	33	$y = -9.6414x^2 + 35.712x + 1034.9$	0.98473	50	$y = 0.1607x^2 - 0.7357x + 10.286$	0.95137
SM	67	$y = 16.033x^2 - 296.7x + 1766.5$	0.99972	175	$y = 0.125x^2 + 1.05x + 5.8$	0.99767
V	62	$y = -1.9668x^2 - 99.415x + 1395.7$	0.90841	171	$y = 0.1786x^2 + 0.0714x + 7.4286$	0.97143
D	53	$y = -8.8953x^2 + 4.1383x + 971.06$	0.99677	100	$y = 0.1786x^2 - 0.1286x + 9.8286$	0.99392
DU	68	$y = -4.3207x^2 - 93.462x + 1403.5$	0.94029	175	$y = 0.1964x^2 + 0.2786x + 7.5714$	0.98874

Table 6. Mean (SE) irradiance (mW/cm^2), RE (J/cm^2), DC (%) and percent decrease in irradiance, RE and DC between the top and bottom surfaces of the RMC specimens

		Irradiance (mW/cm^2)		RE (J/cm^2)		DC (%)	
Surface	LCU	2 mm	8 mm	2 mm	8 mm	2 mm	8 mm
T	O	765.49 (12.11)^{aF}	529.14 (6.03)^{bB}	10.63 (0.16)^{aAB}	10.08 (0.13)^{bBC}	69.53 (0.18)^{aB}	69.33 (0.57)^{aA}
	BS	1023.84 (1.10)^{aD}	696.01 (0.88)^{bA}	10.34 (0.04)^{aAB}	10.29 (0.21)^{aABC}	68.35 (0.48)^{aABC}	67.31 (0.23)^{aA}
	SM	1232.90 (33.65)^{aC}	445.63 (3.33)^{bC}	9.72 (0.24)^{aCD}	9.89 (0.08)^{aC}	70.28 (0.03)^{aA}	67.34 (0.58)^{bAB}
	V	1416.81 (12.41)^{aA}	536.42 (9.41)^{bB}	10.06 (0.04)^{bC}	10.81 (0.19)^{aA}	70.06 (0.75)^{aAB}	67.65 (0.66)^{aAB}
	D	1004.54 (5.71)^{aE}	387.93 (2.95)^{bE}	10.26 (0.05)^{aBD}	10.44 (0.10)^{aAB}	65.33 (0.62)^{aD}	66.04 (0.20)^{aBC}
	DU	1369.49 (1.63)^{aB}	433.96 (2.13)^{bD}	10.54 (0.10)^{aA}	9.83 (0.05)^{bC}	65.78 (0.80)^{aCD}	64.80 (0.57)^{aC}
B	O	82.78 (1.18)^{aD}	64.60 (1.39)^{bB}	1.152 (0.017)^{aA}	1.153 (0.037)^{aC}	66.03 (0.60)^{aA}	64.34 (0.76)^{aABC}
	BS	104.33 (1.67)^{aB}	84.64 (0.85)^{bA}	1.046 (0.019)^{bC}	1.255 (0.015)^{aB}	65.88 (0.10)^{aA}	65.96 (0.76)^{aABC}
	SM	134.63 (4.14)^{aA}	58.52 (0.56)^{bC}	1.065 (0.022)^{bBC}	1.296 (0.017)^{aB}	66.41 (0.18)^{aA}	63.21 (0.33)^{bC}
	V	104.22 (0.94)^{aB}	65.36 (1.12)^{bB}	0.743 (0.007)^{bE}	1.285 (0.029)^{aB}	64.87 (0.48)^{aAB}	66.06 (0.26)^{aA}
	D	91.53 (1.50)^{aC}	55.92 (1.03)^{bC}	0.929 (0.016)^{bD}	1.506 (0.031)^{aA}	63.68 (0.49)^{aB}	64.87 (0.26)^{aB}
	DU	144.05 (1.59)^{aA}	64.12 (0.36)^{bB}	1.106 (0.016)^{bAB}	1.428 (0.015)^{aA}	65.10 (0.56)^{aAB}	64.69 (0.70)^{aABC}
% Decrease	O	89.2*	87.8*	89.2*	88.6*	5.0*	7.2*
	BS	89.8*	87.8*	89.9*	87.8*	3.6*	2.0
	SM	89.1*	86.9*	89.0*	86.9*	5.5*	6.1*
	V	92.6*	87.8*	92.6*	88.1*	7.4*	2.4
	D	90.9*	85.6*	90.9*	85.6*	2.5	1.8
	DU	89.5*	85.2*	89.5*	85.5*	1.0	0.2

The irradiance and RE measurements were collected from a MARC-RC system. The top MARC-RC sensor recorded the irradiance and RE values received on the top surfaces of the RMC specimens at 2 and 8 mm distances from the top surfaces of the specimens. The bottom MARC-RC sensor detected the irradiance and RE values passing through the 2 mm RMC increment specimens at 2 and 8 mm distances from the top surfaces of the specimens. The DC measurements were collected from the top and bottom surfaces of the RMC specimens using micro-Raman spectroscopy. Superscript lowercase letters represent significant differences between 2 and 8 mm curing distances for each measurement. Superscript uppercase letters represent significant differences between the LCUs for each surface. *Represent significant differences between top and bottom surfaces for each LCU at each curing distance. Abbreviations: T, top; B, bottom.

Table 7. ANOVA table of the effect of the LCUs and curing distances on irradiance (mW/cm^2), RE (J/cm^2) and DC (%) on the top and bottom surfaces of the RMC specimens

Measurement	Surface	Effect	Num DF	Den DF	F Value	p-value	Significance
Irradiance	T	distance	1	9.8	8842.27	0.0000	*
		LCU	5	11.9	954.79	0.0000	*
		LCU*distance	5	11.9	8361.59	0.0000	*
	B	distance	1	16.3	2222.33	0.0000	*
		LCU	5	13.6	191.77	0.0000	*
		LCU*distance	5	13.6	187.30	0.0000	*
RE	T	distance	1	29.7	0.23	0.6360	
		LCU	5	12.0	4.26	0.0183	*
		LCU*distance	5	12.0	11.92	0.0003	*
	B	distance	1	36.3	636.13	0.0000	*
		LCU	5	13.8	40.08	0.0000	*
		LCU*distance	5	13.8	40.72	0.0000	*
DC	T	distance	1	15.6	14.02	0.0018	*
		LCU	5	4.6	22.99	0.0026	*
		LCU*distance	5	4.6	4.35	0.0737	
	B	distance	1	15.0	2.61	0.1269	
		LCU	5	7.0	3.32	0.0742	
		LCU*distance	5	7.0	13.78	0.0016	*

Abbreviations: T, top; B, bottom.

Table 8. Correlation among the irradiance (Irr) (mW/cm^2), RE (J/cm^2) and DC (%) on the top and bottom surfaces of the RMC specimens light cured using the LCUs explored at 2 and 8 mm distances

		2 mm			8 mm		
LCU	Surface	Irr-RE	Irr-DC	RE-DC	Irr-RE	Irr-DC	RE-DC
O	T	-0.73	-0.17	-0.55	0.87	0.79	0.39
	B	0.94	0.73	0.46	0.99	-0.62	-0.51
BS	T	-0.16	-0.97	-0.10	0.92	-1.00	-0.88
	B	0.90	1.00	0.91	0.98	0.99	1.00
SM	T	0.92	-0.88	-1.00	0.96	-0.47	-0.22
	B	1.00	-0.52	-0.45	1.00	-0.33	-0.35
V	T	0.57	0.27	-0.63	1.00	0.94	0.95
	B	1.00	0.38	0.34	0.99	-0.75	-0.67
D	T	1.00	0.95	0.92	0.14	-0.63	0.68
	B	1.00	-1.00	-1.00	0.99	-0.59	-0.46
DU	T	-1.00	-0.52	0.56	0.13	0.52	-0.78
	B	0.87	0.66	0.21	0.99	0.56	0.42

Abbreviations: T, top; B, bottom.

Table 9. Mean (SD) radiant power (mW) and irradiance (mW/cm^2) from the QTH and multiple emission peak LED LCUs explored at various spectral ranges and distances using the integrating sphere/spectrometer assembly

Measurement	Spectrum (nm)	LCU	Distance (mm)				
			0	2	4	6	8
Power	380-700	O	579.0 (1.4)	540.0 (1.4)	492.4 (3.3)	439.6 (2.9)	392.7 (1.9)
		BS	647.9 (0.2)	575.1 (0.7)	502.2 (0.5)	421.1 (0.3)	343.8 (0.1)
		SM	853.1 (3.5)	750.9 (2.7)	624.9 (2.9)	535.9 (2.0)	422.9 (1.6)
		V	527.7 (0.3)	497.7 (0.6)	451.8 (0.1)	387.1 (0.1)	321.2 (0.6)
	425-700	O	460.3 (1.2)	425.6 (2.2)	393.7 (1.9)	356.0 (2.5)	318.0 (1.7)
		BS	536.9 (0.1)	483.4 (0.3)	423.8 (0.8)	355.7 (0.0)	291.0 (0.7)
		SM	617.4 (1.9)	552.8 (2.3)	477.1 (4.1)	398.1 (2.2)	318.1 (2.0)
		V	422.8 (0.1)	397.8 (0.4)	358.8 (0.2)	305.4 (0.0)	251.6 (0.1)
	380-425	O	116.0 (0.8)	106.8 (1.0)	96.6 (0.3)	85.3 (0.5)	74.8 (0.2)
		BS	111.9 (0.2)	92.8 (0.1)	78.2 (0.3)	64.8 (0.1)	53.1 (0.1)
		SM	233.6 (0.9)	204.2 (0.6)	161.1 (0.4)	136.4 (0.2)	102.7 (0.4)
		V	104.8 (0.1)	99.7 (0.1)	92.9 (0.1)	81.5 (0.2)	69.5 (0.0)
Irradiance	380-700	O	632.4 (1.6)	589.7 (1.6)	537.8 (3.6)	480.1 (3.2)	428.9 (2.1)
		BS	1019.0 (0.2)	904.5 (1.1)	789.8 (0.8)	662.3 (0.5)	540.7 (0.2)
		SM	1741.1 (7.0)	1532.4 (5.6)	1275.3 (6.0)	1093.6 (4.0)	863.1 (3.4)
		V	714.4 (0.4)	673.8 (0.9)	611.8 (0.1)	524.1 (0.1)	434.9 (0.8)
	425-700	O	502.7 (1.3)	464.8 (2.4)	430.0 (2.1)	388.8 (2.8)	347.3 (1.9)
		BS	844.4 (0.1)	760.2 (0.5)	666.5 (1.3)	559.4 (0.0)	457.6 (1.0)
		SM	1259.9 (4.0)	1128.2 (4.7)	973.8 (8.3)	812.4 (4.6)	649.2 (4.1)
		V	572.4 (0.2)	538.6 (0.6)	485.7 (0.3)	413.5 (0.0)	340.6 (0.1)
	380-425	O	126.7 (0.9)	116.6 (1.0)	105.5 (0.4)	93.1 (0.5)	81.7 (0.2)
		BS	175.9 (0.3)	146.0 (0.2)	123.0 (0.4)	101.9 (0.2)	83.5 (0.1)
		SM	476.8 (1.8)	416.6 (1.2)	328.8 (0.7)	101.9 (0.2)	209.5 (0.7)
		V	141.9 (0.1)	135.0 (0.2)	125.8 (0.2)	110.3 (0.2)	94.1 (0.0)

The irradiance values were calculated using the active light guide tip dimension for each LCU and the corresponding average radiant power value for the individual LCU collected using an integrating sphere/spectrometer assembly.

Table 10. Mean (SD) radiant power (mW) and irradiance (mW/cm^2) measurements from the pulsating single emission peak LED LCUs over the full spectral range (380-700 nm) at multiple curing distances

	LCU		Distance (mm)				
			0	2	4	6	8
Power	D	Max	406.5 (0.7)	378.2 (0.9)	314.9 (2.7)	243.1 (1.2)	177.9 (1.8)
		Min	335.6 (0.2)	309.4 (0.3)	252.3 (1.7)	192.7 (0.7)	140.9 (0.7)
		Mean	371.1 (0.4)	343.8 (0.6)	283.6 (2.2)	217.9 (0.9)	159.4 (1.2)
	DU	Max	539.7 (0.8)	474.8 (0.5)	383.7 (0.4)	299.3 (0.8)	232.2 (1.2)
		Min	471.1 (2.3)	407.7 (2.6)	320.3 (9.1)	252.2 (0.3)	194.9 (0.4)
		Mean	505.4 (1.6)	441.3 (1.3)	352.0 (4.4)	275.7 (0.3)	213.5 (0.8)
Irradiance	D	Max	945.6 (1.5)	879.7 (2.1)	732.5 (6.4)	565.6 (2.8)	413.9 (4.3)
		Min	780.8 (0.4)	719.7 (0.6)	587.0 (3.9)	448.4 (1.5)	327.9 (1.5)
		Mean	863.2 (0.9)	799.7 (1.3)	659.7 (5.1)	507.0 (2.0)	370.9 (2.9)
	DU	Max	1074.3 (1.7)	945.1 (1.0)	763.7 (0.9)	595.6 (1.6)	462.2 (2.4)
		Min	937.6 (4.7)	811.6 (5.2)	637.6 (18.2)	502.1 (0.7)	387.9 (0.7)
		Mean	1006.0 (3.2)	878.3 (2.5)	700.6 (8.9)	548.9 (0.7)	425.0 (1.5)

The average radiant power measurements from the individual LCU collected at each distance over the full spectral range using an integrating sphere/spectrometer assembly. Since the single emission peak LED LCUs are pulsating, the average radiant power values were calculated to show the maximum, minimum and mean power collected from the full spectrum for each LCU. The "mean" power was applied to the corresponding beam profile image collected from the longpass filter using the effective light-emitting area to generate the calibrated irradiance maps. The irradiance values were calculated using the average radiant power values and the corresponding effective light-emitting area.

Table 11. Characterization of the LCUs explored

Effective light-emitting diameter (mm), number and type of the LED chips, spectral distribution and peaks at the long and short spectral range (nm) from the LCUs explored

LCU		Effective light-emitting diameter (mm)	Number of LED chips		Long wavelength spectrum (nm)		Short wavelength spectrum (nm)	
			Blue	Violet	Range	Peak	Range	Peak
QTH	O	10.8	-	-	390-520	487	-	-
Multiple emission peak LED	BS	9	2	1	418-517	456	378-418	408
	SM	*area=49 mm^2	1	1	418-515	450	380-420	400
	V	9.7	2	1	417-520	450	377-417	396
			1 longer blue			460		
Single emission peak LED	D	7.4	1	-	417-520	456	-	-
	DU	8	3	-	417-520	468	-	-

*area value provided by the manufacturer.

Table 12. Number of localized significant comparisons (*) among the %KH reduction measurement points (x-y coordinates) of the RMC specimens at each depth and curing distance using the LCUs explored

Depth (mm)	*no. of comparisons	Distance (mm)	O	BS	SM	V	D	DU
Top	1,224	2	100	50	48	10	55	65
		8	8	107	29	45	130	32
0.5	104	2	0	9	4	6	3	10
		8	1	4	5	12	8	0
0.7	104	2	0		0	7	8	4
		8	1	6		12	15	0
0.9	104	2	10	4	2		0	10
		8	3	10	3	1	25	1
1.1	104	2	7	3	4	14	11	1
		8	14		10	0	6	
1.3	104	2	3	4	0	13	21	12
		8		1	5	0	33	4
1.5	104	2	12	0	1	1	4	3
		8	2	7	0	0	0	
Bottom	104	2	159	38	22	76	158	42
		8	39	93	74	16	65	80
All	3,288	2	303	108	82	128	264	150
		8	70	235	126	86	282	117

*1,224 comparisons among measurement points on the top or bottom surfaces/LCU/distance.

*104 comparisons among measurement points across each depth/LCU/distance.

*3,288 sum comparisons from all measurements across each surface and depth/LCU/distance.

Fewer significant differences indicate that a more consistent %KH reduction was observed across the specimen for a LCU at any given depth. Missing entries in the table were due to lack of convergence for the model.

Table 1. ANOVA table for the %KH reduction significant of x, y and x-y coordinates using the individual LCU across each depth at 2 and 8 mm curing distances

LCU	Depth (mm)	Distance (mm)	Effect	Num DF	Den DF	F-Value	p-value
O	0.9	2	y	2	30.0	3.41	0.0462
	1.3	8	y	2	30.0	3.94	0.0302
	B	2	x	8	100.0	2.56	0.0139
	B	2	y	8	100.0	3.08	0.0038
	B	8	x	8	40.7	2.24	0.0443
BS	0.5	2	y	2	30.0	4.24	0.0238
	0.7	8	y	2	9.3	4.96	0.0341
	0.9	8	y	2	16.6	4.79	0.0227
	B	2	x*y	32	52.3	1.93	0.0169
	B	8	x	8	21.1	2.43	0.0489
SM	B	8	x	8	100.0	2.13	0.0395
V	0.5	8	x*y	8	17.9	2.98	0.0262
	0.7	2	x	4	25.8	5.44	0.0026
	0.7	8	y	2	7.6	9.51	0.0085
	1.1	2	x	4	22.0	2.95	0.0428
D	T	8	y	8	100.0	3.45	0.0015
	0.7	2	y	2	30.0	5.01	0.0133
	0.7	8	y	2	10.9	11.14	0.0023
	0.9	8	x	4	13.5	4.94	0.0114
	0.9	8	y	2	10.8	4.41	0.0397
	0.9	8	x*y	8	15.4	2.98	0.0316
	1.3	2	y	2	9.6	6.05	0.0198
	1.3	8	y	2	10.5	14.01	0.0011
	1.5	2	y	2	14.2	6.22	0.0114
	B	2	x	8	39.9	3.58	0.0032
DU	1.5	2	y	2	24.2	3.60	0.0430

Abbreviations: T, top; B, bottom.

Table 2. Mean (SD) KH-BE, KH-AE (kg/mm^2) and %KH reduction of the RMC specimens across each depth at 2 and 8 mm curing distances using the LCUs explored

		%KH reduction		KH-BE		KH-AE	
Depth (mm)	LCU	2 mm	8 mm	2 mm	8 mm	2 mm	8 mm
T	O	33.4 (0.7)^{c}	46.7 (6.0)^{abc}	60.8 (0.4)	60.4 (1.4)	40.4 (0.4)	32.2 (4.1)
	BS	34.3 (1.4)^{bc}	33.6 (1.7)^{c}	59.7 (1.4)	60.8 (0.1)	39.2 (1.3)	40.3 (1.0)
	SM	38.6 (1.2)^{b}	38.7 (0.4)^{c}	60.9 (0.8)	66.1 (0.1)	37.3 (1.0)	40.4 (0.3)
	V	35.4 (1.7)^{bc}	42.7 (1.0)^{b}*	59.0 (0.7)	60.3 (0.3)	38.1 (1.2)	34.5 (0.7)
	D	50.4 (0.8)^{a}	49.8 (0.8)^{a}	53.7 (0.5)	54.6 (0.8)	26.6 (0.4)	27.4 (0.8)
	DU	50.0 (1.8)^{a}	51.2 (0.6)^{a}	48.8 (0.9)	53.8 (0.9)	24.3 (1.3)	26.2 (0.2)
0.5	O	39.7 (0.7)^{d}	39.5 (2.6)^{ab}	58.1 (0.3)	60.8 (0.4)	35.0 (0.6)	36.8 (1.7)
	BS	42.4 (0.4)^{c}	41.5 (2.8)^{ab}	58.2 (0.8)	62.8 (0.9)	33.4 (0.4)	36.8 (2.0)
	SM	39.1 (2.5)^{bcd}	42.3 (1.1)^{b}	60.5 (1.3)	67.1 (0.4)	36.7 (0.9)	38.6 (0.5)
	V	40.7 (2.2)^{bcd}	42.0 (0.5)^{b}	60.5 (0.8)	65.9 (0.9)	35.9 (1.7)	38.2 (0.8)
	D	50.7 (0.7)^{a}	49.1 (0.6)^{a}	53.5 (0.4)	62.8 (0.6)	26.3 (0.2)	31.9 (0.4)
	DU	48.1 (1.0)^{ab}	45.7 (1.9)^{ab}	51.7 (0.4)	61.2 (2.0)	26.8 (0.4)	33.0 (1.1)
0.7	O	42.7 (1.2)^{c}	41.8 (1.9)^{ab}	57.3 (0.3)	59.2 (0.4)	32.8 (0.5)	34.4 (1.3)
	BS	43.9 (0.7)^{bc}	41.8 (1.5)^{b}	56.2 (0.5)	62.2 (1.2)	31.5 (0.5)	36.2 (1.5)
	SM	40.5 (2.4)^{abc}	42.9 (0.6)^{ab}	59.7 (1.2)	66.0 (0.4)	35.4 (0.7)	37.6 (0.6)
	V	41.9 (1.8)^{bc}	44.1 (0.7)^{ab}	58.6 (0.8)	64.7 (1.1)	34.0 (1.5)	36.1 (1.1)
	D	50.5 (0.1)^{a}	48.9 (1.8)^{a}	53.1 (0.5)	62.2 (1.3)	26.3 (0.3)	31.7 (0.5)
	DU	47.7 (1.1)^{ab}	45.6 (1.3)^{ab}	51.9 (0.5)	61.1 (2.1)	27.2 (0.3)	33.1 (1.1)
0.9	O	46.4 (0.5)^{c}	43.8 (1.5)^{abc}	57.4 (0.0)	57.3 (0.9)	30.7 (0.3)	32.2 (1.2)
	BS	44.6 (1.2)^{bc}	42.7 (1.1)^{c}	54.0 (0.5)	60.4 (0.3)	29.8 (0.6)	34.6 (0.7)
	SM	43.0 (1.3)^{c}	45.2 (0.6)^{bc}	58.4 (0.2)	65.2 (0.9)	33.2 (0.7)	35.7 (0.6)
	V	45.8 (1.0)^{bc}	46.7 (0.6)^{ab}	57.2 (1.1)	64.3 (1.1)	31.0 (1.1)	34.2 (0.9)
	D	50.8 (0.4)^{a}*	48.4 (0.6)^{a}	52.7 (0.6)	62.0 (1.0)	25.9 (0.1)	31.9 (0.3)
	DU	48.4 (0.4)^{b}	46.8 (0.8)^{ab}	51.2 (0.5)	61.1 (1.9)	26.4 (0.1)	32.4 (0.9)
1.1	O	47.4 (0.9)^{a}	45.8 (1.3)^{ab}	57.0 (0.6)	58.1 (1.1)	29.9 (0.5)	31.3 (1.1)
	BS	46.1 (1.8)^{a}	43.4 (1.1)^{b}	54.1 (0.3)	59.9 (0.4)	29.1 (0.9)	33.9 (0.9)
	SM	45.9 (2.4)^{a}	46.9 (1.3)^{ab}	57.2 (1.0)	63.8 (0.3)	30.8 (0.8)	33.8 (0.7)
	V	49.6 (1.4)^{a}	48.2 (0.7)^{a}	55.8 (0.7)	63.2 (1.8)	28.1 (1.1)	32.6 (1.0)
	D	50.5 (0.7)^{a}	48.2 (0.5)^{a}	52.5 (0.3)	61.9 (0.2)	26.0 (0.3)	32.0 (0.3)
	DU	48.3 (1.0)^{a}	46.8 (0.6)^{ab}	52.1 (0.9)	60.9 (1.7)	26.8 (0.1)	32.3 (0.9)
1.3	O	47.6 (1.0)^{b}	47.3 (1.8)^{a}	55.4 (0.5)	56.8 (0.3)	29.0 (0.7)	29.8 (1.1)
	BS	48.0 (1.8)^{ab}	44.2 (1.3)^{a}	53.5 (0.5)	58.9 (0.2)	27.8 (0.7)	32.8 (0.8)
	SM	48.8 (2.1)^{ab}	48.2 (1.1)^{a}	56.5 (0.6)	62.5 (0.9)	28.8 (0.9)	32.3 (0.4)
	V	49.6 (1.3)^{ab}	48.4 (2.0)^{a}	53.8 (1.1)	62.2 (1.6)	27.1 (1.3)	32.0 (1.5)
	D	52.8 (0.4)^{a}*	48.8 (0.3)^{a}	52.0 (0.7)	61.8 (0.2)	24.5 (0.1)	31.6 (0.2)
	DU	48.4 (0.9)^{b}	46.2 (0.7)^{a}	50.9 (0.4)	59.9 (2.4)	26.2 (0.3)	32.1 (1.0)
1.5	O	48.2 (0.2)^{b}	47.5 (2.5)^{ab}	54.2 (0.2)	55.1 (0.3)	28.0 (0.2)	28.9 (1.3)
	BS	48.5 (1.2)^{ab}	45.2 (1.4)^{b}	52.3 (0.2)	58.8 (0.5)	26.9 (0.7)	32.1 (0.9)
	SM	49.1 (2.2)^{ab}	49.2 (1.1)^{ab}	55.5 (1.2)	62.2 (0.0)	28.2 (0.8)	31.6 (0.7)
	V	50.1 (0.6)^{ab}	50.5 (1.2)^{a}	52.4 (1.1)	62.0 (1.3)	26.1 (0.9)	30.7 (1.0)
	D	52.1 (0.5)^{a}*	47.9 (1.0)^{ab}	51.3 (0.1)	61.3 (0.7)	24.5 (0.2)	31.9 (0.5)
	DU	47.8 (0.9)^{b}	45.8 (0.2)^{ab}	50.7 (0.3)	59.6 (1.4)	26.4 (0.4)	32.3 (0.7)
B	O	44.2 (1.1)^{b}	51.6 (1.5)^{ab}*	43.8 (1.7)	51.9 (1.5)	24.3 (0.6)	25.0 (0.4)
	BS	48.8 (3.8)^{ab}	43.3 (1.3)^{c}	56.1 (2.3)	48.7 (1.0)	28.5 (0.9)	27.4 (0.3)
	SM	50.4 (1.3)^{a}	49.9 (0.4)^{a}	52.1 (0.3)	58.4 (1.1)	25.8 (0.8)	29.1 (0.3)
	V	47.2 (0.9)^{ab}	47.8 (0.8)^{abc}	43.6 (0.8)	51.9 (0.8)	22.9 (0.3)	27.0 (0.2)
	D	50.0 (0.3)^{a}*	46.0 (0.9)^{c}	45.6 (0.8)	57.2 (0.6)	22.7 (0.3)	30.8 (0.5)
	DU	50.2 (2.2)^{ab}	46.4 (0.2)^{bc}	49.8 (0.6)	54.4 (0.8)	24.7 (1.2)	29.0 (0.5)

*Asterisk represents significant differences in %KH reduction of the RMC specimens between 2 mm and 8 mm curing distances. Superscript letters represent significant differences among the LCUs at each depth within each column. Abbreviations: T, top; B, bottom.

Table 3. ANOVA table for LCU and curing distance effect on the %KH reduction across each depth of the RMC specimens

Depth (mm)	Effect	Num DF	Den DF	F Value	p-value	Significance
T	Distance	1	4.0	8.18	0.0458	*
	LCU	5	5.1	67.80	0.0001	*
	LCU*distance	5	5.1	3.40	0.1009	
0.5	Distance	1	12.1	0.01	0.9082	
	LCU	5	4.8	25.80	0.0017	*
	LCU*distance	5	4.8	0.85	0.5681	
0.7	Distance	1	14.4	0.16	0.6907	
	LCU	5	5.0	10.91	0.0101	*
	LCU*distance	5	5.0	1.08	0.4669	
0.9	Distance	1	14.8	2.89	0.1099	
	LCU	5	6.8	17.21	0.0009	*
	LCU*distance	5	6.8	2.44	0.1409	
1.1	Distance	1	12.9	3.84	0.0719	
	LCU	5	7.0	5.06	0.0279	*
	LCU*distance	5	7.0	0.33	0.8783	
1.3	Distance	1	15.0	6.69	0.0207	*
	LCU	5	6.6	9.98	0.0052	*
	LCU*distance	5	6.6	1.42	0.3300	
1.5	Distance	1	10.6	4.86	0.0506	
	LCU	5	6.5	6.38	0.0180	*
	LCU*distance	5	6.5	1.70	0.2584	
B	Distance	1	6.8	1.13	0.3251	
	LCU	5	5.5	2.13	0.2017	
	LCU*distance	5	5.5	7.01	0.0212	*

Abbreviations: T, top; B, bottom.

Table 4. Correlation between the localized irradiance beam profiles (mW/cm^2) and localized %KH reduction on the top surfaces of the RMC specimens using the various filters for the multiple LCUs explored at 2 and 8 mm curing distances from the RMC specimens

	Correlation between the localized irradiance and %KH reduction					
	2 mm			8 mm		
LCU	No filter	Longpass filter	Shortpass filter	No filter	Longpass filter	Shortpass filter
O	0.09	0.09	0.09	0.10	0.10	0.10
BS	0.26	0.27	0.05	-0.04	-0.03	-0.13
SM	0.18	0.18	0.13	0.18	0.18	0.06
V	0.27	0.26	0.28	-0.01	-0.01	0.03
D	-0.16	-0.16		-0.19	-0.19	
DU	-0.05	-0.05		0.02	0.02	

Missing correlation coefficients in the table with the linear model could not estimate a correlation.

Table 5. Number of localized significant comparisons (*) among the KH (kg/mm^2) measurements (x-y coordinates) of the RMC specimens across each depth and curing distance using the LCUs explored

Depth (mm)	*no. of comparisons	Distance (mm)	O	BS	SM	V	D	DU
T	1,224	2	72	24	8	16	80	33
		8	31	141	68	58	11	79
0.5	104	2	0	18	2	1	11	0
		8	0	1	6	2	0	0
0.7	104	2	4	21	1	9	3	7
		8	2	10	2	0	2	2
0.9	104	2	3	0	1	12	7	0
		8	0	4	0	1	16	3
1.1	104	2	0		4	7	8	3
		8	14	13	11	1	10	0
1.3	104	2	6	2	3	23	1	6
		8	0		1	0	13	0
1.5	104	2	0	0	1	8	3	4
		8	0	9	8	3	0	1
B	104	2	70	20	33	149	105	110
		8	13	294	11	37	97	34
B/T KH ratio	990	2	42	25	8	30	30	65
		8	86	152	22	33	19	35
All	3,288	2	155	85	54	233	221	167
		8	60	481	115	105	149	120

*1,224 comparisons among measurement points on the top or bottom surfaces/LCU/distance.

*104 comparisons among measurement points across each depth/LCU/distance.

*990 comparisons among bottom/top KH ratio measurement points/LCU/distance.

*3,288 sum comparisons from all measurements across each depth/LCU/distance.

Fewer significant differences indicated that a more consistent KH was observed across the specimen for a LCU at any given depth. Missing entries in the table were due to lack of convergence for the model.

Abbreviations: T, top; B, bottom; B/T KH ratio, bottom/top KH ratio.

Table 6. Number of localized significant comparisons (*) among the DC (%) measurement points (x-y coordinates) across each depth and curing distance of the RMC specimens using the LCUs explored

Depth (mm)	*no. of comparisons	Distance (mm)	O	BS	SM	V	D	DU
Top	1,224	2	76	104	23	104	18	85
		8	84	136	60	53	78	26
0.5	104	2		18	0	6	0	11
		8	2	11	0	1	9	0
0.7	104	2	3	0	0	1	0	8
		8		0	0	0		0
0.9	104	2	6	30	2	14	12	5
		8	0	24	9	3	4	8
1.1	104	2	5	0	0	0	0	1
		8	3	7	12	0	15	15
1.3	104	2	4	0	2	4	7	21
		8		2		8	2	21
1.5	104	2	12	0	11	0	0	9
		8	5	2	0	9	12	0
Bottom	104	2	94	10	52	65	112	64
		8	51	40	78	122	62	38
All	3,288	2	212	162	101	194	149	213
		8	150	224	159	205	194	108

*1,224 comparisons among measurement points on the top or bottom surfaces/LCU/distance.

*104 comparisons among measurement points at each depth/LCU/distance.

*3,288 total comparisons from all measurements across each depth/LCU/distance.

Fewer significant differences indicated that a more consistent DC was observed across the specimen for a LCU at any given depth. Missing entries in the table were due to lack of convergence for the model.

Table 7. ANOVA table for KH (kg/mm^2) significant effect of x, y, x-y coordinates for the individual LCU across each depth at 2 and 8 mm curing distances

LCU	Depth (mm)	Distance (mm)	Effect	Num DF	Den DF	F-Value	p-value
O	T	2	y	8	100.0	2.07	0.0455
	0.7	8	y	2	30.0	4.28	0.0232
	B	2	x	8	42.5	2.47	0.0271
	B/T	8	x	7	90.0	3.43	0.0027
BS	T	8	x	8	100.0	3.66	0.0009
	0.5	2	y	2	8.0	10.03	0.0066
	0.7	2	x	4	17.7	4.60	0.0101
			y	2	15.3	10.05	0.0016
	1.1	8	x	4	24.3	4.86	0.0051
			y	2	27.3	6.38	0.0053
	B	2	x*y	32	63.4	2.18	0.0040
		8	x	8	24.8	5.27	0.0006
	B/T	2	x*y	28	64.4	2.49	0.0013
SM	1.1	2	y	2	12.3	6.07	0.0147
V	0.7	2	y	2	13.9	5.94	0.0136
	1.3	2	y	2	7.7	4.97	0.0415
	B	8	x	8	26.8	2.46	0.0383
D	T	8	y	8	36.3	2.50	0.0284
	0.9	2	y	2	11.2	4.65	0.0339
		8	x	4	19.0	4.54	0.0096
	B	2	x	8	22.1	3.71	0.0068
		8	x	8	100.0	2.17	0.0358
DU	T	8	x	8	56.2	4.02	0.0008
	B	2	x	8	100.0	2.44	0.0187
			y	8	100.0	3.30	0.0022
	B/T	8	x	7	46.9	2.39	0.0355

Abbreviations: T, top; B, bottom; B/T, bottom/top KH ratio.

Table 20. ANOVA table for DC (%) significant effect of x, y, x-y coordinates for the individual LCU across each depth at 2 and 8 mm curing distances

LCU	Depth (mm)	Distance (mm)	Effect	Num DF	Den DF	F-Value	p-value
O	T	2	x	8	100.0	2.19	0.0343
	1.1	2	y	2	14.0	5.21	0.0204
BS	T	8	x	8	100.0	2.42	0.0198
		8	x*y	32	100.0	1.68	0.0269
	0.5	2	y	2	30.0	7.31	0.0026
		8	x	4	30.0	3.28	0.0241
	0.9	2	x*y	8	30.0	4.52	0.0011
		8	x	4	30.0	6.69	0.0006
SM	T	8	x	8	100.0	2.10	0.0426
V	1.5	8	x	4	11.5	4.24	0.0242
D	1.1	8	x*y	8	17.1	3.20	0.0207
	1.5	8	x*y	8	30.0	2.64	0.0255
	B	2	x*y	32	100.0	1.77	0.0170
DU	1.1	8	y	2	24.0	4.66	0.0195
	1.3	2	x*y	8	30.0	3.05	0.0124
		8	x	4	30.0	4.58	0.0052

Abbreviations: T, top; B, bottom.

Table 28. Mean (SE) KH (kg/mm^2) and DC (%) of the RMC specimens across each depth using the LCUs explored at 2 and 8 mm curing distances

		KH (kg/mm^2)		DC (%)	
Depth (mm)	LCU	2 mm	8 mm	2 mm	8 mm
T	O	60.8 (0.4)^{a}	60.4 (1.4)^{ab}	69.5 (0.2)^{b}	69.3 (0.6)^{a}
	BS	59.7 (1.4)^{a}	60.8 (0.1)^{b}	68.3 (0.5)^{abc}	67.3 (0.2)^{a}
	SM	60.9 (0.8)^{a}	66.1 (0.1)^{a}*	70.3 (0.0)^{a}*	67.3 (0.6)^{ab}
	V	59.0 (0.7)^{a}	60.3 (0.3)^{b}	70.1 (0.8)^{ab}	67.7 (0.7)^{ab}
	D	53.7 (0.5)^{b}	54.6 (0.8)^{c}	65.3 (0.6)^{d}	66.0 (0.2)^{bc}
	DU	48.8 (0.9)^{c}	53.8 (0.9)^{c}*	65.8 (0.8)^{cd}	64.8 (0.6)^{c}
0.5	O	58.1 (0.3)^{a}	60.8 (0.4)^{c}*	67.3 (1.7)^{abc}	68.5 (0.2)^{a}
	BS	58.2 (0.8)^{a}	62.8 (0.9)^{bc}*	68.3 (0.4)^{a}	68.7 (0.6)^{a}
	SM	60.5 (1.3)^{a}	67.1 (0.4)^{a}*	67.5 (0.6)^{ab}	67.7 (0.7)^{a}
	V	60.5 (0.8)^{a}	65.9 (0.9)^{ab}*	69.6 (0.2)^{a}*	68.4 (0.2)^{a}
	D	53.5 (0.4)^{b}	62.8 (0.6)^{bc}*	64.6 (0.9)^{bc}	63.8 (0.8)^{b}
	DU	51.7 (0.4)^{c}	61.2 (2.0)^{abc}*	64.5 (0.8)^{c}	64.7 (2.8)^{ab}
0.7	O	57.3 (0.3)^{a}	59.2 (0.4)^{b}*	66.5 (1.0)^{ab}	67.0 (1.3)^{ab}
	BS	56.2 (0.5)^{a}	62.2 (1.2)^{ab}*	67.4 (0.9)^{a}	69.1 (0.6)^{a}
	SM	59.7 (1.2)^{a}	66.0 (0.4)^{a}*	67.7 (1.4)^{ab}	66.7 (1.1)^{ab}
	V	58.6 (0.8)^{a}	64.7 (1.1)^{a}*	66.9 (0.3)^{a}	66.3 (0.5)^{b}
	D	53.1 (0.5)^{b}	62.2 (1.3)^{ab}*	64.0 (0.8)^{b}	66.7 (1.4)^{ab}
	DU	51.9 (0.5)^{b}	61.1 (2.1)^{ab}*	64.2 (1.1)^{ab}	66.8 (0.4)^{ab}
0.9	O	57.4 (0.0)	57.3 (0.9)	66.6 (0.9)^{a}	66.6 (1.1)^{ab}
	BS	54.0 (0.5)	60.4 (0.3)	67.0 (0.2)^{a}	68.1 (0.3)^{a}
	SM	58.4 (0.2)	65.2 (0.9)	67.6 (1.0)^{a}	67.5 (1.1)^{ab}
	V	57.2 (1.1)	64.3 (1.1)	66.6 (0.6)^{a}	66.3 (0.5)^{b}
	D	52.7 (0.6)	62.0 (1.0)	65.3 (0.7)^{a}	65.3 (0.9)^{ab}
	DU	51.2 (0.5)	61.1 (1.9)	66.1 (0.9)^{a}	66.8 (0.3)^{b}
1.1	O	57.0 (0.6)^{a}	58.1 (1.1)^{bc}	65.6 (1.3)^{a}	65.3 (0.7)^{b}
	BS	54.1 (0.3)^{bd}	59.9 (0.4)^{c}*	64.7 (1.0)^{a}	68.3 (0.5)^{a}
	SM	57.2 (1.0)^{ab}	63.8 (0.3)^{a}*	66.1 (1.0)^{a}	67.5 (0.7)^{ab}
	V	55.8 (0.7)^{ab}	63.2 (1.8)^{abc}*	66.7 (1.0)^{a}	66.2 (0.3)^{b}
	D	52.5 (0.3)^{c}	61.9 (0.2)^{b}*	64.8 (1.8)^{a}	65.9 (1.4)^{ab}
	DU	52.1 (0.9)^{cd}	60.9 (1.7)^{abc}*	64.0 (0.8)^{a}	65.2 (1.0)^{ab}
1.3	O	55.4 (0.5)^{ab}	56.8 (0.3)^{c}	63.3 (0.5)^{a}	63.3 (0.6)^{b}
	BS	53.5 (0.5)^{bc}	58.9 (0.2)^{b}*	66.5 (1.6)^{a}	66.3 (0.4)^{a}
	SM	56.5 (0.6)^{a}	62.5 (0.9)^{ab}*	65.9 (0.8)^{a}	65.6 (1.1)^{ab}
	V	53.8 (1.1)^{abcd}	62.2 (1.6)^{abc}*	64.7 (0.8)^{a}	66.3 (1.8)^{ab}
	D	52.0 (0.7)^{cd}	61.8 (0.2)^{a}*	64.5 (0.6)^{a}	64.9 (1.5)^{ab}
	DU	50.9 (0.4)^{d}	59.9 (2.4)^{abc}	65.9 (1.3)^{a}	64.5 (0.5)^{ab}
1.5	O	54.2 (0.2)^{a}	55.1 (0.3)^{c}	65.8 (0.4)^{a}	65.8 (1.2)^{a}
	BS	52.3 (0.2)^{b}	58.8 (0.5)^{b}*	66.1 (0.8)^{a}	67.1 (0.2)^{a}
	SM	55.5 (1.2)^{abc}	62.2 (0.0)^{a}*	66.8 (1.2)^{a}	65.9 (0.8)^{a}
	V	52.4 (1.1)^{abcd}	62.0 (1.3)^{ab}*	65.7 (0.7)^{a}	64.9 (0.9)^{a}
	D	51.3 (0.1)^{cd}	61.3 (0.7)^{ab}*	63.4 (1.2)^{a}	64.9 (0.6)^{a}
	DU	50.7 (0.3)^{d}	59.6 (1.4)^{abc}*	66.8 (0.6)^{a}	66.3 (0.9)^{a}
B	O	43.8 (1.7)^{bd}	51.9 (1.5)^{bcd}*	66.0 (0.6)^{a}	64.3 (0.8)^{abc}
	BS	56.1 (2.3)^{ab}	48.7 (1.0)^{d}	65.9 (0.1)^{a}	66.0 (0.8)^{abc}
	SM	52.1 (0.3)^{a}	58.4 (1.1)^{a}*	66.4 (0.2)^{a}*	63.2 (0.3)^{c}
	V	43.6 (0.8)^{d}	51.9 (0.8)^{cd}*	64.9 (0.5)^{ab}	66.1 (0.3)^{a}
	D	45.6 (0.8)^{cd}	57.2 (0.6)^{ab}*	63.7 (0.5)^{b}	64.9 (0.3)^{b}
	DU	49.8 (0.6)^{b}	54.4 (0.8)^{bc}*	65.1 (0.6)^{ab}	64.7 (0.7)^{abc}
	O	72.1 (2.7)^{de}	86.3 (0.7)^{bc}*		
B/T KH ratio	BS	94.2 (5.8)^{abc}	80.2 (1.8)^{c}		
	SM	85.7 (1.2)^{b}	88.6 (1.7)^{b}		
	V	74.2 (2.1)^{ce}	86.2 (1.0)^{bc}*		
	D	85.1 (1.2)^{bd}	105.0 (2.4)^{a}*		
	DU	102.4 (1.4)^{a}	101.3 (1.7)^{a}		

*Represent significant differences between 2 mm and 8 mm in the same raw for each material property. Superscript letters represent significant differences among the LCUs at each depth within the same column. The analysis model was unable to perform comparisons for the 0.9 mm depth data, most likely due to complexities in the data that could not be overcome with the small sample size. Abbreviations: T, top; B, bottom; B/T, bottom/top KH ratio.

Table 9. ANOVA table of the LCU and curing distance effect on KH (kg/mm^2) across each depth of the RMC specimens

Depth (mm)	Effect	Num DF	Den DF	F Value	p-value	Significance
T	Distance	1	11.7	21.80	0.0006	*
	LCU	5	5.8	77.61	0.0000	*
	LCU*distance	5	5.8	5.06	0.0385	*
0.5	Distance	1	8.8	150.61	0.0000	*
	LCU	5	5.5	20.09	0.0016	*
	LCU*distance	5	5.5	13.51	0.0044	*
0.7	Distance	1	9.9	126.42	0.0000	*
	LCU	5	5.1	14.78	0.0048	*
	LCU*distance	5	5.1	8.87	0.0151	*
0.9	Distance					
	LCU					
	LCU*distance					
1.1	Distance	1	9.3	148.03	0.0000	*
	LCU	5	4.1	9.26	0.0237	*
	LCU*distance	5	4.1	14.21	0.0107	*
1.3	Distance	1	6.7	128.06	0.0000	*
	LCU	5	3.7	7.26	0.0447	*
	LCU*distance	5	3.7	16.12	0.0117	*
1.5	Distance	1	10.0	240.11	0.0000	*
	LCU	5	3.9	11.60	0.0184	*
	LCU*distance	5	3.9	33.14	0.0027	*
B	Distance	1	11.1	61.48	0.0000	*
	LCU	5	7.4	20.84	0.0003	*
	LCU*distance	5	7.4	11.98	0.0020	*
B/T KH ratio	Distance	1	7.0	17.20	0.0044	*
	LCU	5	6.4	51.93	0.0000	*
	LCU*distance	5	6.4	12.53	0.0032	*

The analysis model was unable to perform comparisons for the 0.9 mm depth data, most likely due to complexities in the data that could not be overcome with the small sample size. Abbreviations: T, top; B, bottom; B/T, bottom/top KH ratio.

Table 10. ANOVA table of the LCU and curing distance effect on the DC (%) across each depth of the RMC specimens

Depth (mm)	Effect	Num DF	Den DF	F Value	p-value	Significance
T	Distance	1	15.6	14.02	0.0018	*
	LCU	5	4.6	22.99	0.0026	*
	LCU*distance	5	4.6	4.35	0.0737	
0.5	Distance	1	5.8	0.00	0.9797	
	LCU	5	2.6	15.34	0.0353	*
	LCU*distance	5	2.6	1.44	0.4240	
0.7	Distance	1	16.2	3.01	0.1019	
	LCU	5	7.3	3.10	0.0824	
	LCU*distance	5	7.3	2.19	0.1627	
0.9	Distance	1	15.8	0.26	0.6200	
	LCU	5	8.4	4.20	0.0335	*
	LCU*distance	5	8.4	0.88	0.5334	
1.1	Distance	1	14.8	3.32	0.0887	
	LCU	5	6.7	1.77	0.2404	
	LCU*distance	5	6.7	1.70	0.2562	
1.3	Distance	1	13.4	0.00	0.9793	
	LCU	5	5.3	4.27	0.0637	
	LCU*distance	5	5.3	0.34	0.8726	
1.5	Distance	1	17.1	0.01	0.9241	
	LCU	5	5.8	2.52	0.1489	
	LCU*distance	5	5.8	0.70	0.6415	
B	Distance	1	15.0	2.61	0.1269	
	LCU	5	7.0	3.32	0.0742	
	LCU*distance	5	7.0	13.78	0.0016	*

Abbreviations: T, top; B, bottom.

Table 11. Correlation of the localized irradiance beam profiles with KH and DC values of the RMC specimens using the various LCUs explored and beam profile filters at 2 and 8 mm distances

		2 mm			8 mm		
Measurement	LCU	None	Longpass filter	Shortpass filter	None	Longpass filter	Shortpass filter
KH-BE	O	0.05	0.05	0.05	0.17	0.17	0.17
	BS	0.02	0.01	0.03	-0.06	-0.09	0.22
	SM	-0.04	-0.04	-0.05	0.07	0.07	-0.03
	V	0.18	0.18	0.25	0.02	0.02	0.03
	D	-0.25	-0.25		0.02	0.02	
	DU	0.21	0.21		0.00	0.00	
DC	O	-0.10	-0.09	-0.09	0.11	0.12	0.12
	BS	-0.16	-0.15	-0.15	0.06	0.04	0.26
	SM	0.23	0.23	0.16	-0.08	-0.08	-0.19
	V	-0.21	-0.21	-0.27	0.26	0.26	0.23
	D	0.11	0.11		0.16	0.16	
	DU	0.02	0.02		0.14	0.14	

Correlation coefficients are missing in the table below when the correlation could not be estimated by the linear model.

Table 12. Correlation between the localized (x-y coordinates) DC with KH-BE, KH-AE and %KH reduction using the LCUs explored at 2 and 8 mm curing distances

		Distance					
		2mm			8mm		
LCU	Depth (mm)	KH-BE	KH-AE	%KH reduction	KH-BE	KH-AE	%KH reduction
O	T	-0.25	-0.30	0.13	-0.79	-0.62	-0.60
	0.5		-0.60		-0.25	-0.50	0.37
	0.7	-0.60	-0.19	-0.51	0.84	0.36	
	0.9	0.63	0.60	0.11	-0.69	-0.74	0.45
	1.1	0.39	0.06	0.35	-0.03	-0.13	0.18
	1.3	0.27	-0.38	0.54	-0.19	0.48	-0.51
	1.5	-0.70	0.77	-0.89	0.74	0.79	-0.73
	B	0.66	0.45	0.23	-0.01	0.57	-0.32
BS	T		0.63	-0.53	-0.70	0.29	-0.61
	0.5	0.19	0.60	-0.49	-0.35	0.30	-0.60
	0.7	-0.43	0.02		-0.34	-0.52	0.43
	0.9	0.86	0.68	0.25	-0.23	0.25	-0.38
	1.1	0.75	-0.10	0.61	0.18	-0.02	0.09
	1.3	0.51	-0.83	0.86	-0.37	0.37	-0.44
	1.5	-0.39	0.24		-0.27	0.29	-0.35
	B	0.25	0.12	0.09	0.88	-0.56	0.83
SM	T	-0.62	-0.13	-0.29	0.81	-0.62	0.80
	0.5	-0.11	0.58	-0.45	0.51	-0.27	0.56
	0.7	0.31	-0.01	0.22	-0.55	-0.34	-0.32
	0.9	0.08	-0.02	0.06	0.24	0.24	-0.19
	1.1	-0.62	-0.42	0.15	-0.29	-0.76	0.68
	1.3	0.06	-0.52	0.41	-0.30	0.37	-0.42
	1.5	-0.66	0.58	-0.71	-0.13	-0.04	-0.05
	B	-0.38	0.41	-0.21	0.17	-0.45	0.47
V	T	-0.02	0.35		-0.42	0.01	-0.28
	0.5	-0.68	-0.09	-0.41	-0.24	-0.23	0.11
	0.7	-0.60	0.01	-0.39	-0.02	0.13	-0.16
	0.9	0.71	-0.10	0.61	0.05	-0.05	0.17
	1.1	-0.80	-0.39	-0.41	-0.23	0.20	-0.42
	1.3	0.44	0.71	-0.72	0.64	0.32	0.02
	1.5	-0.55	-0.45	0.12	-0.41	0.54	-0.47
	B	0.41	-0.46	0.43	0.08	0.09	-0.03
D	T	-0.15	0.53	-0.59	0.66	0.11	0.48
	0.5	-0.70	0.23	-0.42	0.30	-0.20	0.39
	0.7	-0.47	-0.05	-0.38		-0.16	
	0.9	-0.18	-0.19	0.11	-0.76	-0.18	-0.55
	1.1	0.00	-0.38	0.24	-0.58	0.54	-0.57
	1.3	-0.12	-0.83	0.61	0.47	-0.21	0.41
	1.5	0.50	0.62	-0.29	0.26	0.47	-0.30
	B	-0.45	-0.36	0.59	-0.17	-0.19	0.09
DU	T			0.60	-0.30	-0.44	0.13
	0.5	0.29		0.41	0.21	-0.24	0.26
	0.7	0.44	0.41	-0.20	-0.19	-0.02	-0.12
	0.9	-0.30	-0.64	0.33		0.15	0.20
	1.1		-0.42	0.41	0.64	-0.91	0.63
	1.3	0.50	-0.75	0.79	-0.08	-0.21	0.18
	1.5	0.75	0.18	0.34	0.45	-0.17	0.57
	B	0.10	-0.61	0.63	0.59	0.31	0.21

Correlation coefficients are missing in the table below when the correlation could not be estimated by the linear model. Abbreviations: T, top; B, bottom.

Table 13. Correlation between the average DC values with KH-BE, KH-AE and %KH reduction values across each depth using the LCUs explored at 2 and 8 mm curing distances

		2 mm			8 mm		
LCU	Depth (mm)	KH-BE	KH-AE	%KH reduction	KH-BE	KH-AE	%KH reduction
O	T	0.99	0.33	0.25	-0.70	-1.00	1.00
	0.5	-0.86	-0.67	0.60	0.45	1.00	-0.98
	0.7	0.52	0.19	-0.01	1.00	0.75	-0.67
	0.9	0.73	0.56	-0.58	-0.82	-0.99	0.84
	1.1	-0.64	0.50	-0.89	-1.00	-0.90	0.81
	1.3	-0.99	-0.70	0.36	0.80	0.84	-0.73
	1.5	-0.28	0.27	-0.66	-0.38	0.99	-0.96
	B	-0.62	-0.27	-0.94	0.22	1.00	-0.37
BS	T	0.59	-0.06	0.77	0.79	0.76	-0.72
	0.5	-0.95	-0.61	-0.85	0.51	0.98	-1.00
	0.7	0.63	-0.26	0.73	-0.83	-0.51	0.18
	0.9	-0.77	0.46	-0.83	0.66	0.89	-0.75
	1.1	0.41	0.74	-0.63	0.65	0.80	-0.85
	1.3	0.99	-0.91	0.95	0.88	0.82	-0.77
	1.5	-1.00	-0.79	0.73	0.05	-0.86	0.96
	B	0.03	-0.44	0.19	0.97	0.58	0.70
SM	T	-0.43	-0.96	0.98	0.92	0.55	-0.36
	0.5	-0.91	0.94	-1.00	-0.60	0.92	-0.84
	0.7	-0.09	0.18	-0.12	-0.66	-0.18	-0.01
	0.9	0.96	0.14	0.02	-0.87	-0.32	-0.59
	1.1	0.77	-0.55	0.65	-0.39	-0.27	0.16
	1.3	0.50	-0.90	0.82	0.20	0.98	-0.54
	1.5	-0.88	0.77	-0.98	-0.45	-0.85	0.85
	B	0.97	0.99	-0.98	-0.48	-0.51	-0.39
V	T	0.99	0.52	-0.20	0.74	0.97	-0.90
	0.5	0.86	0.99	-0.96	-0.42	-0.65	0.92
	0.7	0.76	0.88	-0.91	-0.23	-0.25	0.27
	0.9	0.86	0.42	0.06	-0.40	-0.14	-0.36
	1.1	-0.91	-0.77	0.71	-0.55	-0.05	-0.95
	1.3	0.90	0.94	-0.96	1.00	0.59	-0.06
	1.5	-0.99	-0.99	0.98	0.92	0.89	-0.37
	B	0.41	1.00	-0.33	-0.70	0.53	-0.93
D	T	0.41	-0.92	0.98	-0.90	-0.98	1.00
	0.5	0.74	-0.50	0.62	1.00	0.46	0.29
	0.7	0.78	0.89	-0.99	-0.45	-0.13	-0.18
	0.9	0.71	1.00	0.34	-1.00	-0.73	-0.84
	1.1	0.65	-1.00	0.97	-0.32	0.81	-0.94
	1.3	-0.19	-0.21	-0.20	-0.45	-1.00	0.79
	1.5	-0.25	0.89	-0.80	0.94	-0.30	0.79
	B	1.00	0.99	0.90	0.55	0.94	-0.55
DU	T	0.86	0.69	-0.60	0.92	0.97	0.78
	0.5	-0.73	0.19	-0.44	-0.07	-0.97	0.72
	0.7	0.53	0.13	0.17	-0.35	0.39	-0.99
	0.9	0.58	0.54	0.54	-0.98	-0.77	-0.57
	1.1	0.94	-0.89	0.99	0.25	0.65	-0.86
	1.3	-0.89	0.98	-0.96	0.41	0.17	0.89
	1.5	-0.39	0.99	-0.99	0.36	0.48	-0.59
	B	0.43	-0.55	0.74	0.07	0.34	-0.99

Table 14. Collective significant comparisons (*) summary for the DC, KH, %KH reduction and bottom/top KH ratios of all the data points collected within the entire RMC specimens cured using the LCUs explored at 2 and 8 mm distances

Distance (mm)	Depth (mm)	*no. of comparisons	Measurement	LCU					
				O	BS	SM	V	D	DU
2	All	3,288	DC	346	191	127	272	236	256
			%KH	426	136	96	153	303	154
			KH	202	87	70	307	300	234
	B/T ratio	990	KH	47	2	17	82	82	71
8	All	3,288	DC	222	353	264	261	280	124
			%KH	71	330	187	112	345	141
			KH	136	667	138	120	158	144
	B/T ratio	990	KH	76	195	31	18	9	25

3,288 total comparisons from all measurements across each depth/LCU/distance.

990 comparisons performed among bottom/top KH ratio measurement points/LCU/distance.

The fewer significant difference indicated that more consistent values were observed across the specimen for a LCU at any given depth for a given measurement. Abbreviations: B/T ratio, bottom/top KH ratio.

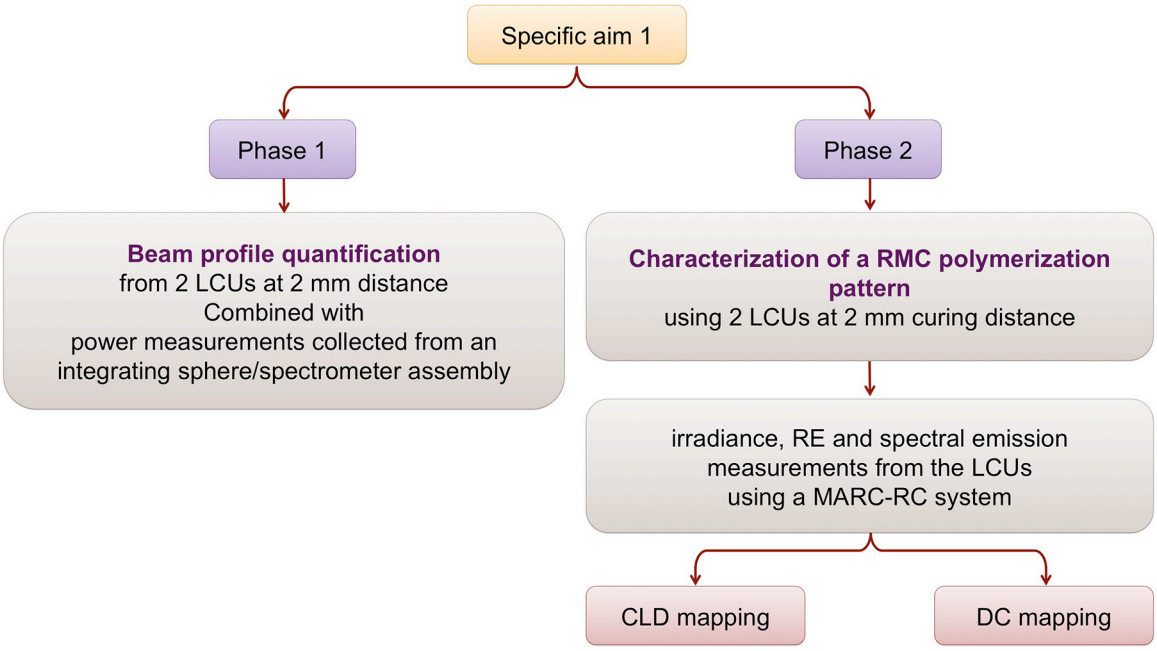

Figure 1. Specific aim 1 phases

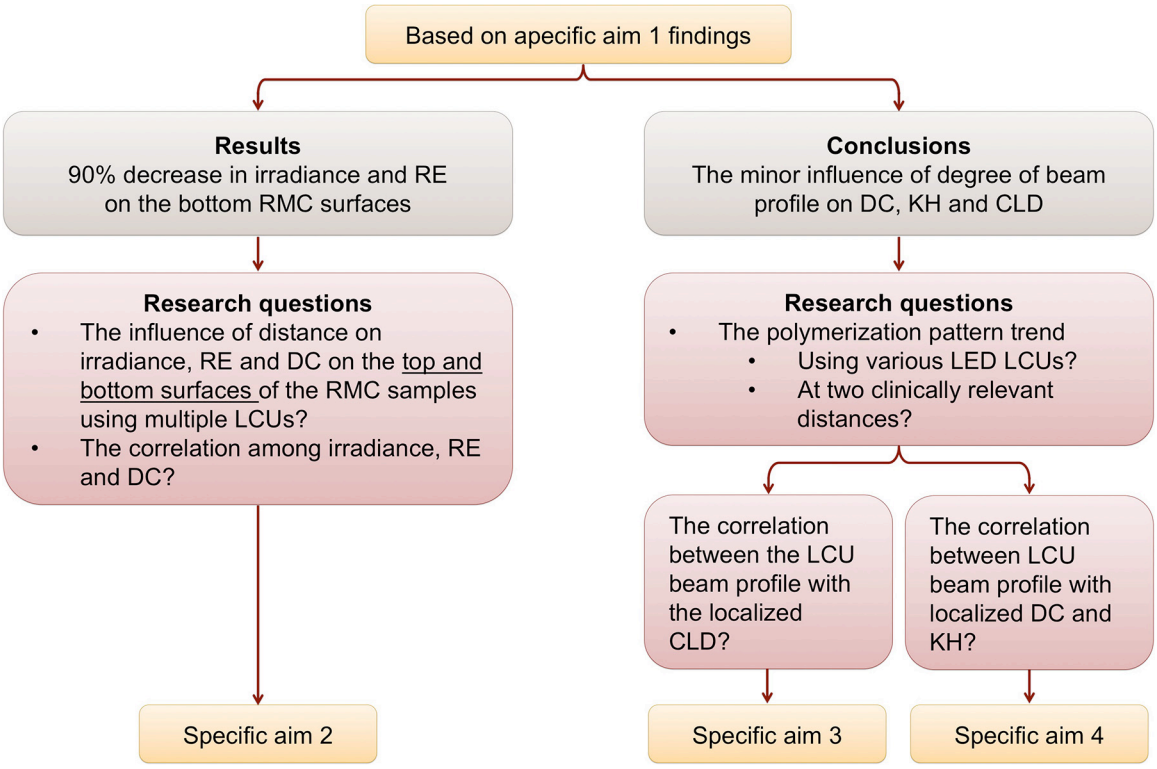

Figure 2. Research questions based on specific aim 1 findings

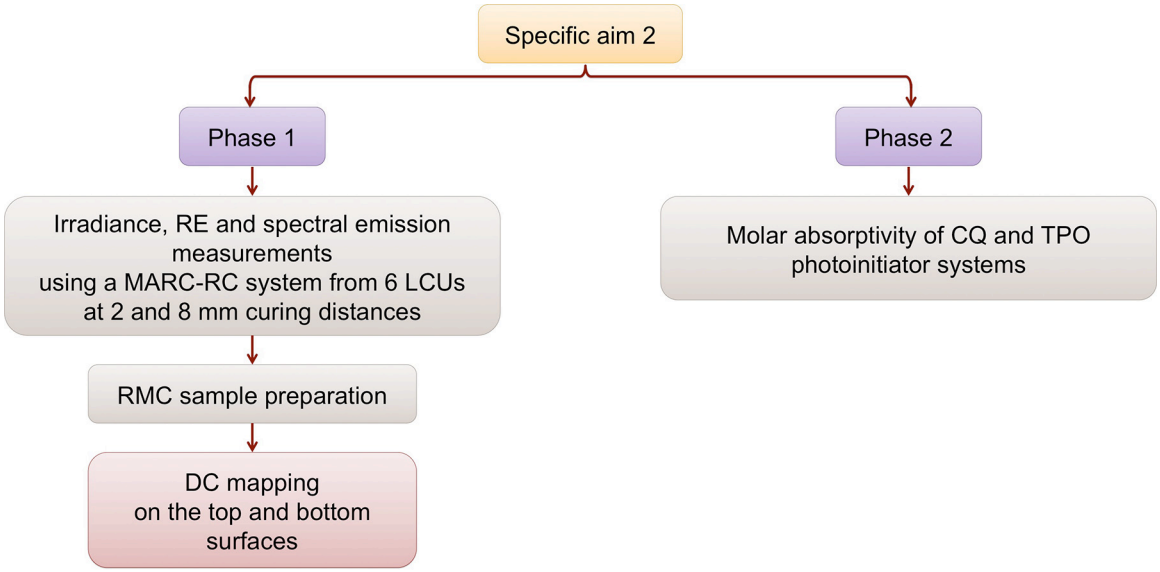

Figure 3. Specific aim 2 phases

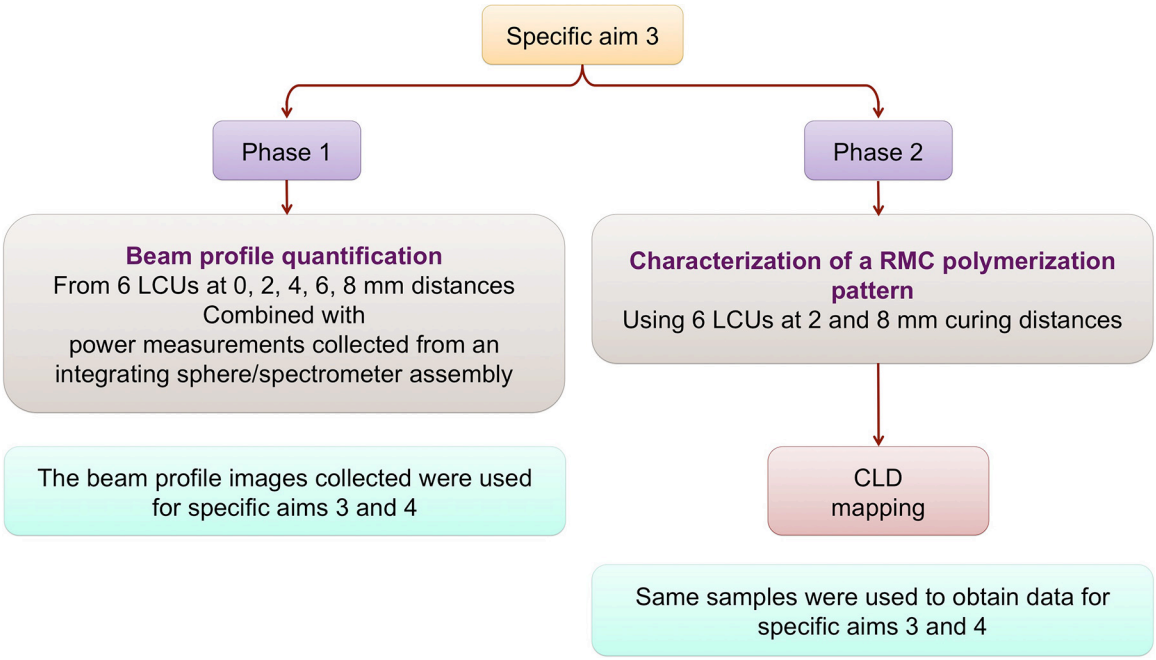

Figure 4. Specific aim 3 phases

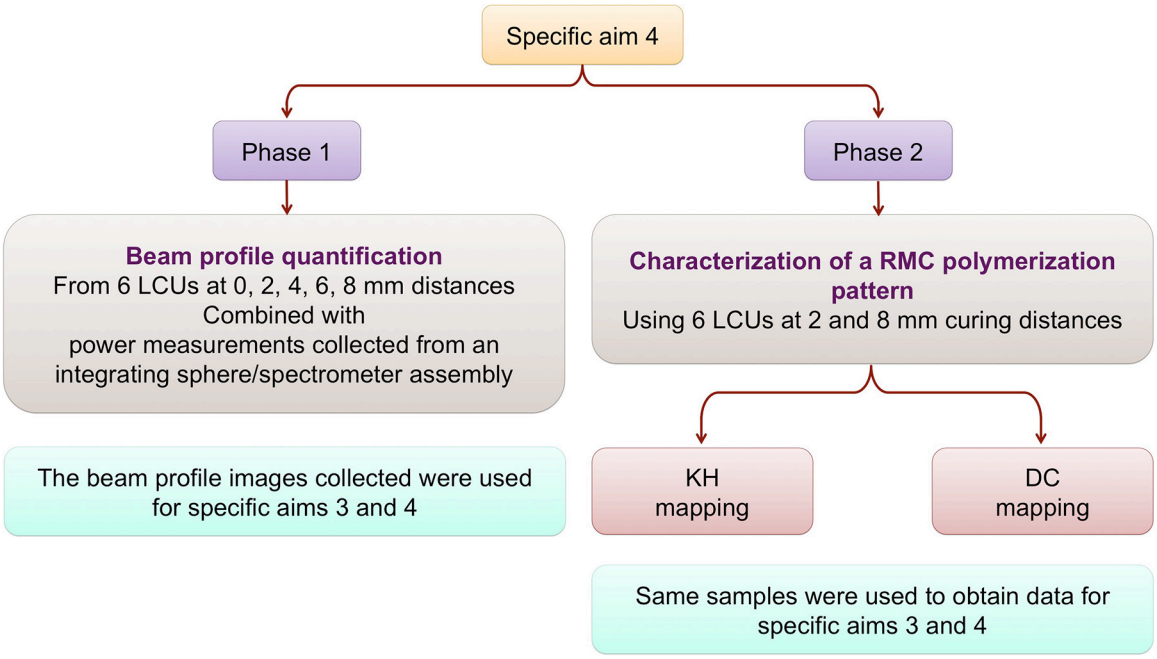

Figure 5. Specific aim 4 phases

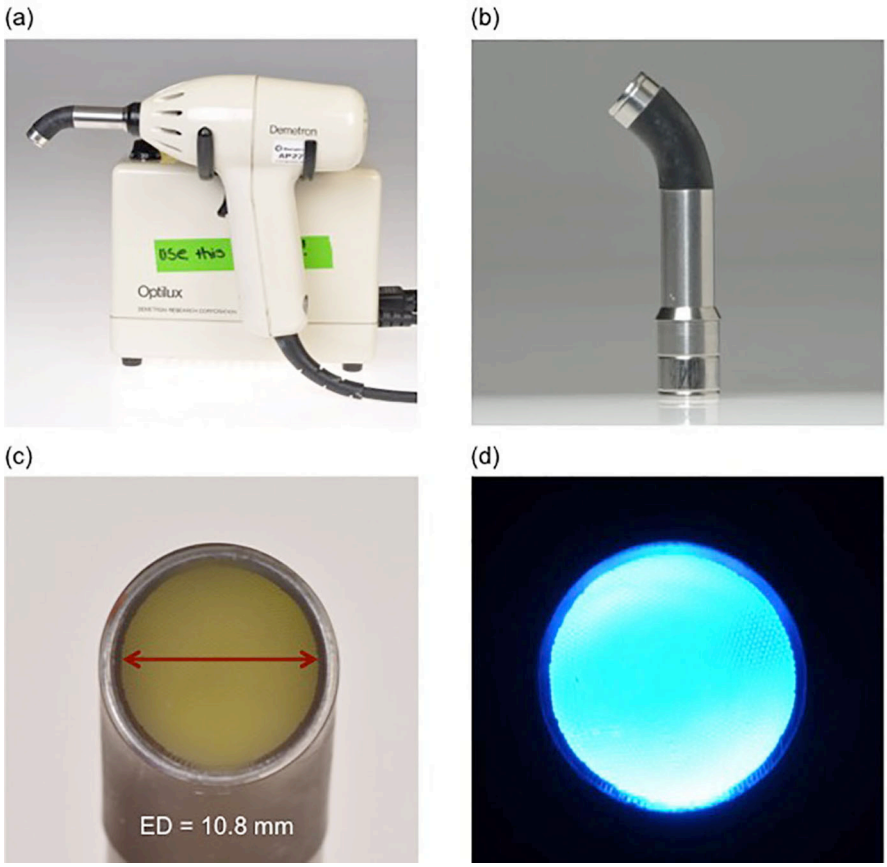

Figure 6. Optilux 401 QTH LCU

(a) The Optilux 401 LCU. (b) Straight fiber optic light guide tip for the LCU. (c) The effective diameter (ED) of the light-emitting portion of the light guide tip. (d) The activated LCU showing a relatively homogenous irradiance beam profile.

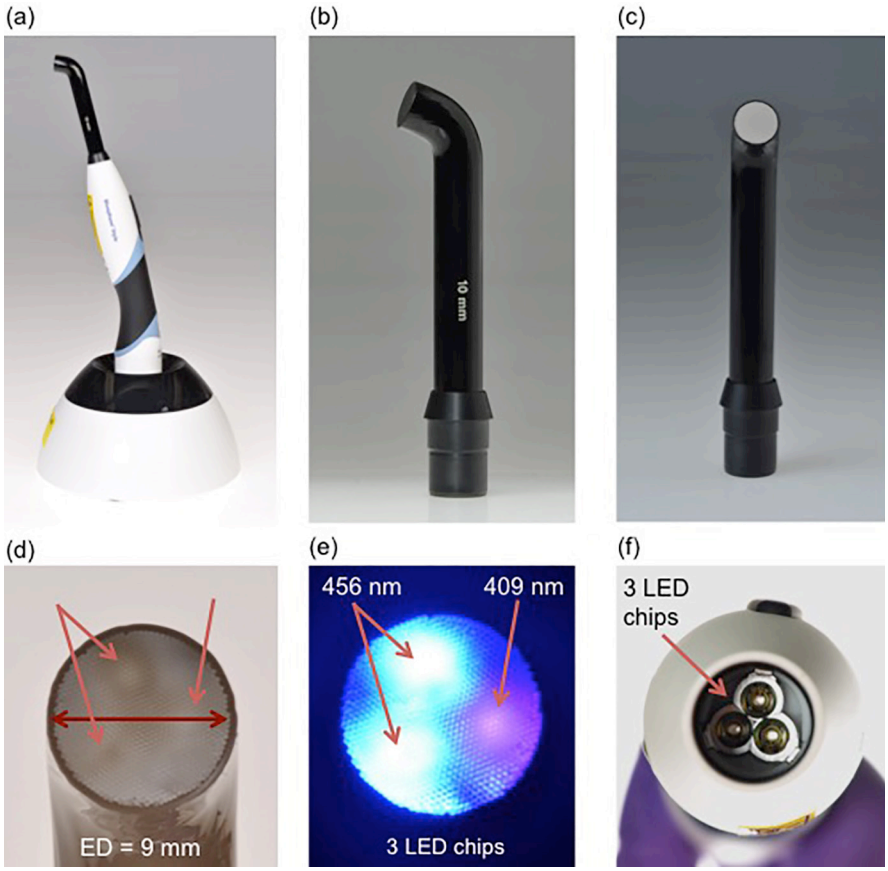

Figure 7. Bluephase Style multiple emission peak LED LCU

(a) The Bluephase Style LCU with the updated light guide tip. (b and c) different views of the straight fiber optic light guide tip for the Bluephase Style LCU. (d) The fiber optic light guide tip showing the effective diameter (ED) of the light-emitting portion of the three LED chips. (e) The activated LCU showing the location of the three LED chips (two blue and one violet). (f) The body of the LED LCU without the fiber optic light guide tip showing the locations of the LED chips.

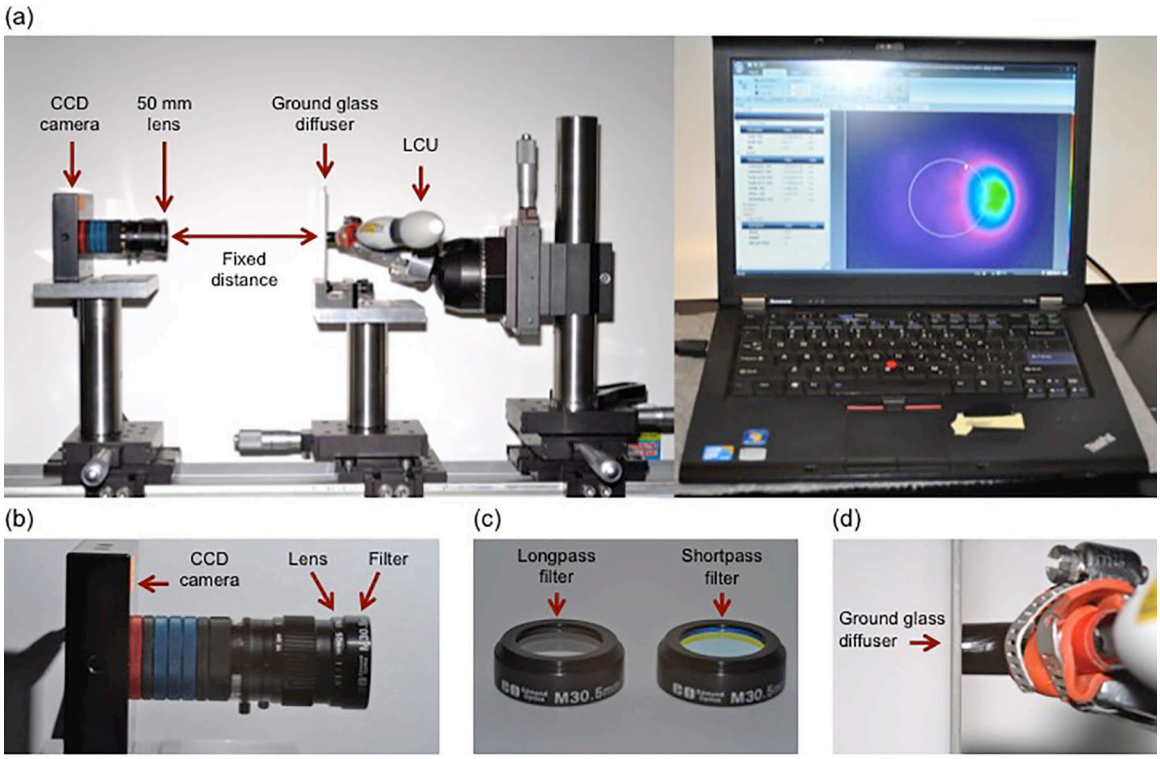

Figure 8. Beam profiler system

(a) The components of the beam profiler system connected to a computer with the beam profiler software. (b) The CCD camera captures the irradiance beam images with a filter attached to the lens. (c) The longpass filter allows wavelengths greater than 425 nm to pass and reach the CCD camera (blue spectrum) and the shortpass filter allows wavelengths below 425 nm to pass through to the CCD camera (violet spectrum). (d) The LCU guide tip setup flat against the ground surface of the glass diffuser.

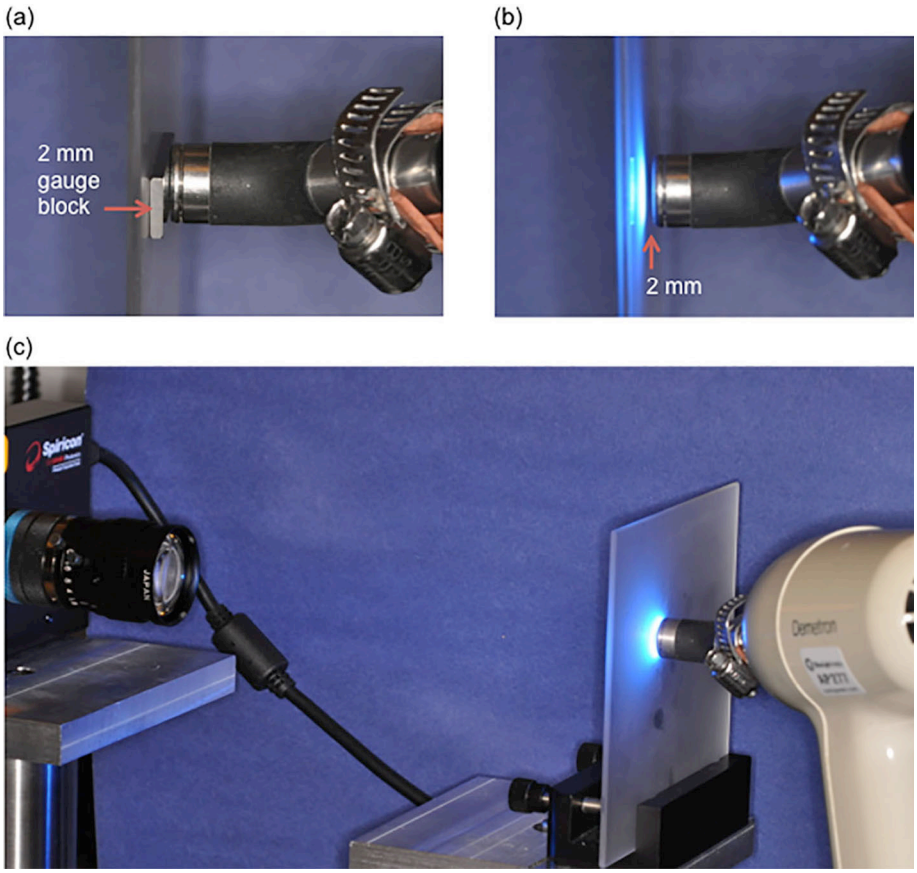

Figure 9. LCU setup on a beam profiler system with the light guide tip at 2 mm distance from a ground glass diffuser

(a) A 2 mm gauge block was used to ensure a 2 mm distance between the light guide tip and ground glass diffuser. (b) The gauge block is removed and the LCU is activated to capture the beam profile images. (c) The CCD camera captures images passing through the glass diffuser and then processed on a computer with the beam gauge software.

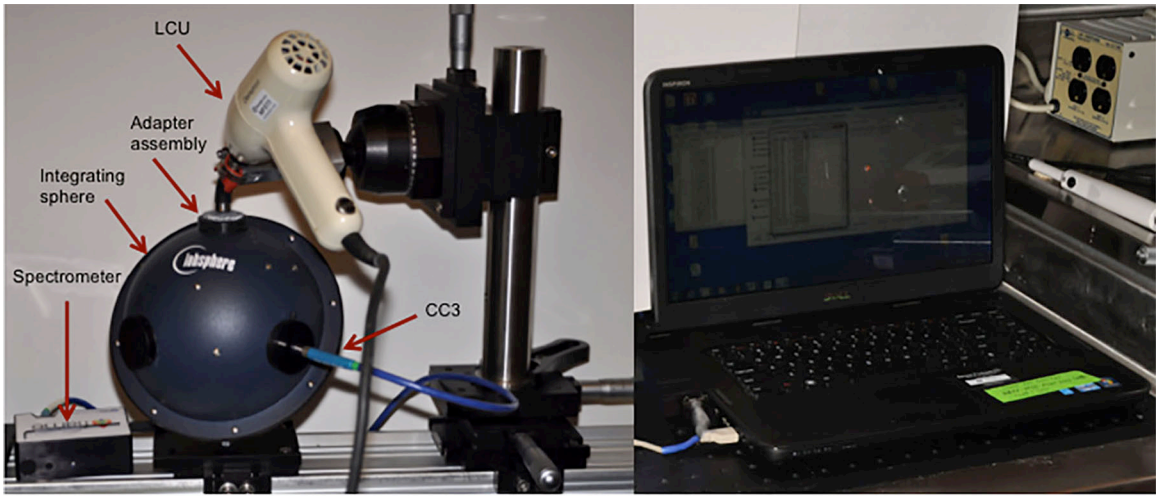

Figure 10. Integrating sphere/spectrometer assembly components and setup

A cosine corrector (CC3) is connected to an Ocean Optics optical spectrometer form one side and to an opening on the 6-inch integrating sphere from the other side. The integrating sphere is connected to a computer with the specific software to collect the measurements. A custom-made adapter assembly matching the dimensions of a light guide tip is placed over an integrating sphere opening and a LCU was placed at 2 mm distance from the adapter assembly to collect power measurements at 2 mm distance and apply the average power value on the beam profile images.

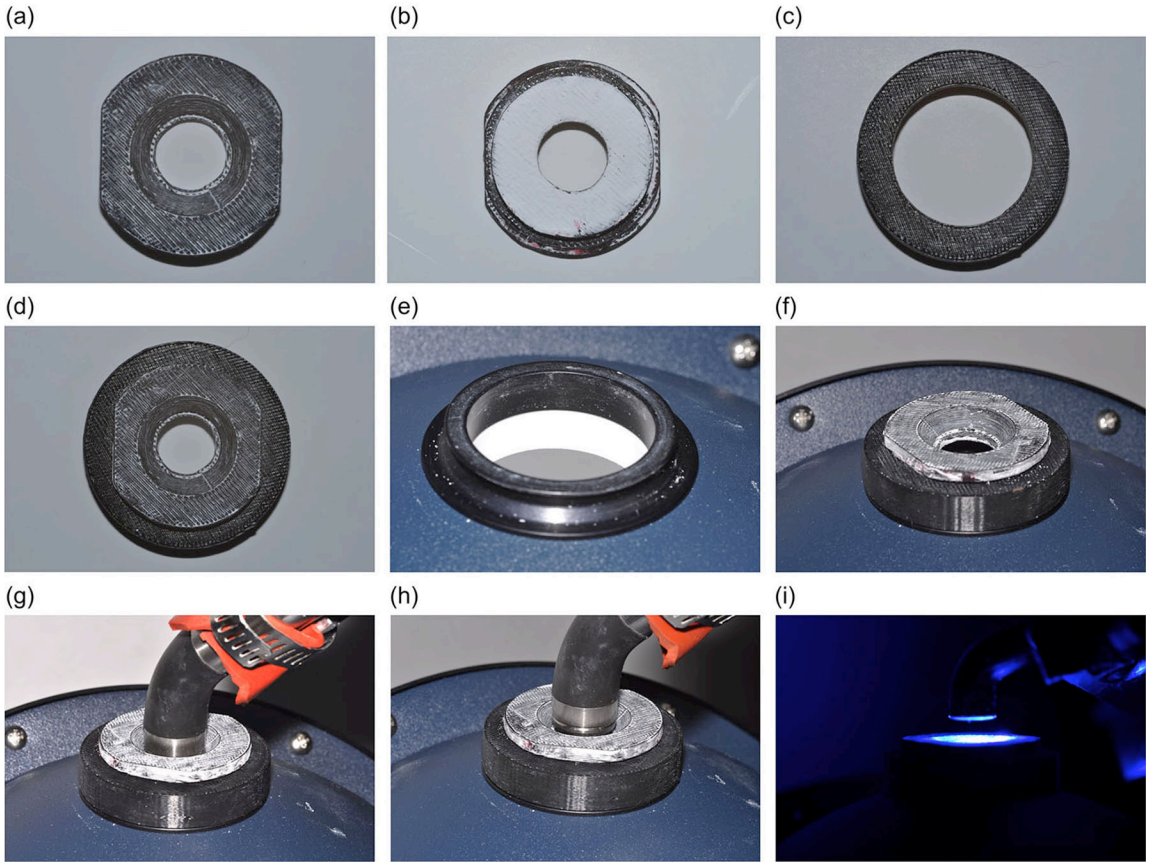

Figure 11. Representative adapter assembly and a LCU setup on an integrating sphere for collecting LCU power measurements

(a) The outer surface of a custom-made adapter. (b) The inner surface of the custom-made adapter coated with highly reflective barium sulfate to match the inner surface of the integrating sphere. (c) A ring that mounts on the integrating sphere opening from its inner surface and holds the custom-made adapter on its outer surface. (d) The adapter assembly composed of the custom-made adapter coupled with a ring that mounts on the integrating sphere opening. (e) The integrating sphere opening. (f) Mounting of the adapter assembly on the integrating sphere opening. (g) Placement of the light guide tip at 0 mm distance to insure the tip is completely flat and seated on the custom-made adapter. (h) Adjustment of the light guide tip at the desired distance using a metric gauge. (i) LCU activation at the desired distance and emitted light is collected through the integrating sphere opening.

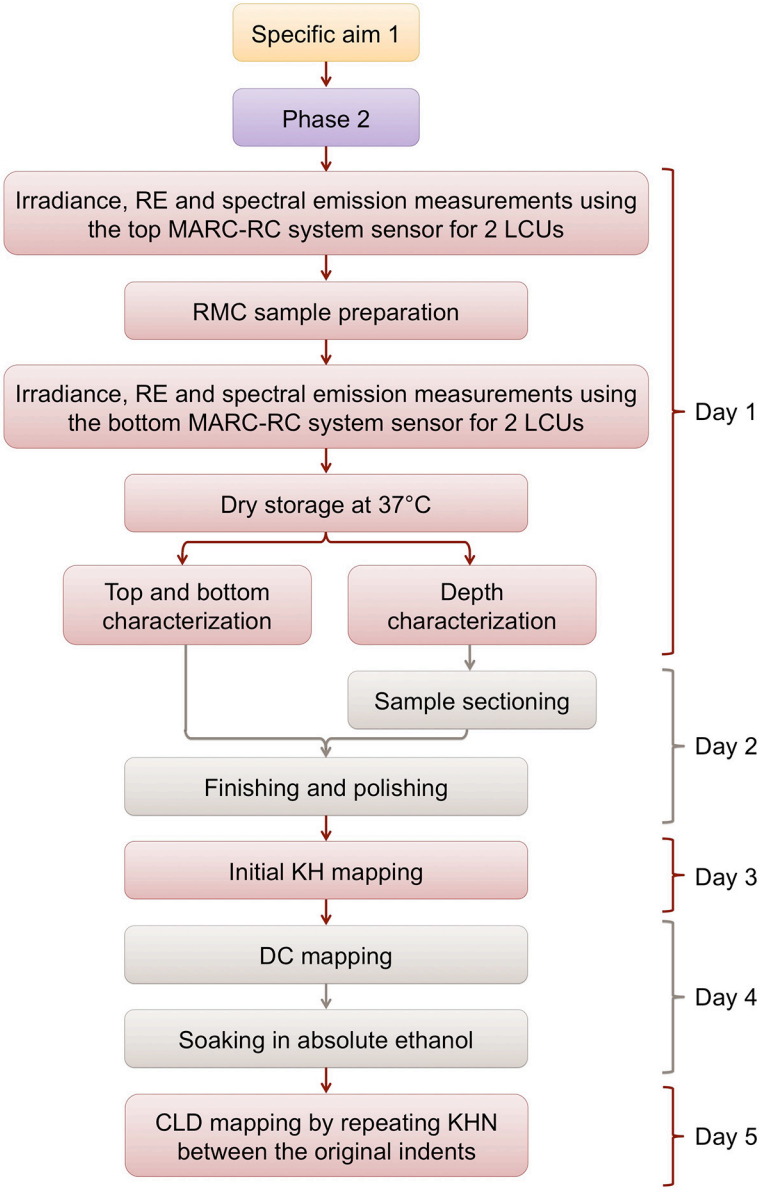

Figure 12. Specific aim 1, phase 2 experimental design

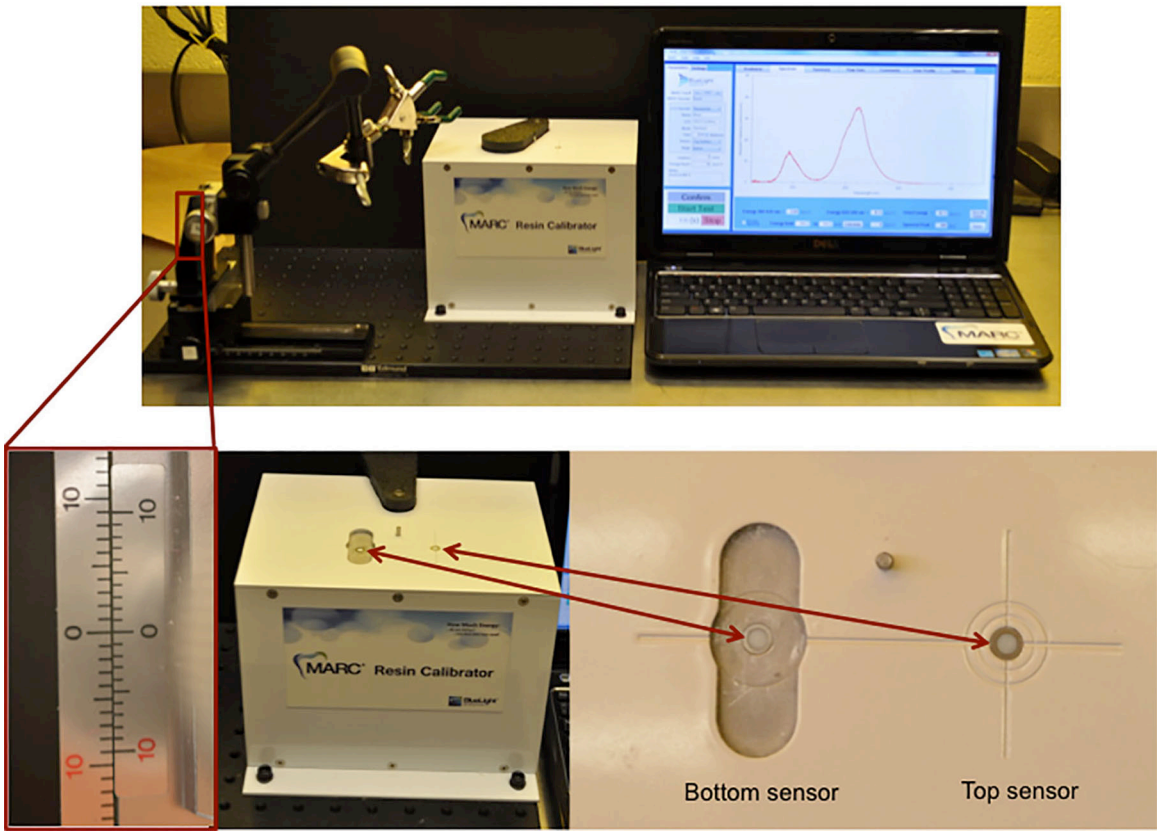

Figure 13. MARC-RC system

The MARC-RC components contain of a miniature spectrometer connected to a top and bottom 4 mm diameter cosine corrector (CC3) sensors. The spectrometer is connected to a computer to measure the LCU irradiance, radiant exposure and spectral distribution detected by the top and bottom MARC-RC sensors. The measurements collected from the top MARC-RC sensor represent the measurements received on the top surfaces of a RMC specimen. The measurements collected from the bottom MARC-RC sensor represent the measurements on the bottom surfaces of a RMC increment. A mechanical arm was used for LCU mounting to fix the position of the LCU, and has a ruler on the side to adjust the distance between the LCU guide tip and the sensor.

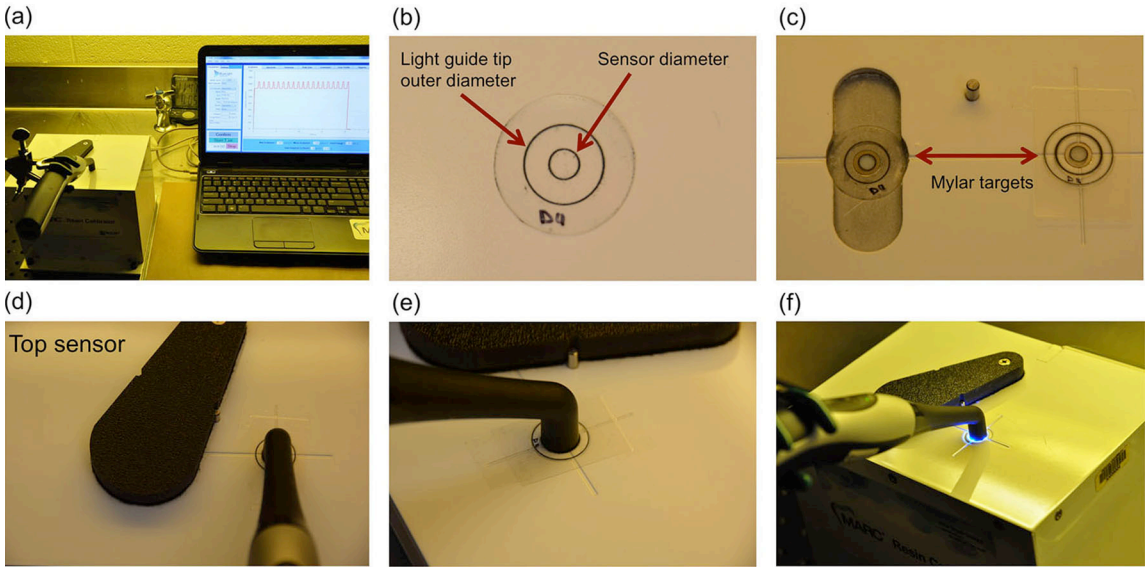

Figure 14. Representative of a LCU setup on the top MARC-RC sensor

(a) A LCU mounted on the MARC-RC mechanical arm. (b) Custom-made Mylar targets that matched the dimensions of the outer borders of a light guide tip. An inner circle that matched the diameter of a sensor was precisely located in the middle of the LCU tip outer dimensions to ensure a light guide tip centering over a MARC-RC sensor. (c) Placement of the Mylar target over the top and bottom sensors. (d) The LCU guide tip and handle was aligned with the MARC-RC crosshead on the surface to standardized x- and y-directions, and the light guide tip was positioned flat and perpendicular against the sensor to standardize the z-direction. (e) Centering of the light guide using the Mylar target over the top or bottom sensor and alignment of the light guide tip flat against the surface. (f) Removal of the Mylar target from the top sensor, adjustment of the desired curing distance using the side ruler, and light activation for collecting the irradiance, RE and spectral emission measurements from the LCU.

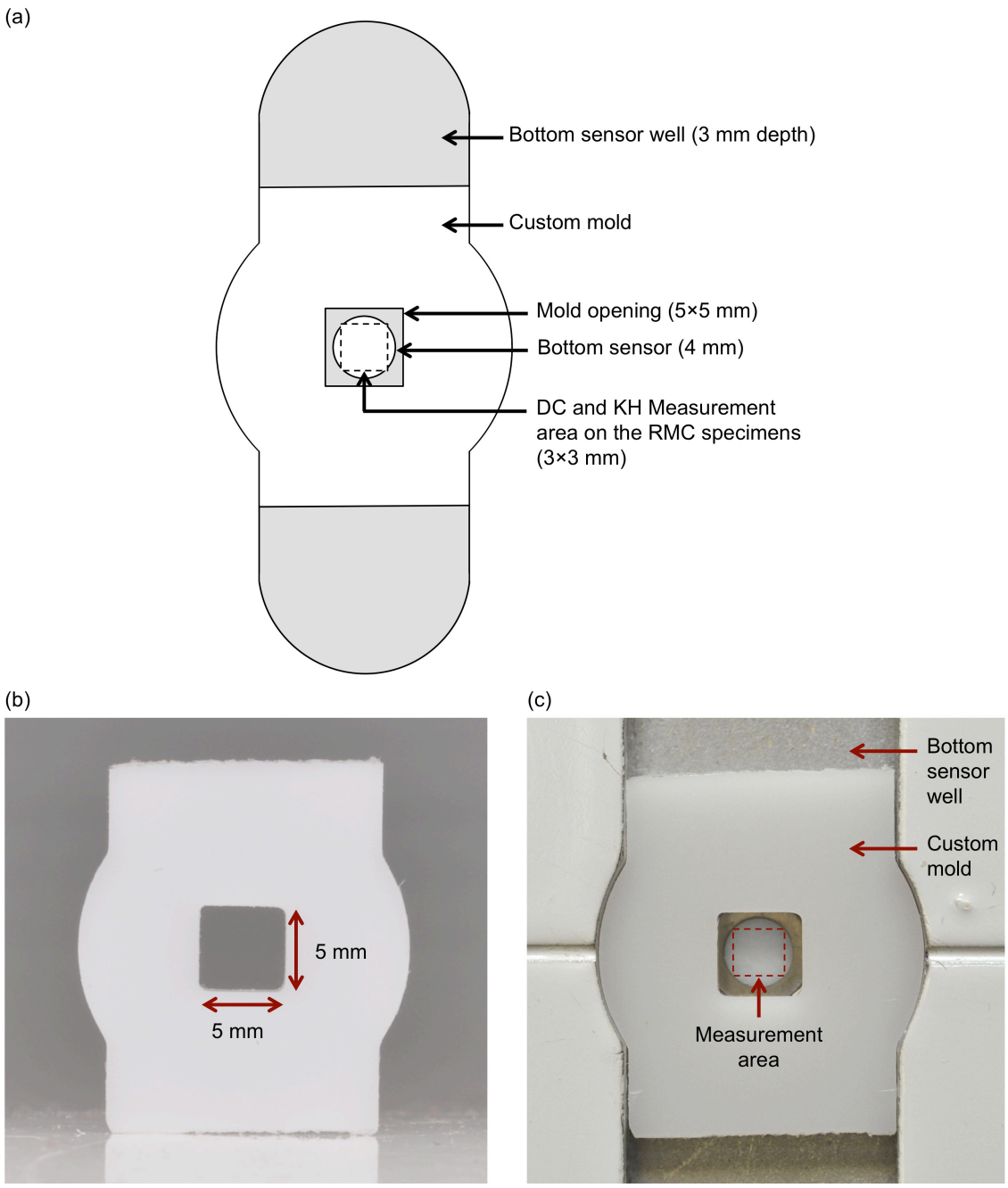

Figure 15. Custom-designed mold for the RMC specimen fabrication

(a) Illustration of the custom mold placement in the bottom MARC-RC sensor well. (b) Custom mold with a 5×5×2 mm square opening. (c) Custom mold designed with a square opening centered over the 4 mm bottom sensor with outer borders that followed the outline of the sensor well. The dashed 3×3 square represent the area where the KH and DC measurements were obtained. The DC and KH measurement area relatively coincided with the 4 mm sensor where the irradiance and RE measurements were collected.

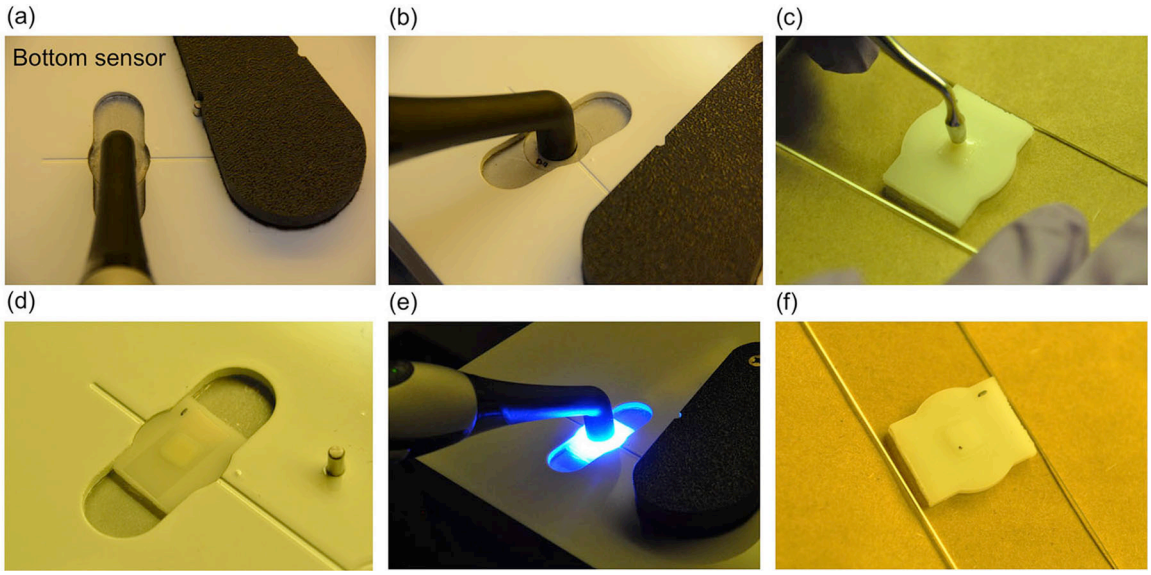

Figure 16. Representative of a LCU setup on the bottom MARC-RC sensor and setup RMC specimen fabrication

(a) A LCU guide tip and handle is aligned with the MARC-RC surface to standardized the x- and y-directions, and the light guide tip was positioned flat and perpendicular against the sensor to standardize the z-direction. (b) Centering of the light guide using the Mylar target over the bottom sensor, then removal of the Mylar target before placement of the mold-filled RMC. (c) Placement of the RMC in the mold. (d) Placement of the mold-filled material sandwiched between two Mylar strips. (e) Adjustment of the desired curing distance between the top surface of the mold and LCU guide tip, light activation from the top surface only using the curing time predetermined using the top sensor, and collecting measurements passing through a RMC increment. (f) Marking the lower right corner of the top surface of the prepared RMC specimen. The mark is placed outside the measurement collection area of the experiments performed.

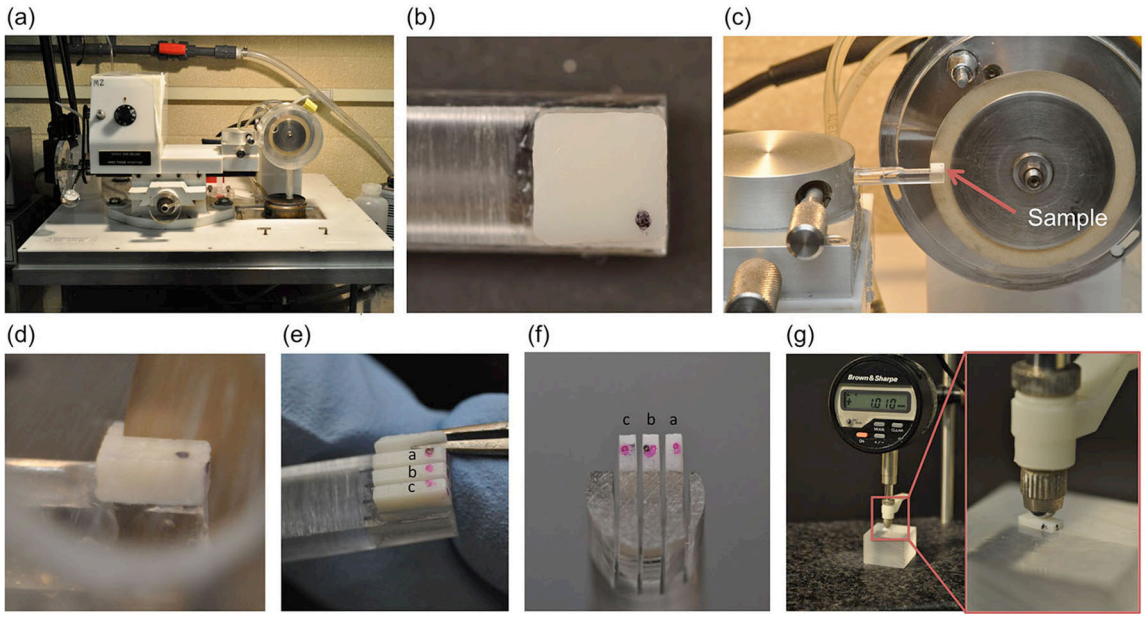

Figure 17. Setup of the RMC specimen sectioning

(a) Hard tissue microtome machine. (b) RMC specimen glued on an acrylic rod using cyanoacrylate glue, the lower right corner of each specimen was marked to identify the top surface and orientation of the specimen. (c) The rod with specimen was mounted on the brass mandrill and positioned in a right angle to the 0.2-mm thick blade. (d) Close-up of the RMC specimen sectioning. (e) Sectioned RMC specimen showing the cuts on the specimen and location of slice-a, -b and -c. (f) The outer edges were discarded and only the three 1 mm middle slices (a, b and c) were used for the depth characterization. (g) Measurement of the harvested slices to ensure each slice is 1 mm thick.

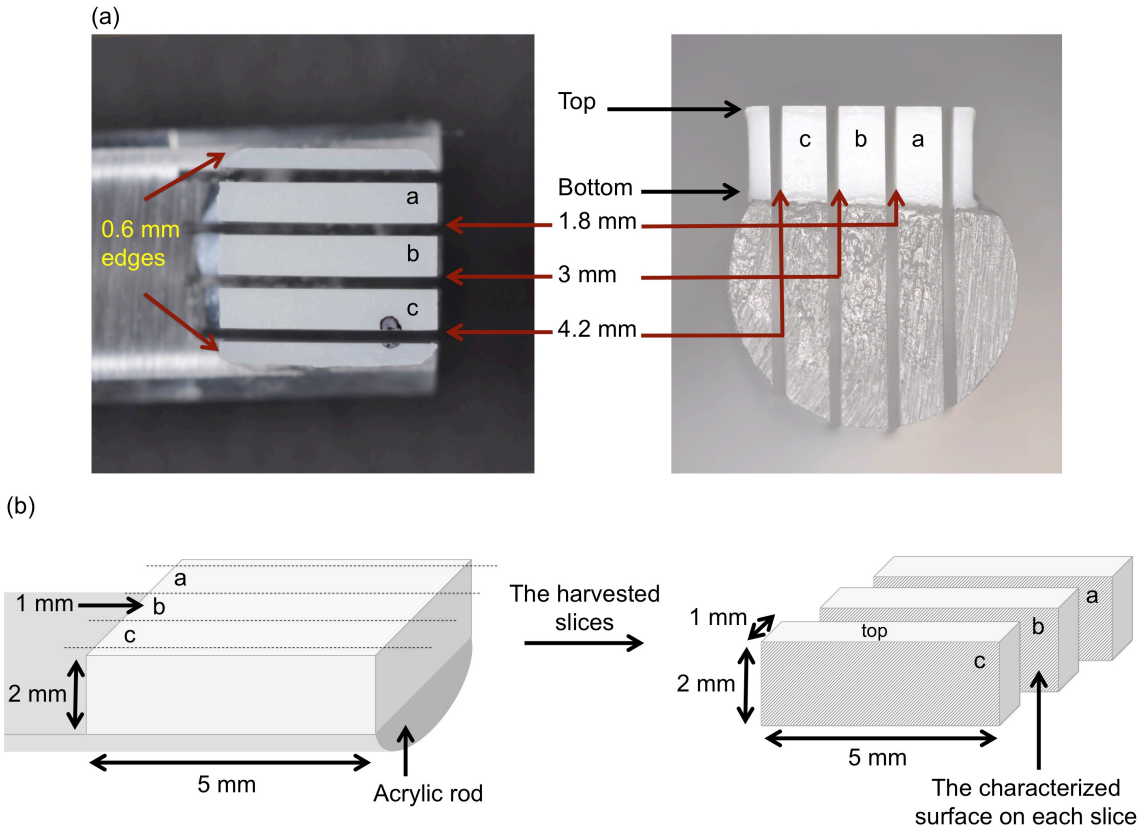

Figure 18. Representative sectioned RMC specimen for depth characterization

(a) Separate square specimens (5×5×2 mm) were prepared for depth characterization, mounted on an acrylic rod using cyanoacrylate glue. (a and b) each specimen was sectioned into three 1 mm thick slices (a, b and c), as illustrated. Since the blade thickness was 0.2 mm, the first cut was made at 0.6 mm and then in 1 mm increments, leaving discarded regions of 0.6 mm thickness from the top and bottom. The surface furthest from the first cut was characterized, as illustrated in the shaded surface: at slice-a=1.8 mm, slice-b=3 mm and slice-c=4.2 mm distance.

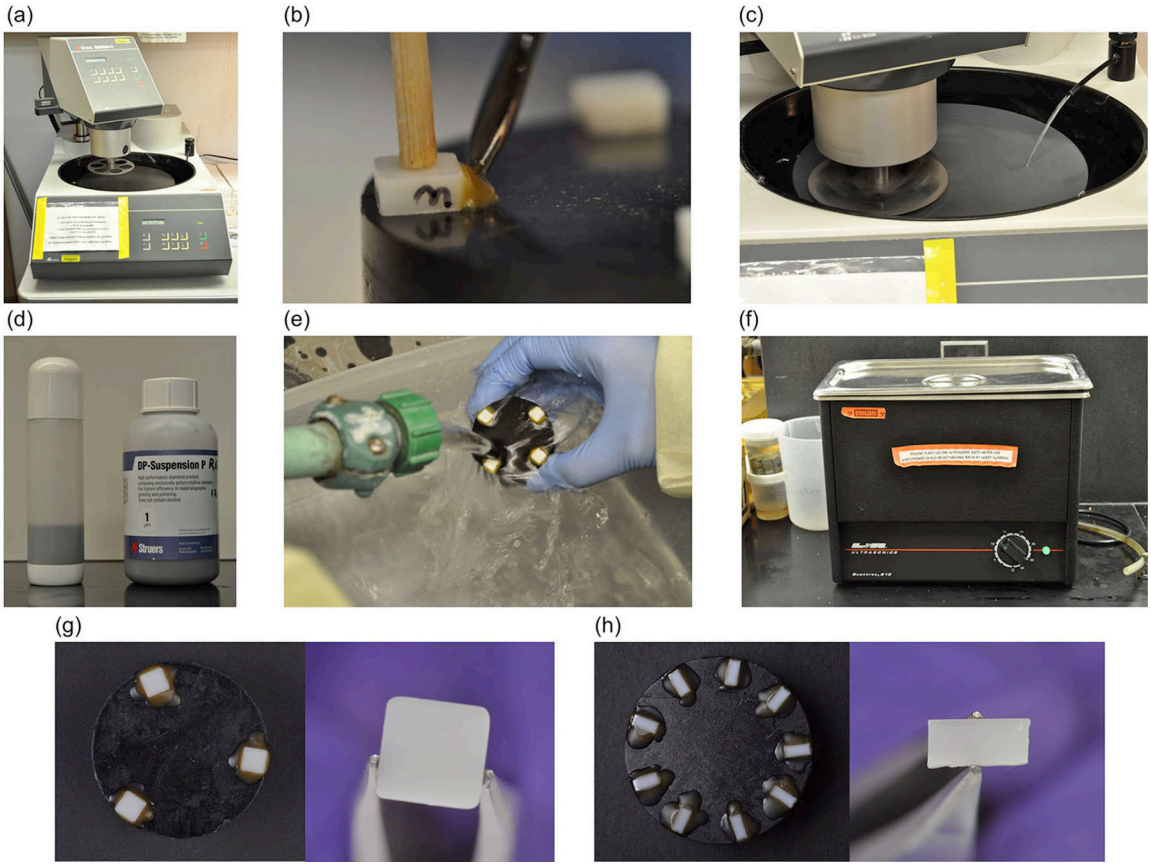

Figure 19. RMC specimens finishing and polishing procedure

(a) The finishing and polishing machine. (b) Mounting of the RMC specimens on blocks using mounting wax. (c) Finishing of the specimens using 1,200, 2,400, and 4,000 grits. (d) The 1-µm diamond polishing suspension. (e) Washing of the specimens under running water for three minutes after finishing and after polishing of the specimens for two cycles with ultrasonically cleaning the specimens between the cycles. (f) Specimens ultrasonically cleansed for 3 minutes after finishing and 20 minutes after polishing. (g) The finished and polished RMC specimens for top and bottom surfaces characterization (n=3/LCU). (h) The finished and polished RMC slices for depth characterization (n=3 slices/specimen/LCU).

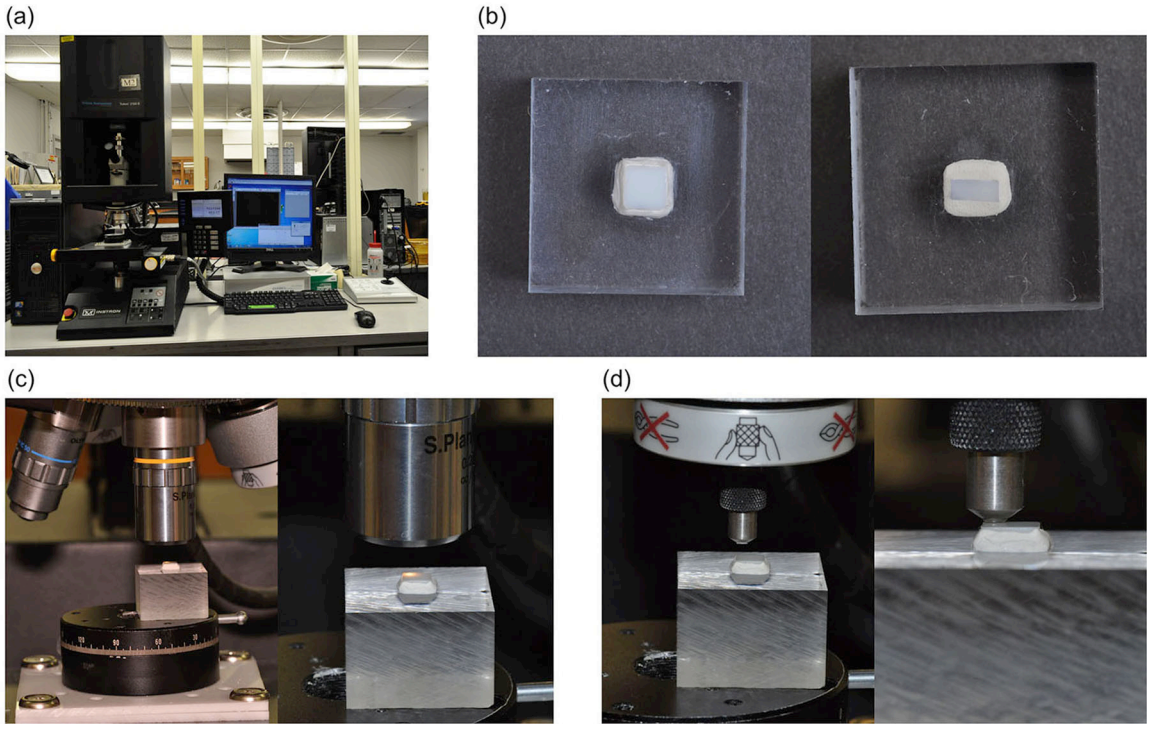

Figure 20. Knoop microhardness test setup

(a) Microhardness tester with an automated stage connected to a computer. (b) The RMC specimens mounted on an acrylic block using a removable mounting putty to stabilize the specimens. (c) Mounted specimens placed on the automated stage. (d) Obtaining KH indentations on the specimens using 50-gram and 10 seconds dwell time.

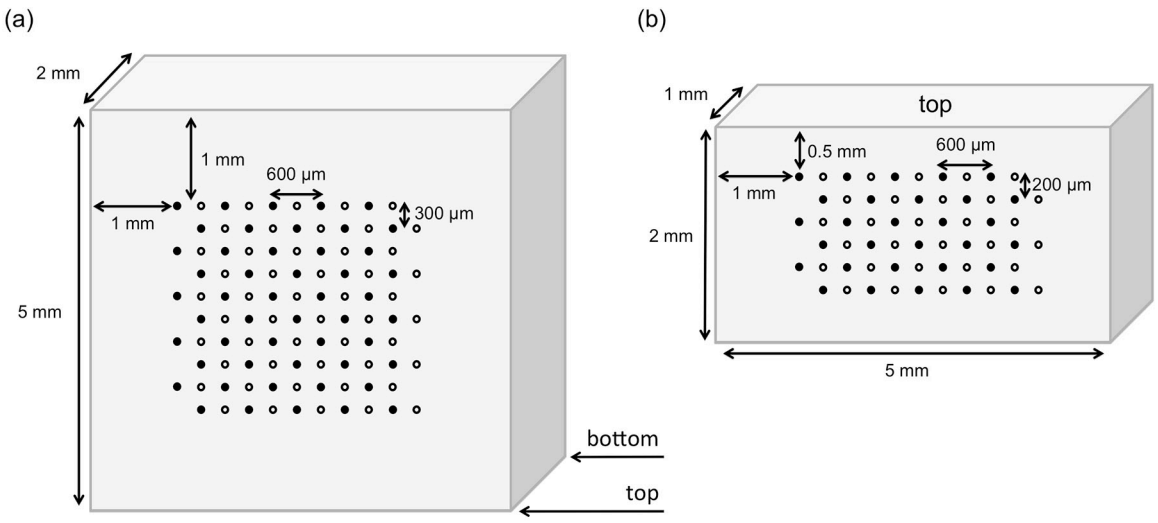

Figure 21. Illustration of the DC and KH mapping on the RMC specimens

(a) Separate square specimens were prepared for the top and bottom KH and DC mapping of the RMC specimen. Top and bottom surfaces characterization of each specimen was performed in a checkerboard pattern (50 points), with the measurements obtained 1 mm away from all edges of the specimen and 600-µm apart in an x-direction and 300-µm apart in a y-direction. (b) Different square specimens were prepared for depth characterization. At the designated surfaces of sections a, b, and c of the specimen, KH and DC mapping was performed in a checkerboard pattern (30 points). The measurement were obtained 1 mm away from the sides and 0.5 mm away from the top and bottom surfaces of the sections and arranged 600-µm apart in an x-direction and 300-µm apart in a y-direction. For (a and b), solid circles represent KH indentations BE and the hollow circles represent KH indentations AE.

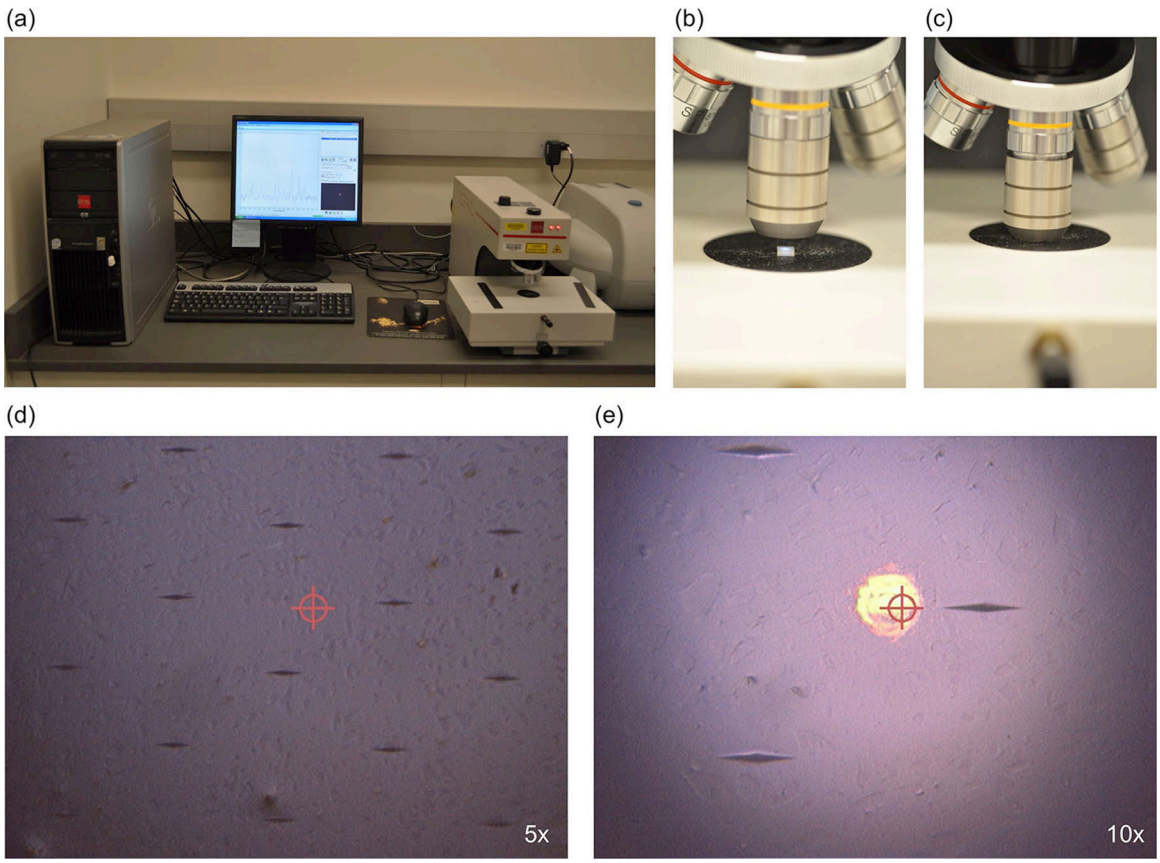

Figure 22. Micro-Raman spectroscopy experiment

(a) Micro-Raman spectroscopy instrument. (b) Placement of the specimen under the microscope. (c) Securing the microscope casing over the specimens before collecting the measurements. (d) Representative image showing the KH indentation on the RMC specimen. (e) Spectra measurement were collected next to each KH indent on all specimens.

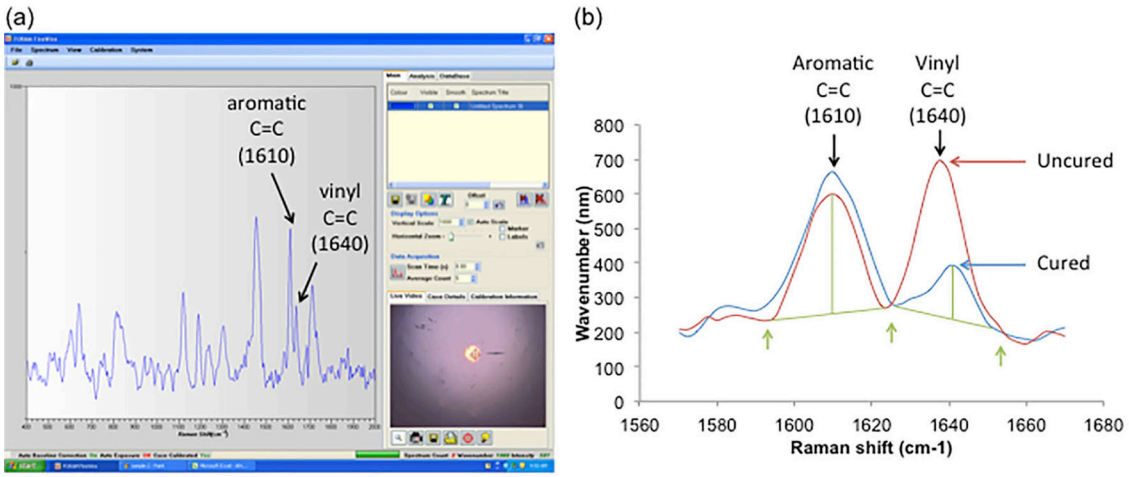

Figure 23. Representative spectra measurement of the peaks of interest collected using a micro-Raman spectroscopy instrument

(a) The peaks of interest on the spectra measurements collected. (b) Peak heights of the cured and uncured RMC curves of interest were calculated by locating the highest point of each peak and locating the middle distance between the curve valleys, as represented by the green lines and arrows. The DC calculations were performed by comparing the relative change of the peak height of the band at 1640 cm^{-1}, representing the C=C stretch before and after the polymerization, to the aromatic C=C reference peak height of the band at 1610 cm^{-1}, which remains unchanged during the polymerization reaction initiated by light curing.

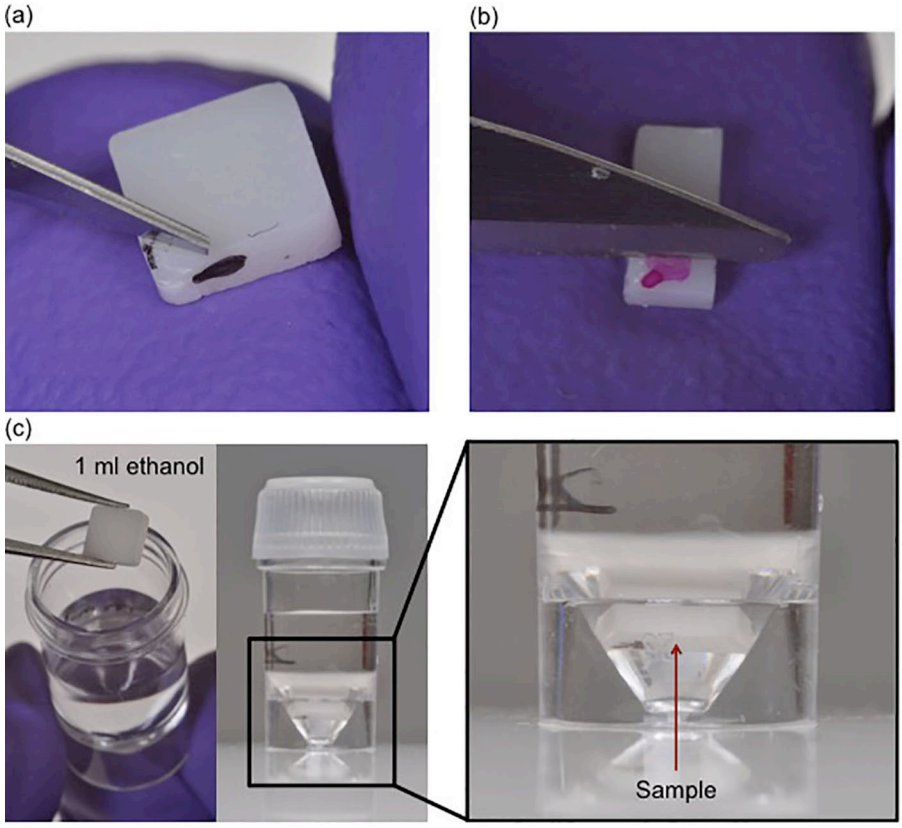

Figure 24. Soaking the RMC specimens in absolute ethanol

(a) A physical scratch was created on the lower right corner on the bottom surfaces of each specimen assigned for top and bottom characterization using a scalpel to identify the specimen orientation after soaking the specimens in ethanol. The scratch was placed in a location away from the KH indent grid. (b) A physical scratch was placed on each slice for depth characterization on the opposite side of the surface being characterized. (c) Each specimen was placed in a vial with a conical bottom that contains 1-ml absolute ethanol to expose all specimen surfaces to the ethanol.

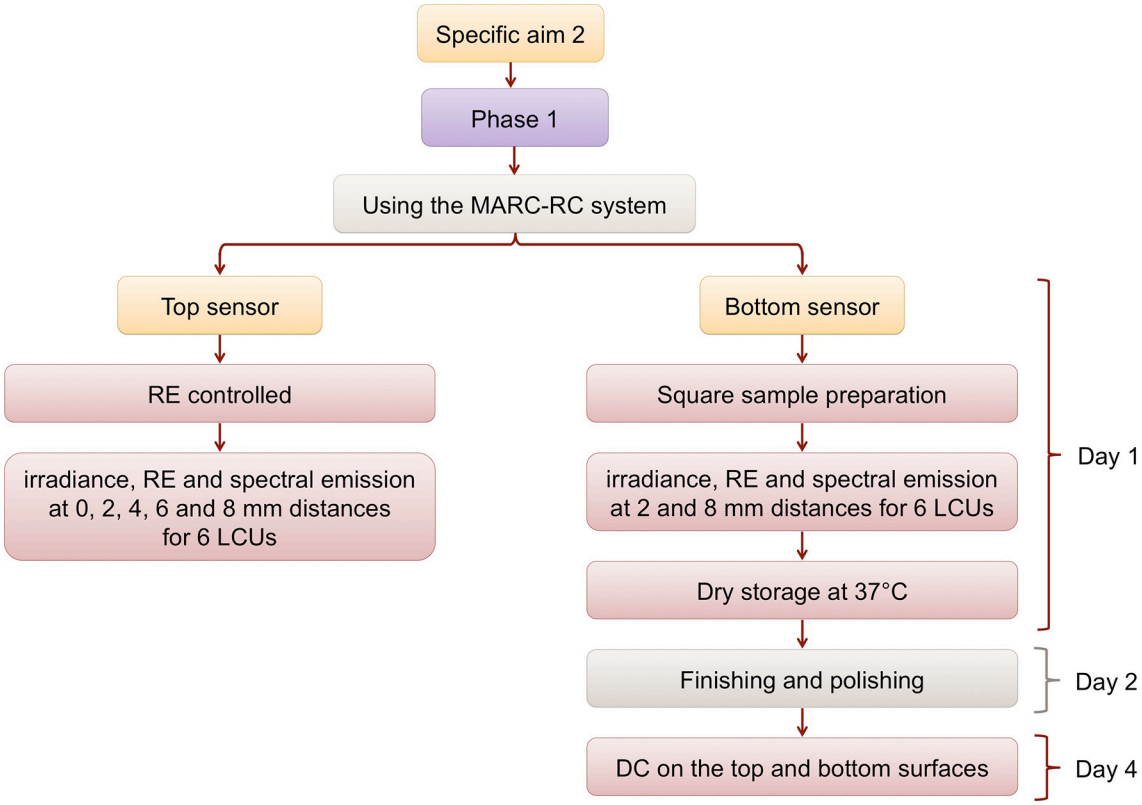

Figure 25. Specific aim 2, phase 1 experimental design

Figure 26. SmartLite Max multiple emission peak LED LCU

(a) The SmartLite Max (SM) LCU. (b) Side view of the light guide head that contains the LED chips. The LED chips are located in the light guide head and not the body of the LCU. The arrow on either sides of the light guide tip represent the location where the emitted light is collimated, and to aid in alignment of the light guide with the target surface. (c) Frontal view of the light guide that contains the LED chips. (d) Effective area of the light-emitting portion. The effective light is emitted through the smooth center of the light guide tip and not from the frosty area. (e) The activated LCU showing part of the blue LED chip and part of the violet LED chip. Only part of the LED chips was captured in the image because they are aligned in an angle. (f) The light guide head positioned in an angle to show the entire blue LED chip. (g) The light guide head positioned in an angle to show the entire violet LED chip.

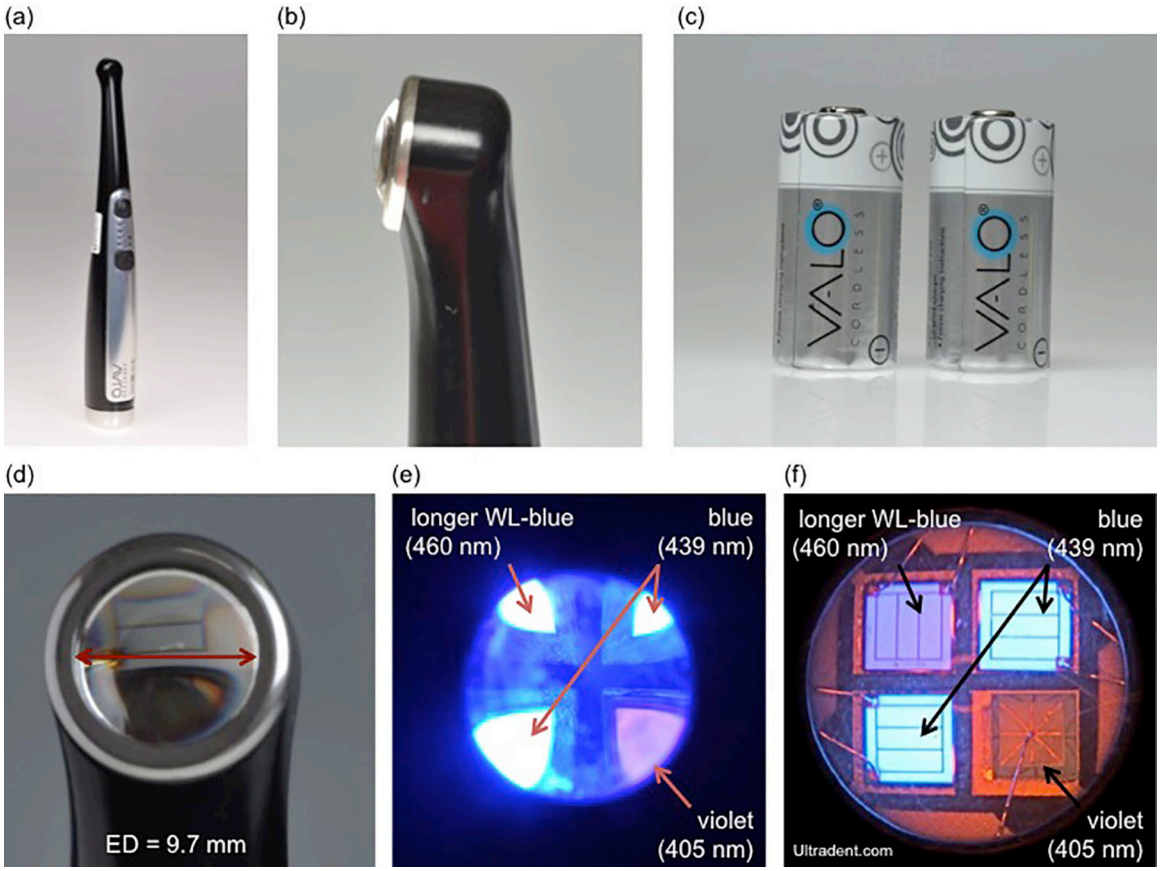

Figure 27. VALO Cordless multiple emission peak LED LCU

(a) The VALO Cordless (V) LCU. (b) Side view of the V LCU showing the concave light guide tip that is designed to collimate the emitted light. (c) The LCU is charged by rechargeable battery. (d) The effective diameter (ED) of the light-emitting portion of the light guide head. All the LED chips are located in the light guide head. (e) The activated LCU showing the locations of the four LED chips. V contains three blue LED chips and one violet LED chip. The LED chips are not clearly seen because the concave tip prevents showing each LED chip effectively. (f) The location of the LED chips in the light guide head.

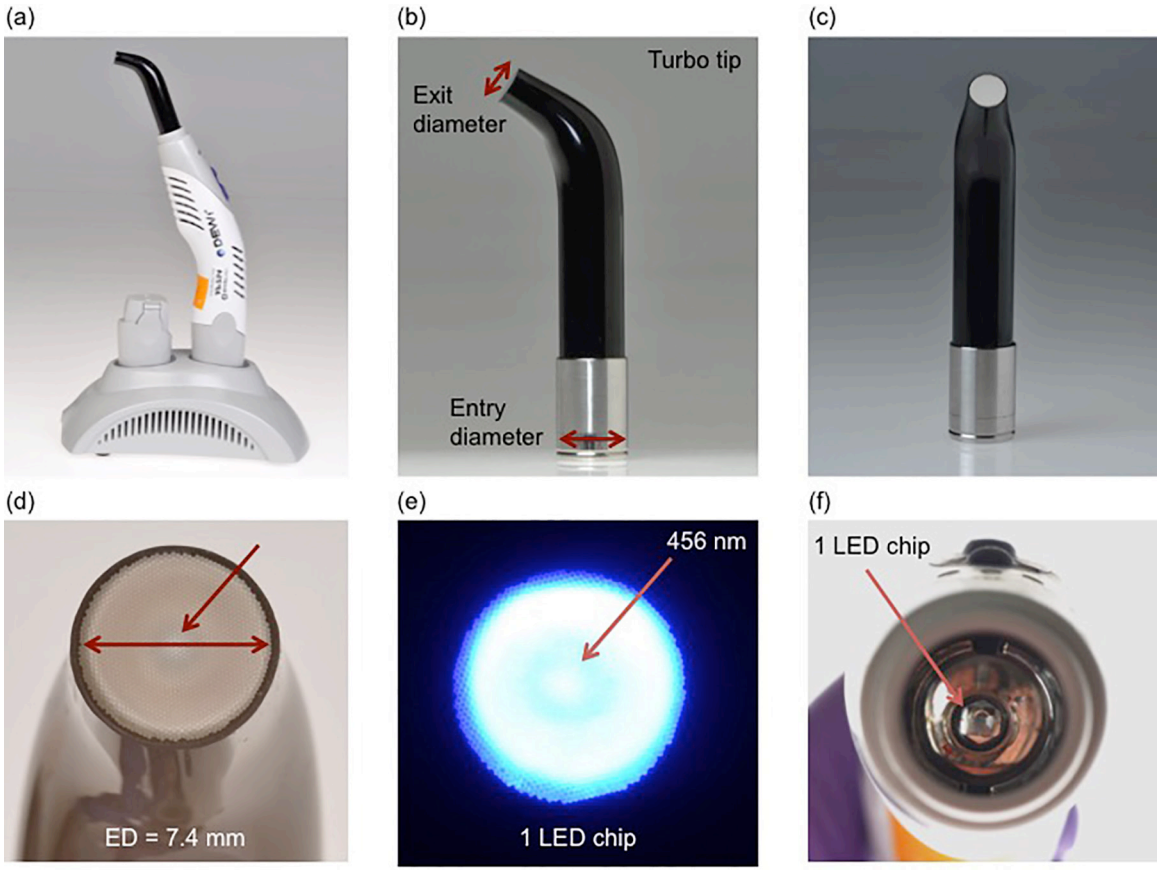

Figure 28. DEMI single emission peak LED LCU

(a) The DEMI (D) LCU. (b) Side view of the fiber optic turbo tip that has an exit diameter that is smaller than the entry diameter. (c) Frontal view of the fiber optic light guide tip. (d) The effective light-emitting diameter (ED) of the light guide tip and the location of the LED chip. (e) The activated LCU showing one blue LED chip. (f) The body of the LCU without the light guide tip showing the location of the blue LED chip.

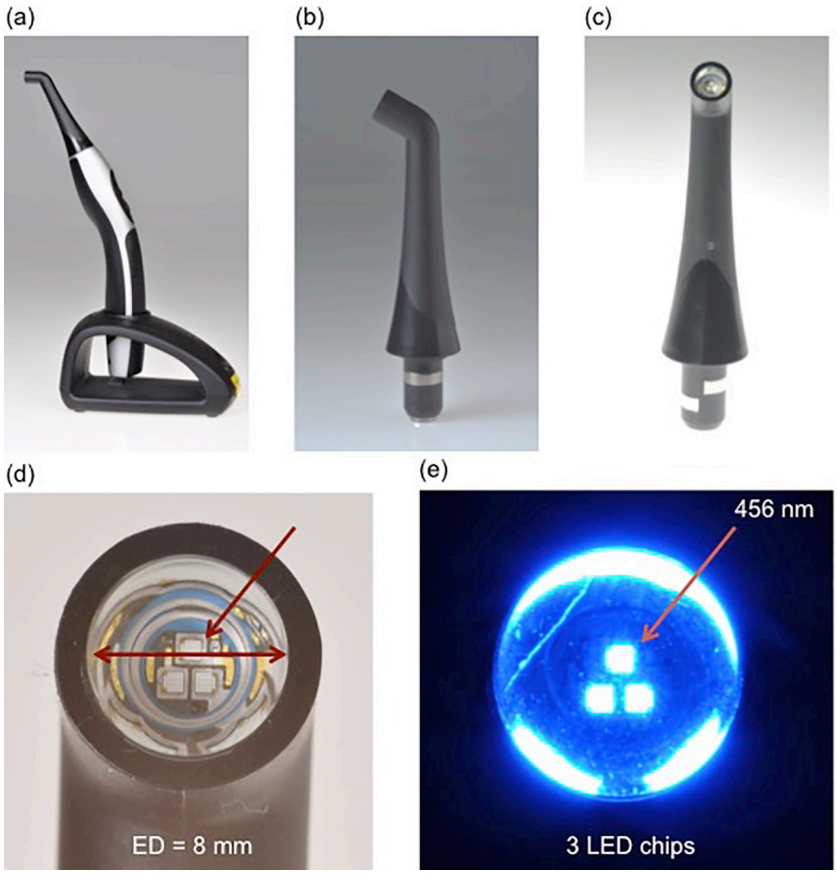

Figure 29. Demi Ultra single emission peak LED LCU

(a) The Demi Ultra (DU) LCU. (b) Side view of the light guide head that contains the LED chips. The LED chips in DU are not located in the body of the LCU. (c) Frontal view of the light guide head. This LCU uses a capacitor instead of a regular battery located in the body of the LCU for fast recharge of the LCU. (d) The effective light-emitting diameter (ED) of the light guide head and location of the three blue LED chips. (e) The activated LCU showing the three blue LED chips.

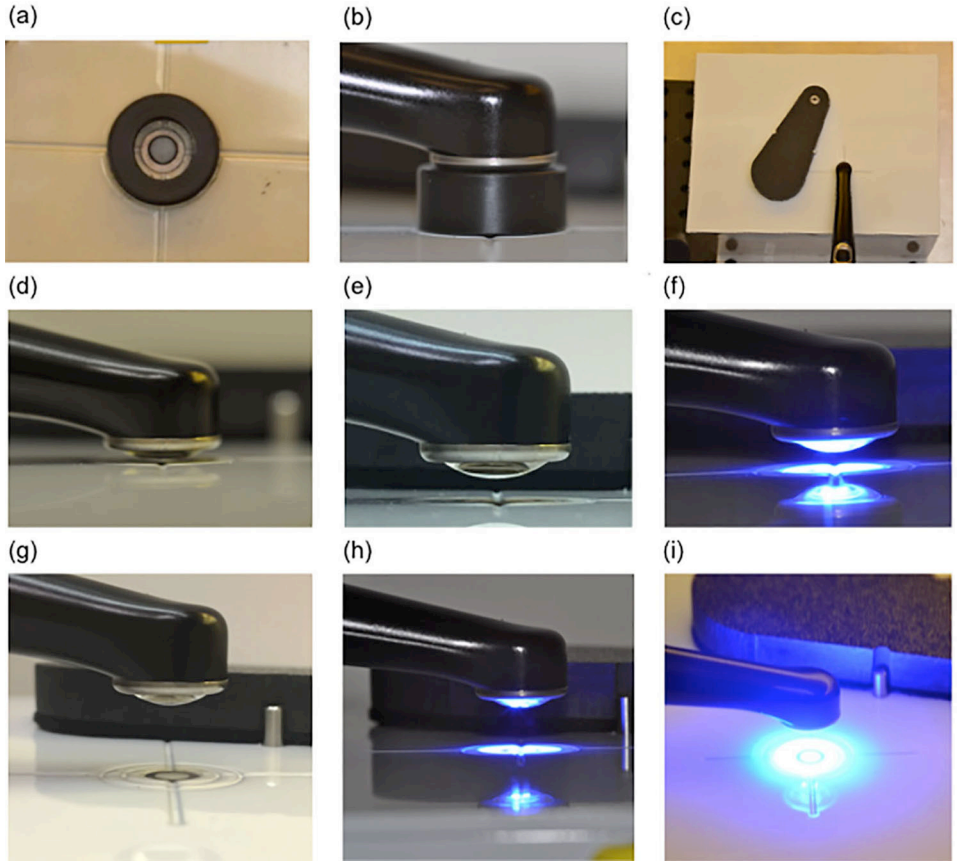

Figure 30. Setup of VALO Cordless on a top MARC-RC sensor

(a) Custom-made adapter centered over the top MARC-RC sensor using a Mylar target. (b) V LCU alignment using the custom-made adapter. (c) LCU alignment over the top sensor in the x- and y-direction along the crosshead on the MARC-RC surface. (d) Removal of the adapter and placement of the V LCU at 0 mm distance against the most concave point. (e) Adjustment of the LCU at the 2 mm distance. (f) Light activation and collecting measurements. (g) Adjustment of the LCU at the 8 mm distance. (h and i) different views of the activated LCU to collect the irradiance, RE and spectral emission measurements detected by the top sensor.

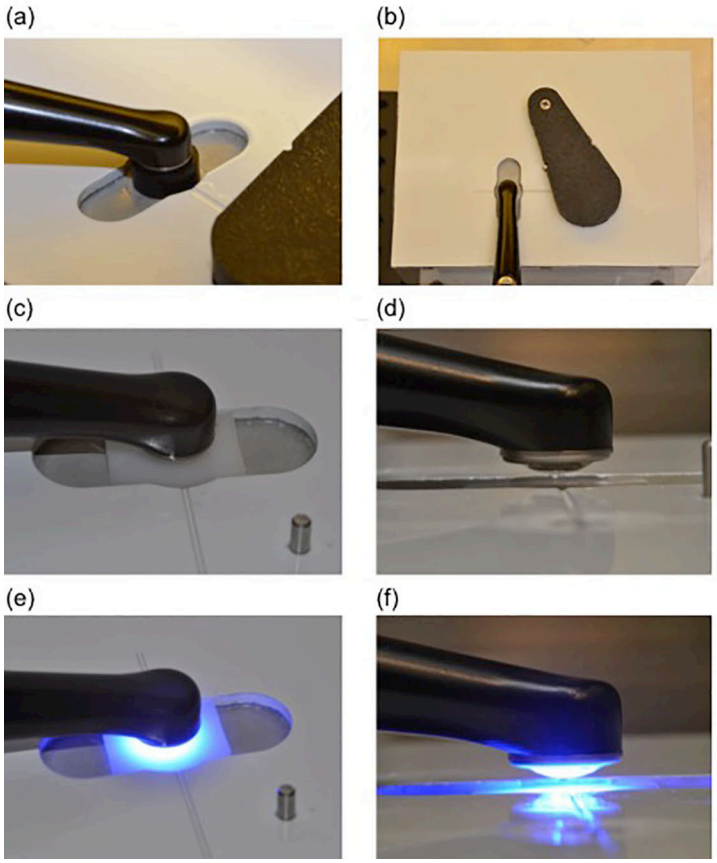

Figure 31. Setup of VALO Cordless on a bottom MARC-RC sensor

(a) Custom-made adapter centered over the bottom MARC-RC sensor using a Mylar target and V LCU alignment. (b) The LCU alignment using over the bottom sensor along the crosshead on the MARC-RC surface. (c) Removal of the adapter and placement of the V LCU at 0 mm distance from the mold with RMC. (d) Adjustment of the LCU at the desired distance. (e and f) two views of the activated LCU to collect irradiance, RE and spectral emission measurements detected by the bottom MARC-RC sensor.

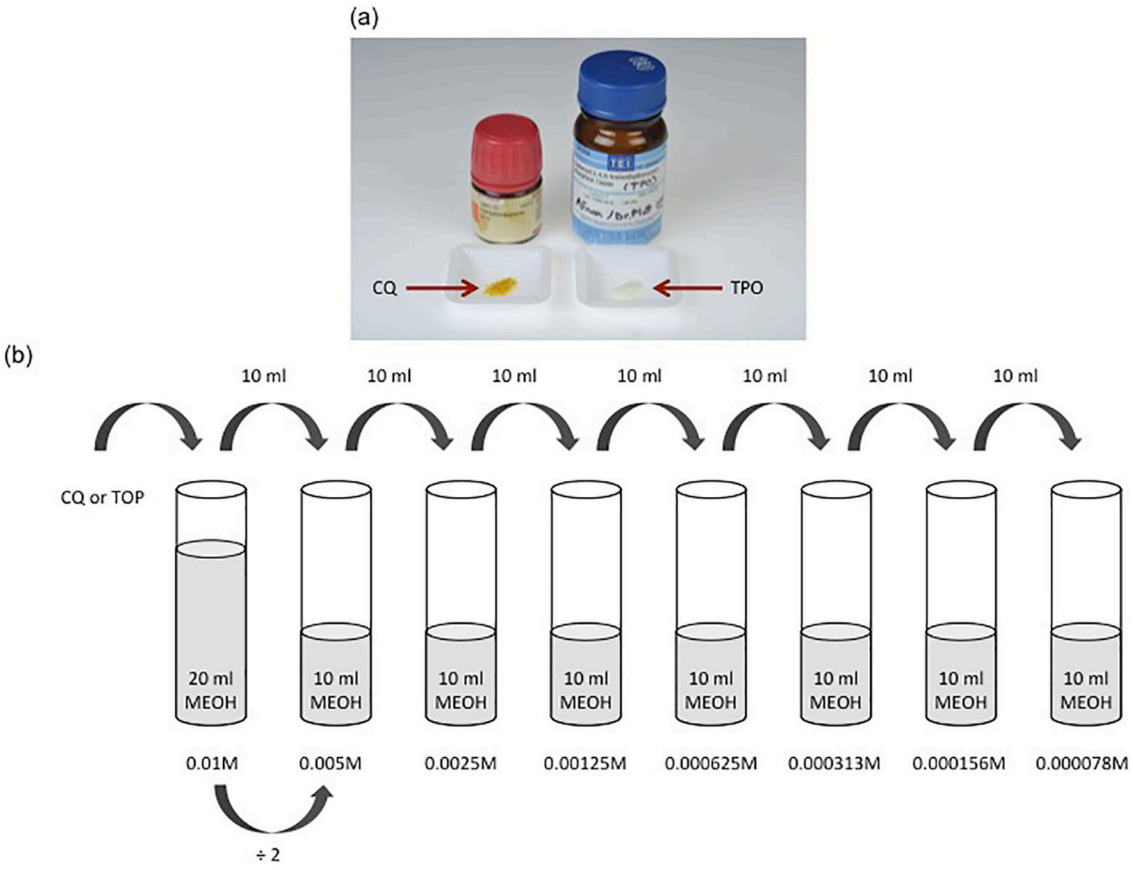

Figure 32. Serial dilutions of the photoinitiator molar absorptivity experiment

(a) The yellowish CQ photoinitiator and the white TPO alternative photoinitiator. (b) Eight calibrant solutions were prepared for each photoinitiator in serial dilutions by mixing CQ or TPO photoinitiator with 20 ml methanol starting from 0.01M concentration.

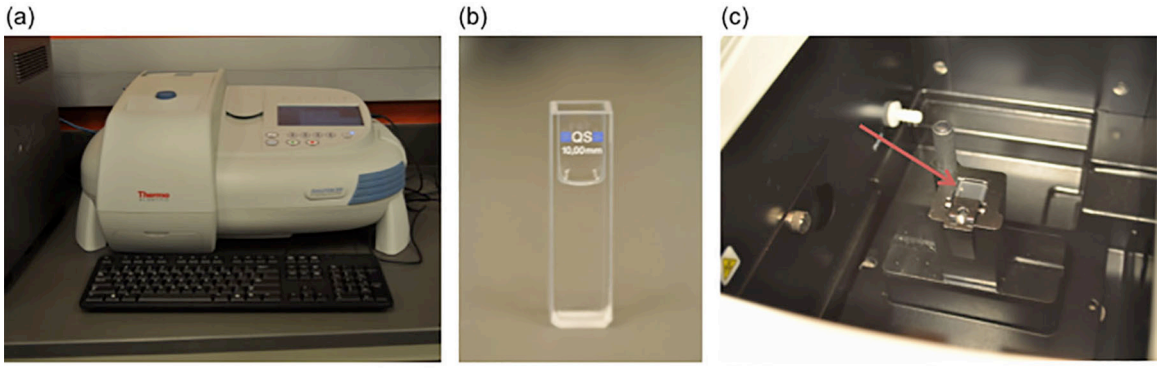

Figure 33. Ultraviolet (UV) spectrophotometry instrument

(a) UV-spectrophotometry for molar absorptivity measurements. (b) Cuvette that contains a prepared CQ or TPO solution. (c) Insertion of the cuvette in the UV-spectrophotometry and measurement collection.

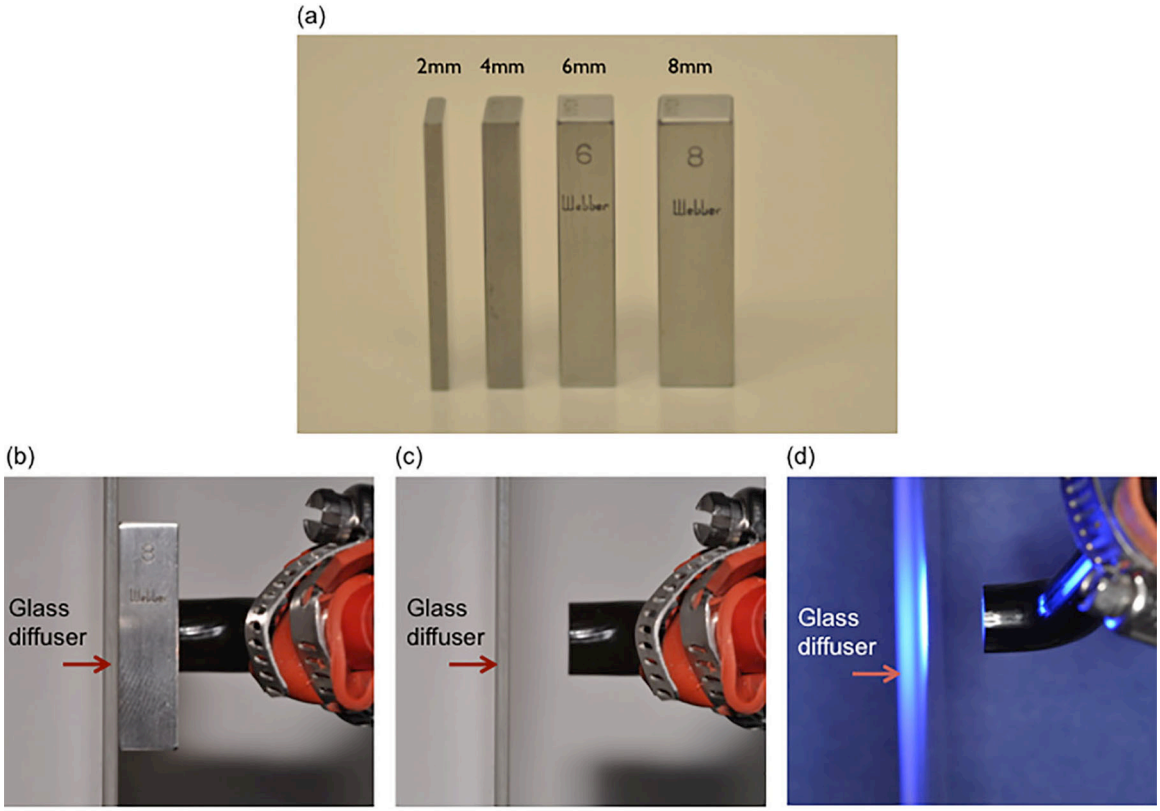

Figure 34. LCU setup against a ground glass diffuser

(a) 2, 4, 6 and 8 mm gauge blocks were used to precisely adjust the desired distance between the light guide tip and ground glass diffuser. (b) Placement of a gauge block against the ground glass diffuser. (c) Removal of the gauge block. (d) Light activation for collecting beam profile measurements.

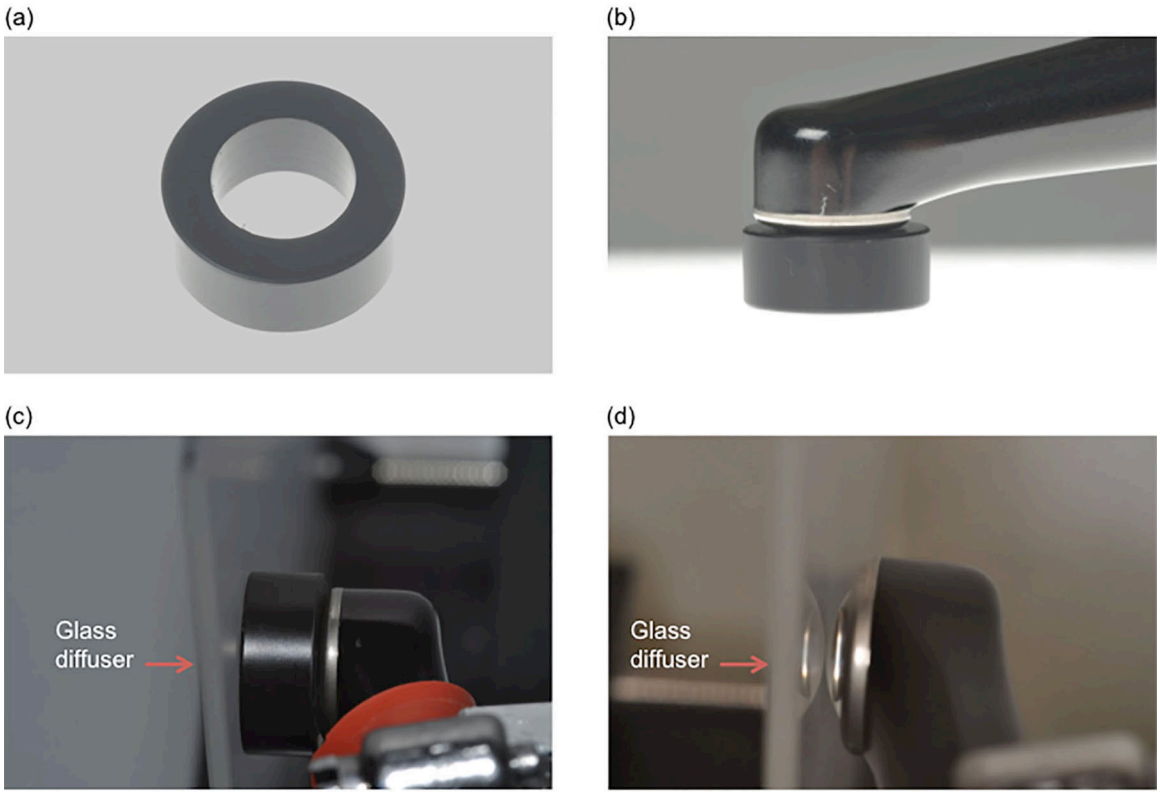

Figure 35. VALO Cordless setup against a ground glass diffuser

(a) The custom-made adapter that matched the dimensions of V. (b) Illustrating the seating of V light guide head on the adapter to ensure the LCU alignment in the x-, y- and z-direction. (c) The setup of V with the adapter against the ground glass diffuser. (d) Removal of the adapter and setup of the most concave point against the ground glass diffuser, which is considered the 0 mm. Then, the LCU is adjusted at the desired distance using the gauge blocks.

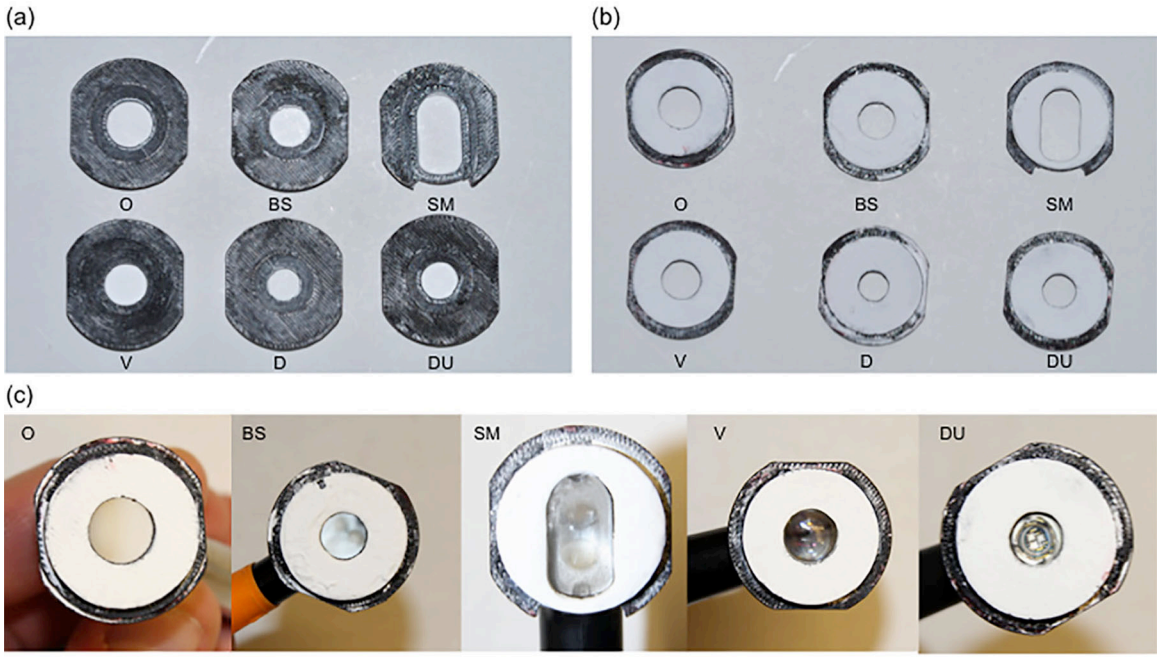

Figure 36. Custom-made 3D printed adapters for placement on an integrating sphere opening

(a) The outer surface of the custom-made adaptors matches the dimensions of the light-emitting portion of the individual LCU guide tip. The light guide tip rests on this side of the adapter. (b) The inner surface of the adapters facing the inside of the integrating sphere was coated with a highly reflective barium sulfate material in order to match the inside of the integrating sphere. (c) The inner surface adaptation of each light-emitting portion of the individual LCU guide tip against the custom-made adapters.

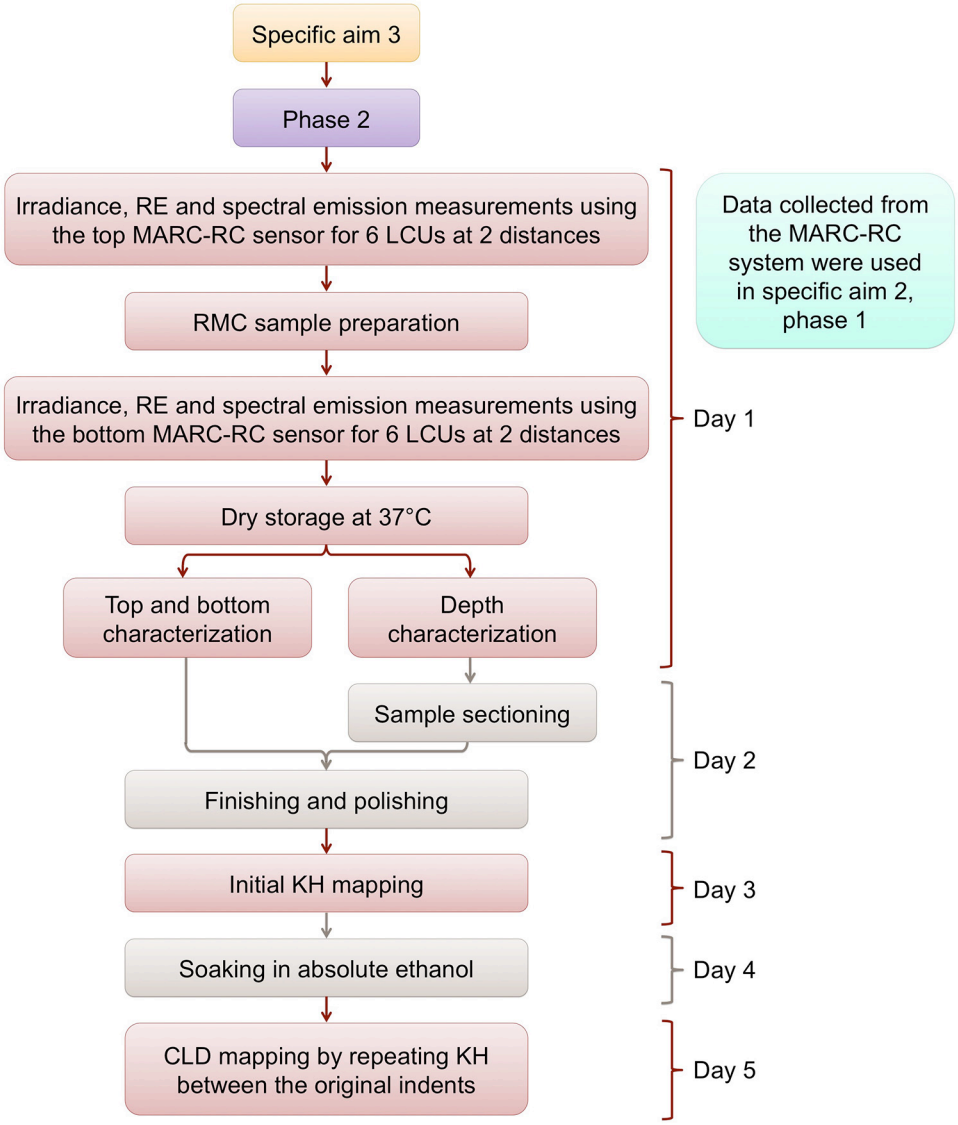

Figure 37. Specific aim 3, phase 2 experimental design

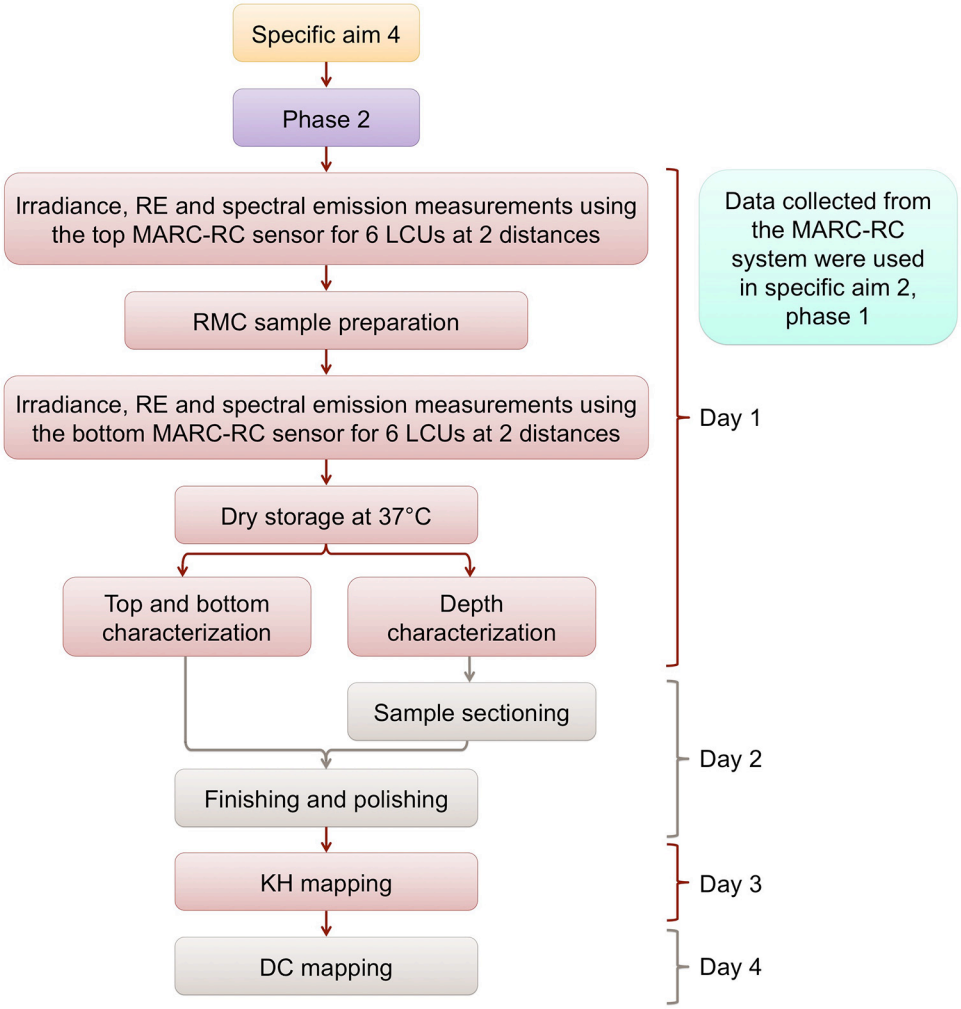

Figure 38. Specific aim 4, phase 2 experimental design

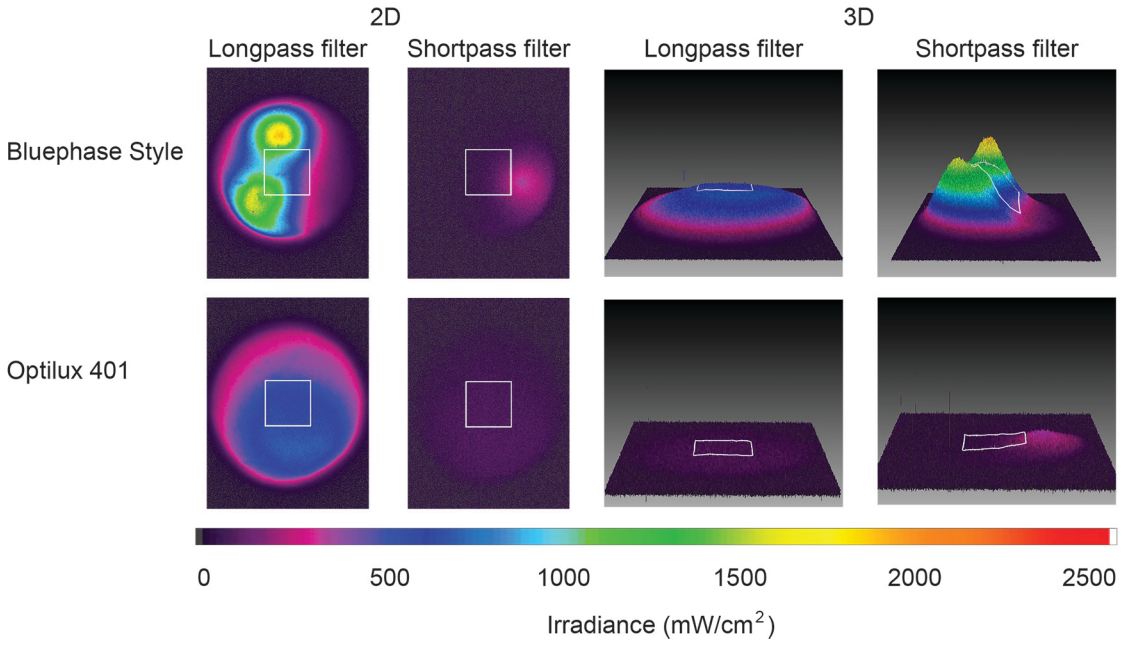

Figure 39. Representative 2D and 3D irradiance beam profiles from the multiple emission peak LED (BS) LCU and QTH (O) LCU measured through a 425 nm longpass or shortpass filter with the light emitting tip at 2 mm distance from a glass diffuser

To compensate for differences in the spectral response of the photodiode within the CCD camera of the beam profiler system, shortpass and longpass optical filters, both having a cut-off wavelength of 425 nm, were used to separate violet light from blue light with peaks at approximately 409 nm and 456 nm, respectively. The shortpass filter allowed only wavelengths below 425 nm to "pass" through to the CCD camera, while the longpass filter was used only to allow wavelengths greater than 425 nm to reach the CCD camera and blocked wavelengths below this value. The square in the center of each irradiance distribution image corresponds to the 3×3 grid where the KH and DC measurements were obtained from the RMC square specimens tested in this study.

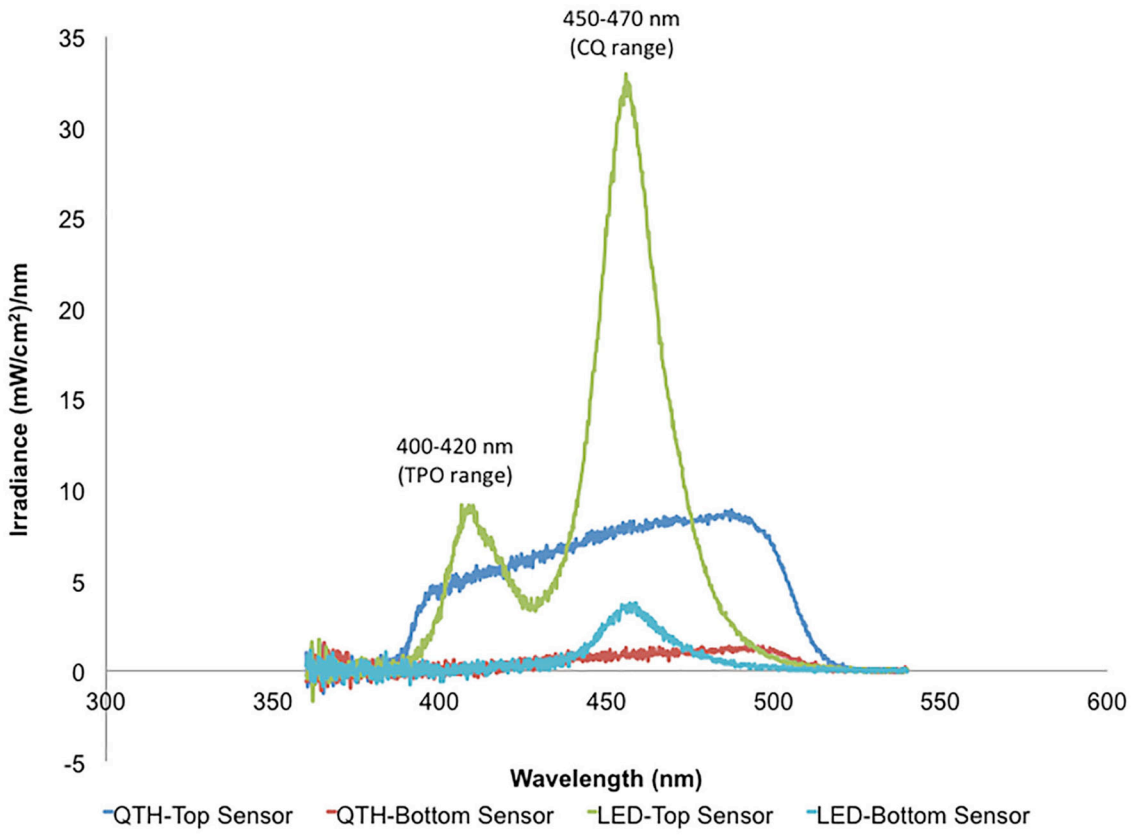

Figure 40. Representative spectral emission curves for the LED (BS) and QTH (O) LCUs

The emission curves were generated using the MARC-RC system. For the curves in the figure denoted "Top Sensor", the light-emitting tip of the LCU was positioned 2 mm above the top sensor of the MARC-RC system. Similarly, for the curves in the figure denoted "Bottom Sensor", the bottom sensor of the MARC-RC system was used to generate the emission curves after light from the LCU passed through a 2 mm RMC specimen with the light emitting tip of the LCU positioned 2 mm above the specimen. The emission curves for the two LCUs show that the spectral distributions of both curves encompass the absorption ranges for both CQ and TPO photoinitiators.

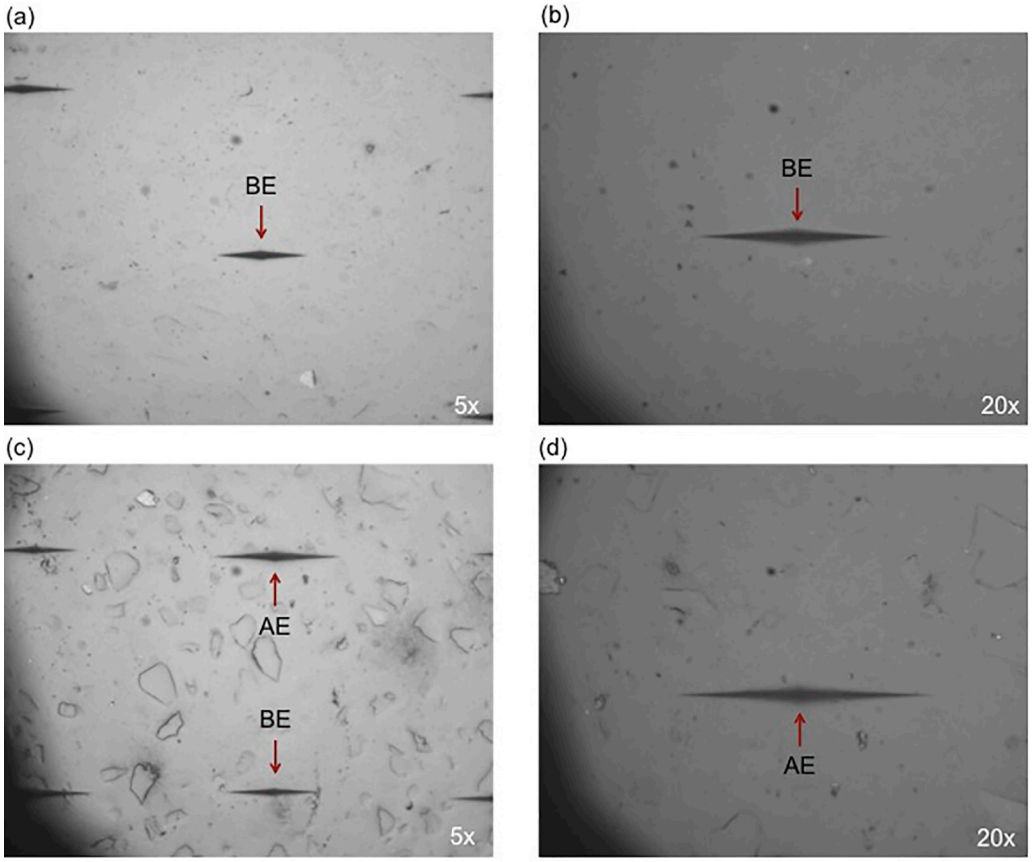

Figure 41. Representative images for the Knoop microhardness indentations BE and AE

(a and b) two different magnifications showing the finished and polished RMC specimen surface with the KH indents BE in a checkerboard pattern. (c and d) two different magnifications showing the rough RMC surface AE exposing the filler particles, and a longer KH indents AE due to ethanol softening. The images also display the KH indents AE placed in a checkerboard pattern between the KH indents performed BE.

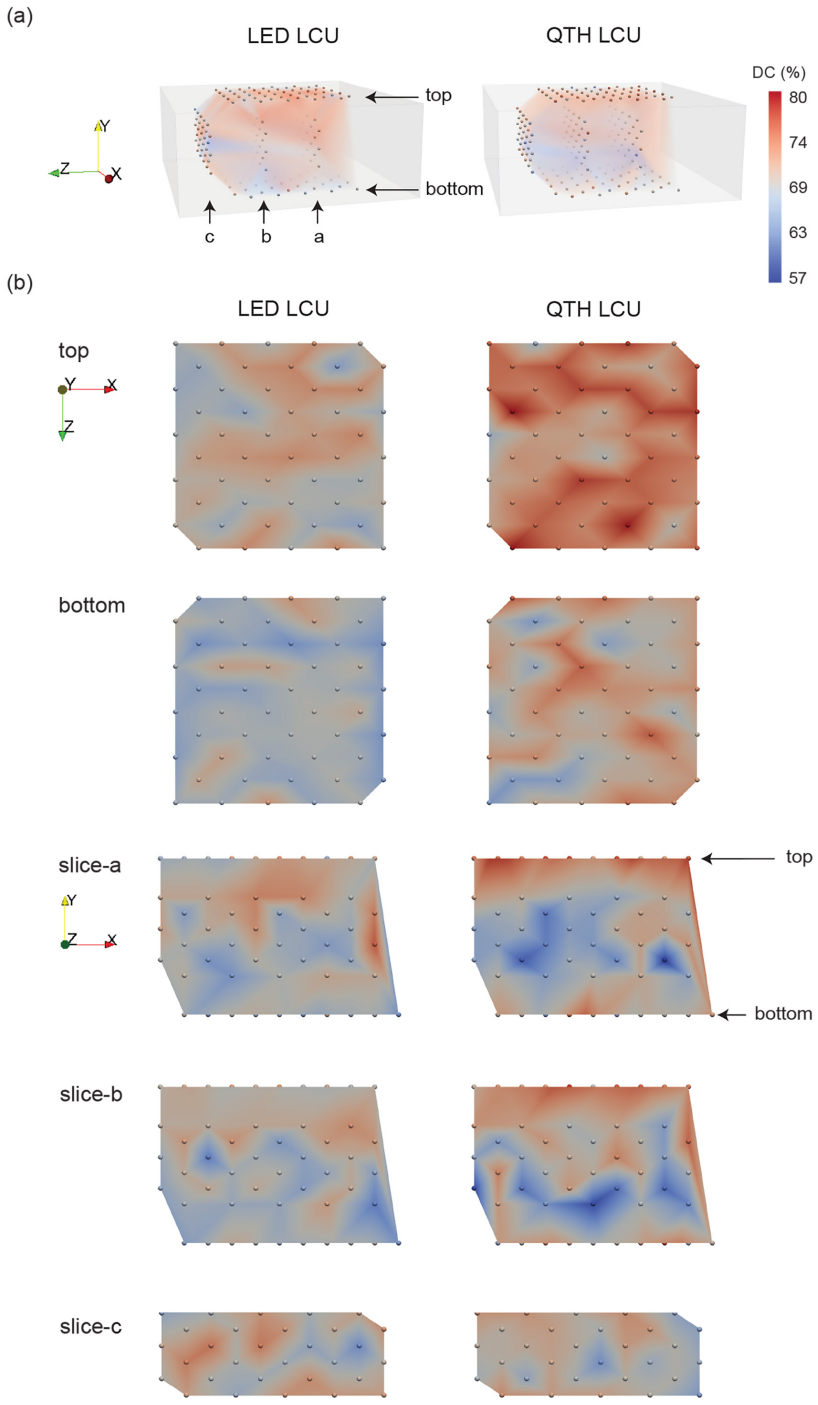

Figure 42. Representative DC (%) 2D contour maps and 3D renderings of RMC specimens light cured with the LED (BS) LCU and the QTH (O) LCU

The Spheres on the renderings represent the location where the DC% measurements were collected. (a) 3D renderings of the DC% of entire specimens cured by each of the LCUs showing the surfaces characterized. (b) 2D renderings of the DC% of the surfaces characterized cured by both LCUs.

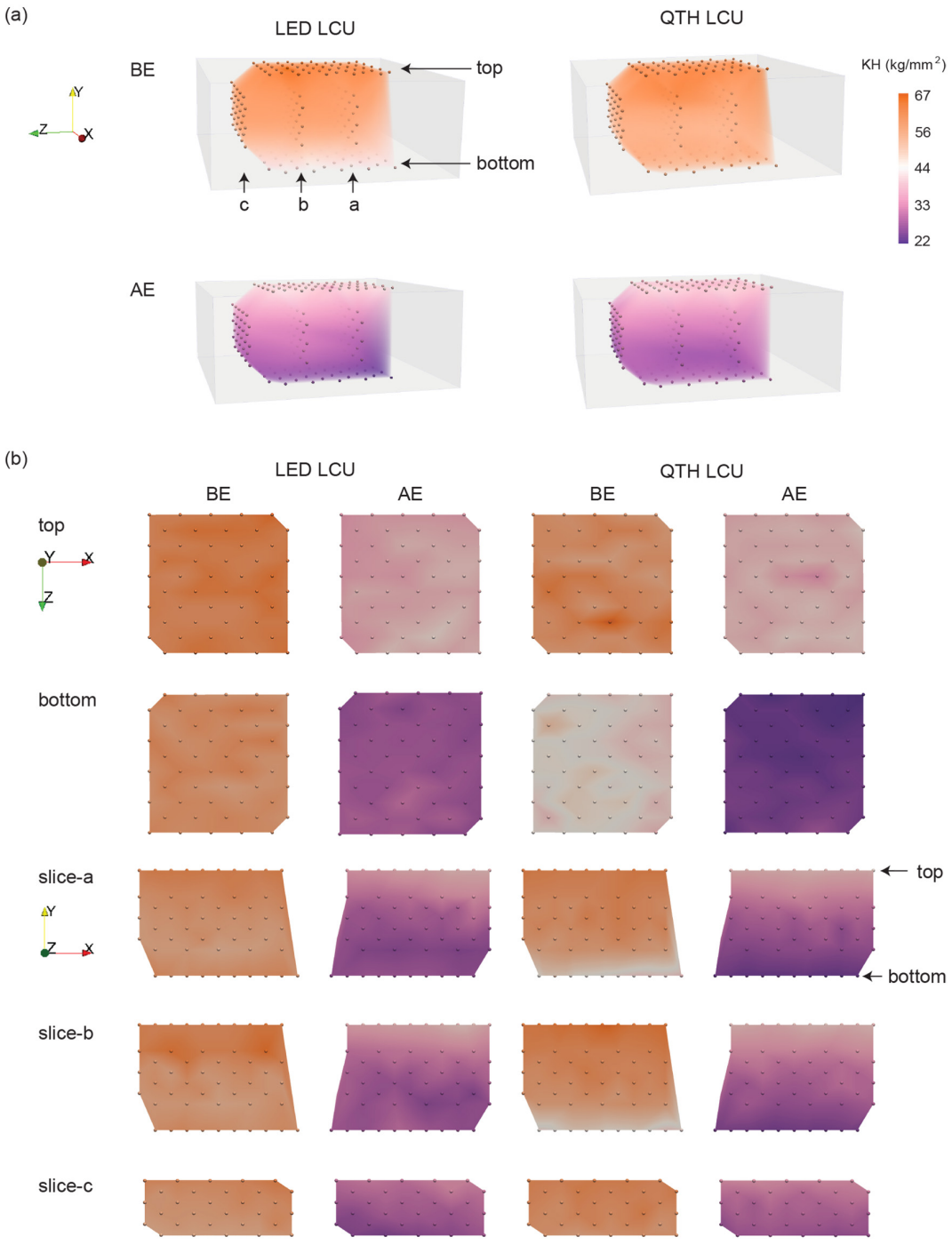

Figure 43. Representative KH (kg/mm^2) 2D contour maps and 3D renderings of the RMC specimens BE and AE that were light cured with the LED (BS) LCU and QTH (O) LCU

The spheres on the renderings represent the locations where the KH measurements were collected. (a) 3D renderings of the KH BE and AE of entire RMC specimens cured by each of the LCU. (b) 2D renderings of the KH BE and AE of each surfaces characterized cured by both LCUs.

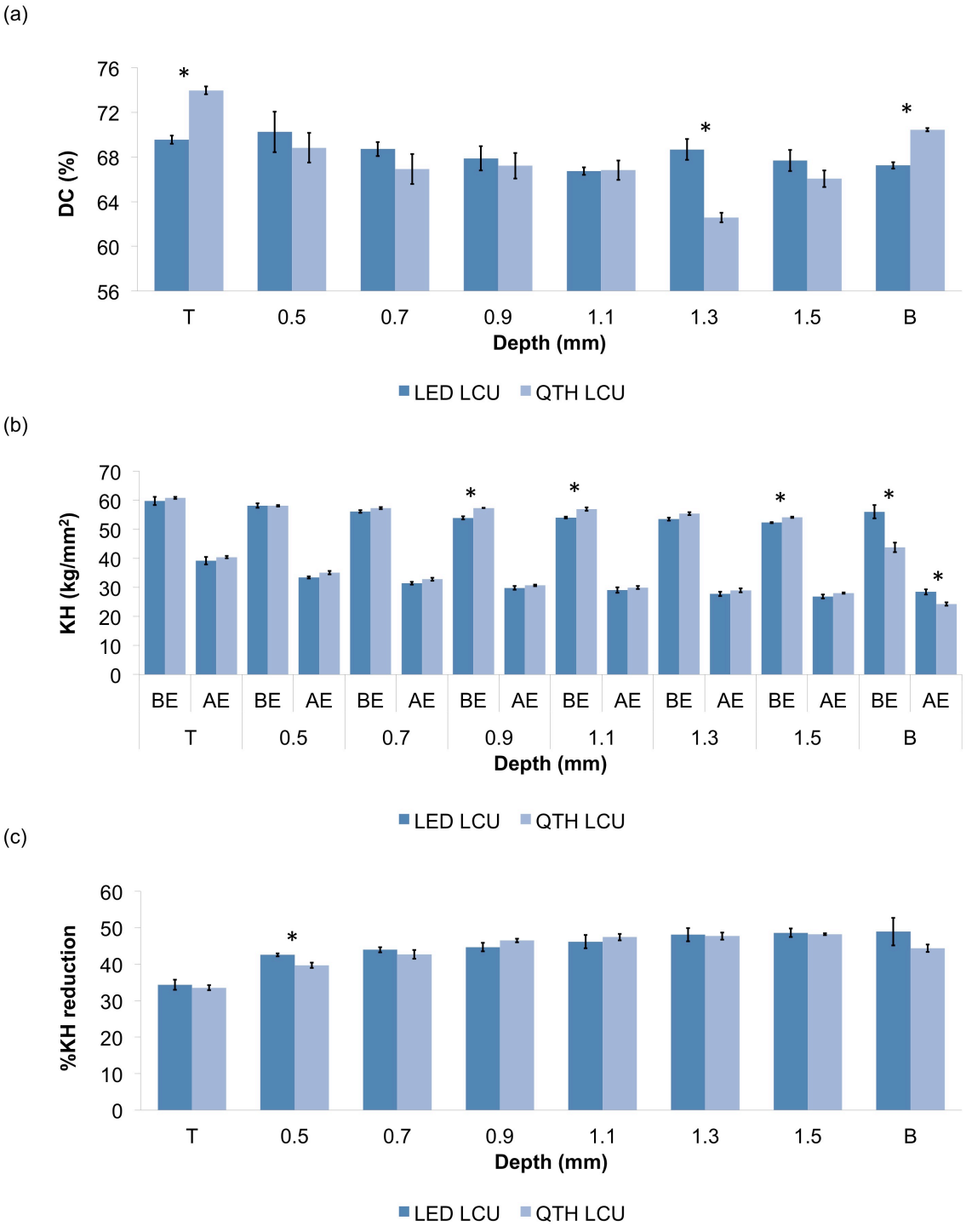

Figure 44. Mean (SE) DC (%), KH-BE and KH-AE (kg/mm^2), and %KH reduction measurements of the RMC specimens cured by the multiple emission peak LED (BS) LCU and the QTH (O) LCU

*Asterisk represents significant differences between the LED LCU and the QTH LCU.

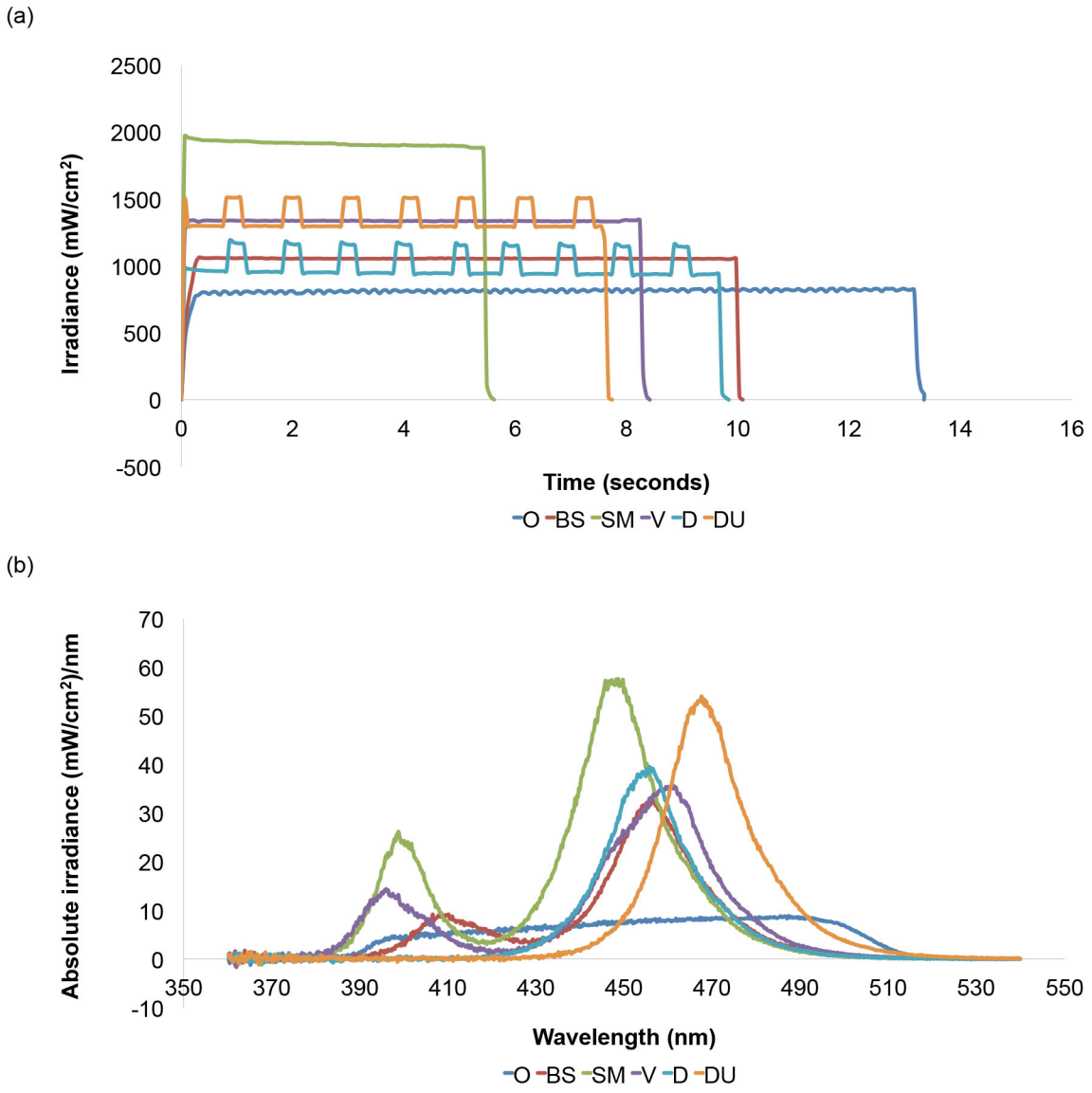

Figure 45. Representative irradiance (mW/cm^2) and spectral distribution curves of the LCUs explored at 0 mm distance from the top MARC-RC sensor needed to achieve 10-11 J/cm^2 to the top surfaces of the RMC specimens

(a) Irradiance and curing time (seconds) needed so that each RMC specimen received 10-11 J/cm^2 on the top surfaces of the RMC specimens at 0 mm distance. (b) Spectral distribution curves of the LCUs at 0 mm distance. The 10-11 J/cm^2 RE was selected following the manufacturer's recommendation to light cure Tetric EvoCeram bleaching shade XL RMC.

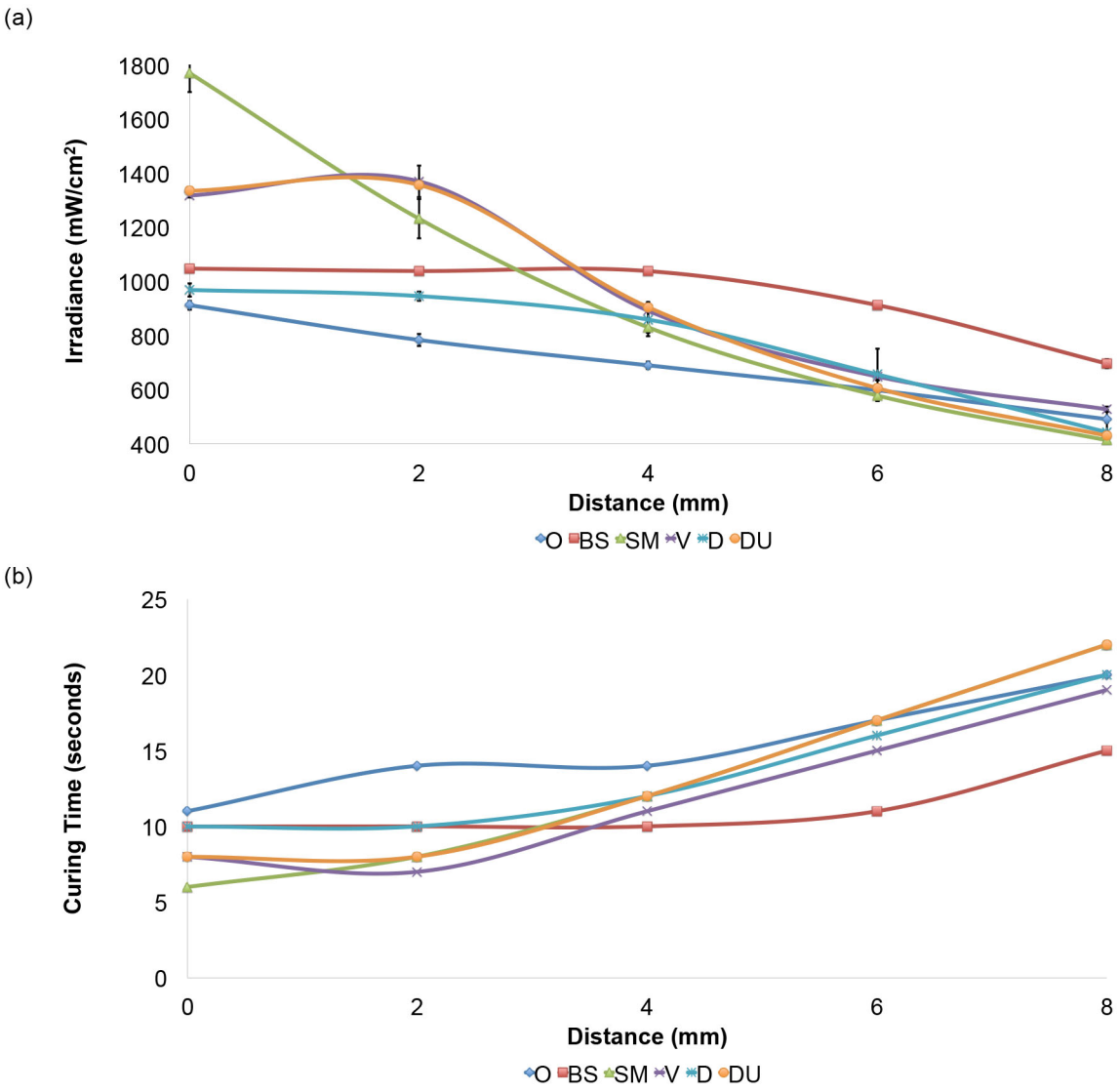

Figure 46. Irradiance mean (SD) and curing times needed to achieve 10-11 J/cm^2 at multiple distances collected using the top MARC-RC sensor for the LCUs explored

(a) The LCUs irradiance collected at 0, 2, 4, 6 and 8 mm distances. It is evident that the irradiance decreased with increasing the distance in a pattern that was unique for each LCU explored. (b) The curing times needed from each LCU explored to achieve 10-11 J/cm^2 at 0, 2, 4, 6 and 8 mm distances. It is evident that the curing time increased with decreasing the distance in a pattern that was distinctive for each LCU explored. The 10-11 J/cm^2 RE was selected following the manufacturer's recommendation to light cure Tetric EvoCeram bleaching shade XL RMC.

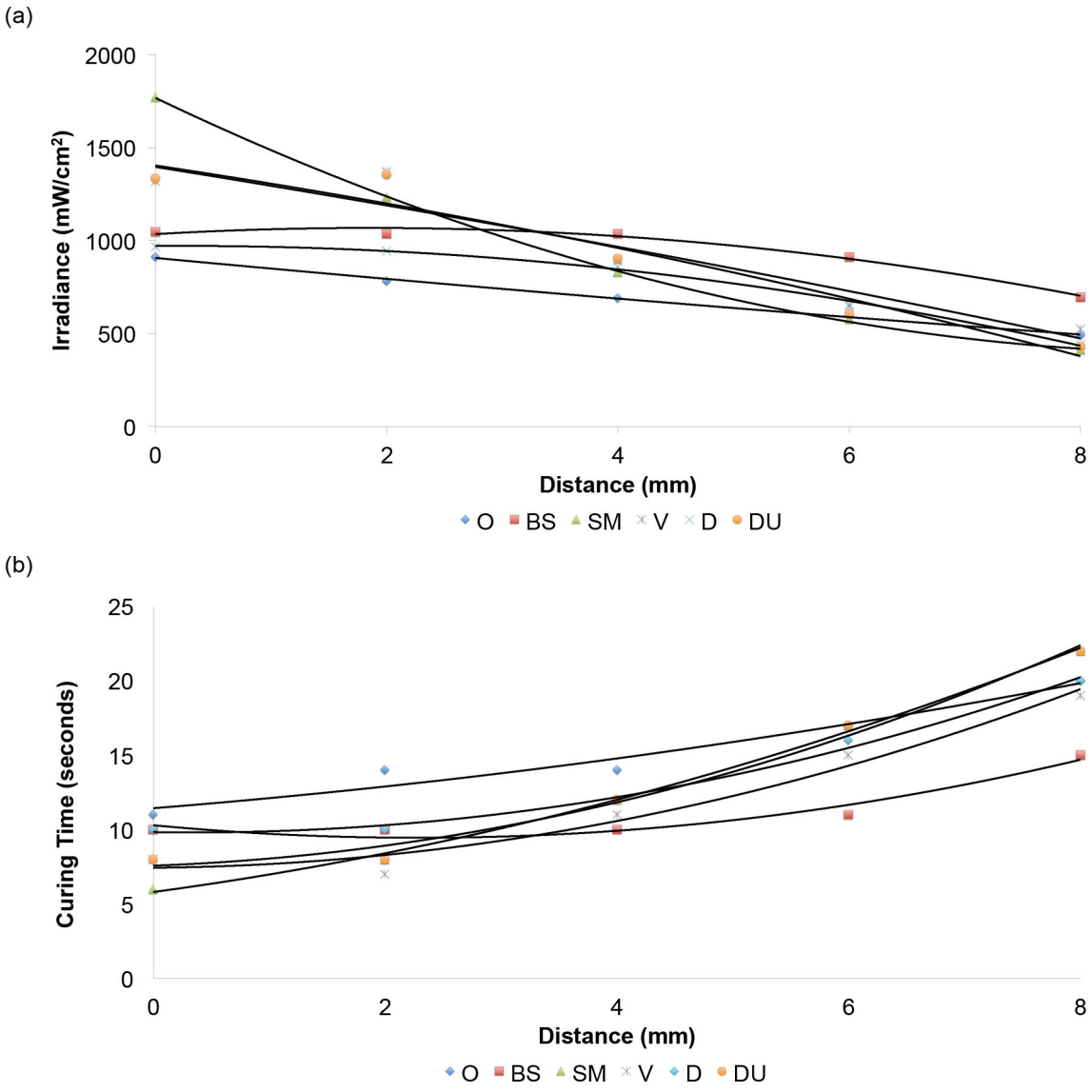

Figure 47. Polynomial (order 2) trendline of the irradiance and curing needed to reach 10-11 J/cm^2 at multiple distances collected using the top MARC-RC sensor

(a) Polynomial (order 2) trendline of the irradiance when increasing the distance for each LCU explored. (b) Polynomial (order 2) trendline of the curing time when increasing the distance for each LCU explored.

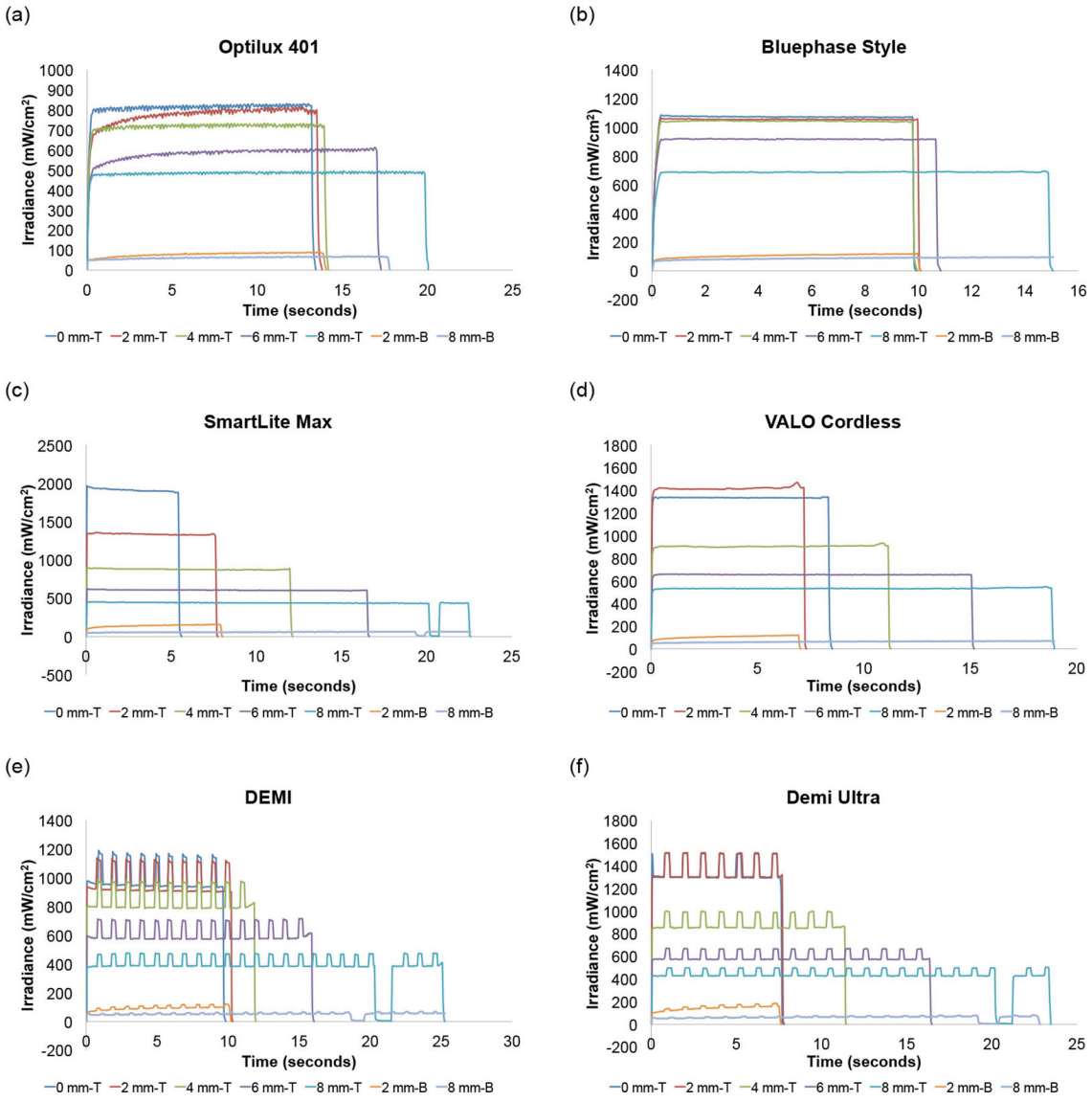

Figure 48. Representative irradiance (mW/cm^2) measurements of the LCUs explored collected using the top and bottom MARC-RC sensors at multiple distances

(a-f) The irradiance and curing time measurements for each LCU were collected using the top and bottom MARC-RC sensors so each specimen received 10-11 J/cm^2 on its top surface. Each LCU guide tip was placed at 0, 2, 4, 6 and 8 mm distances from the top sensor, and the irradiance and curing time measurements were collected. The curing times measured on the top sensor at 2 and 8 mm distances for each LCU was used to cure the specimens placed on the bottom sensor. The bottom sensor detected the irradiance passing through the RMC specimens at 2 and 8 mm distances.

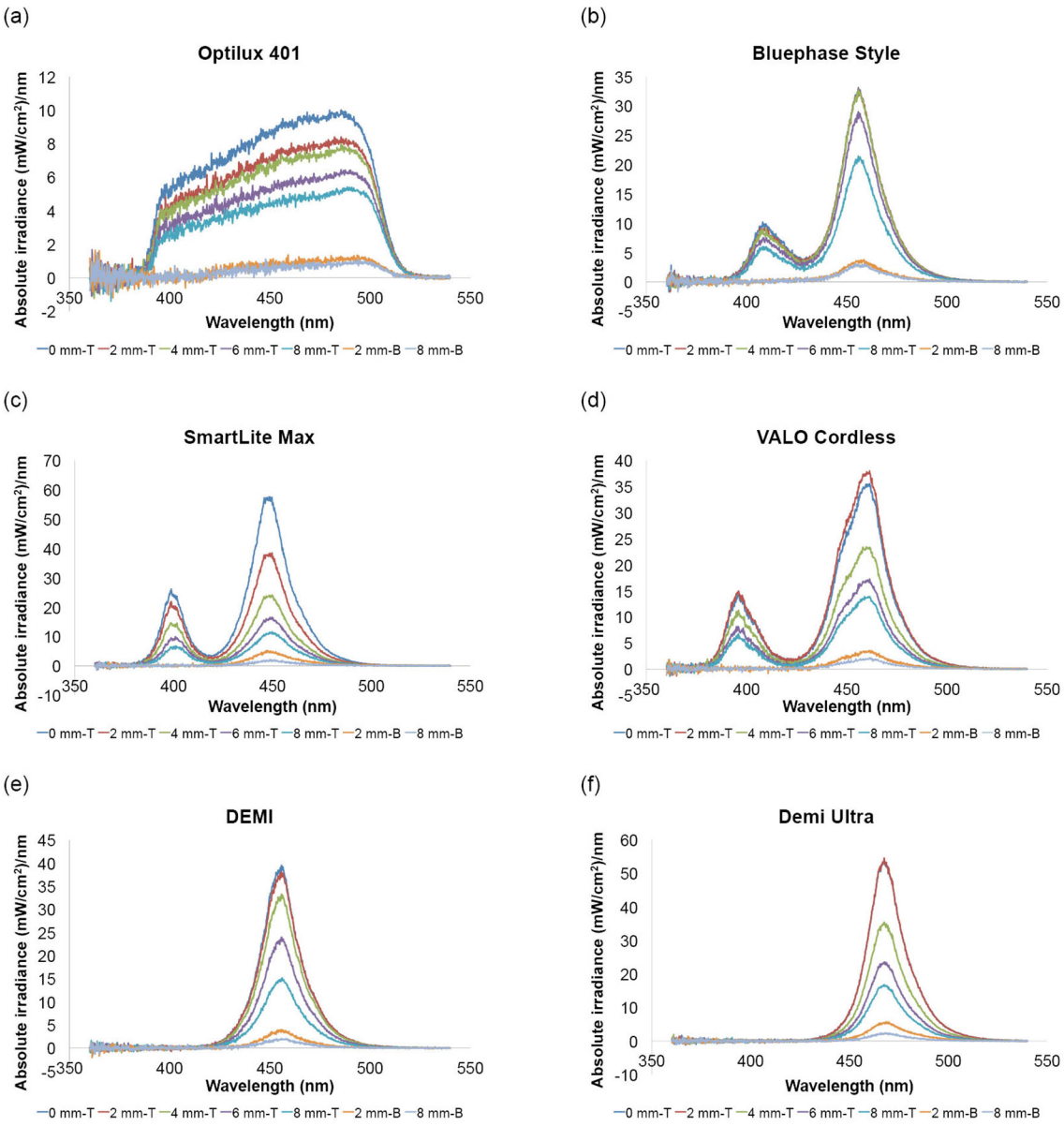

Figure 49. Representative spectral emission curves of the LCUs explored collected using the top and bottom MARC-RC sensors at multiple distances

(a-f) Emission curves were generated using the top and bottom MARC-RC sensors. The light emitting tip of the LCU was positioned at 0, 2, 4, 6 and 8 mm distances above the top MARC-RC sensor representing the spectral emission received on the top surfaces a the RMC specimen. The bottom MARC-RC sensor was used to generate the spectral emission curves after light passed through the 2 RMC specimens with the light-emitting tip positioned at 2 or 8 mm top surfaces of the specimens.

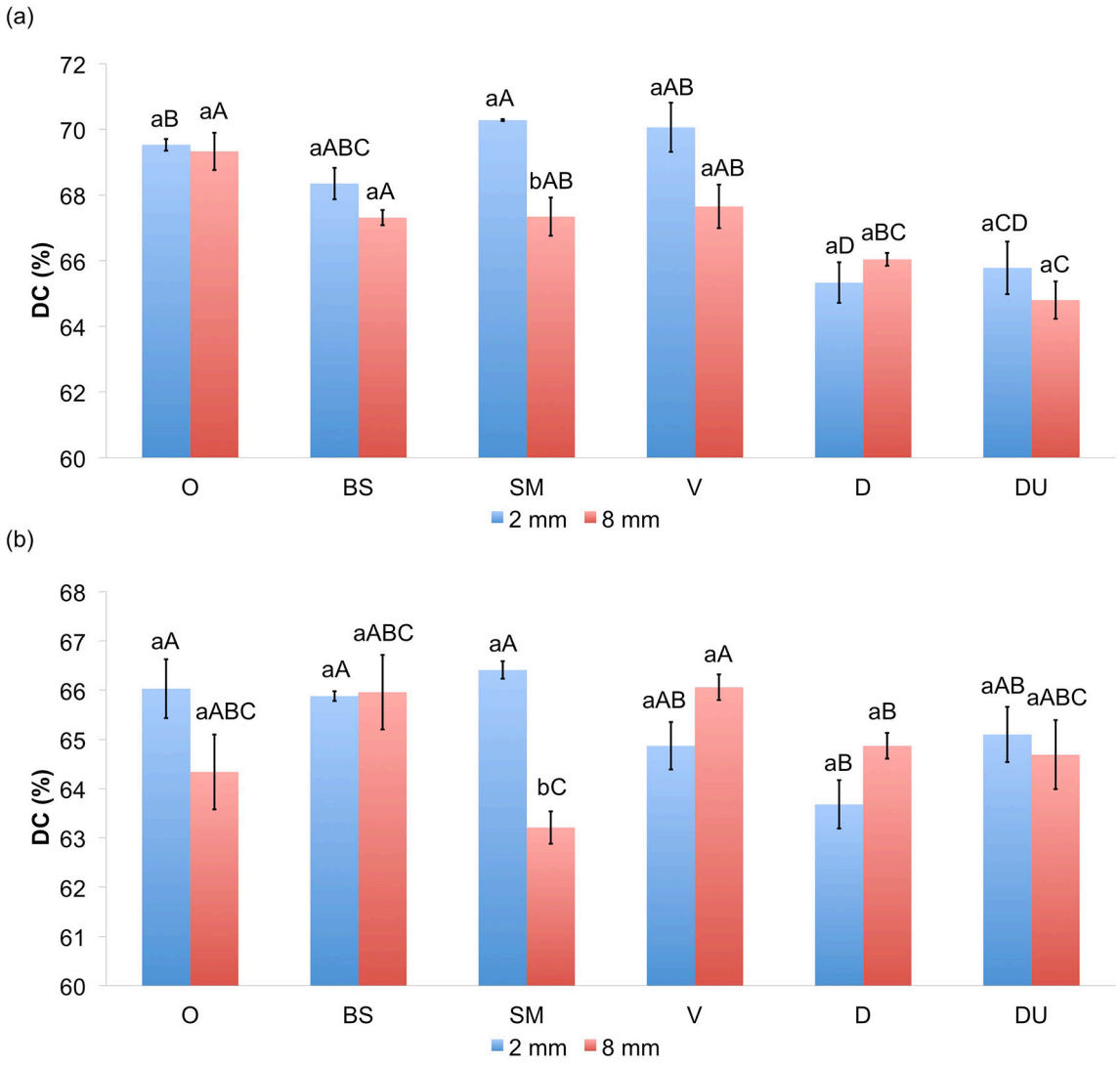

Figure 50. Mean (SE) DC (%) measurements collected from the top and bottom surfaces of the RMC specimen at 2 and 8 mm curing distances

(a) DC values collected form the top surfaces of the RMC specimens at 2 and 8 mm curing distances. (b) DC values collected form the bottom surfaces of the RMC specimens at 2 and 8 mm curing distances. Lowercase letters represent significant differences between 2 and 8 mm curing distances. Uppercase letters represent significant differences between the LCUs for each surface at each curing distance.

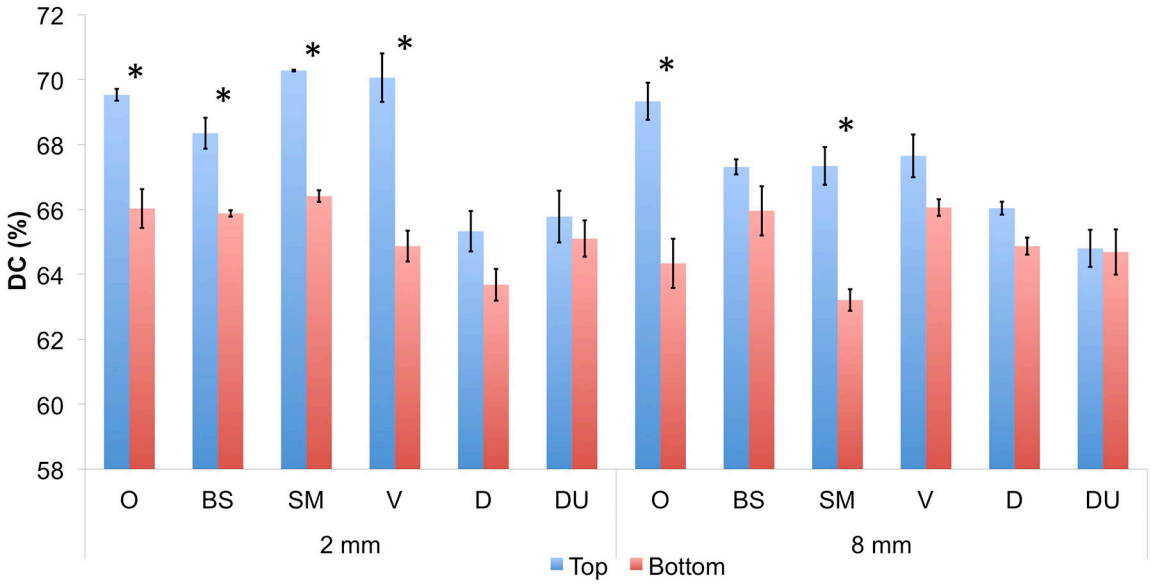

Figure 51. Mean (SE) DC (%) significant differences between top and bottom surfaces for each LCU at 2 and 8 mm curing distances

*Asterisk represents significant differences between the top and bottom for each LCU at each curing distance.

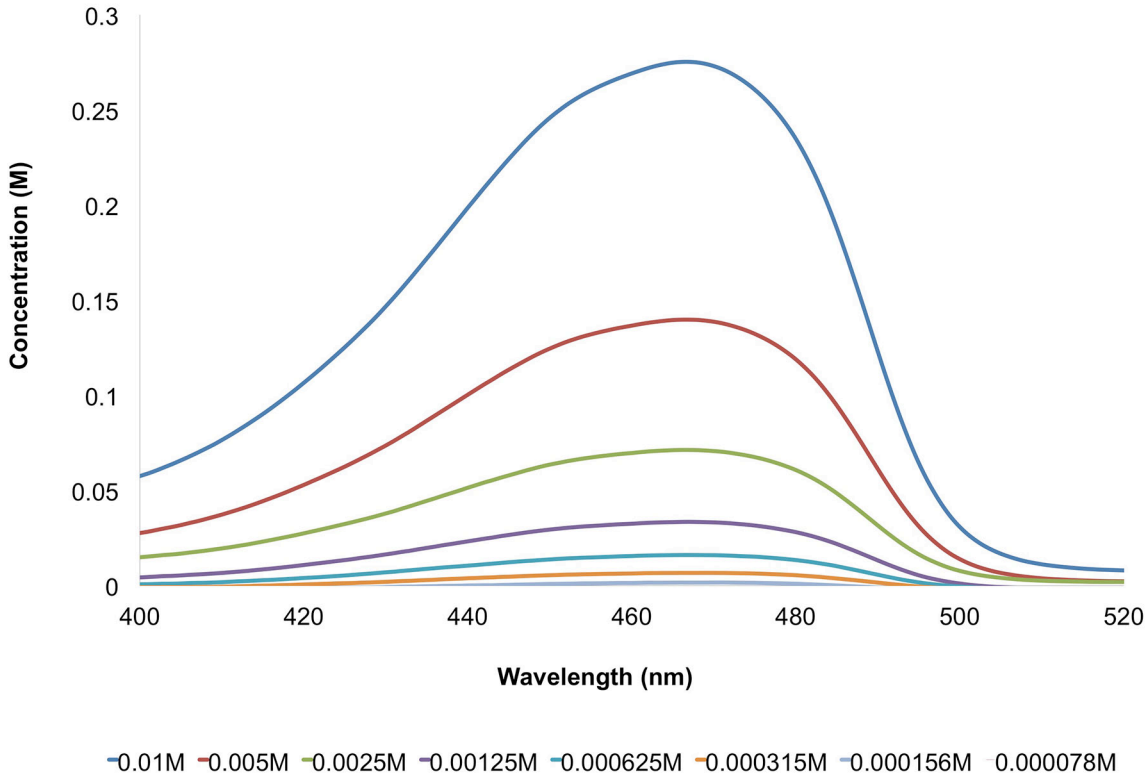

Figure 52. CQ photoinitiator spectral distribution at multiple concentrations measured using a UV-spectrophotometry

Eight calibrant solutions were prepared in serial dilutions by mixing CQ photoinitiator with 20 ml methanol starting from 0.01M concentration.

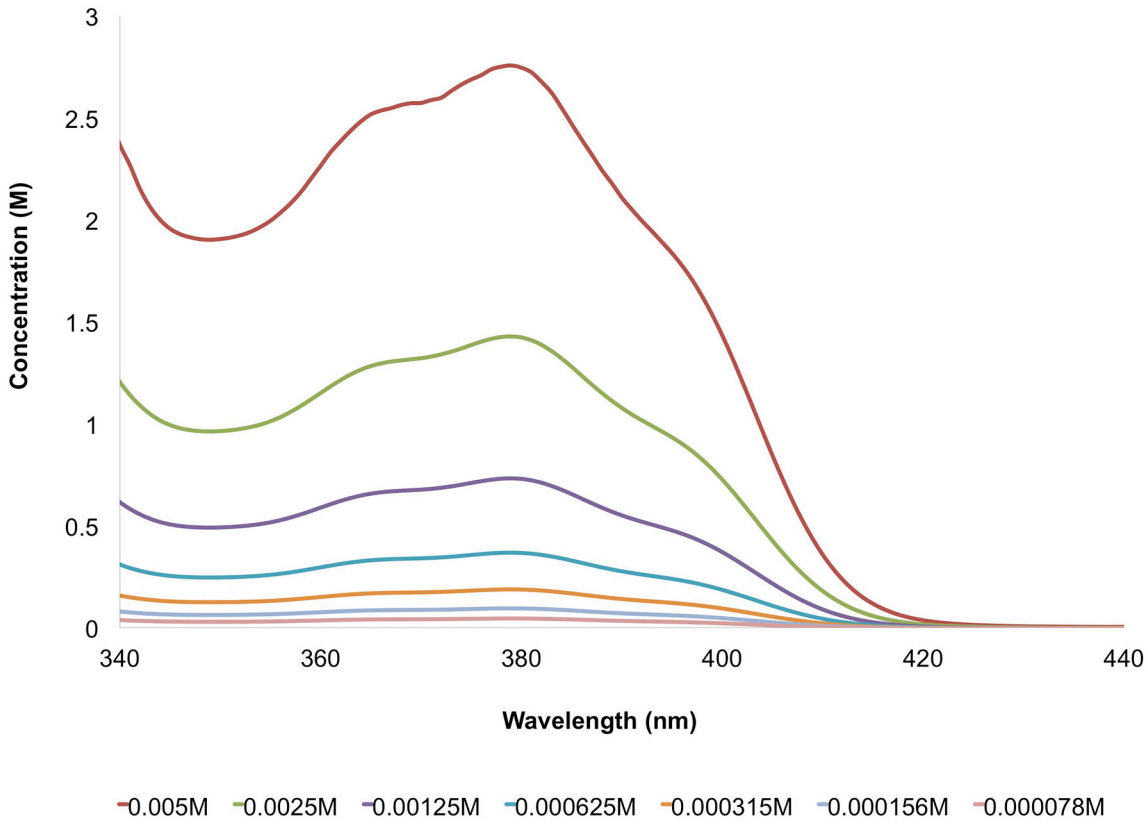

Figure 53. TPO photoinitiator spectral distribution at multiple concentrations measured using a UV-spectrophotometry

Eight calibrant solutions were prepared in serial dilutions by mixing TPO photoinitiator with 20 ml methanol starting from 0.01M concentration.

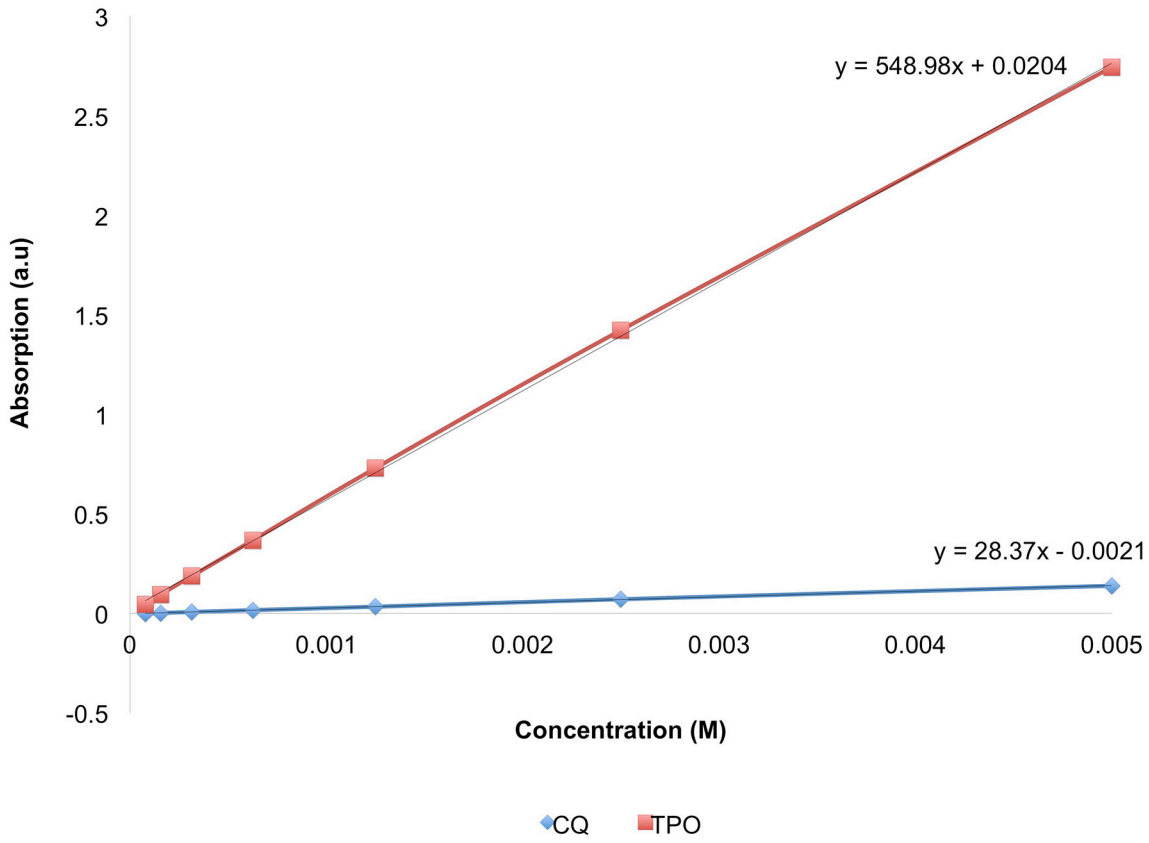

Figure 54. Molar absorptivity of CQ and TPO photoinitiators

The slope represents that the molar absorptivity for TPO was 20-fold more than CQ photoinitiator.

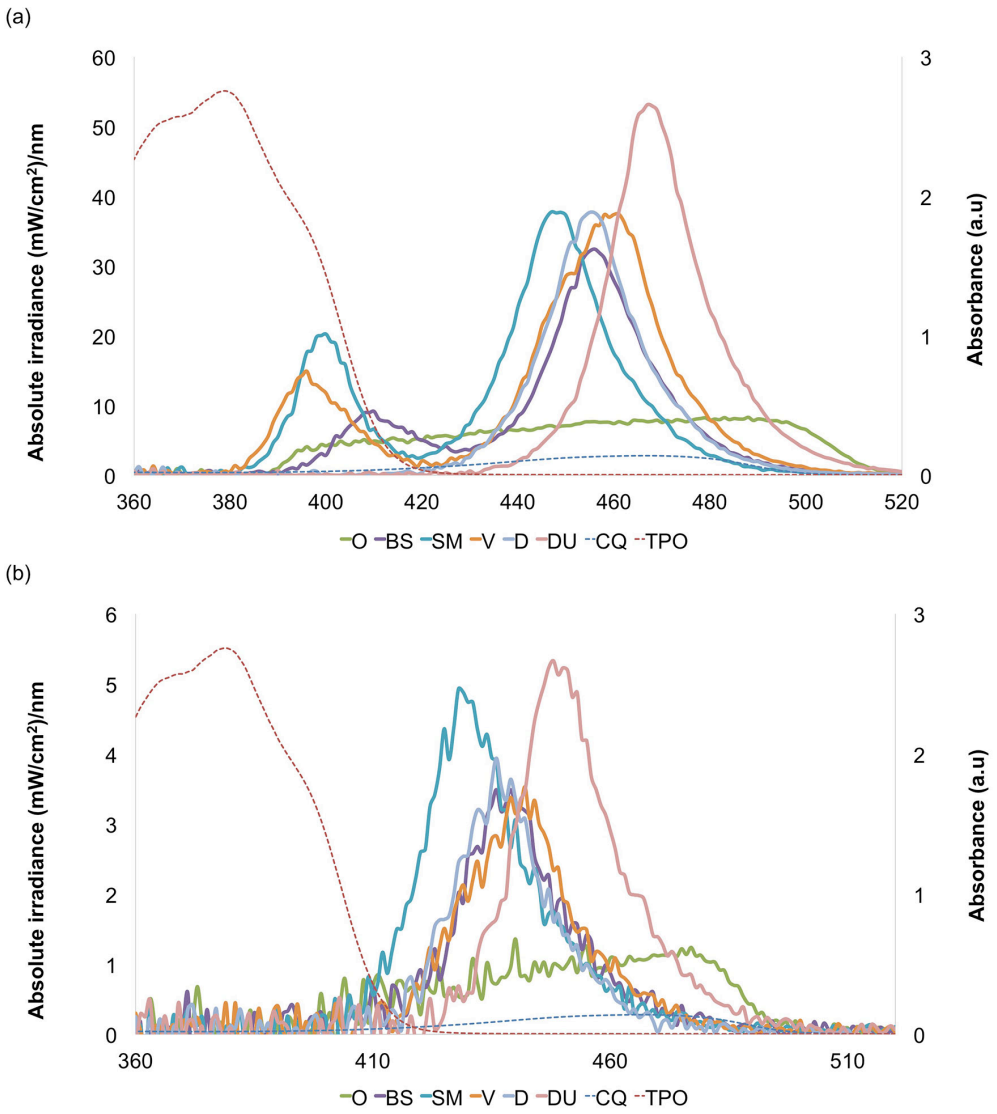

Figure 55. Representative LCU spectral distribution curves collected using the top and bottom MARC-RC sensors combined with the CQ and TPO absorbance spectrum at 0.005M concentration

(a) Spectral distribution curves at 2 mm distance from the top sensor. The spectral distribution of the longer wavelength curve encompasses CQ absorption range, and the spectral distribution of the shorter wavelength curve for the QTH and multiple emission peak LED LCUs encompasses TPO absorption range. (b) Spectral distribution curves at 2 mm distance that passed through the 2 mm increment and was detected by the bottom sensors, representing the irradiance received on the bottom surfaces of the RMC. The spectral distribution dramatically decreased on the bottom. The spectral distribution of the shorter wavelength curve that encompasses TPO absorption range is no longer detected on the bottom sensor using the multiple emission peak LED LCUs.

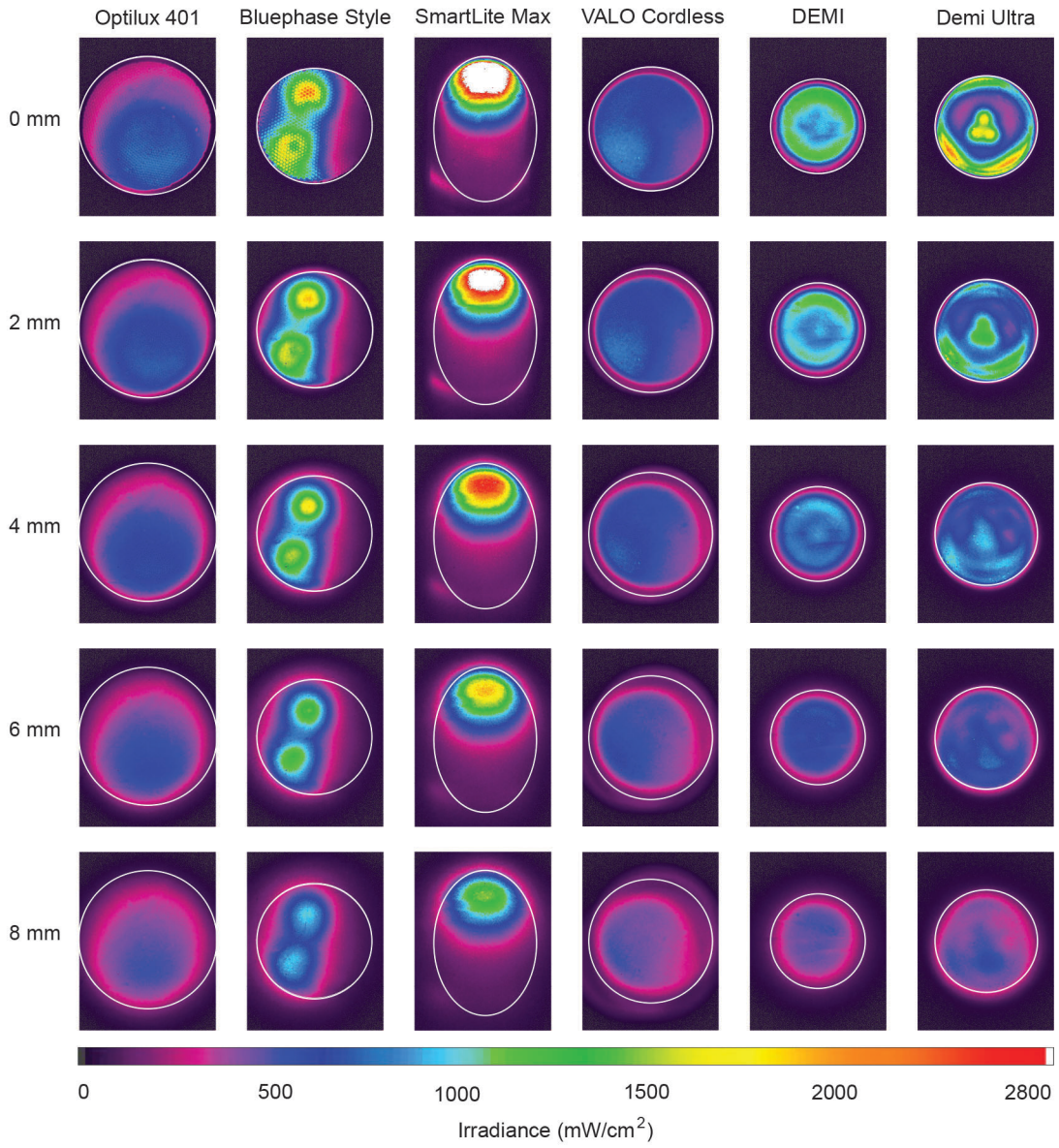

Figure 56. Representative 2D irradiance distribution images measured through a 425 nm longpass filter at multiple distances between each LCU guide tip and glass diffuser

The 425 nm longpass filter was used to filter wavelengths less than 425 nm and allow wavelengths grater than 425 nm to pass. The circle in each beam profile image corresponds to the effective light-emitting dimensions of the each LCU. The average radiant power values collected from the integrating sphere/spectrometer assembly at the long wavelength for each distance were applied to the corresponding beam profile image to generate the calibrated irradiance maps.

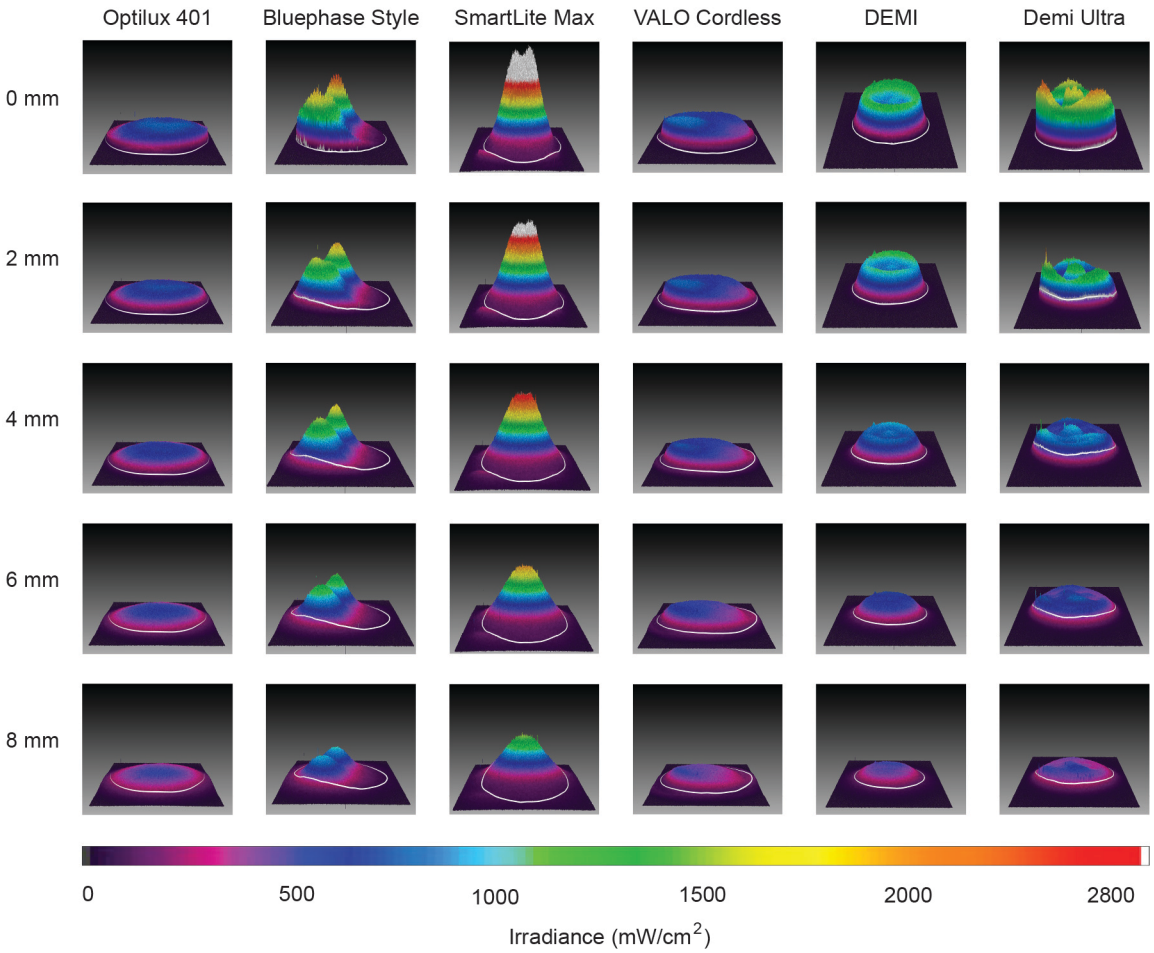

Figure 57. Representative 3D irradiance distribution images explored measured through a 425 nm longpass filter at multiple distances between each LCU guide tip and glass diffuser

The 425 nm longpass filter was used to filter wavelengths less than 425 nm and allow wavelengths greater than 425 nm to pass. The circle in each beam profile image corresponds to the effective light-emitting area of the individual LCU. The average radiant power values collected from the integrating sphere/spectrometer assembly at the long wavelength spectrum (425-700 nm) for each distance were applied to the corresponding beam profile image to generate the calibrated irradiance maps.

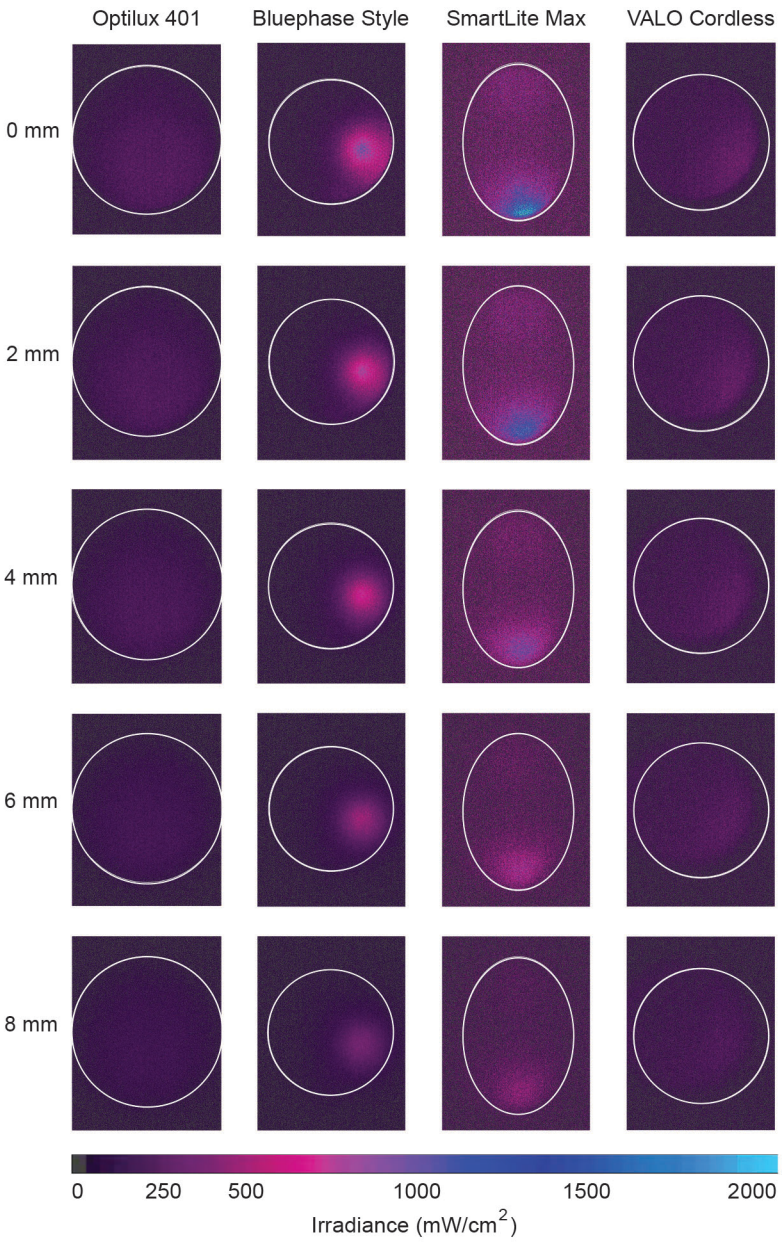

Figure 58. Representative 2D irradiance distribution images measured through a 425 nm shortpass filter at multiple distances between each LCU tip and glass diffuser

The 425 nm shortpass filter was used to filter wavelengths greater than 425 nm and allow wavelengths less than 425 nm to pass. The circle in each beam profile image corresponds to the effective light-emitting area of the individual LCU. The average radiant power values collected from the integrating sphere/spectrometer assembly at the short wavelength spectrum (380-425 nm) for each distance were applied to the corresponding beam profile image to generate the calibrated irradiance maps.

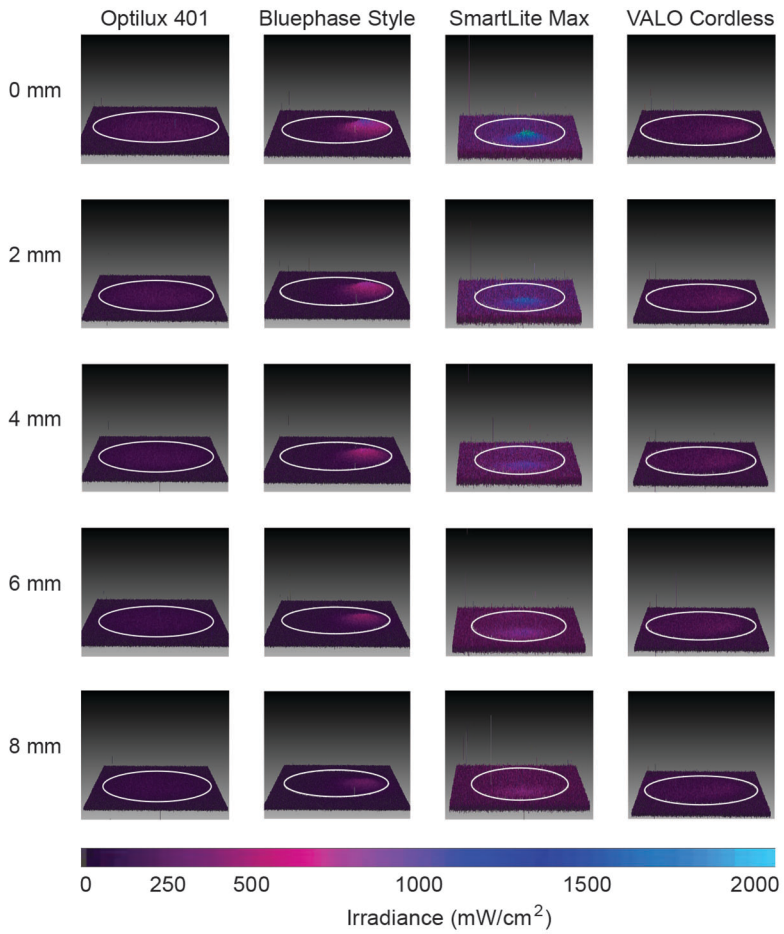

Figure 59. Representative 3D irradiance distribution images measured through a 425 nm shortpass filter at multiple distances between each LCU guide tip and glass diffuser

The 425 nm shortpass filter was used to filter wavelengths greater than 425 nm and allow wavelengths less than 425 nm to pass. The circle in each beam profile image corresponds to the effective light-emitting area of the individual LCU. The average radiant power values collected from the integrating sphere/spectrometer assembly at the short wavelength spectrum (380-425 nm) for each distance were applied to the corresponding beam profile image to generate the calibrated irradiance maps.

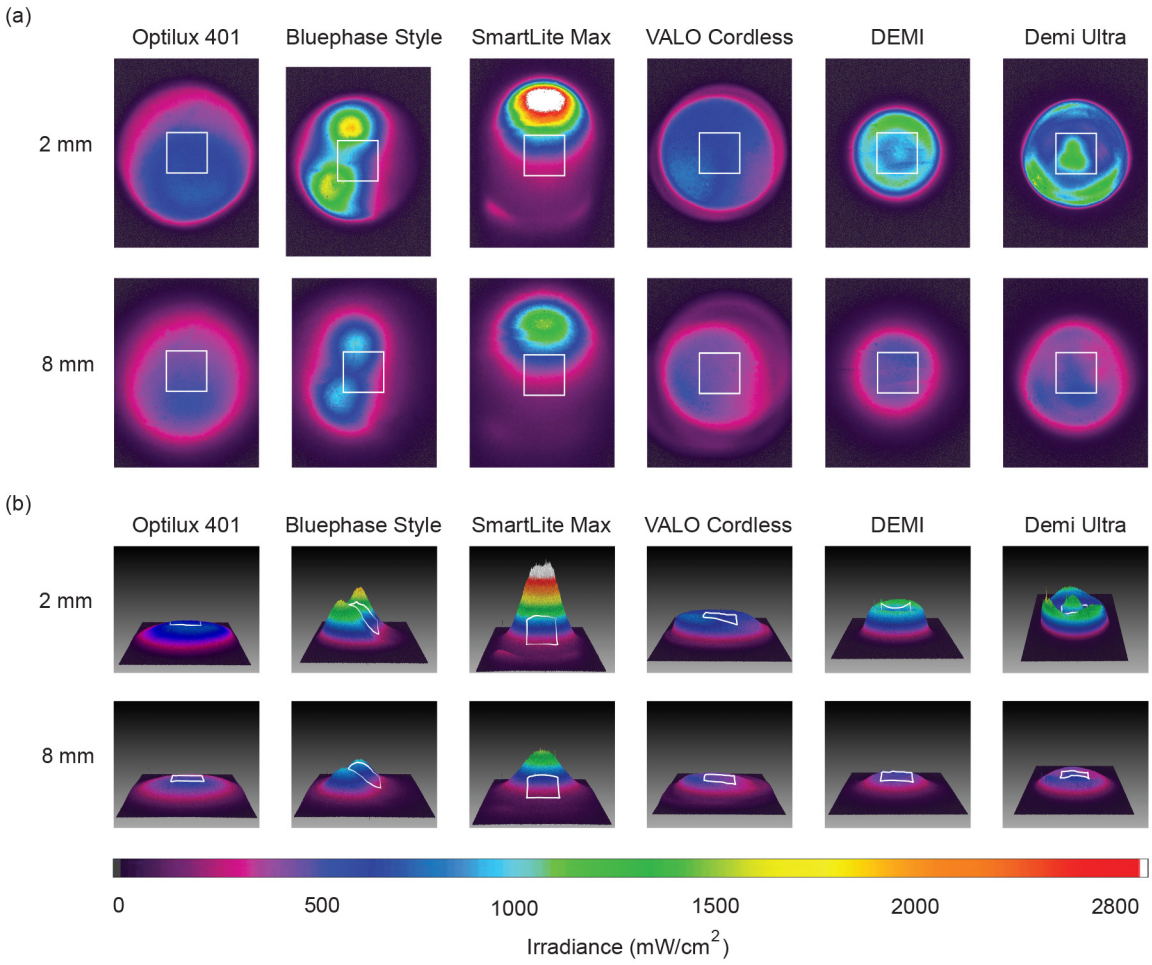

Figure 60. Representative 2D and 3D irradiance distribution images from the LCUs explored measured through a 425 nm longpass filter with the light tip at 2 and 8 mm distance from a glass diffuser

(a) A 2D representation of the LCUs investigated. (b) A 3D representation of the LCUs assessed. To compensate for differences in the spectral response of the photodiode within the CCD camera of the beam profiler system, a longpass optical filter having a cut-off wavelength of 425 nm was used to separate violet light from blue light with peaks at approximately 409 nm and 456 nm, respectively. The longpass filter was used only to allow wavelengths greater than 425 nm to reach the CCD camera and blocked wavelengths less than this value. The square in the center of each irradiance distribution image corresponds to the 3×3 grid where the KH measurements were obtained from the RMC square specimens tested in this study.

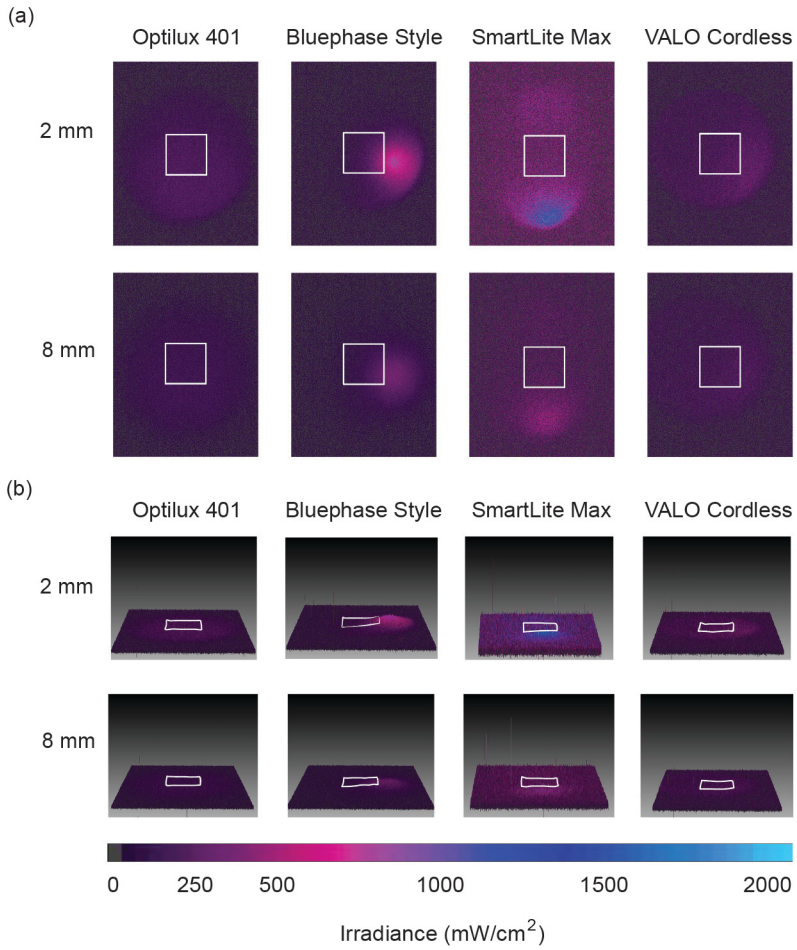

Figure 61. Representative 2D and 3D irradiance distribution images from the LCUs explored measured through a 425 nm shortpass filter with the light tip at 2 and 8 mm distance from a glass diffuser

(a) Representative 2D images of the LCUs investigated. (b) Representative 3D images of the LCUs assessed. To compensate for differences in the spectral response of the photodiode within the CCD camera of the beam profiler system, a shortpass optical filter, both having a cut-off wavelength of 425 nm, were used to separate violet light from blue light with peaks at approximately 409 nm and 456 nm, respectively. The shortpass filter allowed only wavelengths less than 425 nm to "pass" through to the CCD camera. The square in the center of each irradiance distribution image corresponds to the 3×3 grid where the KH measurements were obtained from the RMC square specimens tested in this study.

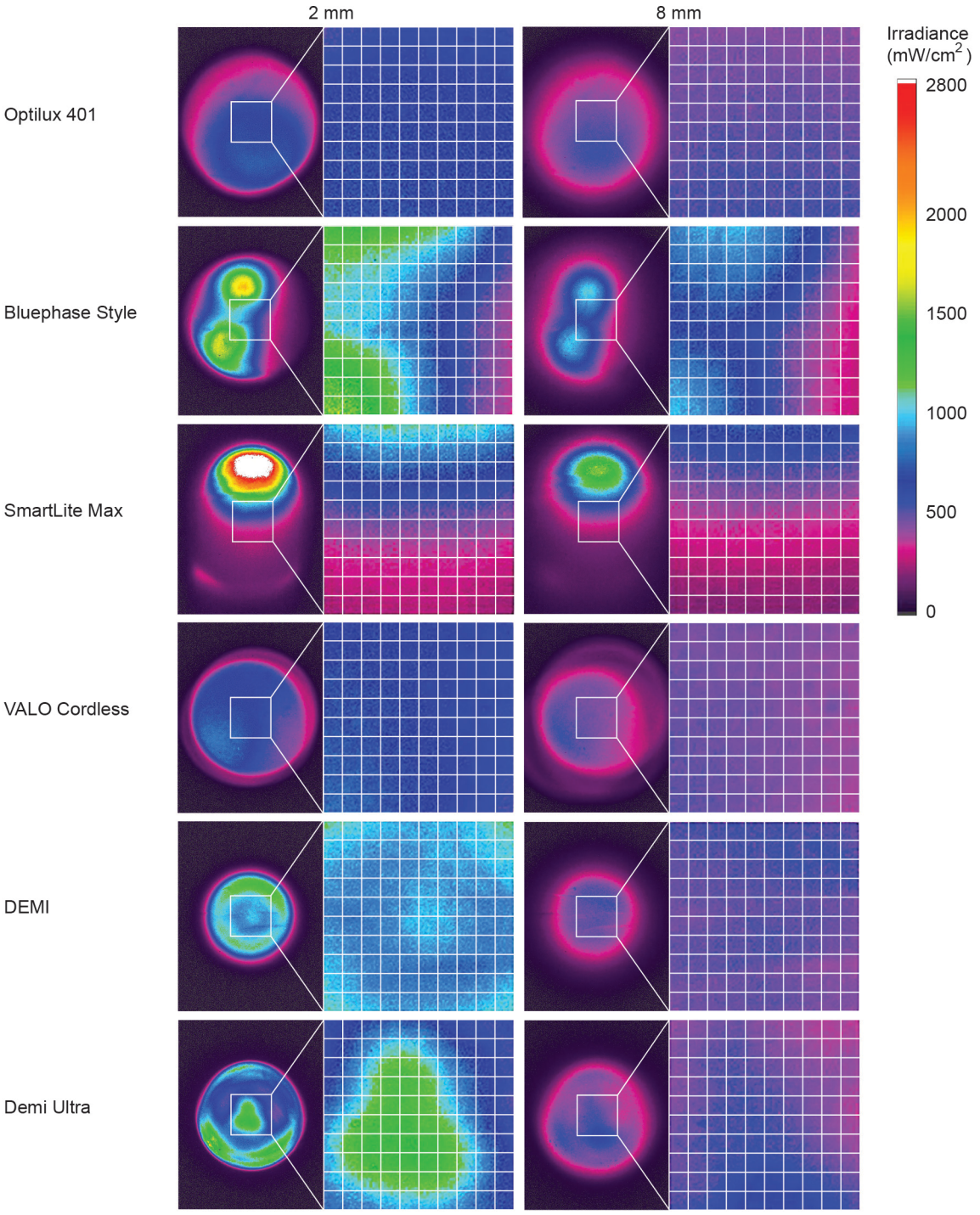

Figure 62. Representative 2D localized irradiance distribution images from the LCUs that were received on the top RMC surfaces measured through a 425 nm longpass filter

Each square in the 10×10 grid of the 3×3 mm area correspond to the locations where the irradiance numerical values were exported, KH and DC measurements were obtained in a checkerboard pattern.

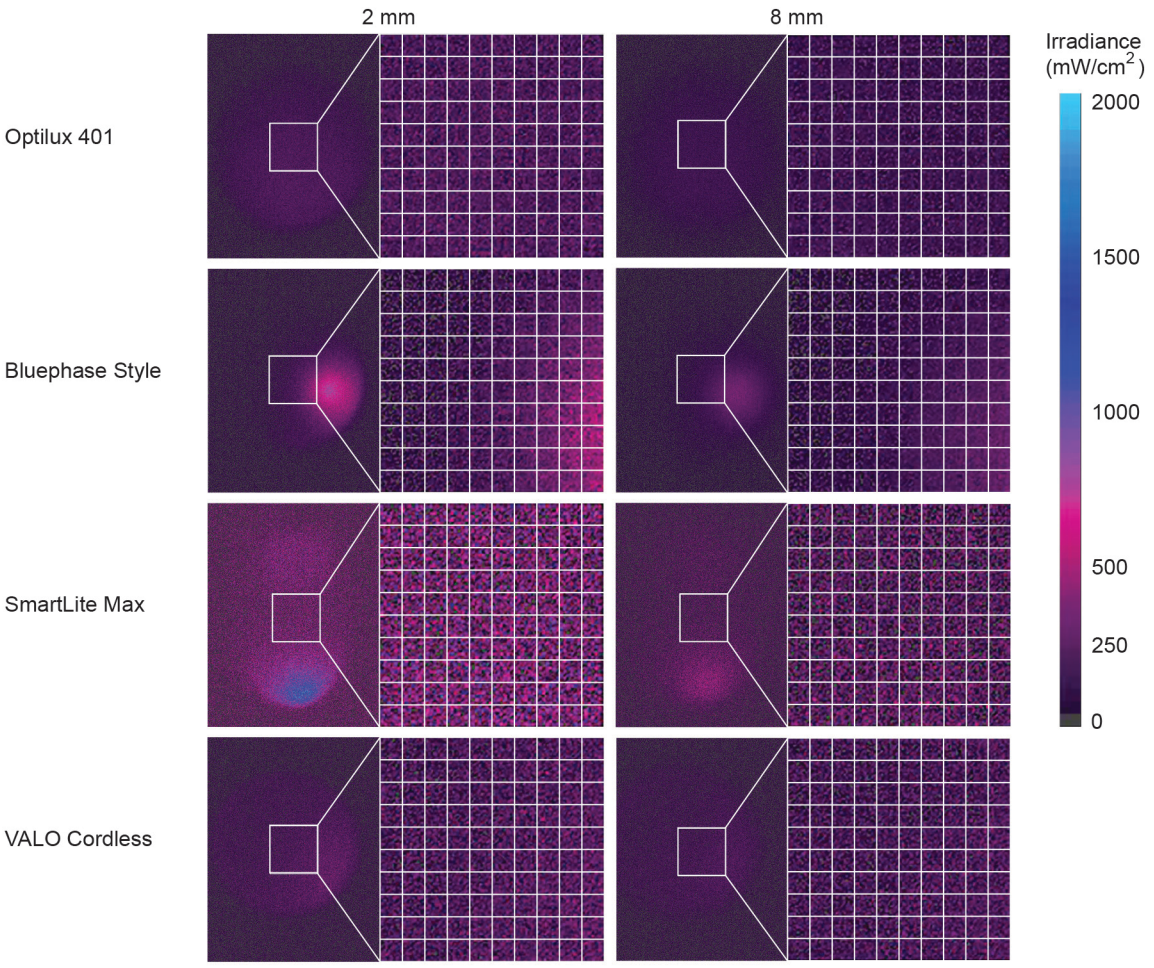

Figure 63. Representative 2D localized irradiance distribution images from the LCUs that were received on the top RMC surfaces measured through a 425 nm shortpass filter

The squares in each image represent the 3×3 area where the KH measurements were obtained from the square specimens. Each square in the 10×10 grid of the enlarged 3×3 area correspond to locations where the irradiance numerical values were exported and where the KH and DC measurements were obtained in a checkerboard pattern.

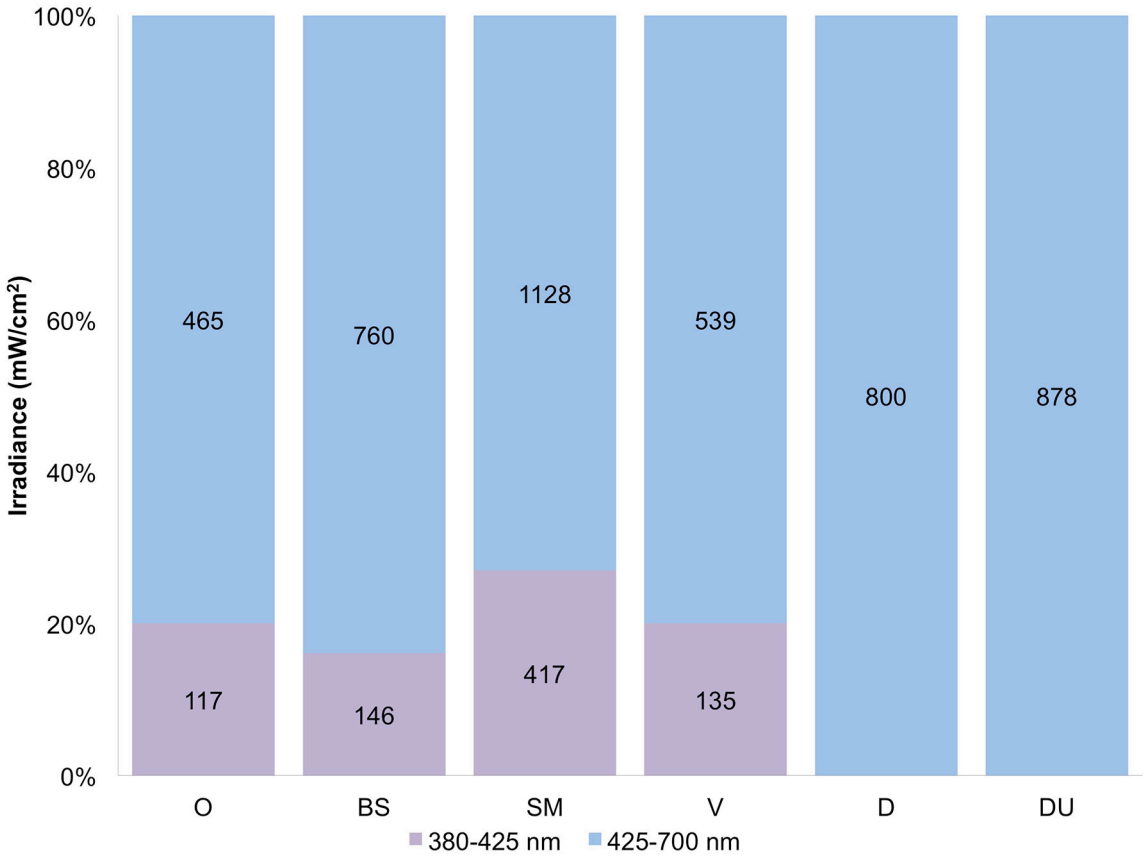

Figure 64. Percent contribution (%) from the blue (425-700 nm) and violet (380-425 nm) spectral region of the LCUs explored at 2 mm curing distance from the integrating sphere opening

The irradiance values were calculated from the average power (mW) measurements collected at 2 mm away from the integrating sphere opening using the effective light-emitting area of the individual LCU.

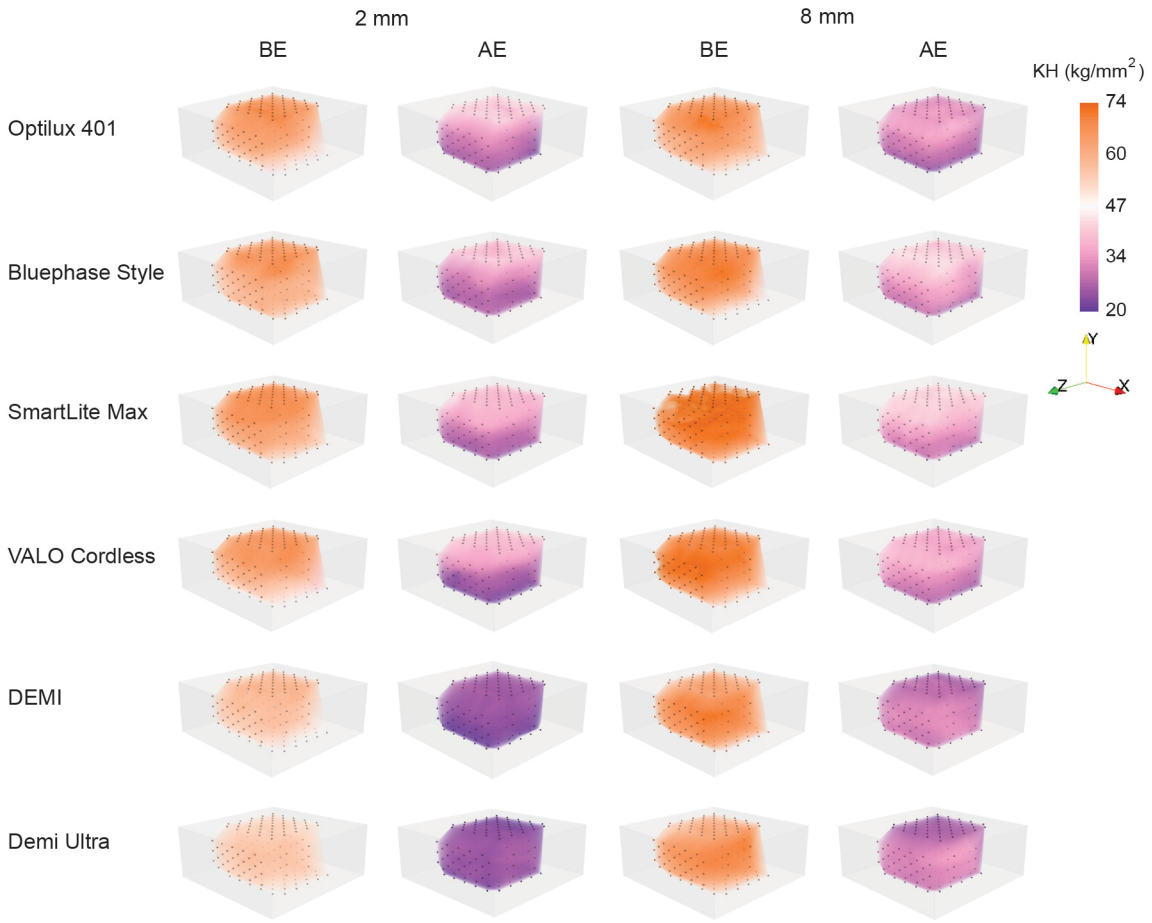

Figure 65. Representative 3D renderings of the localized Knoop microhardness BE and AE (kg/mm^2) of the RMC specimens light cured using the LCUs explored at 2 and 8 mm curing distances

The spheres on the renderings represent the locations where the KH measurements were collected. The renderings represent the KH from the entire RMC specimens cured by the LCUs investigated.

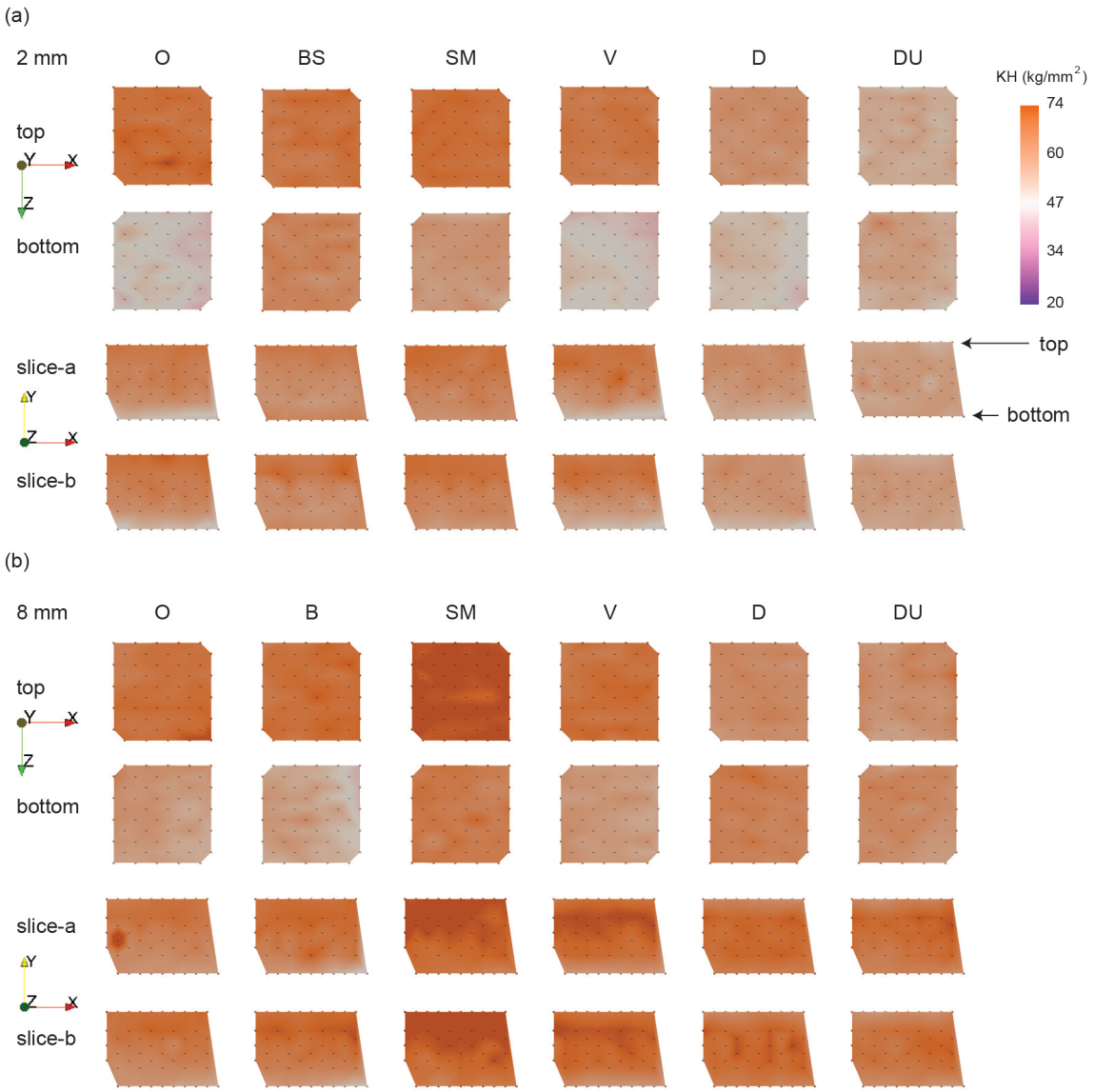

Figure 66. Representative 2D renderings of the localized KH-BE (kg/mm^2) contour maps of the RMC specimens light cured using the LCUs explored

(a) Representative 2D renderings of the localized KH-BE on the top and bottom surfaces along with slice-a, and -b cured by the LCUs investigated at 2 mm distance between the light guide and the top surfaces of the RMC specimens. (b) Representative 2D renderings of the KH-BE on the top and bottom surfaces along with slice-a, and -b cured by the LCUs investigated at 8 mm distance between the light guide and top surfaces of the RMC specimens. The spheres on the renderings represent the locations where the KH-BE measurements were collected.

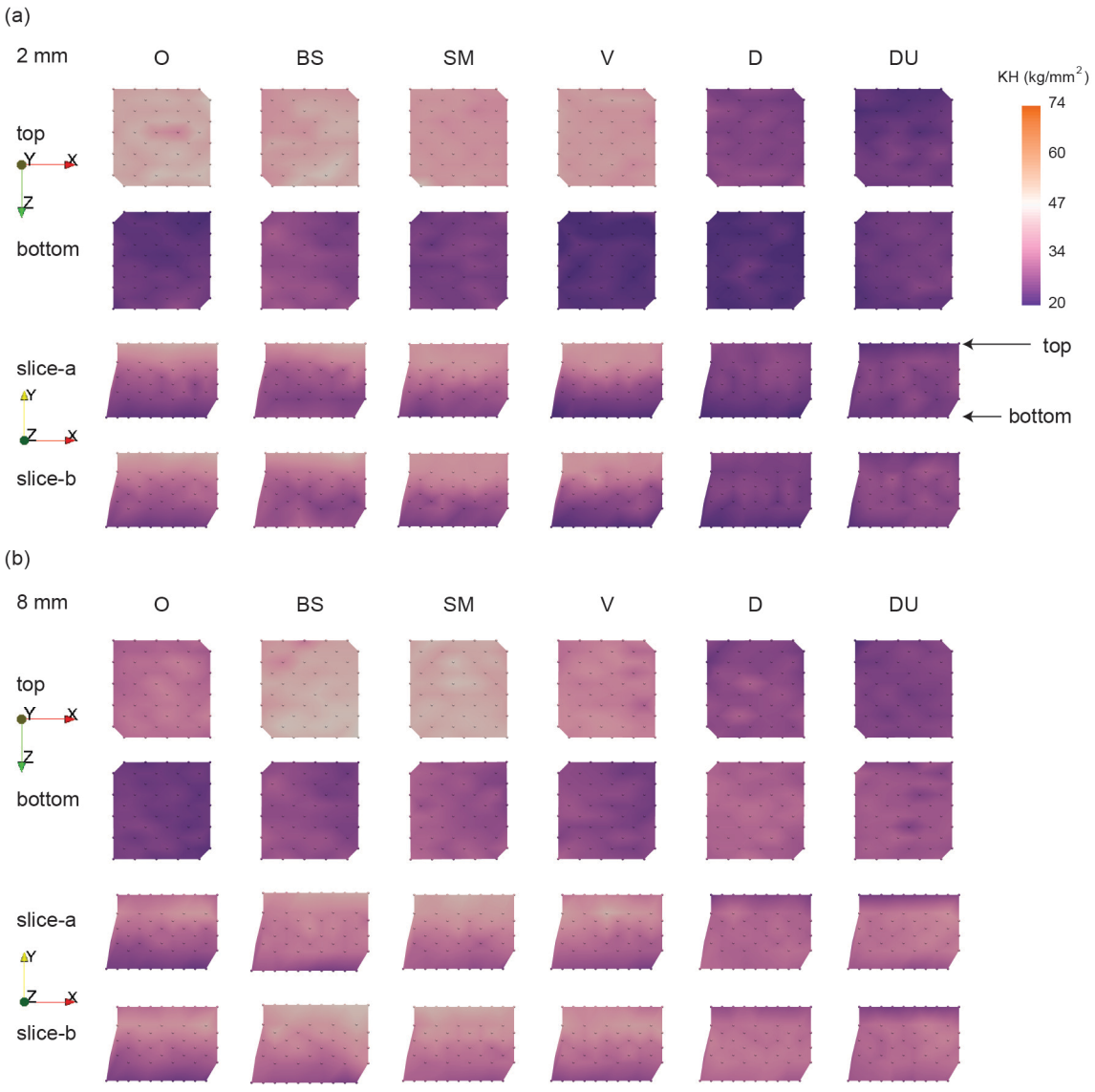

Figure 67. Representative 2D renderings of the localized KH-AE (kg/mm^2) contour maps of the RMC specimens light cured using the LCUs explored

(a) Representative 2D renderings of the localized KH-AE on the top and bottom surfaces along with slice-a, and -b cured by the LCUs assessed at 2 mm curing distance between the light guide and the top surfaces of the RMC specimens. (b) Representative 2D renderings of the localized KH-AE on the top and bottom surfaces along with slice-a, and -b cured by the LCUs assessed at 8 mm curing distance between the light guide and top surfaces of the specimens. The spheres on the renderings represent the locations where the KH-BE measurements were collected.

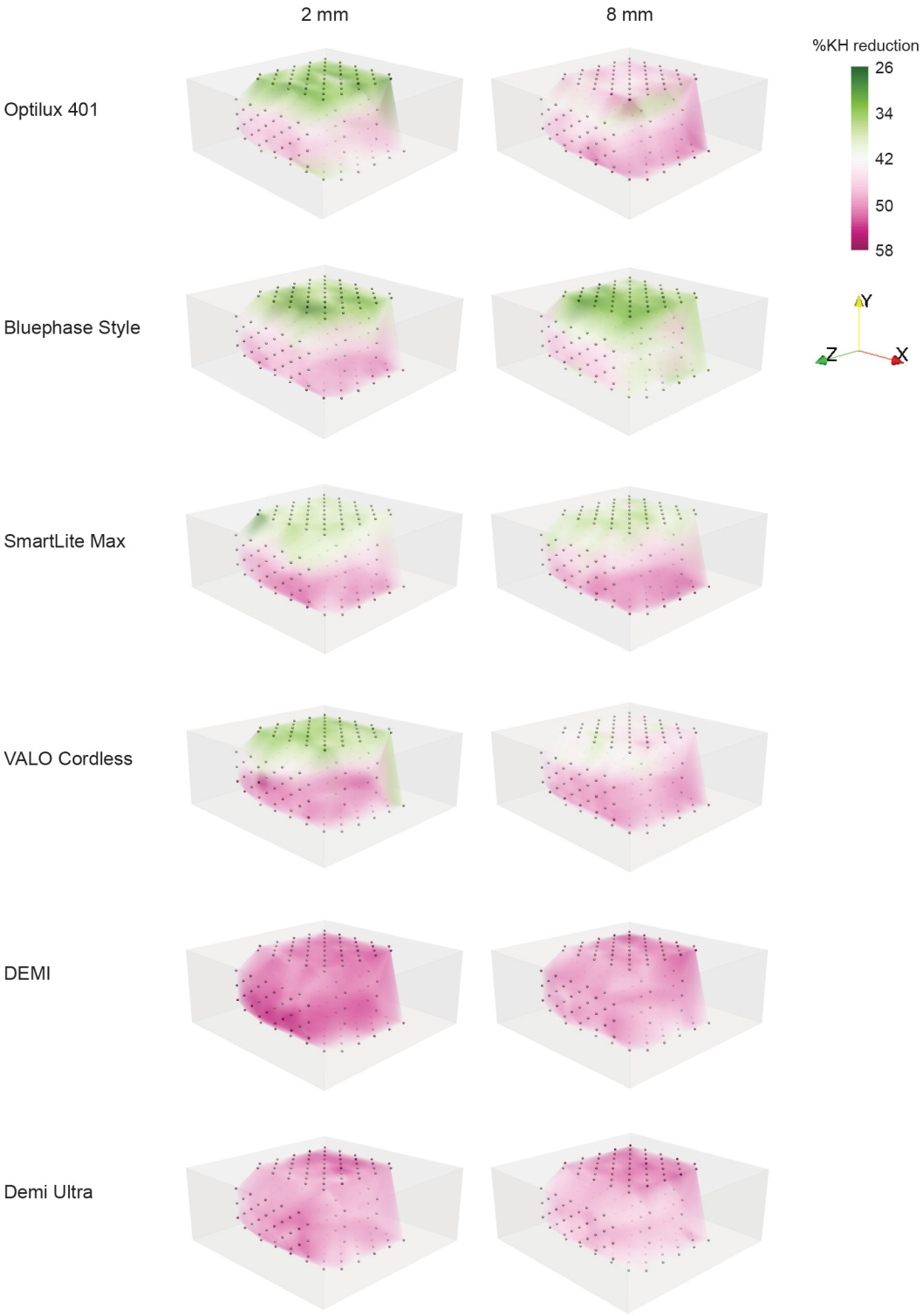

Figure 68. Representative 3D renderings of the localized %KH reduction for the RMC specimens light cured using the LCUs explored at 2 and 8 mm curing distances

The spheres represent the locations of the localized average %KH reduction values.

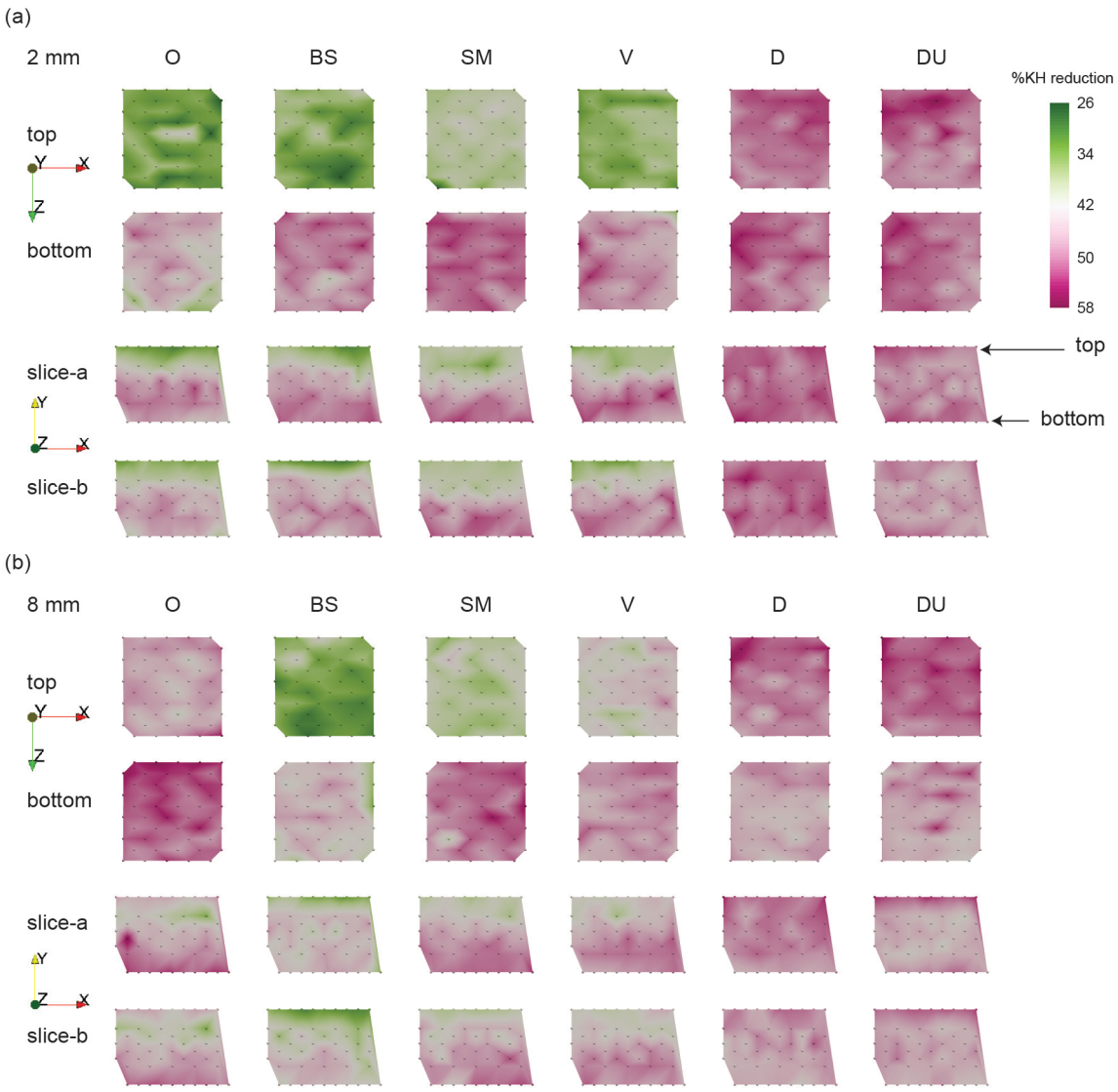

Figure 69. Representative 2D renderings of the localized %KH reduction contour maps of the RMC specimens light cured using the LCUs explored

(a) Representative 2D renderings of the localized %KH reduction on the top and bottom surfaces along with slice-a, -b and c cured by the LCUs investigated at 2 mm distance between the light guide and the top surfaces of the RMC specimens. (b) Representative 2D renderings of the localized %KH reduction on the top and bottom surfaces along with slice-a and -b cured by the LCUs investigated at 8 mm distance between the light guide and top surfaces of the RMC specimens. The spheres on the renderings represent the locations where the %KH reduction measurements were collected.

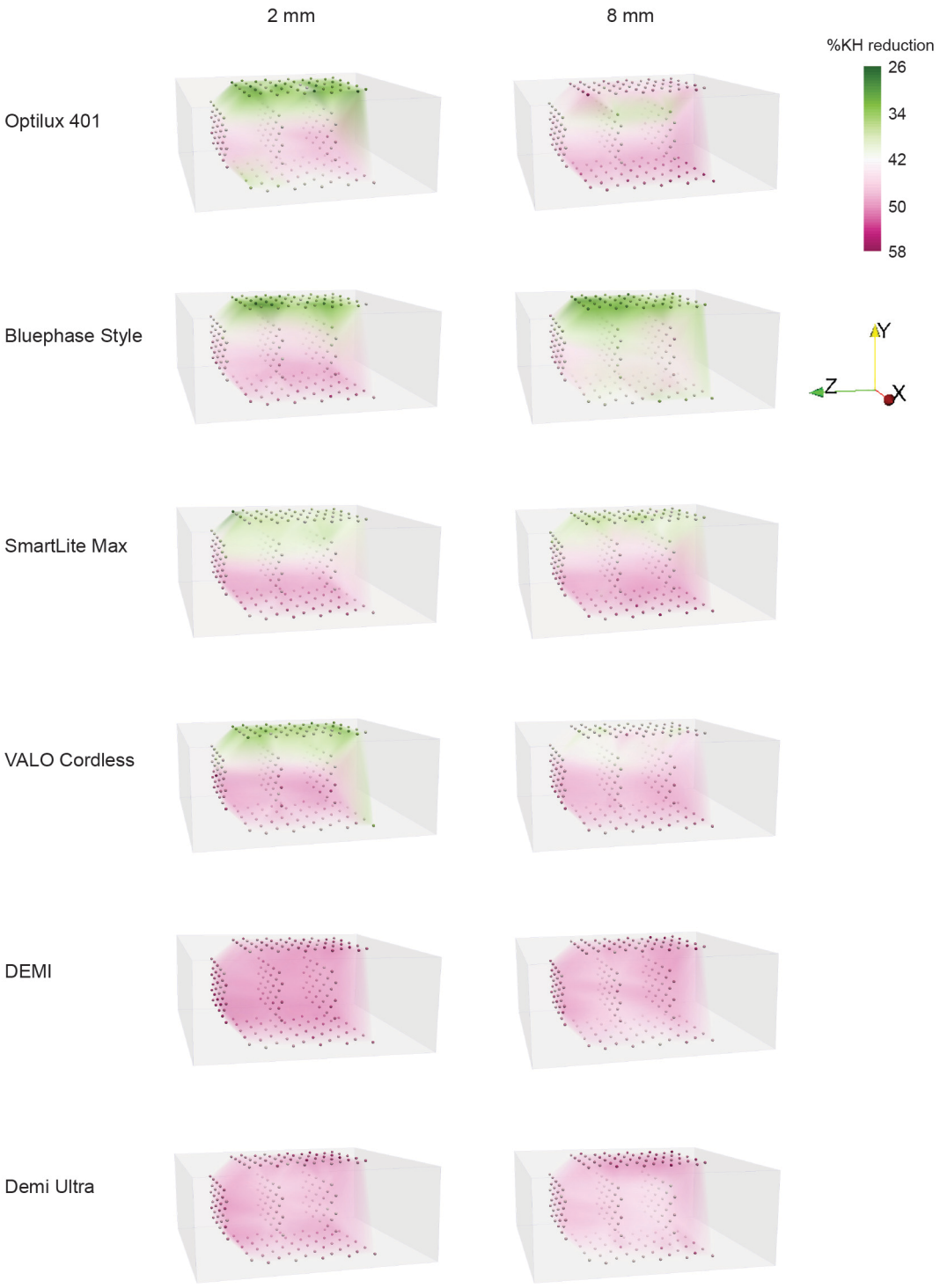

Figure 70. Representative 3D renderings of the localized %KH reduction measurement points at each depth of the RMC specimens light activated using the LCUs explored at 2 and 8 mm distances

The spheres represent the location of the measurements at each depth. The opacity of the rendering was adjusted to clearly visualize all the measurements points.

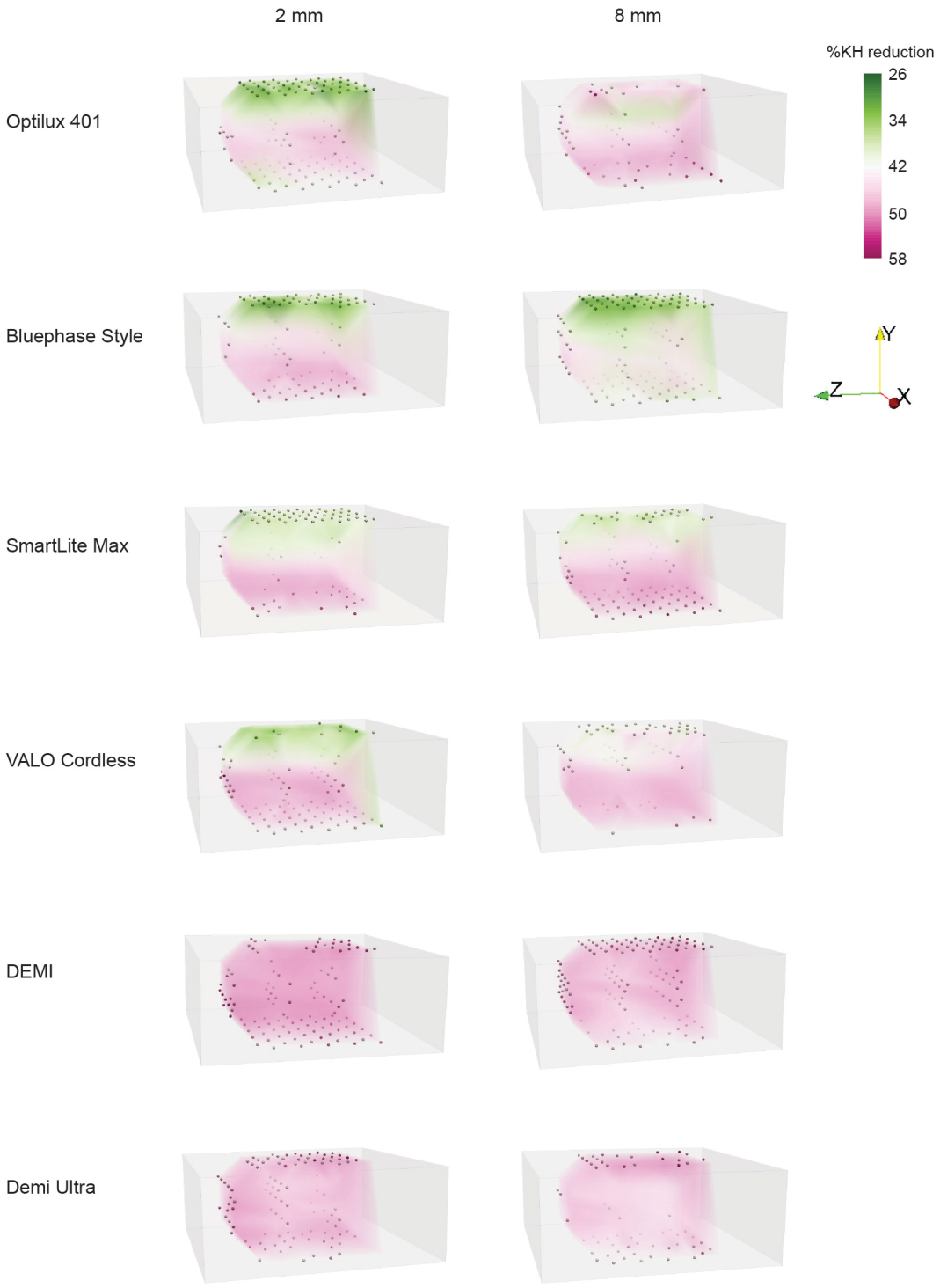

Figure 71. Representative 3D renderings of the localized %KH reduction significant points at each depth of the RMC light cured using the LCUs explored at 2 and 8 mm distances

The spheres represent the location of the significant measurement points at each depth. The opacity of the rendering was adjusted to clearly visualize all the measurement points.

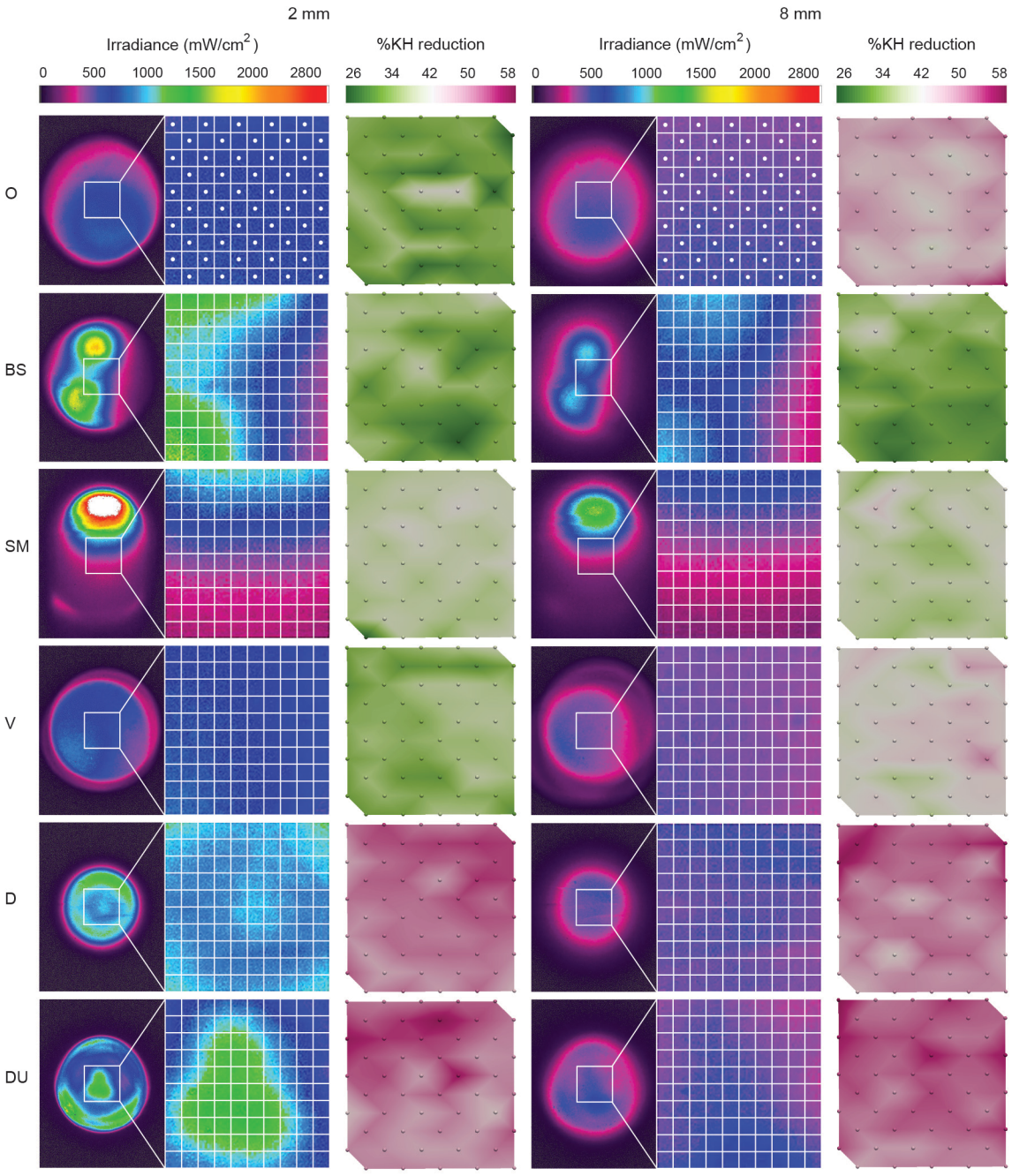

Figure 72. Representatives 2D localized irradiance beam profiles from the LCU explored measured through a 425 nm longpass filter coupled with the corresponding 2D localized %KH reduction contour maps on the top surfaces of the RMC specimens at 2 and 8 mm distances

The white circles in the beam profile image represent the localized irradiance values of each square that was correlated with the corresponding %KH reduction values represented by the spheres on the maps.

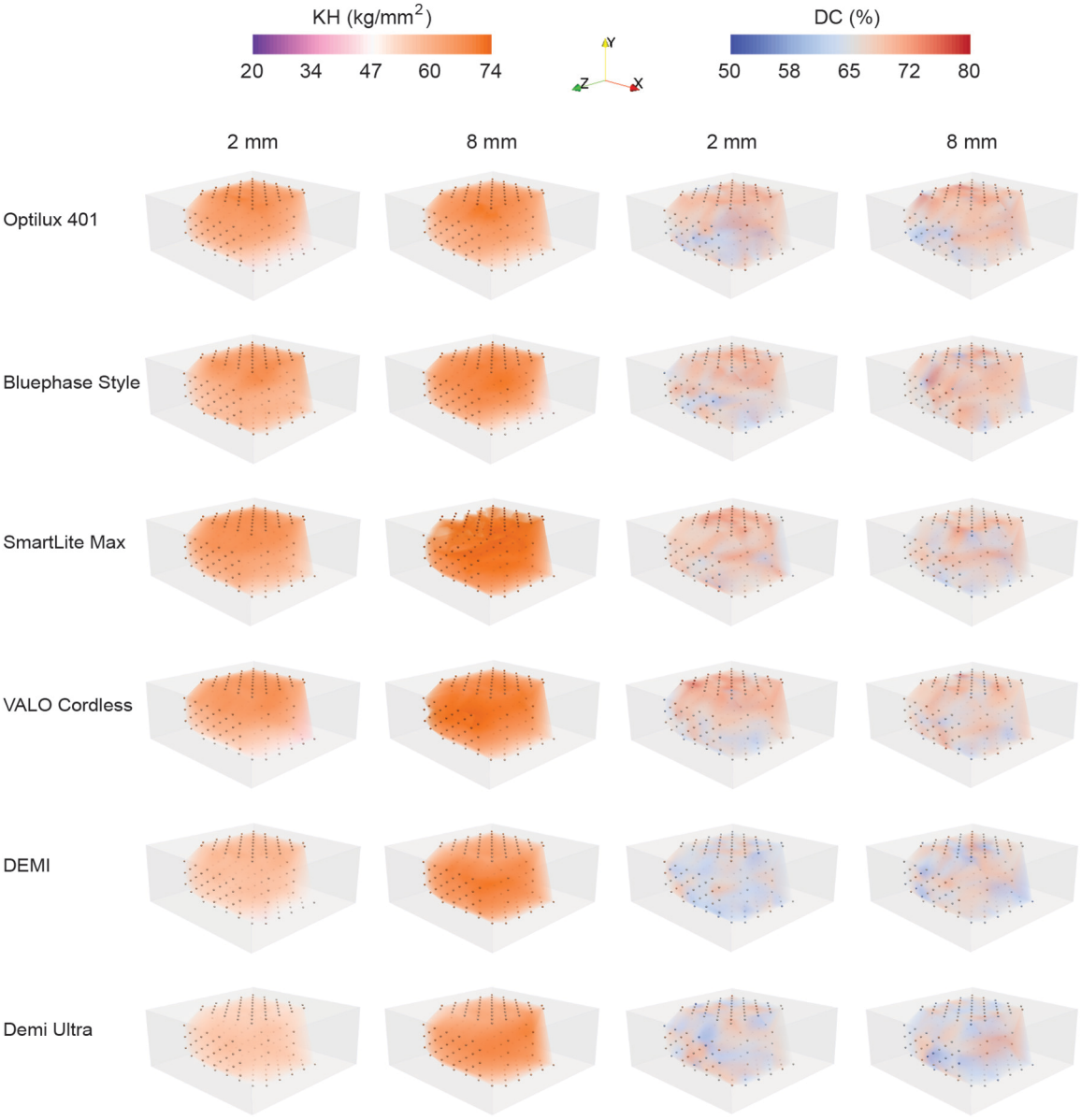

Figure 73. Representative 3D renderings for localized KH (kg/mm^2) and DC (%) values from the RMC specimens light cured using the LCUs assessed at 2 mm and 8 mm curing distances

The spheres represent the significant KH or DC measurements at each depth on the RMC specimens. The renderings illustrate the presence of some localized differences within the specimens using the LCUs explored. KH renderings show a gradual decrease from the top to the bottom of the specimen using the multiple emission peak LCUs and a relatively uniform distribution using the single emission peak LED LCUs. The DC renderings show more localized differences within the specimen that did not have a specific pattern.

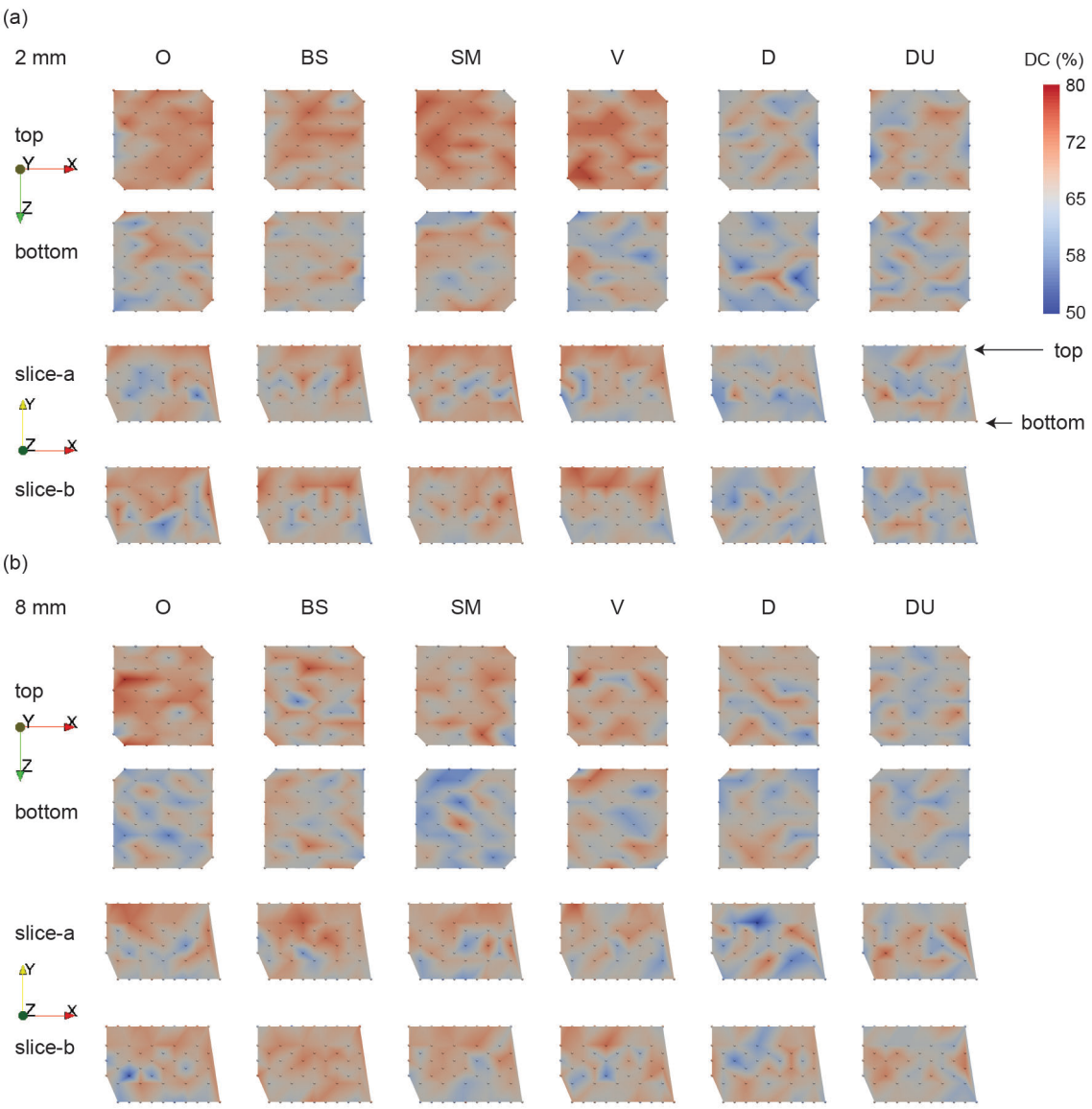

Figure 74. Representative 2D contour maps for the localized DC (%) values light cured using the LCUs assessed at 2 mm and 8 mm curing distances

The spheres represent the locations of the localized DC measurements at each depth on the RMC specimens. (a) Representative 2D renderings of the localized DC on the top and bottom surfaces along with slice-a, and -b cured by the LCUs investigated at 2 mm distance between the light guide and the top surfaces of the RMC specimens. (b) Representative 2D renderings of the localized DC on the top and bottom surfaces along with slice-a, and -b cured by the LCUs investigated at 8 mm distance between the light guide and top surfaces of the RMC specimens. The spheres on the renderings represent the locations where the DC reduction measurements were collected.

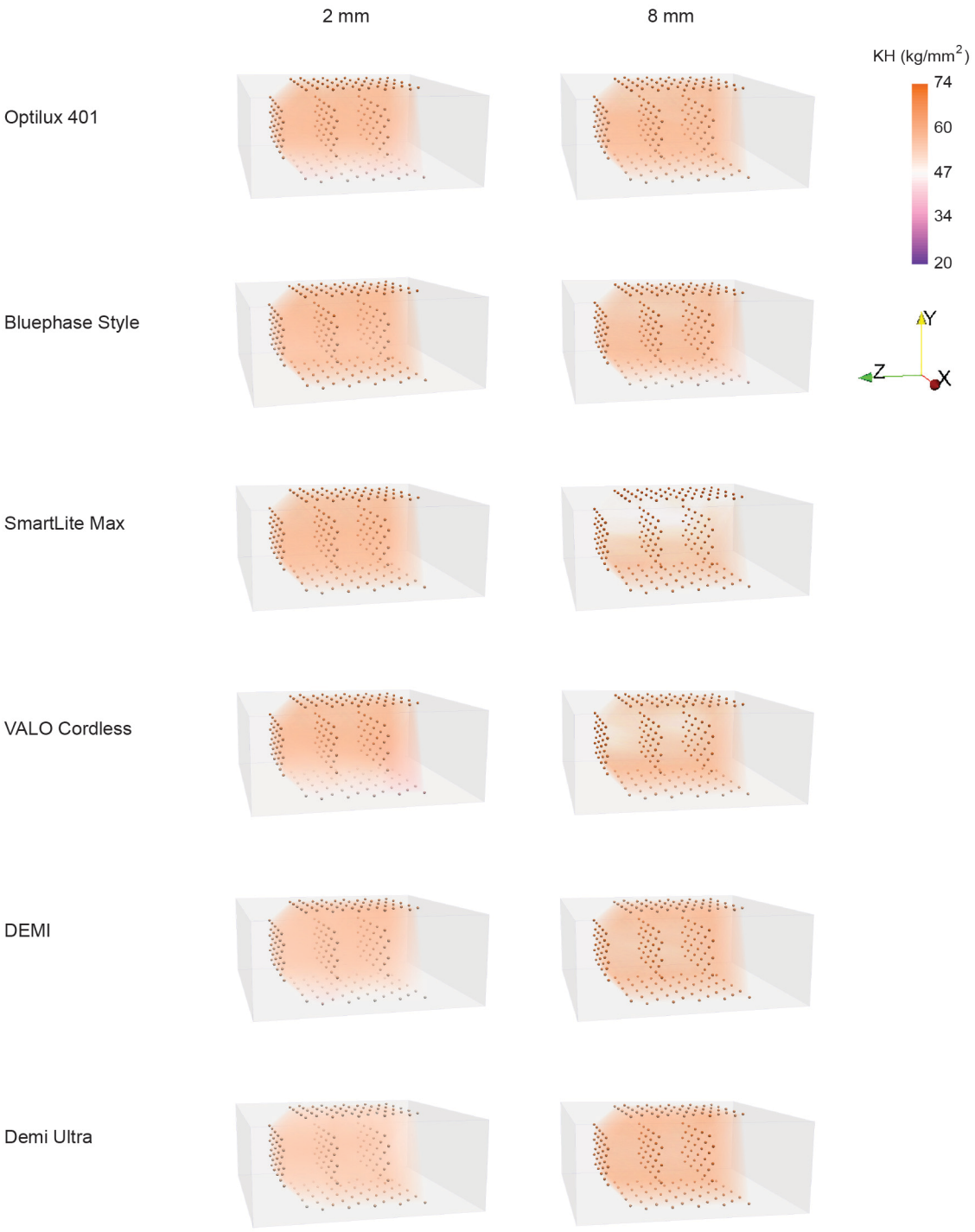

Figure 75. Representative 3D renderings of the localized KH (kg/mm^2) measurement points at each depth of the RMC specimens light cured using the LCUs explored at 2 and 8 mm curing distances

The spheres represent the location of the measurement points at each depth. The opacity of the rendering was adjusted to clearly visualize all the measurement points.

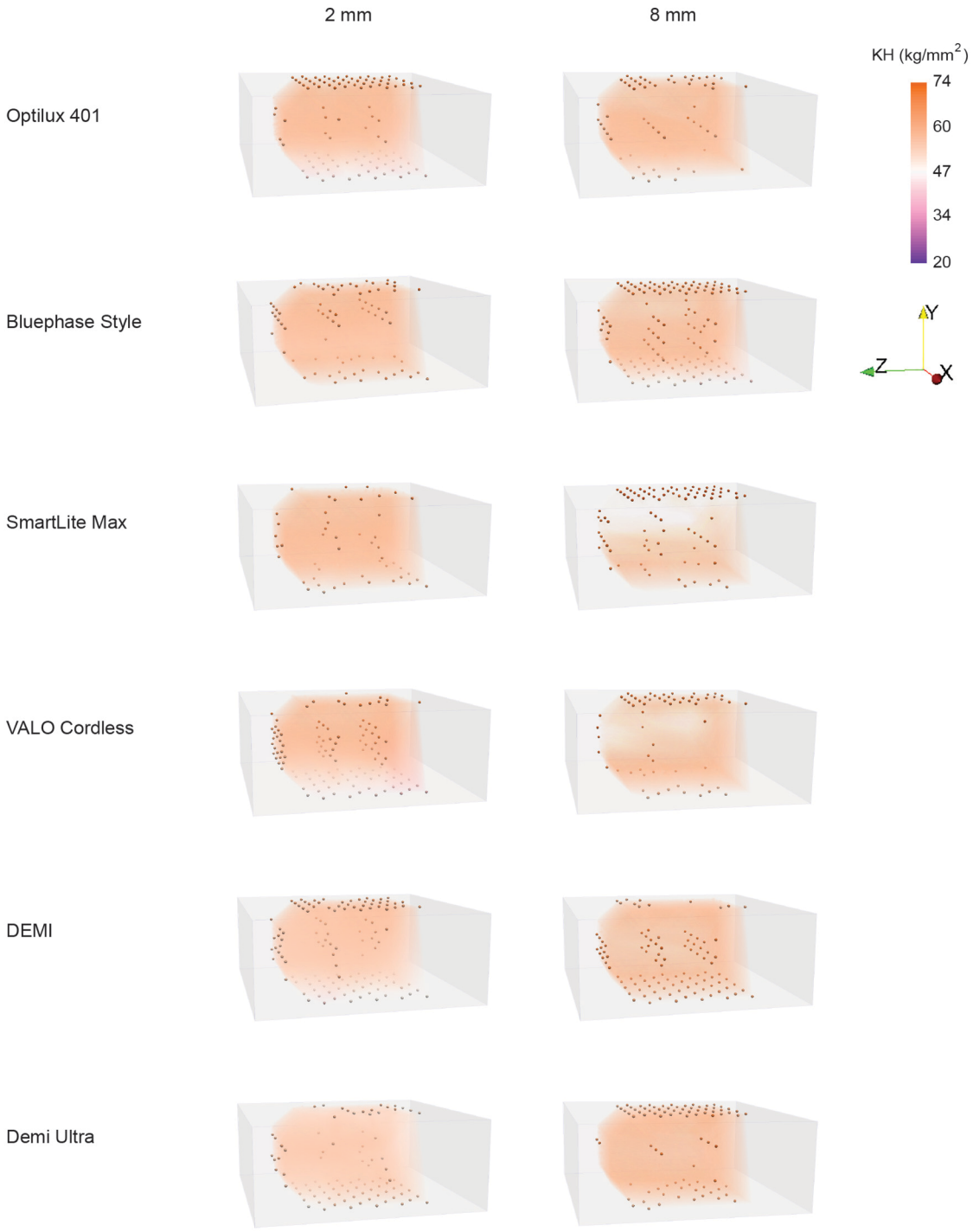

Figure 76. Representative 3D renderings of the localized KH (kg/mm^2) significant measurement points at each depth of the RMC specimens light cured using the LCUs explored at 2 and 8 mm distances

The spheres represent the location of the significant measurement points at each depth. The opacity of the rendering was adjusted to clearly visualize all the measurement points.

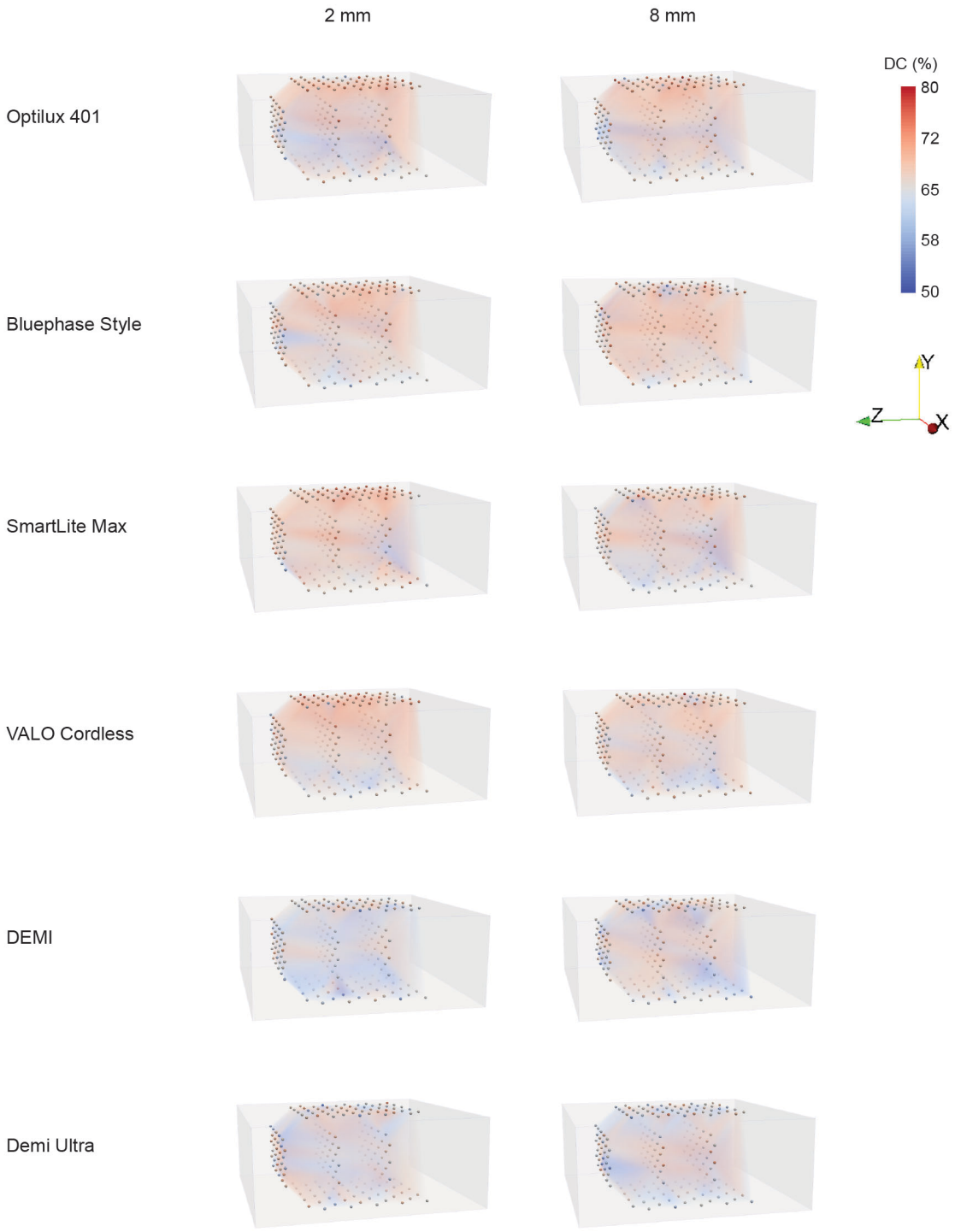

Figure 77. Representative 3D renderings of the localized DC (%) measurement points at each depth of the RMC specimens cured using the LCUs explored at 2 and 8 mm curing distances

The spheres represent the location of the measurement points at each depth. The opacity of the rendering was adjusted to clearly visualize all the measurement points.

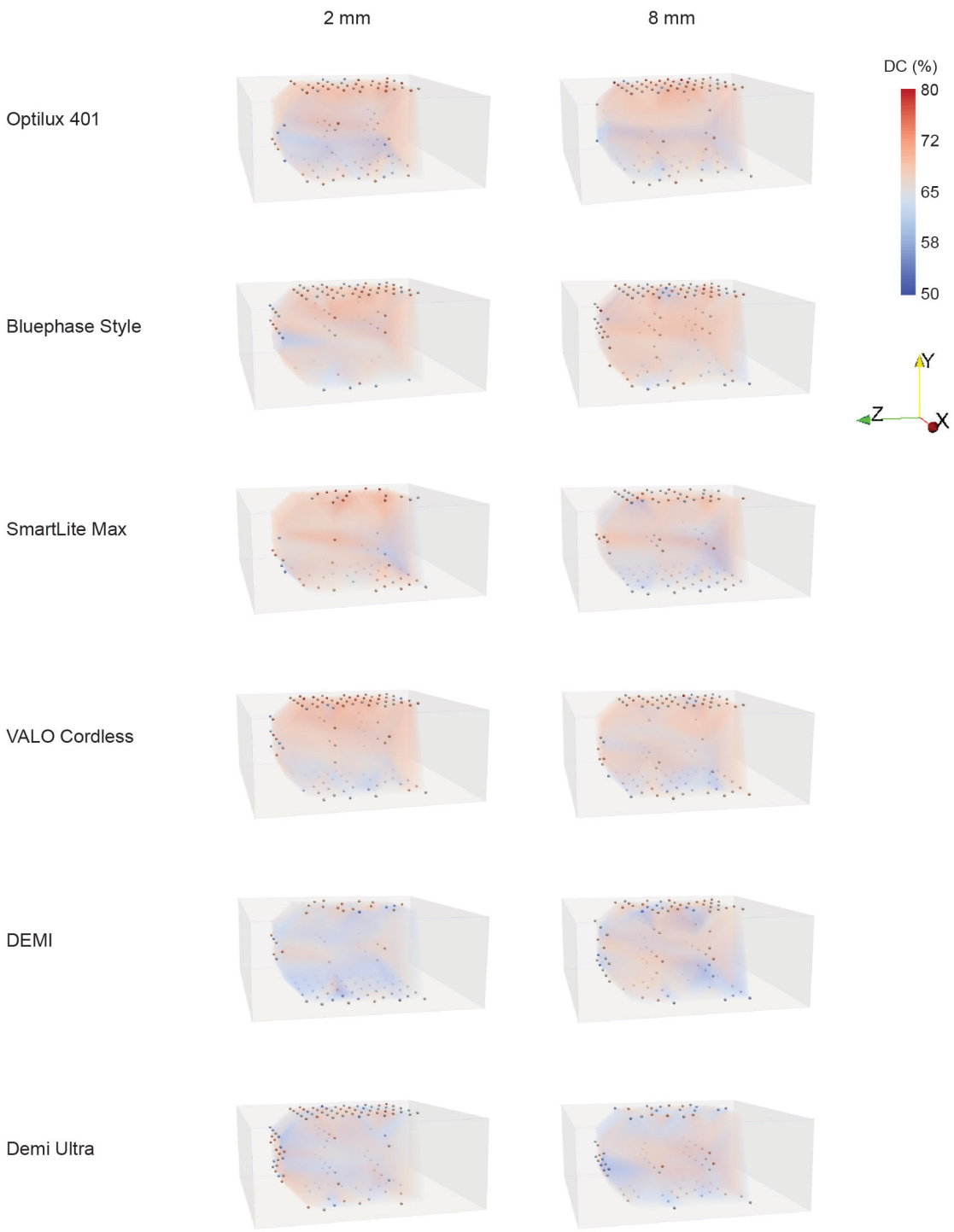

Figure 78. Representative 3D renderings of the localized DC (%) significant measurement points at each depth of the RMC specimens light cured using the LCUs explored at 2 and 8 mm curing distances

The spheres represent the location of the significant measurement points at each depth. The opacity of the rendering was adjusted to clearly visualize all the measurement points.

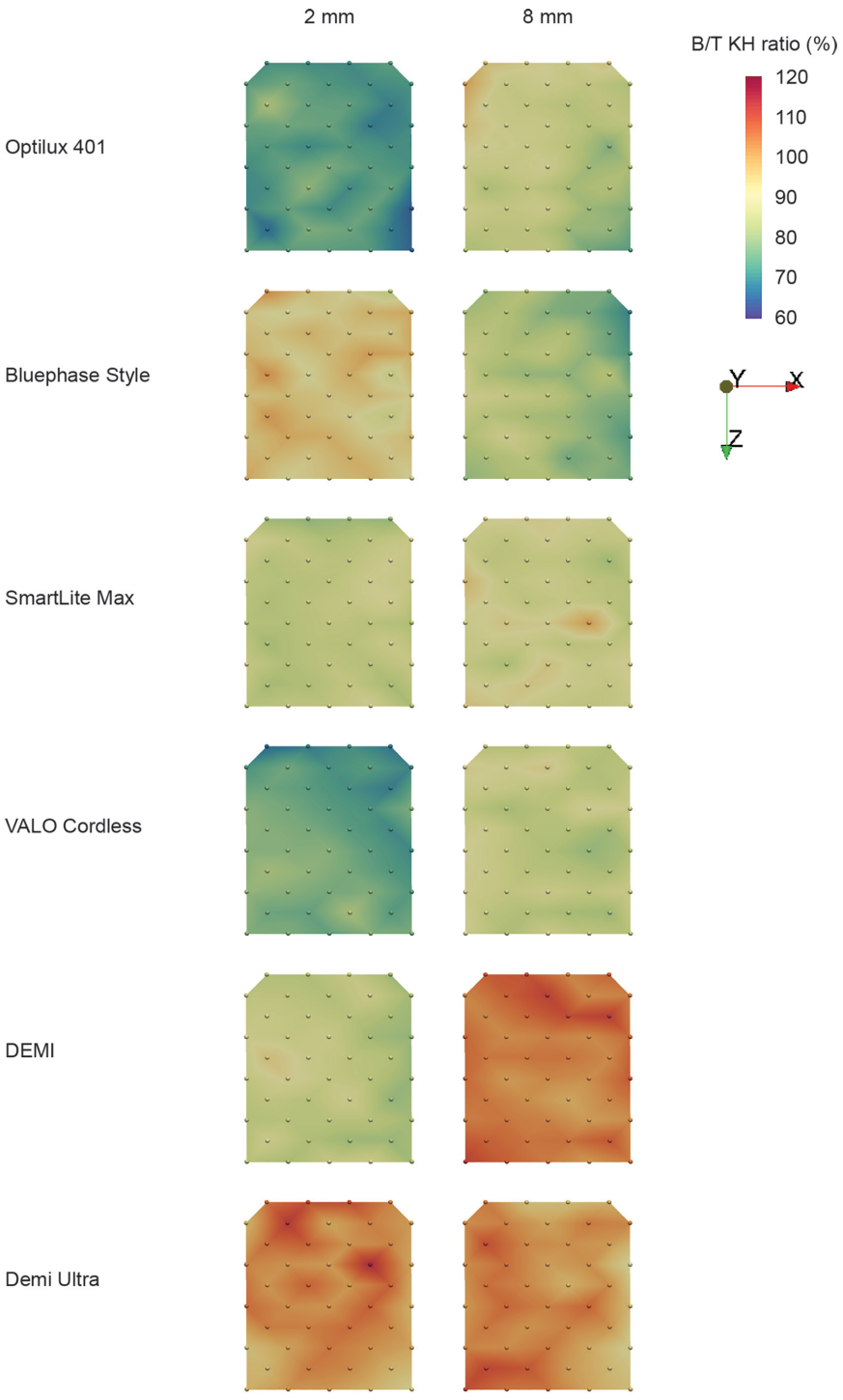

Figure 79. 2D contour plots to visualize the localized bottom/top KH ratios (%) at each measurement point on the RMC specimens cured using the LCUs explored at 2 and 8 mm curing distances

The spheres represent the location of each measurement on the bottom surface divided by the corresponding measurement on the top surface.

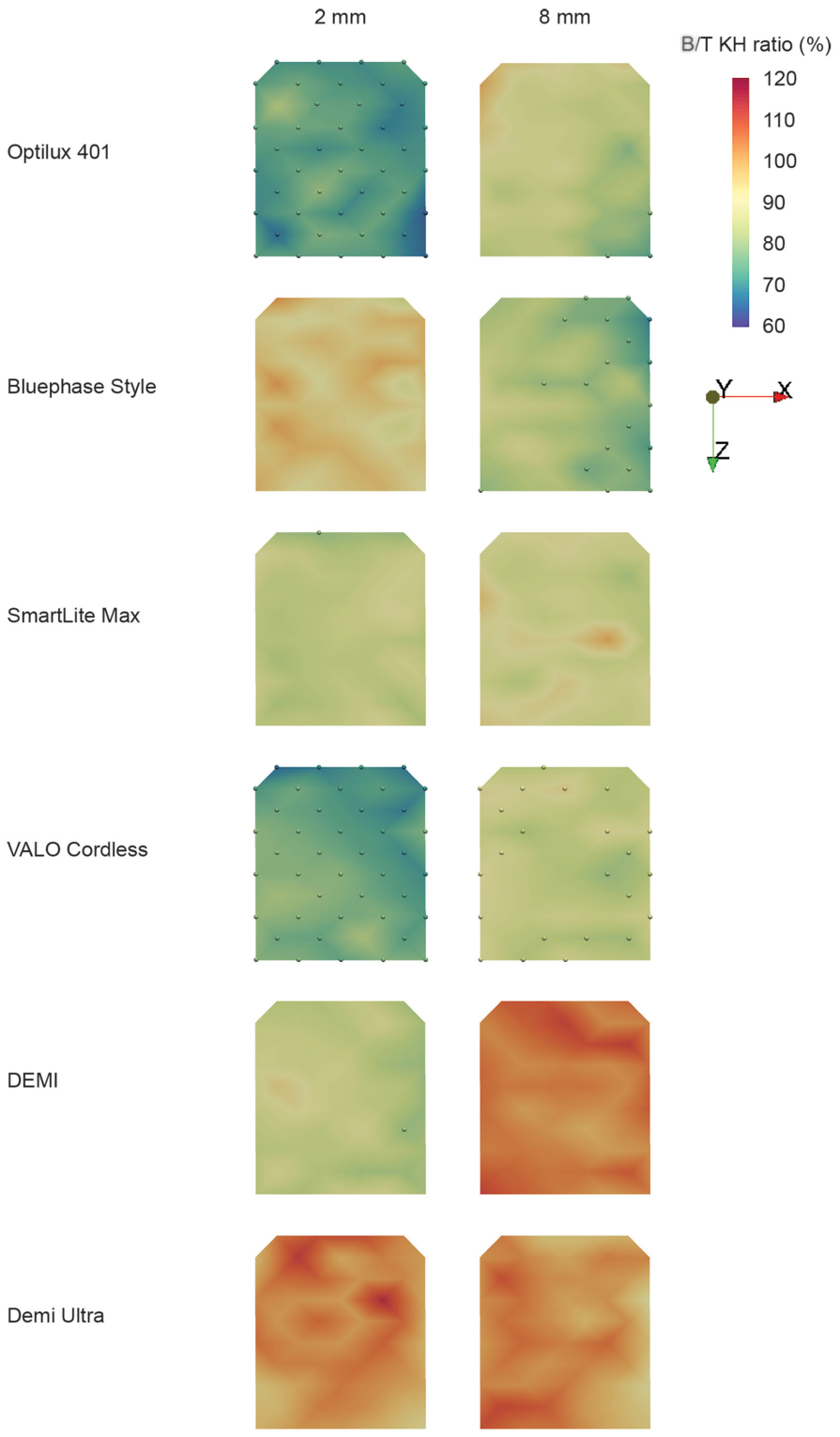

Figure 80. 2D contour plots to visualize the localized %bottom/top KH ratios that are less than 80% at each point on the RMC specimens cured using the LCUs explored at 2 and 8 mm distances

The spheres represent the location of the points with bottom/top KH ratios less than 80%.

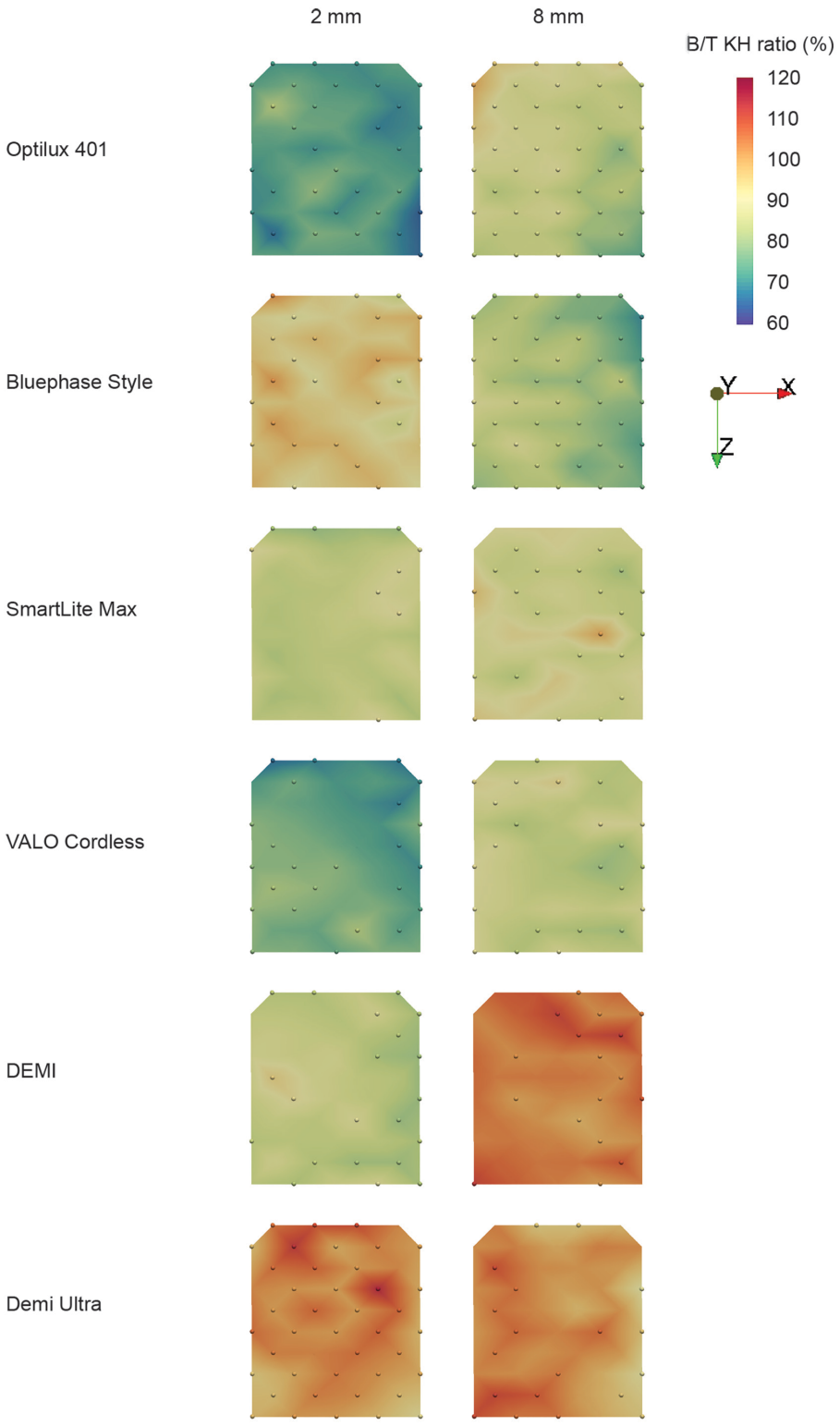

Figure 81. 2D contour plots to visualize the localized significant %bottom/top KH ratios among the point on the RMC light cured using the LCUs explored at 2 and 8 mm distances

The spheres represent the location of the significant measurement points using each LCU.

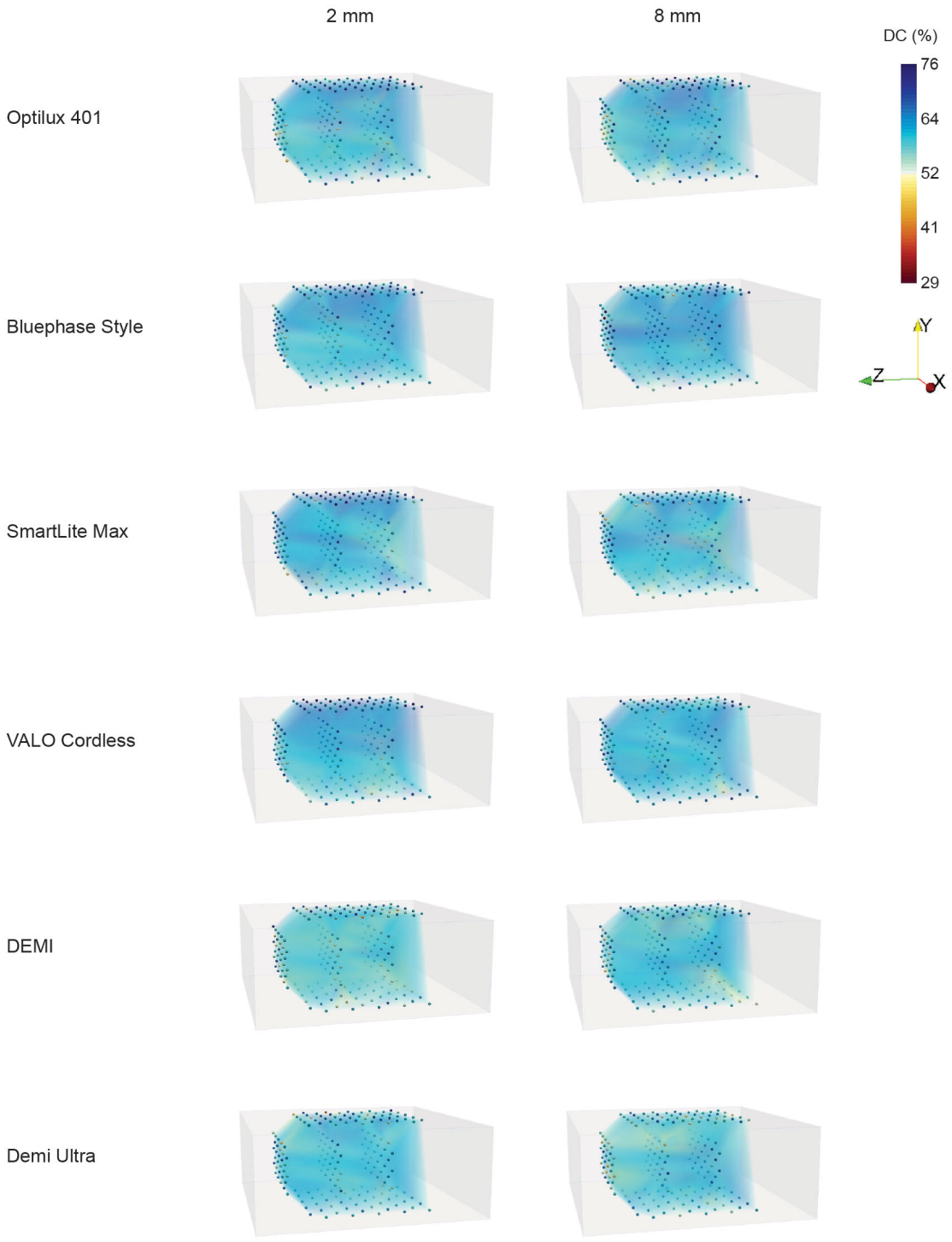

Figure 82. Representative 3D renderings of the localized minimum DC (%) measurement points at each depth of the RMC specimens light cured using the LCUs explored at 2 and 8 mm curing distances

The spheres represent the location of the measurement points at each depth. The opacity of the rendering was adjusted to clearly visualize all the measurement points.

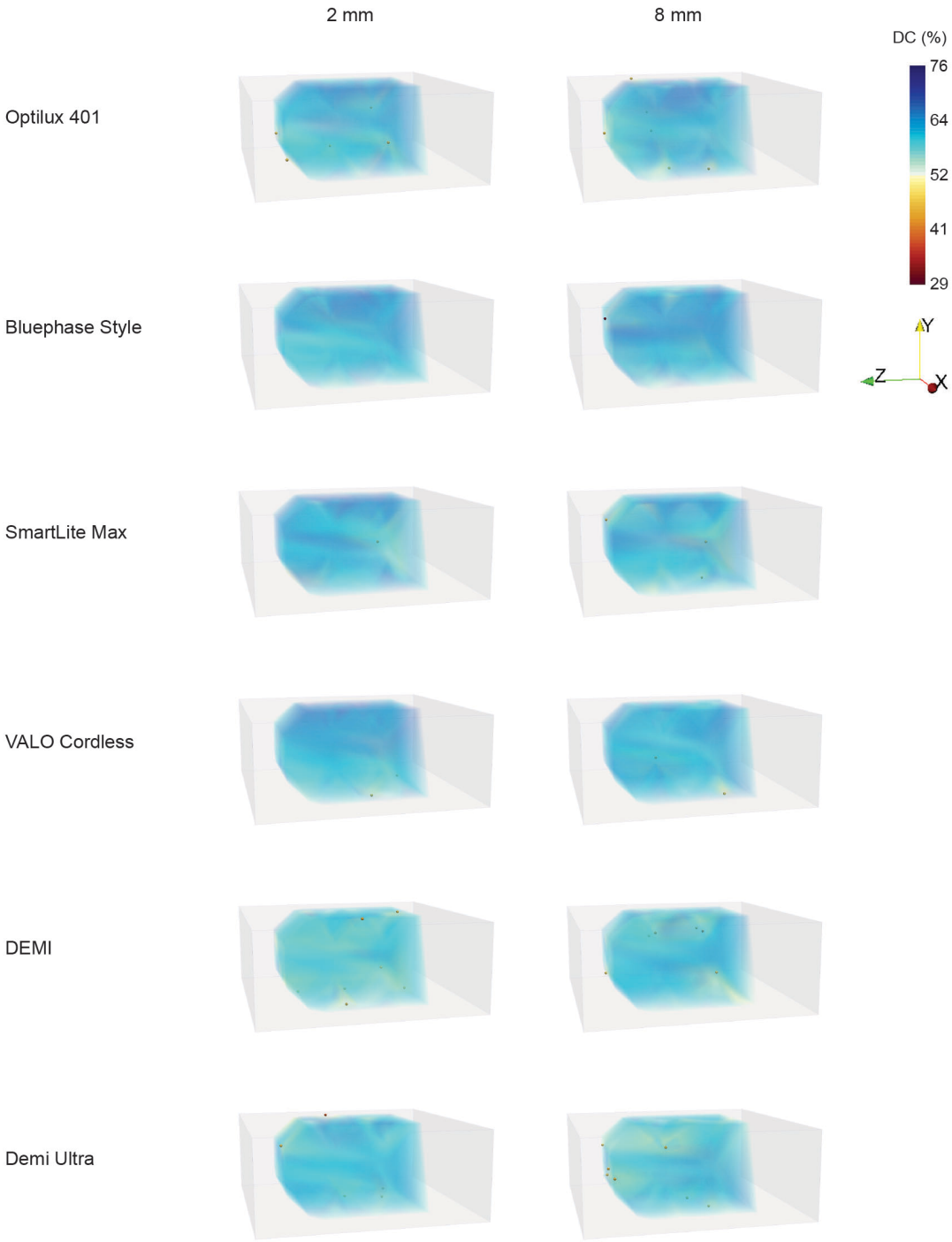

Figure 83. Representative 3D renderings of the localized minimum DC values that are less than 50% on the RMC specimens light cured using the LCUs explored at 2 and 8 mm distances

The spheres represent the location of the measurement points with a DC less than 50% at each depth. The opacity of the rendering was adjusted to clearly visualize all the measurement points.

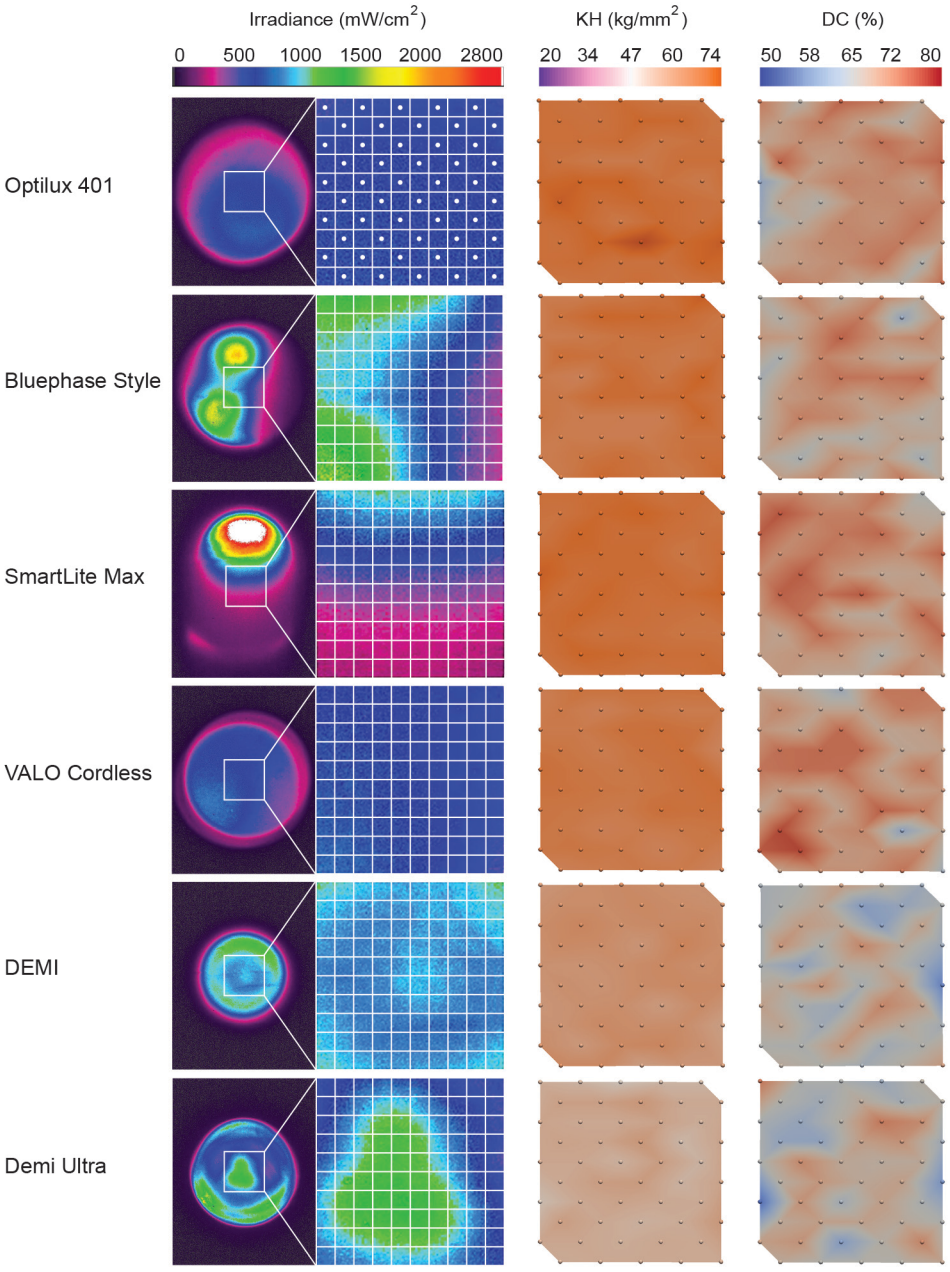

Figure 84. Representative 2D images of the localized irradiance beam profiles from the LCU explored measured through a 425 nm longpass filter coupled with the corresponding 2D localized KH and DC contour maps at 2 mm distance from the target surface

The square in each beam profile image corresponds to the 3×3 mm area on the specimens where the numerical power values were exported and from which the irradiance values were calculated. The white circles represent the irradiance values that were with the corresponding KH and DC measurements.

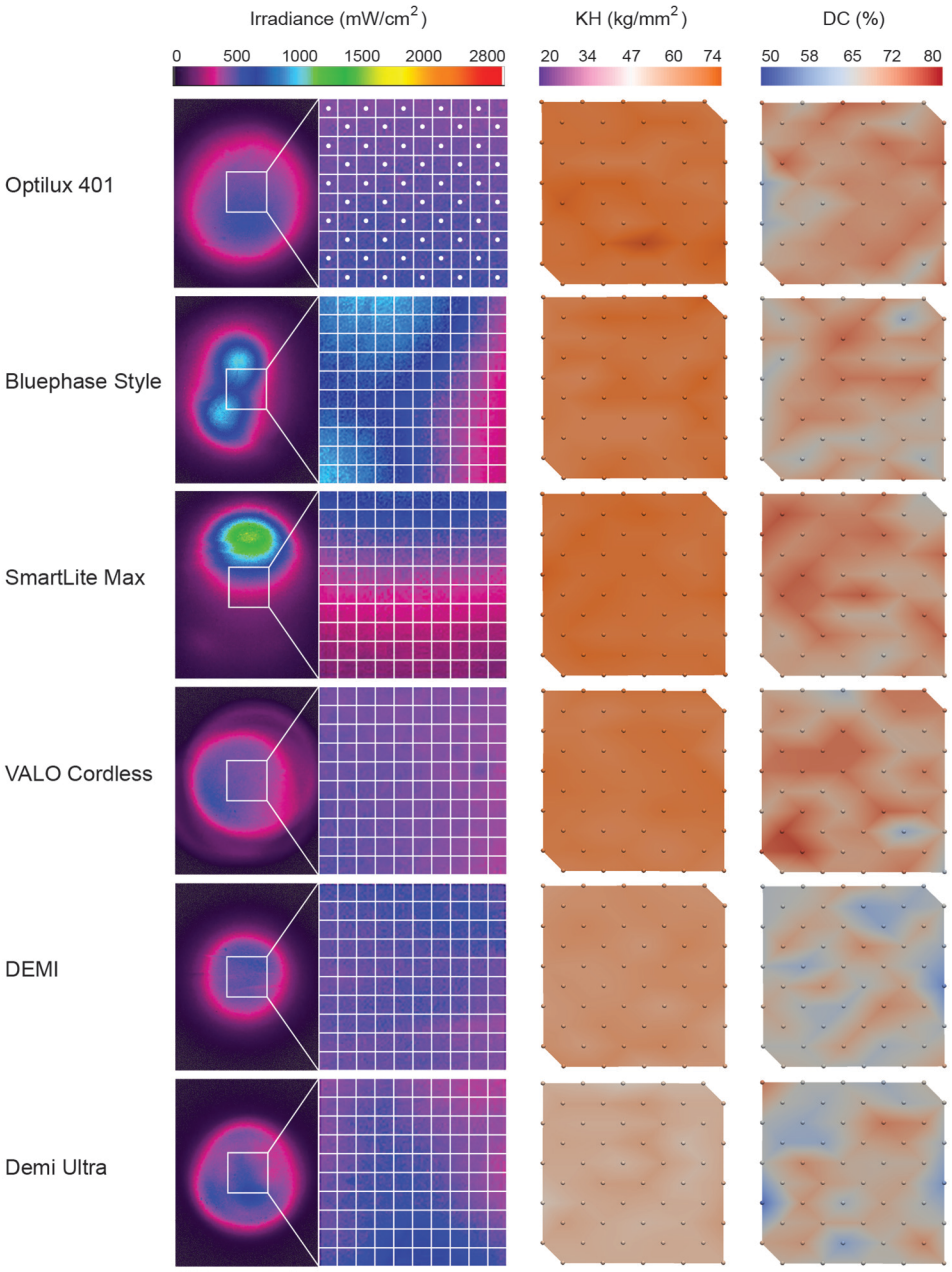

Figure 85. Representative 2D images of the localized irradiance beam profiles from the LCU explored measured through a 425 nm longpass filter coupled with the corresponding 2D localized KH and DC contour maps at 8 mm distance from the target surface

The square in each beam profile image corresponds to the 3×3 mm area on the RMC specimens where the numerical power values were exported and from which the irradiance values were calculated. The white circles represent the irradiance values that were with the corresponding KH and DC measurements.

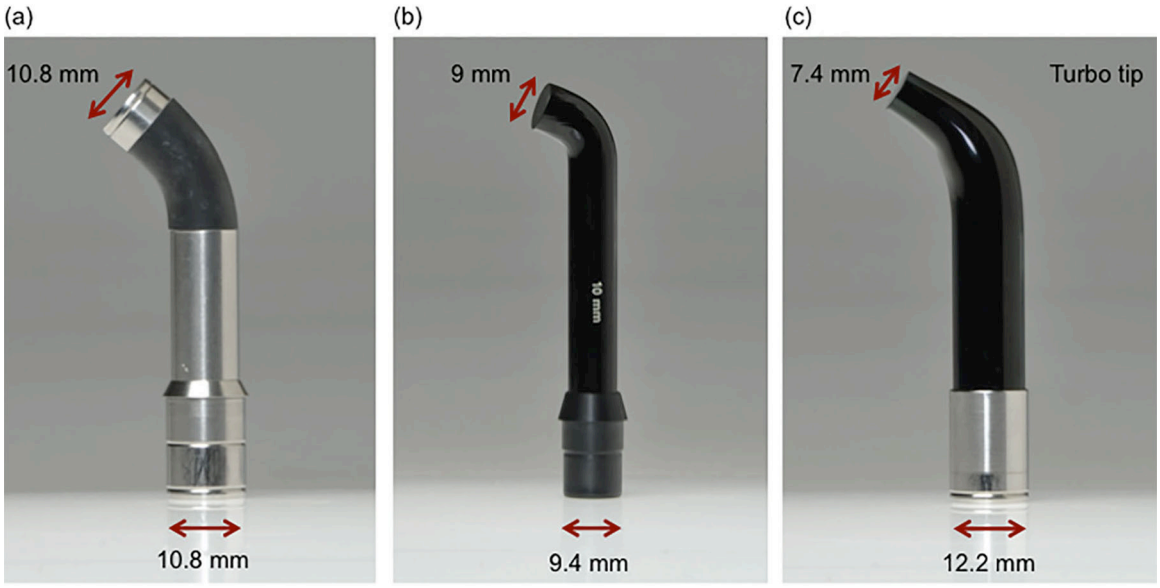

Figure 86. Diameter of the fiber optic light guide tip entry and exit for the removable light guide tips of the LCUs explored

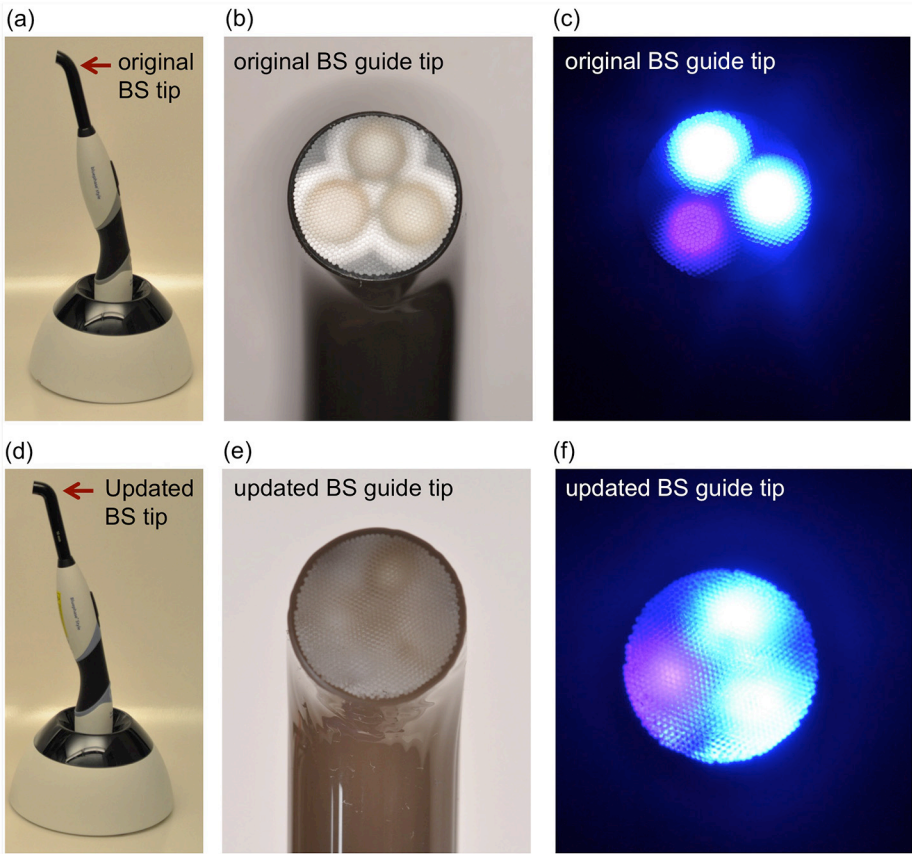

Figure 87. Differences between the original and updated BS fiber optic light guide tips

(a and d) The light guide tip angulation differences between both BS LCUs. The body of both units is similar. (a) BS LCU with the original light guide tip. (b) The three LED chips are distinctively shown through the original fiber optic tip. (c) Each LED chip is distinctively shown through the original fiber optic tip. (d) BS LCU with the updated light guide tip. (e) The three LED chips are not so obvious in the updated fiber optic light guide tip. (f) Each LED chip is not distinctively separate through the updated fiber optic tip when the LCU is activated.

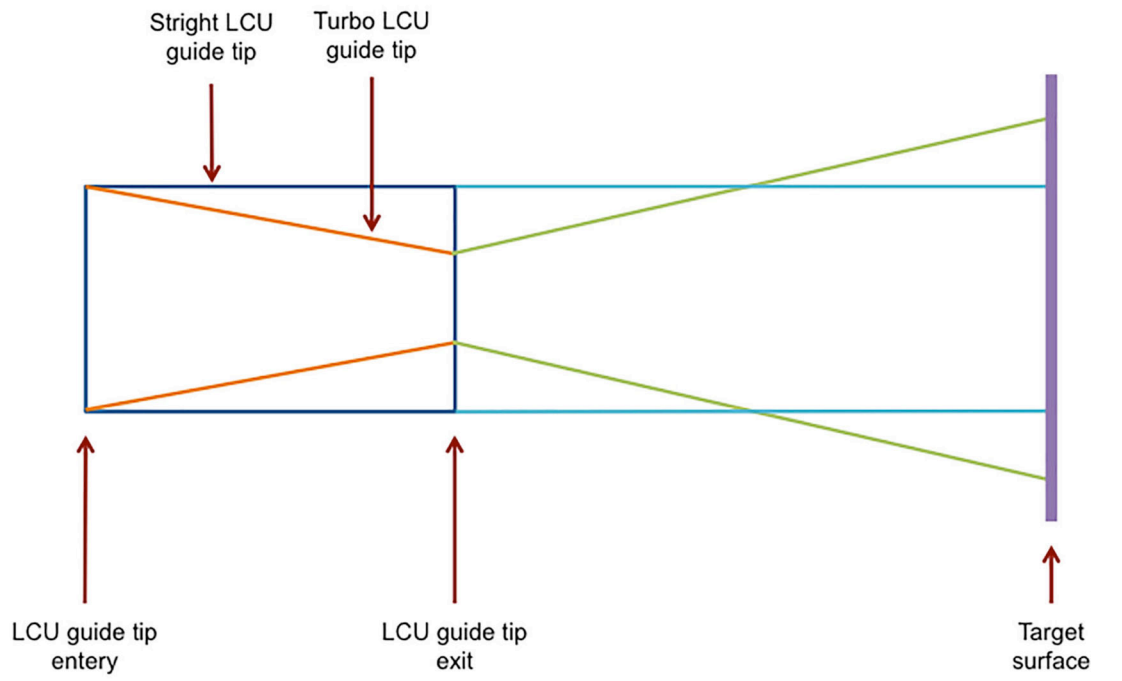

Figure 88. Illustration of the Spectral Reflection Law

The cone of light generated is reflected outward in a specular manner that causes a “Turbo” fiber optic light guide tip to spread over a wider area compared to a straight light guide tip.

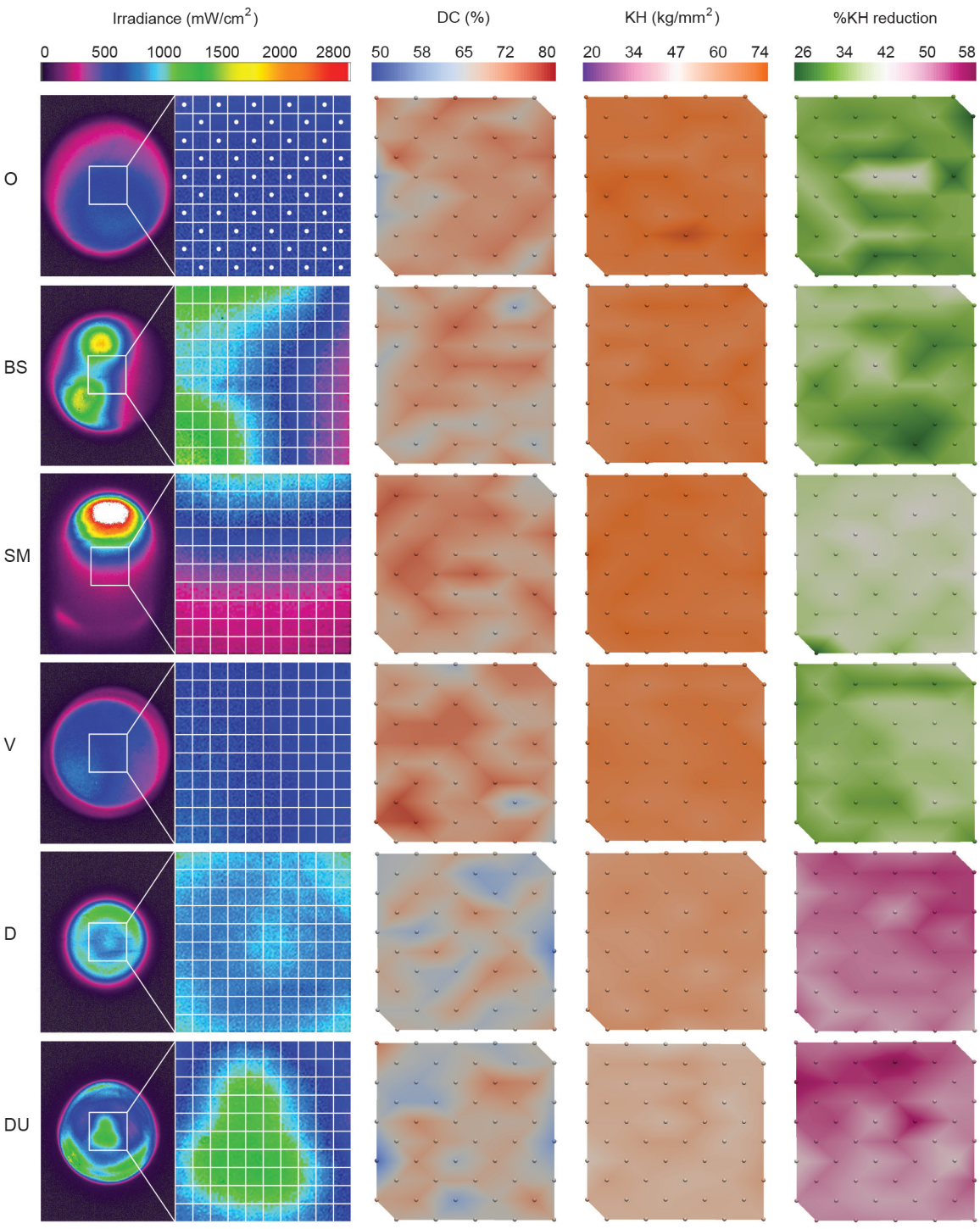

Figure 89. Representatives 2D images of the localized irradiance beam profiles from the LCUs explored measured through a 425 nm longpass filter coupled with the corresponding 2D localized DC, KH and %KH reduction values on the top surfaces of the specimens at 2 mm distance from the target surface

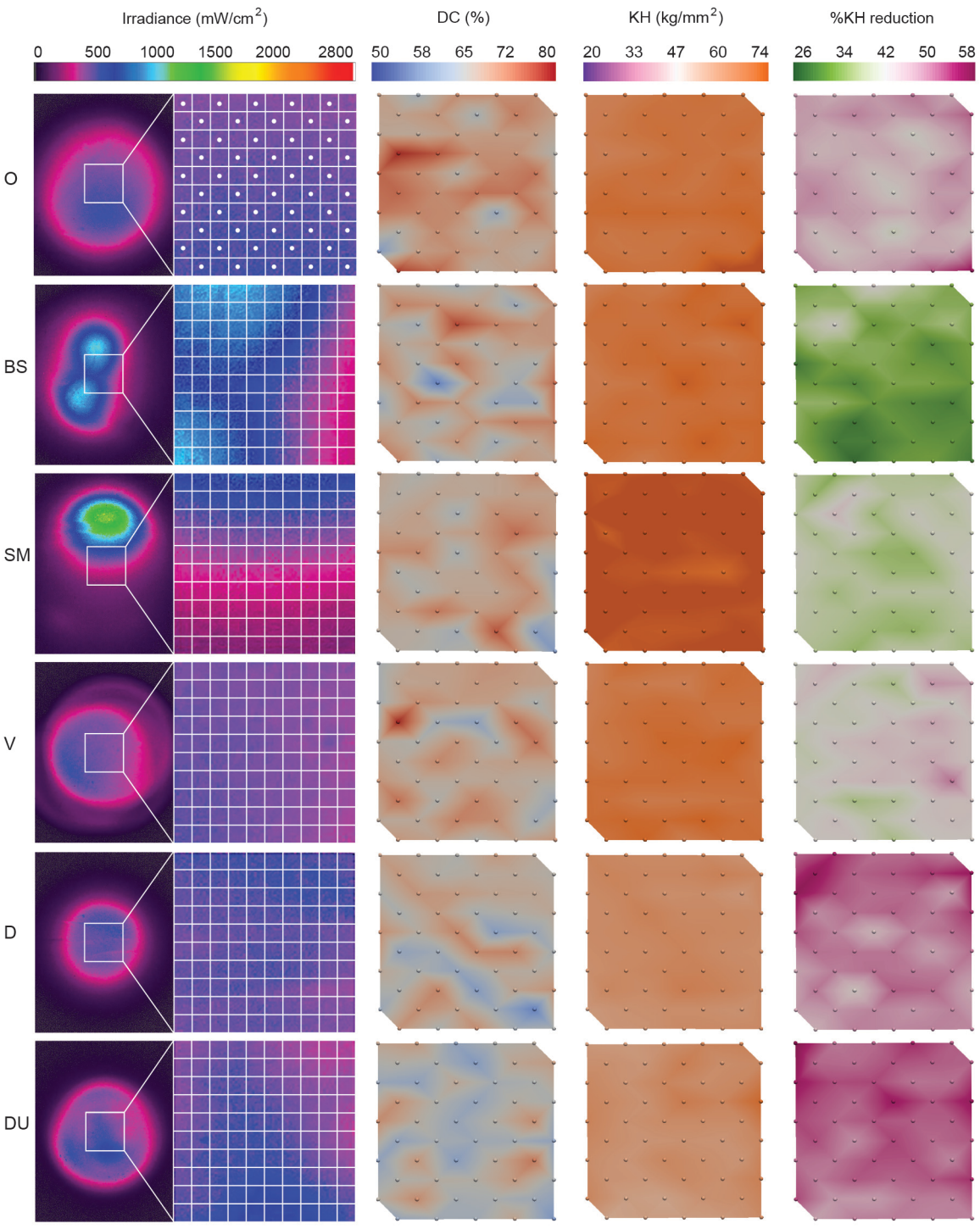

Figure 90. Representatives 2D images of the localized irradiance beam profiles from the LCUs explored measured through a 425 nm shortpass filter coupled with the corresponding 2D localized DC, KH and %KH reduction values on the top surfaces of the specimens at 8 mm distance from the target surface

APPENDICES

Appendices are provided in a supplementary document, preceded by an index, as pages 224-709.

REFERENCES

Aguiar, F. H., A. T. Braceiro, G. M. Ambrosano, and J. R. Lovadino. 2005. "Hardness and diametral tensile strength of a hybrid composite resin polymerized with different modes and immersed in ethanol or distilled water media." *Dent Mater* 21 (12):1098-103. doi: 10.1016/j.dental.2004.11.010.

Albino, L. G., J. A. Rodrigues, Y. Kawano, and A. Cassoni. 2011. "Knoop microhardness and FT-Raman evaluation of composite resins: influence of opacity and photoactivation source." *Braz Oral Res* 25 (3):267-73.

Alshali, R. Z., N. A. Salim, J. D. Satterthwaite, and N. Silikas. 2015. "Post-irradiation hardness development, chemical softening, and thermal stability of bulk-fill and conventional resin-composites." *J Dent* 43 (2):209-18. doi: 10.1016/j.jdent.2014.12.004.

Alshali, R. Z., N. Silikas, and J. D. Satterthwaite. 2013. "Degree of conversion of bulk-fill compared to conventional resin-composites at two time intervals." *Dent Mater* 29 (9):e213-7. doi: 10.1016/j.dental.2013.05.011.

Alvanforoush, N., J. Palamara, R. Wong, and M. F. Burrow. 2016. "A Comparison between published clinical success of direct resin composite restorations in vital posterior teeth in 1995-2005 and 2006-2016 periods." *Aust Dent J*. doi: 10.1111/adj.12487.

Arikawa, H., K. Fujii, T. Kanie, and K. Inoue. 1998. "Light transmittance characteristics of light-cured composite resins." *Dent Mater* 14 (6):405-11.

Arikawa, H., H. Takahashi, Y. Minesaki, K. Muraguchi, T. Matsuyama, T. Kanie, and S. Ban. 2011. "A method for improving the light intensity distribution in dental light-curing units." *Dent Mater J* 30 (2):151-7.

Asmussen, E. 1982. "Factors affecting the quantity of remaining double bonds in restorative resin polymers." *Scand J Dent Res* 90 (6):490-6.

Asmussen, E., and A. Peutzfeldt. 2001a. "Influence of pulse-delay curing on softening of polymer structures." *J Dent Res* 80 (6):1570-3.

Asmussen, E., and A. Peutzfeldt. 2001b. "Influence of selected components on crosslink density in polymer structures." *Eur J Oral Sci* 109 (4):282-5.

Astvaldsdottir, A., J. Dagerhamn, J. W. van Dijken, A. Naimi-Akbar, G. Sandborgh-Englund, S. Tranaeus, and M. Nilsson. 2015. "Longevity of posterior resin composite restorations in adults - A systematic review." *J Dent* 43 (8):934-54. doi: 10.1016/j.jdent.2015.05.001.

Ayachit, Utkarsh. 2015. "The ParaView Guide: A Parallel Visualization Application, Kitware." http://www.paraview.org/.

Beolchi, R. S., C. Moura-Netto, R. M. Palo, C. Rocha Gomes Torres, and B. Pelissier. 2015. "Changes in irradiance and energy density in relation to different curing distances." *Braz Oral Res* 29. doi: 10.1590/1807-3107BOR-2015.vol29.0060.

Beun, S., C. Bailly, A. Dabin, J. Vreven, J. Devaux, and G. Leloup. 2009. "Rheological properties of experimental Bis-GMA/TEGDMA flowable resin composites with various macrofiller/microfiller ratio." *Dent Mater* 25 (2):198-205. doi: 10.1016/j.dental.2008.06.001.

Brandt, W. C., R. R. de Moraes, L. Correr-Sobrinho, M. A. Sinhoreti, and S. Consani.

2008. "Effect of different photo-activation methods on push out force, hardness and cross-link density of resin composite restorations." *Dent Mater* 24 (6):846-50. doi: 10.1016/j.dental.2007.09.012.

Brewer, Cynthia A. 2017. "colorbrewer.org." http://colorbrewer2.org/ -type=sequential&scheme=BuGn&n=3.

Bucuta, S., and N. Ilie. 2014. "Light transmittance and micro-mechanical properties of bulk fill vs. conventional resin based composites." *Clin Oral Investig* 18 (8):1991-2000. doi: 10.1007/s00784-013-1177-y.

Cassoni, A., O. Ferla Jde, J. A. Shibli, and Y. Kawano. 2008. "Knoop microhardness and FT-Raman spectroscopic evaluation of a resin-based dental material light-cured by an argon ion laser and halogen lamp: an in vitro study." *Photomed Laser Surg* 26 (6):531-9. doi: 10.1089/pho.2007.2212.

Cook, W. D., and P. M. Standish. 1983. "Cure of resin based restorative materials. II. White light photopolymerized resins." *Aust Dent J* 28 (5):307-11.

Corciolani, G., A. Vichi, C. L. Davidson, and M. Ferrari. 2008. "The influence of tip geometry and distance on light-curing efficacy." *Oper Dent* 33 (3):325-31. doi: 10.2341/07-94.

Cramer, N. B., J. W. Stansbury, and C. N. Bowman. 2011. "Recent advances and developments in composite dental restorative materials." *J Dent Res* 90 (4):402-16. doi: 10.1177/0022034510381263.

de Oliveira, D. C., M. G. Rocha, A. Gatti, A. B. Correr, J. L. Ferracane, and M. A. Sinhoret. 2015. "Effect of different photoinitiators and reducing agents on cure efficiency and color stability of resin-based composites using different LED wavelengths." *J Dent* 43 (12):1565-72. doi: 10.1016/j.jdent.2015.08.015.

Demarco, F. F., K. Collares, F. H. Coelho-de-Souza, M. B. Correa, M. S. Cenci, R. R. Moraes, and N. J. Opdam. 2015. "Anterior composite restorations: A systematic review on long-term survival and reasons for failure." *Dent Mater* 31 (10):1214-24. doi: 10.1016/j.dental.2015.07.005.

Dewaele, M., E. Asmussen, A. Peutzfeldt, E. C. Munksgaard, A. R. Benetti, G. Finne, G. Leloup, and J. Devaux. 2009. "Influence of curing protocol on selected properties of light-curing polymers: degree of conversion, volume contraction, elastic modulus, and glass transition temperature." *Dent Mater* 25 (12):1576-84. doi: 10.1016/j.dental.2009.08.001.

Dewaele, M., D. Truffier-Boutry, J. Devaux, and G. Leloup. 2006. "Volume contraction in photocured dental resins: the shrinkage-conversion relationship revisited." *Dent Mater* 22 (4):359-65. doi: 10.1016/j.dental.2005.03.014.

Dunn, W. J., and A. C. Bush. 2002. "A comparison of polymerization by light-emitting diode and halogen-based light-curing units." *J Am Dent Assoc* 133 (3):335-41.

Durner, J., J. Obermaier, M. Draenert, and N. Ilie. 2012. "Correlation of the degree of conversion with the amount of elutable substances in nano-hybrid dental composites." *Dent Mater* 28 (11):1146-53. doi: 10.1016/j.dental.2012.08.006.

Fan, P. L., R. M. Schumacher, K. Azzolin, R. Geary, and F. C. Eichmiller. 2002. "Curing-light intensity and depth of cure of resin-based composites tested according to international standards." *J Am Dent Assoc* 133 (4):429-34; quiz 491-3.

Feitosa, V. P., A. P. Fugolin, A. B. Correr, L. Correr-Sobrinho, S. Consani, T. F. Watson,

M. A. Sinhoreti, and S. Sauro. 2012. "Effects of different photo-polymerization protocols on resin-dentine muTBS, mechanical properties and cross-link density of a nano-filled resin composite." *J Dent* 40 (10):802-9. doi: 10.1016/j.jdent.2012.05.014.

Felix, C. A., and R. B. Price. 2003. "The effect of distance from light source on light intensity from curing lights." *J Adhes Dent* 5 (4):283-91.

Feng, L., and B. I. Suh. 2007. "Exposure reciprocity law in photopolymerization of multi-functional acrylates and methacrylates." *Macromolecular Chemistry and Physics* 208 (3):295-306. doi: 10.1002/macp.200600480.

Ferracane, J. L. 1985. "Correlation between hardness and degree of conversion during the setting reaction of unfilled dental restorative resins." *Dent Mater* 1 (1):11-4. doi: 10.1016/s0109-5641(85)80058-0.

Ferracane, J. L. 1994. "Elution of leachable components from composites." *J Oral Rehabil* 21 (4):441-52.

Ferracane, J. L. 2006. "Hygroscopic and hydrolytic effects in dental polymer networks." *Dent Mater* 22 (3):211-22. doi: 10.1016/j.dental.2005.05.005.

Ferracane, J. L., J. C. Mitchem, J. R. Condon, and R. Todd. 1997. "Wear and marginal breakdown of composites with various degrees of cure." *J Dent Res* 76 (8):1508-16.

Fujita, K., T. Ikemi, and N. Nishiyama. 2011. "Effects of particle size of silica filler on polymerization conversion in a light-curing resin composite." *Dent Mater* 27 (11):1079-85. doi: 10.1016/j.dental.2011.07.010.

Goncalves, F., F. C. Calheiros, M. F. Witzel, Y. Kawano, and R. R. Braga. 2007. "Effect of photoactivation protocol and radiant exposure on monomer conversion and flexural strength of a resin composite after water and ethanol storage." *J Biomed Mater Res B Appl Biomater* 82 (1):89-92. doi: 10.1002/jbm.b.30708.

Gritsch, K., S. Souvannasot, C. Schembri, P. Farge, and B. Grosgogeat. 2008. "Influence of light energy and power density on the microhardness of two nanohybrid composites." *Eur J Oral Sci* 116 (1):77-82. doi: 10.1111/j.1600-0722.2007.00506.x.

Hadis, M., J. G. Leprince, A. C. Shortall, J. Devaux, G. Leloup, and W. M. Palin. 2011. "High irradiance curing and anomalies of exposure reciprocity law in resin-based materials." *J Dent* 39 (8):549-57. doi: 10.1016/j.jdent.2011.05.007.

Haenel, T., B. Hausnerova, J. Steinhaus, R. B. Price, B. Sullivan, and B. Moeginger. 2015. "Effect of the irradiance distribution from light curing units on the local micro-hardness of the surface of dental resins." *Dent Mater* 31 (2):93-104. doi: 10.1016/j.dental.2014.11.003.

Hansen, E. K. 1983. "After-polymerization of visible light activated resins: surface hardness vs. light source." *Scand J Dent Res* 91 (5):406-10.

Harlow, J. E., B. Sullivan, A. C. Shortall, D. Labrie, and R. B. Price. 2016. "Characterizing the output settings of dental curing lights." *J Dent* 44:20-6. doi: 10.1016/j.jdent.2015.10.019.

Hofmann, N., B. Hugo, and B. Klaiber. 2002. "Effect of irradiation type (LED or QTH) on photo-activated composite shrinkage strain kinetics, temperature rise, and hardness." *Eur J Oral Sci* 110 (6):471-9.

Ikemura, K., and T. Endo. 2010. "A review of the development of radical

photopolymerization initiators used for designing light-curing dental adhesives and resin composites." *Dent Mater J* 29 (5):481-501.
Ilie, N., and K. Stark. 2014. "Curing behaviour of high-viscosity bulk-fill composites." *J Dent* 42 (8):977-85. doi: 10.1016/j.jdent.2014.05.012.
ISO. 2004. 10650-1:2004 dentistry-powered polymerizationactivators: part 1: quartz tungsten halogen lamps. Geneva,Switzerland: International Standards Organization.
ISO. 2007. "10650-2:2007 dentistry-powered polymerizationactivators: part 2: light-emitting diode (LED) lamps. Geneva,Switzerland: International Standards Organization.":7.
Jandt, K. D., and R. W. Mills. 2013. "A brief history of LED photopolymerization." *Dent Mater* 29 (6):605-17. doi: 10.1016/j.dental.2013.02.003.
Knezevic, A., D. Zeljezic, N. Kopjar, and Z. Tarle. 2008. "Cytotoxicity of composite materials polymerized with LED curing units." *Oper Dent* 33 (1):23-30. doi: 10.2341/07-16.
Leprince, J. G., M. Hadis, A. C. Shortall, J. L. Ferracane, J. Devaux, G. Leloup, and W. M. Palin. 2011. "Photoinitiator type and applicability of exposure reciprocity law in filled and unfilled photoactive resins." *Dent Mater* 27 (2):157-64. doi: 10.1016/j.dental.2010.09.011.
Leprince, J. G., P. Leveque, B. Nysten, B. Gallez, J. Devaux, and G. Leloup. 2012. "New insight into the "depth of cure" of dimethacrylate-based dental composites." *Dent Mater* 28 (5):512-20. doi: 10.1016/j.dental.2011.12.004.
Leprince, J. G., W. M. Palin, M. A. Hadis, J. Devaux, and G. Leloup. 2013. "Progress in dimethacrylate-based dental composite technology and curing efficiency." *Dent Mater* 29 (2):139-56. doi: 10.1016/j.dental.2012.11.005.
Leprince, J., G. Lamblin, D. Truffier-Boutry, S. Demoustier-Champagne, J. Devaux, M. Mestdagh, and G. Leloup. 2009. "Kinetic study of free radicals trapped in dental resins stored in different environments." *Acta Biomater* 5 (7):2518-24. doi: 10.1016/j.actbio.2009.04.034.
Li, J., H. Li, A. S. Fok, and D. C. Watts. 2009. "Multiple correlations of material parameters of light-cured dental composites." *Dent Mater* 25 (7):829-36. doi: 10.1016/j.dental.2009.03.011.
Lohbauer, U., C. Rahiotis, N. Kramer, A. Petschelt, and G. Eliades. 2005. "The effect of different light-curing units on fatigue behavior and degree of conversion of a resin composite." *Dent Mater* 21 (7):608-15. doi: 10.1016/j.dental.2004.07.020.
Lucey, S. M., A. Santini, and E. M. Roebuck. 2015. "Degree of conversion of resin-based materials cured with dual-peak or single-peak LED light-curing units." *Int J Paediatr Dent* 25 (2):93-102. doi: 10.1111/ipd.12104.
Manga, R. K., D. G. Charlton, and C. W. Wakefield. 1995. "In vitro evaluation of a curing radiometer as a predictor of polymerization depth." *Gen Dent* 43 (3):241-3; quiz 245-6.
Manojlovic, D., M. D. Dramicanin, V. Miletic, D. Mitic-Culafic, B. Jovanovic, and B. Nikolic. 2017. "Cytotoxicity and genotoxicity of a low-shrinkage monomer and monoacylphosphine oxide photoinitiator: Comparative analyses of individual toxicity and combination effects in mixtures." *Dent Mater*. doi: 10.1016/j.dental.2017.02.002.

Megremis, S. J., V. Ong, H. Lukic, and H. Shepelak. 2014. "An ada laboratory evaluation of light-emitting diode curing units." *J Am Dent Assoc* 145 (11):1164-6. doi: 10.14219/jada.2014.97.

Michaud, P. L., R. B. Price, D. Labrie, F. A. Rueggeberg, and B. Sullivan. 2014. "Localised irradiance distribution found in dental light curing units." *J Dent* 42 (2):129-39. doi: 10.1016/j.jdent.2013.11.014.

Miletic, V., and A. Santini. 2012. "Micro-Raman spectroscopic analysis of the degree of conversion of composite resins containing different initiators cured by polywave or monowave LED units." *J Dent* 40 (2):106-13. doi: 10.1016/j.jdent.2011.10.018.

Mills, R. W., K. D. Jandt, and S. H. Ashworth. 1999. "Dental composite depth of cure with halogen and blue light emitting diode technology." *Br Dent J* 186 (8):388-91.

MM, A. LShaafi, T. Haenel, B. Sullivan, D. Labrie, M. Q. Alqahtani, and R. B. Price. 2016. "Effect of a broad-spectrum LED curing light on the Knoop microhardness of four posterior resin based composites at 2, 4 and 6-mm depths." *J Dent* 45:14-8. doi: 10.1016/j.jdent.2015.11.004.

Moin Jan, C., Y. Nomura, H. Urabe, M. Okazaki, and H. Shintani. 2001. "The relationship between leachability of polymerization initiator and degree of conversion of visible light-cured resin." *J Biomed Mater Res* 58 (1):42-6.

Moore, B. K., J. A. Platt, G. Borges, T. M. Chu, and I. Katsilieri. 2008. "Depth of cure of dental resin composites: ISO 4049 depth and microhardness of types of materials and shades." *Oper Dent* 33 (4):408-12. doi: 10.2341/07-104.

Moraschini, V., C. K. Fai, R. M. Alto, and G. O. Dos Santos. 2015. "Amalgam and resin composite longevity of posterior restorations: A systematic review and meta-analysis." *J Dent* 43 (9):1043-50. doi: 10.1016/j.jdent.2015.06.005.

Moreland, Kenneth. 2009. "Diverging Color Maps for Scientific Visualization." In *Advances in Visual Computing: 5th International Symposium, ISVC 2009, Las Vegas, NV, USA, November 30-December 2, 2009. Proceedings, Part II*, edited by George Bebis, Richard Boyle, Bahram Parvin, Darko Koracin, Yoshinori Kuno, Junxian Wang, Renato Pajarola, Peter Lindstrom, André Hinkenjann, Miguel L. Encarnação, Cláudio T. Silva and Daniel Coming, 92-103. Berlin, Heidelberg: Springer Berlin Heidelberg.

Mousavinasab, S. M., and I. Meyers. 2011. "Comparison of Depth of Cure, Hardness and Heat Generation of LED and High Intensity QTH Light Sources." *Eur J Dent* 5 (3):299-304.

Musanje, L., and B. W. Darvell. 2003. "Polymerization of resin composite restorative materials: exposure reciprocity." *Dent Mater* 19 (6):531-41.

Musanje, L., and B. W. Darvell. 2006. "Curing-light attenuation in filled-resin restorative materials." *Dent Mater* 22 (9):804-17. doi: 10.1016/j.dental.2005.11.009.

Nedeljkovic, I., W. Teughels, J. De Munck, B. Van Meerbeek, and K. L. Van Landuyt. 2015. "Is secondary caries with composites a material-based problem?" *Dent Mater* 31 (11):e247-77. doi: 10.1016/j.dental.2015.09.001.

Neumann, M. G., W. G. Miranda, Jr., C. C. Schmitt, F. A. Rueggeberg, and I. C. Correa. 2005. "Molar extinction coefficients and the photon absorption efficiency of dental photoinitiators and light curing units." *J Dent* 33 (6):525-32. doi:

10.1016/j.jdent.2004.11.013.
Nitta, K. 2005. "Effect of light guide tip diameter of LED-light curing unit on polymerization of light-cured composites." *Dent Mater* 21 (3):217-23. doi: 10.1016/j.dental.2004.03.008.
Nomoto, R. 1997. "Effect of light wavelength on polymerization of light-cured resins." *Dent Mater J* 16 (1):60-73.
Ogunyinka, A., W. M. Palin, A. C. Shortall, and P. M. Marquis. 2007. "Photoinitiation chemistry affects light transmission and degree of conversion of curing experimental dental resin composites." *Dent Mater* 23 (7):807-13. doi: 10.1016/j.dental.2006.06.016.
Opdam, N. J., E. M. Bronkhorst, J. M. Roeters, and B. A. Loomans. 2007. "A retrospective clinical study on longevity of posterior composite and amalgam restorations." *Dent Mater* 23 (1):2-8. doi: 10.1016/j.dental.2005.11.036.
Palin, W. M., D. P. Senyilmaz, P. M. Marquis, and A. C. Shortall. 2008. "Cure width potential for MOD resin composite molar restorations." *Dent Mater* 24 (8):1083-94. doi: 10.1016/j.dental.2008.01.001.
Par, M., O. Gamulin, D. Marovic, E. Klaric, and Z. Tarle. 2014. "Effect of temperature on post-cure polymerization of bulk-fill composites." *J Dent* 42 (10):1255-60. doi: 10.1016/j.jdent.2014.08.004.
Par, M., O. Gamulin, D. Marovic, E. Klaric, and Z. Tarle. 2015. "Raman spectroscopic assessment of degree of conversion of bulk-fill resin composites--changes at 24 hours post cure." *Oper Dent* 40 (3):E92-101. doi: 10.2341/14-091-L.
Park, J. G., Q. Ye, E. M. Topp, C. H. Lee, E. L. Kostoryz, A. Misra, and P. Spencer. 2009. "Dynamic mechanical analysis and esterase degradation of dentin adhesives containing a branched methacrylate." *J Biomed Mater Res B Appl Biomater* 91 (1):61-70. doi: 10.1002/jbm.b.31374.
Pilo, R., and H. S. Cardash. 1992. "Post-irradiation polymerization of different anterior and posterior visible light-activated resin composites." *Dent Mater* 8 (5):299-304.
Platt, J. A., and R. B. Price. 2014. "Light curing explored in Halifax." *Oper Dent* 39 (6):561-3. doi: 10.2341/1559-2863-39.6.561.
Price, R. B., T. Derand, M. Sedarous, P. Andreou, and R. W. Loney. 2000. "Effect of distance on the power density from two light guides." *J Esthet Dent* 12 (6):320-7.
Price, R. B., J. Fahey, and C. M. Felix. 2010. "Knoop microhardness mapping used to compare the efficacy of LED, QTH and PAC curing lights." *Oper Dent* 35 (1):58-68. doi: 10.2341/09-055-L.
Price, R. B., and C. A. Felix. 2009. "Effect of delivering light in specific narrow bandwidths from 394 to 515nm on the micro-hardness of resin composites." *Dent Mater* 25 (7):899-908. doi: 10.1016/j.dental.2009.01.098.
Price, R. B., C. A. Felix, and P. Andreou. 2005. "Knoop hardness of ten resin composites irradiated with high-power LED and quartz-tungsten-halogen lights." *Biomaterials* 26 (15):2631-41. doi: 10.1016/j.biomaterials.2004.06.050.
Price, R. B., C. A. Felix, and P. Andreou. 2006. "Third-generation vs a second-generation LED curing light: effect on Knoop microhardness." *Compend Contin Educ Dent* 27 (9):490-6; quiz 497, 518.
Price, R. B., J. L. Ferracane, and A. C. Shortall. 2015. "Light-Curing Units: A Review of What We Need to Know." *J Dent Res* 94 (9):1179-86. doi:

10.1177/0022034515594786.
Price, R. B., D. Labrie, F. A. Rueggeberg, and C. M. Felix. 2010. "Irradiance differences in the violet (405 nm) and blue (460 nm) spectral ranges among dental light-curing units." *J Esthet Restor Dent* 22 (6):363-77. doi: 10.1111/j.1708-8240.2010.00368.x.
Price, R. B., D. Labrie, F. A. Rueggeberg, B. Sullivan, I. Kostylev, and J. Fahey. 2014. "Correlation between the beam profile from a curing light and the microhardness of four resins." *Dent Mater* 30 (12):1345-57. doi: 10.1016/j.dental.2014.10.001.
Price, R. B., D. Labrie, J. M. Whalen, and C. M. Felix. 2011. "Effect of distance on irradiance and beam homogeneity from 4 light-emitting diode curing units." *J Can Dent Assoc* 77:b9.
Price, R. B., F. A. Rueggeberg, D. Labrie, and C. M. Felix. 2010. "Irradiance uniformity and distribution from dental light curing units." *J Esthet Restor Dent* 22 (2):86-101. doi: 10.1111/j.1708-8240.2010.00318.x.
Rasines Alcaraz, M. G., A. Veitz-Keenan, P. Sahrmann, P. R. Schmidlin, D. Davis, and Z. Iheozor-Ejiofor. 2014. "Direct composite resin fillings versus amalgam fillings for permanent or adult posterior teeth." *Cochrane Database Syst Rev* 3:CD005620. doi: 10.1002/14651858.CD005620.pub2.
Rencz, A., R. Hickel, and N. Ilie. 2012. "Curing efficiency of modern LED units." *Clin Oral Investig* 16 (1):173-9. doi: 10.1007/s00784-010-0498-3.
Rho, Y. J., C. Namgung, B. H. Jin, B. S. Lim, and B. H. Cho. 2013. "Longevity of direct restorations in stress-bearing posterior cavities: a retrospective study." *Oper Dent* 38 (6):572-82. doi: 10.2341/12-432-C.
Rueggeberg, F. A. 2011. "State-of-the-art: dental photocuring--a review." *Dent Mater* 27 (1):39-52. doi: 10.1016/j.dental.2010.10.021.
Rueggeberg, F. A., W. F. Caughman, and J. W. Curtis, Jr. 1994. "Effect of light intensity and exposure duration on cure of resin composite." *Oper Dent* 19 (1):26-32.
Santini, A., V. Miletic, M. D. Swift, and M. Bradley. 2012. "Degree of conversion and microhardness of TPO-containing resin-based composites cured by polywave and monowave LED units." *J Dent* 40 (7):577-84. doi: 10.1016/j.jdent.2012.03.007.
Schneider, L. F., R. R. Moraes, L. M. Cavalcante, M. A. Sinhoreti, L. Correr-Sobrinho, and S. Consani. 2008. "Cross-link density evaluation through softening tests: effect of ethanol concentration." *Dent Mater* 24 (2):199-203. doi: 10.1016/j.dental.2007.03.010.
Schneider, L. F., C. S. Pfeifer, S. Consani, S. A. Prahl, and J. L. Ferracane. 2008. "Influence of photoinitiator type on the rate of polymerization, degree of conversion, hardness and yellowing of dental resin composites." *Dent Mater* 24 (9):1169-77. doi: 10.1016/j.dental.2008.01.007.
Selig, D., T. Haenel, B. Hausnerova, B. Moeginger, D. Labrie, B. Sullivan, and R. B. Price. 2015. "Examining exposure reciprocity in a resin based composite using high irradiance levels and real-time degree of conversion values." *Dent Mater* 31 (5):583-93. doi: 10.1016/j.dental.2015.02.010.
Shortall, A. C., W. M. Palin, and P. Burtscher. 2008. "Refractive index mismatch and monomer reactivity influence composite curing depth." *J Dent Res* 87 (1):84-8.
Shortall, A. C., R. B. Price, L. MacKenzie, and F. J. Burke. 2016a. "Guidelines for the selection, use, and maintenance of LED light-curing units - Part 1." *Br Dent J*

221 (8):453-460. doi: 10.1038/sj.bdj.2016.772.
Shortall, A. C., R. B. Price, L. MacKenzie, and F. J. Burke. 2016b. "Guidelines for the selection, use, and maintenance of LED light-curing units - Part II." *Br Dent J* 221 (9):551-554. doi: 10.1038/sj.bdj.2016.814.
Silikas, N., G. Eliades, and D. C. Watts. 2000. "Light intensity effects on resin-composite degree of conversion and shrinkage strain." *Dent Mater* 16 (4):292-6.
Sim, J. S., H. J. Seol, J. K. Park, F. Garcia-Godoy, H. I. Kim, and Y. H. Kwon. 2012. "Interaction of LED light with coinitiator-containing composite resins: effect of dual peaks." *J Dent* 40 (10):836-42. doi: 10.1016/j.jdent.2012.06.008.
Sobrinho, L. C., M. F. Goes, S. Consani, M. A. Sinhoreti, and J. C. Knowles. 2000. "Correlation between light intensity and exposure time on the hardness of composite resin." *J Mater Sci Mater Med* 11 (6):361-4.
Soh, M. S., and A. U. Yap. 2004. "Influence of curing modes on crosslink density in polymer structures." *J Dent* 32 (4):321-6. doi: 10.1016/j.jdent.2004.01.012.
Soh, M. S., A. U. Yap, and K. S. Siow. 2004. "Comparative depths of cure among various curing light types and methods." *Oper Dent* 29 (1):9-15.
Soh, M. S., A. U. Yap, T. Yu, and Z. X. Shen. 2004. "Analysis of the degree of conversion of LED and halogen lights using micro-Raman spectroscopy." *Oper Dent* 29 (5):571-7.
Stahl, F., S. H. Ashworth, K. D. Jandt, and R. W. Mills. 2000. "Light-emitting diode (LED) polymerisation of dental composites: flexural properties and polymerisation potential." *Biomaterials* 21 (13):1379-85.
Sunnegardh-Gronberg, K., J. W. van Dijken, U. Funegard, A. Lindberg, and M. Nilsson. 2009. "Selection of dental materials and longevity of replaced restorations in Public Dental Health clinics in northern Sweden." *J Dent* 37 (9):673-8. doi: 10.1016/j.jdent.2009.04.010.
Truffier-Boutry, D., S. Demoustier-Champagne, J. Devaux, J. J. Biebuyck, M. Mestdagh, P. Larbanois, and G. Leloup. 2006. "A physico-chemical explanation of the post-polymerization shrinkage in dental resins." *Dent Mater* 22 (5):405-12. doi: 10.1016/j.dental.2005.04.030.
Turssi, C. P., J. L. Ferracane, and K. Vogel. 2005. "Filler features and their effects on wear and degree of conversion of particulate dental resin composites." *Biomaterials* 26 (24):4932-7. doi: 10.1016/j.biomaterials.2005.01.026.
Vaidyanathan, T. K., J. Vaidyanathan, P. P. Lizymol, S. Ariya, and K. V. Krishnan. 2017. "Study of visible light activated polymerization in BisGMA-TEGDMA monomers with Type 1 and Type 2 photoinitiators using Raman spectroscopy." *Dent Mater* 33 (1):1-11. doi: 10.1016/j.dental.2016.09.002.
Vandewalle, K. S., J. L. Ferracane, T. J. Hilton, R. L. Erickson, and R. L. Sakaguchi. 2004. "Effect of energy density on properties and marginal integrity of posterior resin composite restorations." *Dent Mater* 20 (1):96-106.
Watts, D. C., O. M. Amer, and E. C. Combe. 1987. "Surface hardness development in light-cured composites." *Dent Mater* 3 (5):265-9. doi: 10.1016/S0109-5641(87)80085-4.
Watts, D. C., and A. J. Cash. 1994. "Analysis of optical transmission by 400-500 nm visible light into aesthetic dental biomaterials." *J Dent* 22 (2):112-7.
Wydra, J. W., N. B. Cramer, J. W. Stansbury, and C. N. Bowman. 2014. "The reciprocity

law concerning light dose relationships applied to BisGMA/TEGDMA photopolymers: theoretical analysis and experimental characterization." *Dent Mater* 30 (6):605-12. doi: 10.1016/j.dental.2014.02.021.
Yap, A. U., and C. Seneviratne. 2001. "Influence of light energy density on effectiveness of composite cure." *Oper Dent* 26 (5):460-6.
Yap, A. U., M. S. Soh, T. T. Han, and K. S. Siow. 2004. "Influence of curing lights and modes on cross-link density of dental composites." *Oper Dent* 29 (4):410-5.

CURRICULUM VITAE

Afnan Omar AlZain

Education

2010-2017	Ph.D. in Dental Sciences. Dental Biomaterials Track. Indiana University, Indianapolis, IN, USA.
2008-2010	Master of Science in Dental (M.S.D.). Major in Operative Dentistry, Minor in Dental Materials and Preventive Dentistry. Certificate in Operative Dentistry. Indiana University School of Dentistry (IUSD), Indianapolis, IN, USA.
1999-2005	Bachelor of Dental Science Degree (B.D.S.). King Abdulaziz University, Faculty of Dentistry, Jeddah, Saudi Arabia.

Honors and Awards

2017	Sherry Queener Graduate Student Excellence Award. Indiana University Purdue University Indianapolis (IUPUI), Indianapolis, IN, USA.
2017	Graduate and Professional Student Government Legislative Incentive, IUPUI, Indianapolis, IN, USA.
2017	GlaxoSmithKline Ph.D. Student Oral Presentation Award. IUSD Annual Research Day, Indianapolis, IN, USA.
2016	Dr. Jason T. Sprat Scholarship. IUPUI's 5th Annual Student Leadership Reception, IUPUI, Indianapolis, IN, USA.
2016	Elite 50 Award. Elite 50 Celebration Dinner. IUPUI, Indianapolis, IN, USA.
2016	Best in School Recognition Certificate. Elite 50 Celebration Dinner. IUPUI, IN, USA.

2016	Premier 10 Award. Elite 50 Celebration Dinner. IUPUI, Indianapolis, IN, USA.
2016	Shofu Ph.D. Student Award for Best Oral Poster Presentation. IUSD Annual Research Day, Indianapolis, IN, USA.
2016	King Saud University Travel Award. IUSD Annual Research Day, Indianapolis, IN, USA.
2015, 2016	Graduate and Professional Educational Grant. IUPUI, Indianapolis, IN, USA.
2012, 2013	Educational Enhancement Grant. IUPUI, Indianapolis, IN, USA.
2011	Shofu Graduate Student Award. IUSD Annual Research Day, Indianapolis, IN, USA.
2008-2017	Full scholarship for Master and Ph.D. Graduate Studies. King Abdulaziz University. Jeddah, Saudi Arabia.
2008	Certificate of Appreciation for the Scientific Contribution entitled "Posture Evaluation of Dental Students in King Abdulaziz University". The 2nd International King Abdulaziz University/The 19th Saudi Dental Society Conference.
2007	Plaque of Honor for Appointed as a Demonstrator (Teacher Assistant). King Abdulaziz University, Jeddah, Saudi Arabia.
2006	Plaque of Academic Honor for Achieving GPA with a Second Honor Degree. King Abdulaziz University, Jeddah, Saudi Arabia.
2006	Certificate of Appreciation for Participating in Health day. Dorm Female section. King Abdulaziz University, Jeddah, Saudi Arabia.
2006	Comprehensive Care Clinic Internship Award for Outstanding Clinical Performance. King Abdulaziz University, Jeddah, Saudi Arabia.
2006	Academic Honor, Certificate Honor for High Scientific Achievements. King Abdulaziz University, Jeddah, Saudi Arabia.

Professional Experience

2016	Lecture Dental Material Seminar course for Ph.D. students. IUSD, Indianapolis, IN, USA.
2013	Lecture an Operative Seminar to Master in Operative Dentistry students. IUSD, Indianapolis, IN, USA.
2012-2017	Senior Resident of the Dental Biomaterials Laboratory. IUSD, Indianapolis, IN, USA.
2012-2013	Critical Thinking Skills Facilitator. IUSD, Indianapolis, IN, USA.
2013-2017	IUSD Representative for the Graduate and Professional School Government. IUPUI, Indianapolis, IN, USA.
2012-2017	Representative of the Ph.D. students. IUSD, Indianapolis, IN, USA.
2012-2016	President of the Advanced Graduate Organization. IUSD, Indianapolis, IN, USA.
2012-2016	Member of the Advanced Graduate Council. IUSD, Indianapolis, IN, USA.
2011-2017	Bench instructor for pre-doctoral dental students in pre-clinical lab and research projects. IUSD, Indianapolis, IN, USA.
2007-2008	Demonstrator (Teacher Assistant). Operative Dentistry Division, Conservative Dental Sciences Department, Faculty of Dentistry, King Abdulaziz University**,** Jeddah, Saudi Arabia.
2005-2006	Intern/Dentist at Faculty of Dentistry. King Abdulaziz Uuniversity, King Fahd Armed Forces Hospital, King Abdulaziz Medical City and King Fahd General Hospital. Jeddah, Saudi Arabia.

Conferences, Courses & Workshops

Attended over 300 hours of continuous education conferences, courses and workshops.

2017 International Association of Dental Research, San Francisco, CA, USA.

2017 American Dental Education Association. Long Beach, CA, USA.

2017 E.C. Moore Symposium on Excellence in Teaching. IUPUI, Indianapolis, IN, USA.

2016 Academy of Dental Materials Annual Meeting. Chicago, IL, USA.

- Workshop. Breakfast and Learn: How to publish in Dental Materials?. Dr. Nick Silicas, University of Manchester, England.
- Workshop. Breakfast and Learn: Bio-Degradation of adhesive and its interfaces. Is it a problem? Dr. Ricardo Marins Carvalho, University of British Colombia, Canada.
- Workshop. Breakfast and Learn: Factors influencing the effective use of light-curing units. Dr. Spiro Megremis. American Dental Association, USA.

2016 Ralph Phillips Symposium on Dental Biomaterials. IUSD, Indianapolis, IN, USA.

2016 American Association of Dental Research, Los Angeles, CA, USA.

2016 Midwinter meeting. Chicago, IL, USA.

2015 International Association of Dental Research, Boston, MA, USA.

2015 Midwinter meeting. Chicago, IL, USA.

2014 Biomaterials Day. UK, Lexington, KY, USA.

2013 Preparing Future Faculty. Indiana University Purdue University Indianapolis, Indianapolis, IN, USA.

2013 International Association of Dental Research, Seattle, WA, USA.

2012	American Association of Dental Research, Tampa, FL, USA.
2011-2017	Various CE lectures. IUSD, Indianapolis, IN, USA.
2011-2017	IUPUI Student Research Day. Indianapolis, IN, USA.
2011	International Association of Dental Research, San Diego, California, USA.
2009-2017	IUSD Annual Research Day. Indianapolis, IN, USA.
2009	Straumann Implant Workshop. IUSD, Indianapolis, IN, USA.
2009	Strategies for Efficient Diagnosis and Effective Management of Mucocutaneous Diseases and Salivary Gland Disorders. IUSD, Indianapolis, IN, USA.
2009	The 38th Annual Meeting of the Academy of Operative Dentistry Conference. Chicago, Illinois, USA.
2008	The 2nd International KAU and the 19th Saudi Dental Society Conference. Jeddah, Saudi Arabia.
2008	Hi-Tech. Dentistry Lectures. Jeddah, Saudi Arabia.
2005-2007	Various Saudi Dental Society monthly scientific lectures. Jeddah, Saudi Arabia.
2007	3rd Jeddah Dental Esthetic Conference. Jeddah, Saudi Arabia.
2007	Hi-Tech. Dentistry Lectures. Jeddah, Saudi Arabia.
2007	The 18th Saudi International Dental Congress. Riyadh, Saudi Arabia.
2006	2nd Jeddah Dental Esthetic Conference. Jeddah, Saudi Arabia.
2006	Implant Dentistry from Examination to Restoration Workshop. Jeddah, Saudi Arabia.
2006	Dental and Facial Esthetic Symposium. Jeddah, Saudi Arabia.
2006	Achieving Maximum Esthetic Results with Bleaching and/or Porcelain Veneers Workshop. Jeddah, Saudi Arabia.

2006 Modern Approach in Esthetic Dentistry Workshop. Jeddah, Saudi Arabia.

2006 Evidence Based Dentistry Workshop. Jeddah, Saudi Arabia.

2006 The 17th Saudi International Dental Congress. Riyadh, Saudi Arabia.

2005 Six Points of Efficient Non-Surgical Endodontic Treatment Workshop. Al-Khubar, Saudi Arabia.

2005 Second Gulf Scientific Dental Conference. Al-Khubar, Saudi Arabia.

2005 Strategic Development Course. Jeddah, Saudi Arabia.

Published Abstracts

- **Oral Presentation**
  - Al-Zain AO, Lukic H, Eckert GJ, Megremis SJ, Platt JA. Localized Irradiance From LCUs Influence on Resin-matrix Composite Cross-link Density. March 2017. International Association of Dental Research Meeting.
- **Posters**
  1. Al-Zain AO, Lukic H, Eckert GJ, Megremis SJ, Platt JA. Localized Irradiance From LCUs Influence on Resin-matrix Composite Cross-link Density. April 2017. IUPUI Student Research Day. IUSD Annual Research Day.
  2. Eshmawi Y, Al-Zain AO, Eckert GJ, Platt JA. Impact of beam profile on resin-matrix composite conversion and micro-flexural strength. March and April 2017. International Association of Dental Research Meeting. IUSD Annual Research Day.
  3. Alqahtani S, Soto-Rojas AE, Al-Zain AO, Platt JA, Cook NB. Evaluation of polywave and monowave light curing units efficiency on the degree of conversion and microhardness of resin fissure sealants. March and April 2017. International Association of Dental Research Meeting. IUSD Annual Research Day.

4. Al-Zain AO, Eckert GJ, Goodpaster JV, Platt JA. Distance's influence on exposure reciprocity and degree of conversion. 2016. Academy of Dental Materials Annual Meeting.
5. Al-Zain AO, Lukic H, Eckert GJ, Megremis SJ, Platt JA. Beam Profile Characterization of Light-Emitting Diode Curing Units and Its Effect on Polymerization of Resin-Matrix Composites. 2016. American Association of Dental Research meeting. IUPUI Student Research Day. IUSD Annual Research Day.
6. Al-Zain AO, Xie D, Platt JA. Evaluation of various properties of novel urethane-based resin composites. 2015. International Association of Dental Research/American Association of Dental Research meeting. IUPUI Student Research Day. IUSD Annual Research Day.
7. Feitosa SA*, Munshow EA, Al-Zain AO*, Kamocki K, Platt JA, Bottino MC. Synthesis and characterization of novel hallosite-incorporated adhesive resins. 2015. International Association of Dental Research/American Association of Dental Research meeting.
8. Al-Shehri E*, Al-Zain AO*, Sabrah AH, Al-Angari SS, Al Dehailan L, Eckert GJ, Platt JA, Bottino MC. The effect of combined cyclic loading and thermocycling on the Shear-Bond Strength and Surface Roughness of Y-TZP Zirconia. 2015. International Association of Dental Research/American Association of Dental Research meeting. IUSD Annual Research Day.
9. Al-Zain AO, Xie D, Platt JA. Chemical and Mechanical Characterization of a Novel Urethane-Based Composite. 2014. IUPUI Student Research Day. IUSD Annual Research Day.
10. Al-Zain AO, Eckert GJ, Platt JA. Microtensile bond strength and microleakage of HEMA-free one-step self-etch adhesive. 2013. International Association of Dental Research/American Association of Dental Research meeting. IUSD Annual Research Day.

11. Al-Zain AO, Eckert GJ, Platt JA. Evaluation of microtensile bond strength and micoleakage of a one-step self-etch adhesive. 2012. American Association of Dental Research meeting. IUPUI Student Research Day. IUSD Annual Research Day.
12. Al-Zain AO, Eckert GJ, Platt JA. Evaluation of microtensile bond strength of a one-step self-etch adhesive. 2011. American Association of Dental Research meeting. IUSD Annual Research Day.
13. Al-Zain AO, Chu TM. The ion release behaviors of a novel resin-based calcium phosphate cement. 2010. International Association of Dental Research/American Association of Dental Research meeting. IUPUI Student Research Day. IUSD Annual Research Day.

Publications

1. Al-Zain AO, Eckert GJ, Lukic H, Megremis S, Platt JA. Influence of distance on the degree of conversion, microhardness and cross-link density within a resin-matrix composite cured using multiple LED curing units. Clin Oral Investig. 2017 (Manuscript in preparation).
2. Al-Zain AO, Eckert GJ, Platt JA. The influence of distance on the degree of conversion of a resin-matrix composite light cured using multiple LED light-curing units. Clin Oral Investig. 2017 (Manuscript in preparation).
3. Eshmawi Y, Al-Zain AO, Eckert GJ, Platt JA. Impact of beam profile on resin-matrix composite conversion and micro-flexural strength. Journal of American Dental Association. 2017 (Manuscript in preparation).
4. Alqahtani S, Soto-Rojas AE, Al-Zain AO, Platt JA, Cook NB. Evaluation of polywave and monowave light curing units efficiency on the degree of conversion and microhardness of resin fissure sealants. 2017 (Manuscript in preparation).

5. Al-Zain AO, Eckert GJ, Lukic H, Megremis S, Platt JA. Degree of conversion and cross-link density within a resin-matrix composite. J Biomed Mater Res B Appl Biomater. 2017 (Submitted).
6. Al-Shehri E*, Al-Zain AO*, Sabrah AH, Al-Angari SS, Al Dehailan L, Eckert GJ, Özcan M, Platt JA, Bottino MC. The effect of combined cyclic loading and thermocycling on the Shear-Bond Strength and Surface Roughness of Y-TZP Zirconia. Restor Dent Endod. 2016 (accepted for publication). *First two authors contributed equally to the paper.
7. Yassen GH, Huang R, Al-Zain A, Yoshida T, Gregory RL, Platt JA. Clin Oral Investig. Evaluation of selected properties of a new root repair cement containing surface pre-reacted filled glass ionomer fillers. 2016 Jan 20.
8. Feitosa SA*, Munshow EA*, Al-Zain AO*, Kamocki K, Platt JA, Bottino MC. Synthesis and characterization of novel hallosite-incorporated adhesive resins. Journal of Dentistry. J Dent. 2015 Nov;43(11):1316-22. *First three authors contributed equally to the paper.
9. Yousef MK, Al-Zain AO. Posture Evaluation of Dental Students in King Abdulaziz University. JKAU: Med. Sci., Vol. 16, No. 2, pp: 51-68. 2009 AD/ 1430 AH.